Convection-Diffusion Models

for

Competition and Segregation

in

Granular Material

vorgelegt von
Joel Braun
aus Göttingen

2003

Contents

List of Figures

v

The various figures in this thesis are complemented by a flip-book illustration in order to demonstrate the dynamics of segregation in shaken granular material. The pictures at the bottom of the odd pages make up a sequence illustrating the so-called *Brazil nut effect*: The depicted vessel contains a mixture of grains of three different types. All of them have the same specific weight and spherical shape, but their sizes vary considerably. During the shaking process, the larger particles tend to move up, while the smaller ones fall into the gaps and move down. The pictures on the even pages show a granular material composed of only two types of particles. This time, all of them have equal size and shape, but their specific densities differ largely. We observe a clear tendency of the lighter grains to move up. This *buoyancy effect* is consistent with our everyday experience.

Zusammenfassung in deutscher Sprache

Inhalt dieser Arbeit sind die Untersuchung und der Vergleich von Wettbewerbsmodellen in Form sogenannter Konvektions-Diffusions-Gleichungen und ihre Anwendung vorwiegend im Bereich der granularen Medien. Während die qualitative Theorie der Reaktions-Diffusions-Gleichungen gut entwickelt ist, da diese als Modelle immer da auftreten, wo Interaktionen zwischen verschiedenen Spezies zusammen mit Ausbreitungsvorgängen untersucht werden, erscheinen die hier betrachteten Systeme von Konvektions-Diffusions-Gleichungen als recht neuartig. Sie stehen in enger Verbindung mit Viskositätsansätzen für Erhaltungsgleichungen, werden hier aber als eigenständige Systeme untersucht. Das Ziel der Arbeit ist es, diese Gleichungen als Modelle für Phänomene insbesondere bei granularen Medien zu rechtfertigen, z. B. durch Übergang von Partikelsystemen, und ihre mathematischen Eigenschaften zu untersuchen.

Das Prinzip, welches besagt, dass "zwei ähnliche Arten nicht denselben Lebensraum bewohnen können", war schon Naturforschern im 19. und frühen 20. Jahrhundert bekannt. So untersuchte beispielsweise A. Hansmann in [Hansmann57] die beiden eng verwandten Vogelarten *Phylloscopus trochilus* und *Phylloscopus bonelli* (Laubsänger) und führte die räumliche Trennung ihrer Lebensräume auf den Wettbewerb zwischen beiden zurück. Der Beitrag von V. Volterra ([Volterra26], [Volterra28]) prägte die theoretische Forschung auf dem Gebiet der Koexistenz. Er konstruierte ein Modell für zwei Spezies, die um eine begrenzt zur Verfügung stehende Nahrungsquelle kämpfen und zeigte, dass fast immer eine der beiden Arten ausstirbt. Zusammen mit A. J. Lotka gab er den heute bekannten Lotka-Volterra Wettbewerbsmodellen den Namen. Diese Gleichungen lassen, abhängig von den Parametern, in ihrer allgemeinen Form sowohl die Koexistenz als auch das wettbewerbsbedingte Aussterben einer Art zu. Volterras Arbeit schuf die Voraussetzungen für die bedeutenden theoretischen und experimentellen Studien von G. F. Gause (siehe [Gause34]), welcher im Jahre 1935 die ökologische Hypothese formulierte, dass zwei Arten mit vergleichbaren Eigenschaften nicht denselben Lebensraum bewohnen können. Auch bei nur geringfügigen Unterschieden wird eine der beiden Arten aussterben. Um diesem Prinzip zu entgehen, muss demnach wenigstens eine der beiden Arten ihre ökologische Nische wechseln oder erweitern. R. McGehee und R. A. Armstrong ([McGehee77]) schließlich stellten das Problem der Persistenz und Koexistenz auf eine solidere mathematische Basis, gaben einen Überblick über verschiedene Wettbewerbsmodelle und führten strikte Beweise der bekannten Hypothesen.

Das Prinzip des *wettbewerbsbedingten Ausschlusses* spielt heutzutage auf zahlreichen Gebieten wissenschaftlichen Interesses eine unverzichtbare Rolle. Im Bereich der Genetik beispielsweise ermöglicht erst die große Zahl unterschiedlicher Allele, welche an ein und demselben Genlokus auftreten und in gewisser Weise um ihr *Überleben* in der Population kämpfen, eine ausreichende Anpassung der Art an wechselnde Umwelteinflüsse. Dies gilt als eine treibende Kraft für die Evolution. Aber auch die wirtschaftliche Entwicklung beispielsweise wird seit jeher offensichtlich durch Gesetze des Wettbewerbs geprägt. So liegt es nahe, dass die Entstehung von Monopolen in den westlichen Industrienationen auf ähnliche Mechanismen zurückzuführen ist. Es stellt sich die Frage, inwieweit das Kartellrecht dieser Entwicklung entgegenzuwirken vermag, indem es durch globale und nationale Bestimmungen den Wettbewerb reglementiert. Neben der Garantie einer gewissen Sozialverträglichkeit ist hier das Hauptziel, die Vielschichtigkeit des Marktes zu erhalten: Die Voraussetzungen für eine *Koexistenz* mehrerer Konkurrenten sollen durch die Reglementierung geschaffen werden.

In dieser Arbeit lösen wir uns von der Anschauung des Wettbewerbs zwischen Menschen oder Tieren und verallgemeinern das Konzept auf leblose *Arten*. Letztere mögen chemische Substanzen sein, welche in einem Reagenzglas miteinander reagieren, es kann sich aber auch um feste Teilchen handeln, die der Gravitation ausgesetzt sind und sich in ihrer Bewegung gegenseitig beeinflussen. Vor allem während der letzten Jahre hat der Bereich der granularen Materie in der Physik, aber auch in der Mathematik, an Bedeutung gewonnen. Die Dynamik des Systems wird hier durch die Interaktion von Partikeln verschiedener Größe, Form und Oberflächenbeschaffenheit und unterschiedlicher spezifischer Dichte bestimmt. Diese mischen oder entmischen sich und können unter dem Einfluss äußerer Kräfte wie Schüttelbewegungen oder Vibration Muster ausbilden. In diesem Sinne stehen also auch leblose Teilchen im *Wettbewerb* miteinander. Man könnte sagen, sie *kämpfen* um eine Position in der gegebenen Geometrie. Die Modelle, die wir benutzen, bestehen aus Systemen sogenannter *Konvektions-Diffusions*-Gleichungen. Derartige parabolische partielle Differentialgleichungen wurden bereits auf dem Gebiet der Konvektion von Flüssigkeiten untersucht, ihre Anwendung im Bereich der granularen Medien ist jedoch weitgehend unerforscht. Wir vertiefen uns daher in der vorliegenden Arbeit auf dieses Gebiet und untersuchen, inwieweit die durch die Modelle getroffenen Aussagen mit Computersimulationen oder Experimenten übereinstimmen. Zu diesem Zweck wurde ein Vielteilchenmodell implementiert, welches das Schütteln eines mit granularem Material gefüllten Behälters simuliert. Darüberhinaus hatten wir die Gelegenheit, im Labor von H. Herrmann am Institut für Computeranwendungen I der Universität Stuttgart selbst Schüttelexperimente durchzuführen und so unsere theoretischen Modelle zu perfektionieren. Neben der Untersuchung von granularen Medien betrachten wir im Rahmen dieser Arbeit auch verwandte Modelle, welche ähnliche physikalische und biologische Sachverhalte beschreiben, zum Beispiel Sedimentation oder den

Chemostaten mit Diffusion. Regelmäßig werden wir zu der eingangs gestellten Frage zurückkehren, inwieweit die Beschreibung solcher Vorgänge mit Hilfe von Konvektions-Diffusions-Gleichungen möglich ist.

Kapitel 2 dient vorwiegend der Herleitung eines Konvektions-Diffusions-Modells aus elementaren mikroskopischen Gesetzmäßigkeiten, welche für die Dynamik in Vielteilchensystemen verantwortlich sind. Wir beginnen mit einem *Random-Walk*-Prozess, welcher die Bewegung einzelner Partikel in einem vertikalen Gefäß beschreibt und ergänzen die Gleichung Schritt für Schritt, um so vor allem dem Einfluss unterschiedlicher Korngrößen und unterschiedlicher spezifischer Dichte auf die globale Dynamik Rechnung zu tragen. Das Gefäß wird hierbei der Einfachheit halber auf ein Intervall $[0, l]$ reduziert, wobei $l > 0$ dann die Höhe des Gefäßes darstellt. Auf diese Weise gelangen wir schließlich zu zwei verschiedenen Modellen. Das eine erzeugt Segregation durch Auftrieb großer Teilchen. Das andere bewirkt die Trennung der Medien durch den sogenannten Paranuss-Effekt, d.h. kleine Partikel füllen die Lücken zwischen den größeren Körnern und gelangen so nach unten. Beide Modelle haben die Form einer Konvektions-Diffusions-Gleichung

$$u_t = (d(u)u_x)_x - f(u)_x \tag{1}$$

auf dem Intervall $[0, l]$ mit Neumann-Randbedingung

$$d(u)u_x = f(u) \tag{2}$$

in $x = 0, l$, wobei die Komponenten des Vektors u die relativen Partikeldichten bezeichnen und $d(u)$ ein skalarer Diffusionskoeffizient ist, welcher von den Dichten abhängt. Im folgenden Kapitel 3 werden derartige Systeme parabolischer partieller Differentialgleichungen in der allgemeinen Form (1), (2) untersucht. Wir zeigen, dass Lösungen unter relativ schwachen Voraussetzungen an die Konvektionsfunktion f für alle Zeit existieren, dass die Gesamtmassen im Gefäß erhalten bleiben und dass die Konzentrationen keine unphysikalischen Werte außerhalb des Intervalls $[0, 1]$ annehmen können. Darüberhinaus konvergieren die Lösungen im Falle einer Mischung zweier Teilchenarten stets zu einem stationären Zustand des Systems. Modelle der Form (1), (2) können schließlich auf den Fall der sogenannten *Replikator-Dynamik* angewandt werden, welche aus dem Bereich der Populationsdynamik bekannt sind. Für diesen speziellen Fall zeigen wir gar Eindeutigkeit der Gleichgewichtszustände.

In Kapitel 4 lösen wir uns von den Neumann-Randbedingungen (2) und ermöglichen das Ein- und Austreten von Substanz durch Deckel und Boden des Gefäßes. Das sogenannte Zweipunkt-Randwertproblem schreibt Dirichlet-Randbedingungen der Form

$$u(0) = a, \ u(l) = b$$

mit festen Konzentrationsvektoren a und b vor. Wir verallgemeinern einen Existenzbeweis für stationäre Lösungen von B. Di Bella (siehe [DiBella02]) und

zeigen Eindeutigkeit des Gleichgewichtes im skalaren Fall.

Sedimentation ist ein weiterer Prozess, welcher sich durch Gleichungen der Form
(1), (2) modellieren lässt. Wir adaptieren in Kapitel 5 Modellansätze von G. G.
Stokes, G. J. Kynch, G. K. Batchelor und J. H. Masliyah (siehe zum Beispiel
[Stokes51], [Kynch52], [Batchelor82.1], [Batchelor82.2] und [Masliyah79]) und
vergleichen die Resultate vor allem in Bezug auf die Trennung verschiedener
Korngrößen. In diesem Zusammenhang untersuchen wir auch die Auswirkungen
eines variablen Diffusionskoeffizienten und versuchen so, die Abhängigkeit der
Sedimentationszeit von der Gefäßhöhe zu berücksichtigen.

In Kapitel 6 analysieren wir ein allgemeines Chemostatmodell für zwei intera-
gierende Spezies und eine limitierende Nahrungsquelle. Die Konzentrationen der
Spezies und des Substrates werden dabei als homogen betrachtet. Im Vergleich
zu zahlreichen Arbeiten von G. J. Butler, S. B. Hsu oder S. K. Wolkowicz
(e.g. [Butler85.1], [Hsu94.1], [Wolkowicz92]) werden hier sehr allgemeine, monoto-
ne Nahrungsaufnahmefunktionen und Auswaschraten betrachtet. Für eine große
Klasse von Modellen wird die Konvergenz zu einem Koexistenzpunkt nachgewie-
sen. Die Erkenntnisse aus diesem System gewöhnlicher Differentialgleichungen be-
nutzen wir in Kapitel 7. Dort wird ein Chemostat mit inhomogenen Konzentra-
tionen modelliert, indem die Gleichungen aus dem vorigen Kapitel durch einen
Diffusionsterm ergänzt werden. Das resultierende System parabolischer partieller
Differentialgleichungen

$$s_t = D_0(1-s) - uf(s) + \delta_s s_{xx},$$
$$u_t = u\left[f(s) - D_1\right] + \delta_u u_{xx}$$

erzeugt unter gewissen Umständen laufende Wellen auf der reellen Achse.
Dabei ist s die Konzentration des Substrates und u die der Spezies, welche
sich von s ernährt. Die monotone Funktion f bestimmt die Nahrungsaufnahme
der Lebewesen, während die Konstanten D_0 und D_1 den Zufluss von Substrat
bzw. die Mortalitätsrate der Art beschreiben. δ_s und δ_u sind die jeweiligen
Diffusionskonstanten.

Die analytischen Resultate vor allem aus den Kapiteln 2, 3 und 5 werden in
Kapitel 8 mit Simulationen eines zweidimensionalen Vielpartikelmodells ver-
glichen. Die Grundlage bildet ein Algorithmus, welcher für eine vorgegebene
Zahl kreisförmiger Teilchen unterschiedlichen spezifischen Gewichts und unter-
schiedlicher Größe die Newtonschen Bewegungsgleichungen löst. Diese Teilchen
kollidieren mit benachbarten Partikeln, die Stöße werden dabei als teilelastisch
angenommen. Im Laufe der Zeit verliert das gesamte System durch die Stöße
Energie und die Teilchen sinken zu Boden. In regelmäßigen Abständen erhält
das Material nun einen nach oben gerichteten Impuls. Dieser Prozess simuliert
die Schüttelbewegung des Gefäßes. Die Beobachtungen aus den analytischen

Modellen bestätigen sich in der Teilchensimulation: Wir erreichen eine Trennung der Medien, der Grad der Entmischung wird dabei in erster Linie durch Größe und spezifisches Gewicht der Partikel beeinflusst. Kapitel 9 schließlich dient der Untermauerung der Theorie durch Schüttelexperimente. Neben dem bekannten Paranuss-Effekt beobachten wir vor allem auch die Ausbildung von Konvektionszellen in vibrierendem granularem Material. Vergleichbar mit dem aus der Konvektion von Flüssigkeiten bekannten *Rayleigh-Bénard*-Effekt bilden sich hier Bereiche aus, in denen Teilchen bestimmter Größe und Masse an die Oberfläche treten und an anderer Stelle wieder versinken.

Chapter 1

Introduction

The idea that "two similar species are not likely to live together" was already held by naturalists in the nineteenth and early twentieth centuries. The earliest known reference is to a remark of A. Hansmann. In his paper published in 1857 (see [Hansmann57]), he describes the natural habitats of two closely allied bird species, the willow warbler (*Phylloscopus trochilus*) and Bonelli's warbler (*P. bonelli*). He comes to the conclusion that their similarity forces these two species to occupy different ecological niches. However, the first known use of the word *niche* in an ecological context did not occur until the year 1910 (see [Johnson10]). The theoretical contribution that really started investigation of the subject of coexistence was that of V. Volterra (see [Volterra26], [Volterra28]). He constructed a model of two species competing for a single resource and showed that one of the species almost always must go extinct. Together with A. J. Lotka (see [Lotka32]), he gave the name to the well-known Lotka-Volterra models, which describe competition between two species. These equations in their general form admit both *coexistence* and *competitive exclusion*, depending on the parameters. Volterra's work stimulated the incisive theoretical and experimental studies of G. F. Gause, who in 1935 (see [Gause34]) formulated an ecological contention, stating that two species with similar ecology cannot live together in the same place. In other words, if two non-interbreeding populations occupy the same ecological niche and if they are sympatric, in the sense that they occupy the same territory, then even a slight difference in their reproduction potentials will eventually lead to a complete extinction of the disadvantaged species. In order for both of them to coexist, at least one must come to occupy a different ecological niche. Thus, species standing in competition are forced to adapt to the changing environmental influences. The principle of the *survival of the fittest*, as crude and straightforward as it may seem, is crucial for the advancement of any kind and stands at the origin of evolution. Gause's definition of the term *competition* and its consequences in an ecological context is consistent with the modern description as "the act or action of seeking to gain at the same time and usually under or as if under fair or equitable rules and circumstances" and a "more or less active
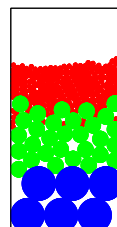
demand by two or more organisms or kinds of organisms at the same time for some environmental resource in excess of the supply available, typically resulting in ultimate elimination of the less effective organisms from the particular ecologic niche" (see [Merriam-Webster93]). R. McGehee and R. A. Armstrong (see [McGehee77]) reformulated the problem of coexistence and competitive exclusion and analyzed various examples. They placed the discussion on a solid mathematical basis and gave proofs of the known results. A chronological summary of the scientific discussion on competition and coexistence is given in [Hutchinson78].

The principles of competition and of competitive exclusion unquestionably play an indispensable role in many fields of scientific interest, some rather alien to ecology. Often, microscopic biological processes follow the same patterns. In genetics, for example, the large number of different alleles being found at the same gene locus, competing for *survival* within a certain population of organisms, enables adequate adaptation of the species to a changing environment and is the driving factor of evolution itself. But also economic thinking has long been dominated by the concept of competition, and the often desired persistence of a multifaceted community of competitors on the market frequently depends crucially on global as well as national regulations and relatively strong legislative restrictions. The end of the formerly eulogized free market economy giving free rein to unrestricted competition and ruled solely by the interplay of offer, demand and price, is most often a monopoly, which many countries in the modern economical world have set out to prohibit. As a result, the society as such, rather than the individual competitors, are forced to band together in order to ensure ongoing free competition, which, not to forget, is seen as the major driving force for an accelerated progress and new inventions.

In the present thesis, we abandon the idea of human beings or animals being in competitive relationship with each other and generalize the concept of competition to lifeless *species*. The latter could be chemical substances reacting in a test tube in a fluid medium or solid particles, which are subject to gravity and which influence and constrain each other in their movement. Especially during the past years, the field of research of granular material has gained in esteem among both physicists and mathematicians. Here, the dynamics of the system is ruled by the interplay of grains of different size, weight, shape or surface structure, which mix, segregate or form patterns and thereby try to *defy* gravity and reach a position high in the reaction vessel. Accordingly, the particles in a metaphorical sense *compete* for a position on the vertical axis. The models we use are for the most part systems of partial differential equations said of *convection-diffusion* type. Such parabolic equations have been employed to describe diffusive effects in fluids, but their application in the field of granular matter is recent. We set out to investigate, to which extent these models are capable of predicting and reproducing the effects observed in experiments and simulations. To this end, we implemented a multi-particle model in order to compare its results to the
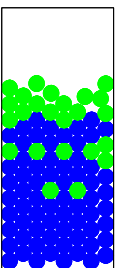
theory and to shaking experiments, which we conducted in the laboratory of H. Herrmann at the Institute of Computational Physics I of the University of Stuttgart. At the same time, we intend to compare our convection-diffusion equations to other models describing competition, such as sedimentation models or the diffusive chemostat. Consistently throughout this thesis, we will return to the questions of competitive exclusion and coexistence of species and, more generally, to the global effects of the microscopic interaction.

In chapter 2, we start by setting up a very simple discrete model describing the compaction of a single particle species in a vertical container due to gravitation. With a certain scaling of space and time, we can take the corresponding difference equation to a continuous-time-continuous-space limit, the resulting partial differential equation is shown to satisfy the basic properties required by the physical setup in mind. In the following, the simple discrete model is amended step by step in order to take into account mixtures of particles of varying size, shape and surface coarseness. Furthermore, the species are allowed to interact, thus giving rise to segregation phenomena. The most famous example is the so-called *Brazil nut* or *müsli* effect, which owes its name to the observation, that nuts and other large particles found in cereals always form the topmost layer. The heuristic interpretation agreed upon to date is the following: During the shaking process (for example when the cereals are bagged), small grains fill up the gaps left in between the larger ones, and the latter move up. The second half of the chapter is concerned with discrete systems incorporating undirected random motion in addition to directed convection, and their continuous counterparts, the so-called convection-diffusion models. The latter are more adequate to describe natural processes, which, due to the large number of interacting individuals, are practically always afflicted with a random component. Simulations at the end of the chapter illustrate the sedimentation and segregation process. The examples of convection-diffusion partial differential equations derived and analyzed in chapter 2 are generalized in chapter 3. Under relatively weak restrictions on the convection term, we can show the existence of global solutions as well as the convection to stationary solutions of the equation for a general number n of species. This general parabolic equation plays a central role in the present thesis. Even though it is derived with the specific idea of mixing granular material in mind, the model itself is very unspecific and leaves room for applications in the biological or chemical field (see for example chapters 5 and 7). While the models discussed in chapters 2 and 3 both describe a mixture of granular material in a container with closed lid and solid bottom, the system in chapter 4 models compaction and segregation in an *open* vessel, the ends of which are connected to reservoirs with prescribed saturation levels. Here, particles can enter and leave the container, the concentrations of the species on the boundary are prescribed by those in the surrounding medium. The aim of chapter 5 is to interpret and to generalize the phenomenon of sedimentation in the setting of convection-diffusion equations. Previous work by G. J. Kynch and J. H.
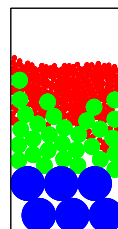
Masliyah ([Kynch52], [Masliyah79]) can be connected to the present problem. We also present a new approach to modeling sedimentation via variable diffusion coefficients. In chapter 6, we discuss a different type of competition models, the so-called *chemostat* system. Unlike previous work by G. J. Butler, S. B. Hsu, P. Waltman, G. S. K. Wolkowicz and others (see for example [Butler83], [Butler85.1], [Butler85.2], [Butler86], [Butler87], [Wolkowicz92], [Wolkowicz95], [Wolkowicz96], [Wolkowicz97], [Wolkowicz98.1] and [Wolkowicz98.2]), we treat a general equation admitting arbitrary monotone nutrient uptake functions and washout rates. We analyze existence and stability of stationary points and show convergence to the coexistence state for a large class of uptake functions. Chapter 6 represents the spadework for the following chapter 7, which is dedicated to the study of the diffusive chemostat model. At the origin is again the ODE from chapter 6, which is now furnished with a diffusive term. The resulting chemostatic interaction on the real axis exhibits traveling waves. The theory is again fortified by computer simulations. In chapter 8, we conduct multi-particle simulations. On the basis of simple, partly elastic particle collisions between spherical grains, we observe sedimentation and segregation effects and illustrate the dependence of the latter on particle sizes and specific weights. Chapter 9 collects the results of some exemplary shaking experiments, which we conducted in order to back the theoretical results. While the segregation properties of different mixtures of seeds and small balls are compared, we also try to explain the appearance of convection cells in vibrated material. The latter effect is similar to the so-called *Rayleigh-Bénard* phenomenon observed in heated fluid. Material rises in the center of such a convection cell and sinks again at its edge.

Resuming our main results, we can say that systems of convection-diffusion partial differential equations to a large extend fulfill the demands made on models describing competition in granular material. Due to their general form, they leave room for applications in various related fields as well. Some of the phenomena, which are familiar to the reader from everyday experience, such as basic properties of sedimenting material, the Brazil nut effect or simple pattern formation and compaction effects in shaken or vibrated granular mixtures can be predicted by our models and are reproduced by computer simulations. But many other effects remain to date unexplained. For future work on the field of granular matter modeling, it would be desirable to refine the influence of particle shape and surface condition on the global interaction between the *species* composing a granular mixture. We would like to get deeper insight into the mechanisms causing complex effects, such as the convection rolls (see chapter 9) or horizontal asymmetries. Such phenomena have so far only been explained heuristically. On the mathematical side, we still owe a detailed characterization of convection-diffusion systems exhibiting a unique equilibrium state. While chapter 3 reveals examples of such systems, a general classification could not be performed. One of our main goals will be to determine conditions which ensure the uniqueness of the stationary constellation for arbitrary numbers of granular
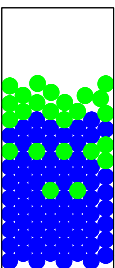
components in the mixture.

Thursday, May 8, 2003
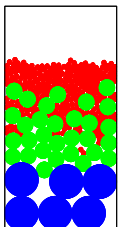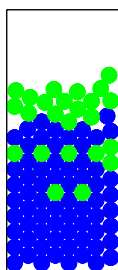
Chapter 2

Random walk models for particle segregation and compaction

Summary. The present chapter is devoted to the elementary study of random walk processes describing the migration of particles in a closed container. This approach produces simple models in the form of conservation laws, i.e. hyperbolic partial differential equations, which are discussed in the first half of the chapter. The following sections deal with more elaborate models incorporating a diffusive component. They can be interpreted as viscosity versions of the hyperbolic equations. The mathematical analysis of the resulting diffusion-convection equations will be the topic of later chapters.

2.1 Introduction

The main goal of this work is to study mathematical models for segregation, compaction and sedimentation processes in granular matter under the influence of gravity and other forces, such as stochastic reshuffling. In the simplest case of a single species of particles, segregation of material is not observed and the movement of the individual grains results in mere sedimentation and compaction. In general, the mixture is composed of several species. Due to different physical qualities, such as size, weight, overall shape or microscopic surface structure, the grains are then apt to cant or to pass each other more or less smoothly. In a typical experiment, the particles are grains of sand, pebbles or different kinds of seeds. They are encased in a container, usually a high glass cylinder, which is vibrated or rotated, or they are poured from an elevated source onto a heap. Typically, the patterns emanating from segregation processes are horizontal stripes, which can be distinguished by color.

If the particles have identical size and shape but differ in weight, we expect
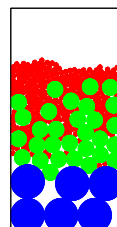
buoyancy effects to dominate the segregation process and drive the lighter grains to the top. In case the particles all have the same specific weight and similar shapes, while their sizes vary considerably, the large grains will move up. This quite unexpected phenomenon is widely known as the *Brazil nut* or *müsli* effect (see [Barker90], [Barker93] or [Rosato87]). If particles differ in more than one aspect, for example in specific weight and size, the type of occurring patterns cannot be predicted as easily (see for example [Hong01]).

Throughout this thesis, we look at the physical processes involved in the segregation dynamics as if the particles were *competing* for certain positions on a vertical scale. This view is supported by the fact that very similar mathematical models arise on the one hand in sedimentation theory, e.g. the Masliyah and Kynch models (see [Bürger00.1], [Bürger00.2], [Kynch52] or [Masliyah79]), and, on the other hand, in the theory of molecular evolution, e.g. the so-called replicator equations (see [Eigen79], [Hofbauer98]). These analogies between models for granular mixtures and models for the evolution of molecular or animal and plant species suggests to include into the present modeling approach other aspects such as competition and fitness. Of course, we merely exploit analogies; we do not claim that fitness is actually a character of sand grains or seeds. In a much wider context, our models could be adapted in order to describe living beings interacting actively and competing for some vital source, such as food or habitat.

Many authors have studied theoretical models to describe particle interaction in sedimenting or segregating granular material. In most cases, complex procedures describing the interaction of individual particles were implemented, and the resulting computer simulations were compared to experimental data. In contrast to most of the work in this field over the past years, we set out to derive a relatively simple mathematical model from elementary considerations concerning the physical properties of the particle species. Starting with the simplest case of a granular material composed of a single type of grains, we then extend the model in order to incorporate various grain types and more complex laws of interaction. Our considerations are guided by general ideas and approaches developed for example in [Duran93], [Jullien92], [Luding96.2], [McNamara99], [Rosato87] or [Vladimirova99]. Last but not least, some helpful ideas were taken from [deLarrard99].

In sections 2.2 through 2.8, we gradually develop more and more realistic models still without the diffusive component mentioned above. Due to the quality of the resulting systems of equations, we have to deal with regularity aspects and the formation of shocks. Via the viscosity solution approach discussed in section 2.5, we then bridge to diffusion-convection equations. Throughout the remainder of the chapter, we present various approaches and compare them on the basis of computer simulations. Our main interest will always be the question whether the system describes the physical realities reasonably well and exhibits the phenomena
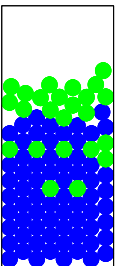
of sedimentation and segregation observed in experiments. In section 2.15, we discuss some general results concerning the stationary solutions of the segregation models. In this context, we fall back on some properties of so-called *competitive* systems of ordinary differential equations.

2.2 Discrete models without random movement

As a first step in the development of our segregation model, we derive a simple discrete model incorporating gravitation but neglecting random movement of particles. We think of the vertical container as of a set of stacked compartments numbered from $i = 0$ at the bottom to $i = N + 1$ at the uppermost level. We consider one type of grains, hence the capacity of the compartment is a fixed number C. Let us denote by a the transition rate from one compartment to the one directly below. To begin with, we will restrict to simple linear transition rates. Since our idea is to model particle movement in a closed container, we have to impose boundary conditions satisfying the physical requirements of a solid lid and bottom. For example, we could say that the lowest layer $i = 0$ is already filled with grains such that no more particles can be added. For the uppermost level $i = N + 1$, we impose an empty cell. Since particle transition from one cell to the other can only take place downward, this means that the only compartments of interest are the intermediate ones numbered $i = 1$ to N.

Let $u_i = u_i(t)$ be the number of grains in the ith cell at time t. If there is empty space in the cell below, particles can fall down and gradually fill up the lower cell. Suppose that the particle flow is proportional to both the number u_i and the remaining capacity in cell number $i-1$. Hence the change in the ith compartment during a small time interval Δt is

$$u_i(t + \Delta t) - u_i(t) = a[(C - u_i(t))u_{i+1}(t) - (C - u_{i-1}(t))u_i(t)] \Delta t + o(\Delta t). \quad (2.1)$$

Letting $\Delta t \to 0$, we get the system of ordinary differential equations

$$\dot{u}_i = a[(C - u_i)u_{i+1} - (C - u_{i-1})u_i], \quad (2.2)$$

$i = 1, \ldots, N$, with boundary condition

$$\begin{aligned} u_0 &= C, \\ u_{N+1} &= 0. \end{aligned} \quad (2.3)$$

This set of differential equations is defined in $\mathbb{R}^N$. We are only interested in solutions which correspond to physically realistic situations. With this restriction in mind, we have two different sets which we call $\mathcal{M}$ and $\hat{\mathcal{M}}$. The set $\mathcal{M}$ is the set of all possible particle distributions,

$$\mathcal{M} = \{u = (u_i) : 0 \leq u_i \leq C \text{ for } i = 1, \ldots, N\},$$
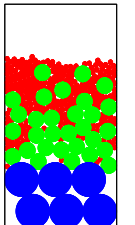
while $\hat{\mathcal{M}}$ is the set of all monotonous particle distributions with the property that the particle density decreases from bottom to top,

$$\hat{\mathcal{M}} = \{u \in \mathcal{M} : u_i \geq u_{i+1} \text{ for } i = 1, \ldots, N-1\}.$$

The following proposition summarizes some basic properties of system (2.2) (2.3).

Proposition 2.2.1 (Positivity, total mass and monotonicity of the discrete system.)
(i) Solutions starting from initial data in $\mathcal{M}$ exist for all positive times and stay in $\mathcal{M}$.
(ii) Solutions starting in $\hat{\mathcal{M}}$ stay in $\hat{\mathcal{M}}$ for all positive times.
(iii) Solutions starting in $\mathcal{M}$ preserve total mass, i.e.

$$\frac{d}{dt} \sum_{i=1}^{N} u_i = 0.$$

(iv) The stationary solutions of system (2.2), (2.3) are contained in $\hat{\mathcal{M}}$. They have the form

$$\begin{aligned}
u_i &= C, \quad i = 1, \ldots, i_0 - 1, \\
0 &\leq u_{i_0} \leq C, \\
u_i &= 0, \quad i = i_0 + 1, \ldots, N
\end{aligned}$$

for some $i_0 \in \{1, \ldots, N\}$. Furthermore, these equilibria are completely characterized by their total mass $C(i_0 - 1) + u_{i_0}$, i.e. i_0 is determined by the equation

$$C(i_0 - 1) + u_{i_0} = \sum_{i=1}^{N} u_i^0,$$

where $u_i^0 = u_i(t = 0)$ is the number of grains in the cell i at time $t = 0$.
(v) The potential energy

$$E = \sum_{i=1}^{N} i u_i$$

is non-increasing along trajectories.
(vi) Every solution starting in $\mathcal{M}$ converges to the stationary state with the total mass given by the initial distribution.

Proof. (i) Invariance of $\mathcal{M}$:
Positivity: Suppose u_i vanishes for some i. Then, obviously, $\dot{u}_i = C u_{i+1} \geq 0$. This is sufficient to ensure that u_i cannot drop below zero ([Amann83], theorem 16.9, p. 240).
Upper bound: If $u_i = C$ then the argument works in the same way. We have $\dot{u}_i = -(C - u_{i-1})u_i \leq 0$.
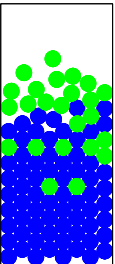
Hence, if the initial data satisfy $0 \leq u_i \leq C$, this property is preserved for all positive times.

(ii) Straightforward calculation yields

$$\frac{1}{a}\dot{v}_i = -(C - v_i)v_i + (C - u_{i+1})v_{i+1} + u_i v_{i-1},$$

where $v_i = u_i - u_{i+1}$. Suppose v_i reaches zero from above. Then $\dot{v}_i/a = u_i v_{i-1} + (C - u_{i+1})v_{i+1} \geq 0$, which, by the same argument, guarantees non-negativity of v_i for all times.

As in (i), two neighboring particle numbers u_i and u_{i+1} can not become equal if they are not equal from the beginning.

(iii) Straightforward calculation yields

$$\frac{d}{dt}\sum_{i=1}^{N} u_i = \sum_{i=1}^{N} \dot{u}_i = 0,$$

i.e. total mass is preserved.

(iv) Let $u = (u_i)$ be an equilibrium state in $\mathcal{M}$. From $u_0 = C$ and $(C - u_1)u_2 = 0$ it follows that either $u_1 = C$ or $u_1 \leq C$, $u_2 = 0$. Suppose it has been shown that $u_i \leq C$, $u_{i+1} = 0$. By induction it follows that also $u_{i+2} = 0$.

(v) Check that

$$\frac{d}{dt}\sum_{i=1}^{N} iu_i = \sum_{i=1}^{N} ia[(C - u_i)u_{i+1} - (C - u_{i-1})u_i]$$

$$= -a\sum_{i=1}^{N-1}(C - u_i)u_{i+1}$$

$$\leq 0.$$

Actually, as we will see in (vi), the potential energy functional E only vanishes on stationary solutions.

(vi) By (v), E is a Lyapunov functional. On the ω-limit set of any trajectory in $\mathcal{M}$, we have $(C - u_i)u_{i+1}$ for $i = 1, \ldots, N - 1$. But by (iv), these are exactly the equilibrium states of the system.

This proves proposition 2.2.1. $\square$.

In a physical context, proposition 2.2.1 states that particles gradually fall down in the container and fill it up to a certain level, depending on the total number of particles and the size of the vessel. The latter has a solid bottom, and no grains can enter through the top. Once the grains are densely packed from the bottom upward and no particles are left in the top part, the uppermost non-void compartment might be only partly filled with grains. In experiments, due to the restriction to downward particle motion, the density of the packing will decrease with growing height in the vessel. (For an illustration see figure 2.1.) In reality, a
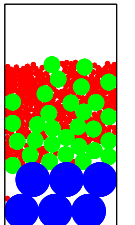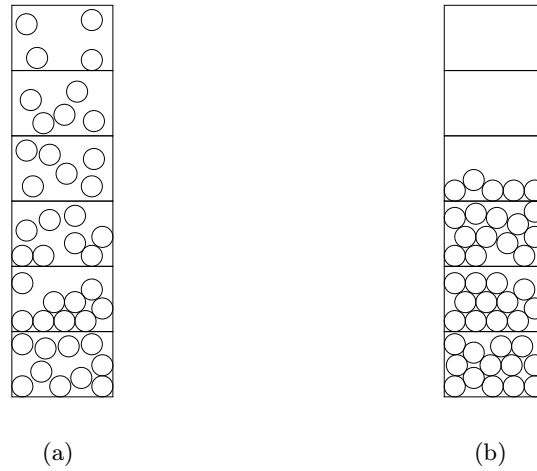
Figure 2.1: The simplest discrete model. A container is divided in vertical direction in a certain number of compartments, each containing particles of the same size and weight (a). Under the influence of gravity, particles start to fall down from one cell to the one below and gradually fill up the lower cells (b).

physical system will never reach the optimal (or *virtual*) packing density, which is equal to 0.74 for mono-size spheres in three dimensions (see [Aste00]). Depending on the compaction process or the type of external forces applied in order to shake the material, for mono-size spheres values between 0.6 and 0.7 are feasible.

2.3   A first continuum model

In a next step, we derive a continuum model from (2.2), (2.3). We divide the interval $\Omega = [0, l]$ representing the vessel into thin layers and describe solutions in the limit as continuous functions on Ω. Now the quantity C is the capacity per length. Furthermore, normalize the rate parameter to $a = 1$. As in section 2.2, we first write down a difference equation governing the changes in particle numbers in both discrete time and space steps. Instead of numbering the cells from $i = 0$ to $i = N$, let us introduce a space variable x and denote by Δx the height of one layer in the vessel. Let $u = u(t, x)$ be the number of grains per length, hence $u(t, x)\Delta x$ is the number of grains in a cell which occupy the section from x to $x + \Delta x$ in the container. Thus, we get

$$[u(t + \Delta t, x) - u(t, x)]\Delta x = \{[C - u(t, x)]u(t, x + \Delta x) - \\ -[C - u(t, x - \Delta x)]u(t, x)\} \Delta t.$$
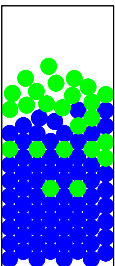
After rearranging and division by $\Delta x \Delta t$, we get

$$\frac{u(t+\Delta t, x) - u(t, x)}{\Delta t} = C\frac{u(t, x+\Delta x) - u(t, x)}{\Delta x} - \frac{u(t, x+\Delta x) - u(t, x-\Delta x)}{\Delta x}. \tag{2.4}$$

Taking both sides of (2.4) to the limit as $\Delta t, \ \Delta x \longrightarrow 0$, we end up with the conservation law

$$u_t = Cu_x - (u^2)_x \tag{2.5}$$

with boundary condition

$$\begin{aligned} u(t, 0) &= C, \\ u(t, l) &= 0 \end{aligned} \tag{2.6}$$

for some positive l, the height of the container. Note that (2.5) is very similar to the well-known Burgers' equation. An example is given in [Renardy93].

As before, we are only interested in physically feasible grain distributions. Therefore, define

$$\mathcal{M}_c = \{u \in \mathcal{C}^1[0, l] : 0 \leq u(x) \leq C \text{ for } 0 \leq x \leq l\},$$
$$\hat{\mathcal{M}}_c = \{u \in \mathcal{M}_c : u'(x) \leq 0 \text{ for } 0 \leq x \leq l\}.$$

$\mathcal{M}_c$ is the set of particle distributions with concentrations varying between 0 and C, while the subset $\hat{\mathcal{M}}_c$ contains only monotone functions. With these definitions, the continuous analogon of proposition 2.2.1 holds, at least formally: The solutions have the desired physical properties, as long as they exist. But they may cease to exist due to the evolution of shocks.

Proposition 2.3.1 (Positivity, total mass and monotonicity of the continuous system.) *(i) Solutions starting in $\mathcal{M}_c$ exist up to some time $t_s > 0$ and stay in $\mathcal{M}_c$ for $0 \leq t < t_s$.*
(ii) Solutions starting in $\hat{\mathcal{M}}_c$ stay in $\hat{\mathcal{M}}_c$ for $0 \leq t < t_s$.
(iii) Solutions starting in $\mathcal{M}_c$ preserve total mass,

$$\frac{d}{dt}\int_0^l u dx = 0.$$

(iv) The formal equilibrium states of (2.5), (2.6) are not contained in $\mathcal{M}_c$. They are characterized by their total mass and have the form

$$\bar{u}(x) = \begin{cases} C & x < l_0 \\ 0 & x > l_0 \end{cases} \tag{2.7}$$
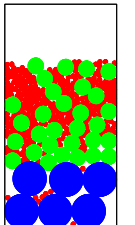
for some $l_0 \in [0, l]$.

(v) The potential energy

$$E_c = \int_0^l xu(x)dx$$

is non-increasing along trajectories.

(vi) Every solution starting in $\mathcal{M}_c$ converges in a weak sense to the equilibrium determined by the total mass.

Proof.

(i) We anticipate the result of proposition 2.4.1 of section 2.4. Hence we know, that there is a strictly positive time t_s until which no shocks occur. For all $t \in [0, t_s)$, the solution inherits the upper and lower bounds as well as the regularity of the initial function $u_0 = u(0, \cdot)$.

(ii) Again by proposition 2.4.1, solutions are monotone for all $0 \le t < t_s$ if the initial function is in $\hat{\mathcal{M}}_c$.

(iii) Verify that

$$\frac{d}{dt} \int_0^l u(t,x)dx = \int_0^l u_t dx$$
$$= [u(C - u)]_0^l$$
$$= 0$$

due to the boundary condition, i.e. total mass is preserved.

(iv) Stationary solutions of (2.5), (2.6) are characterized by $Cu_x = 2uu_x$, i.e. $u(C - u) = const = 0$ due to (2.6). Therefore, $u^2 = Cu$, i.e. $u = C$ or $u = 0$ everywhere. In view of (ii), the only feasible equilibria are the step functions $\bar{u}(x) = C$ for $x < l_0$ and $\bar{u} = 0$ above l_0. Theoretically, any arbitrary step function taking values $\bar{u} = 0$ and $\bar{u} = C$ also represents a stationary solution to system (2.5), (2.6). In order to find the physically correct equilibrium, we interpret the non-continuous solutions as *viscosity solutions*. We postpone the question of choosing *adequate* discontinuous solutions to section 2.5.

(v) Check that

$$\dot{E}_c = \int_0^l xu_t dx$$
$$= [x(u(C - u))]_0^l - \int_0^l u(C - u)dx$$
$$\le 0$$

due to the boundary condition (2.6) and (i), i.e. E_c is non-increasing along solutions.

(vi) Once we agree to choose the discontinuous functions in (iv) as the appropriate stationary states of our system, we have $E_c(\bar{u}) = Cl_0^2/2$ and $\dot{E}_c(\bar{u}) = 0$, i.e.
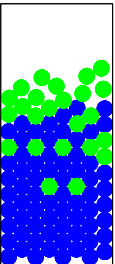
$E_c - Cl_0^2/2$ is a Lyapunov functional. Note that the value l_0 depends uniquely on the initial distribution $u_0(x) = u(0, x)$. In fact,

$$l_0 = \frac{1}{C} \int_0^l u_0(x)dx.$$

This proves proposition 2.3.1. $\square$.

2.4 The propagation of shocks

Equation (2.5) is a conservation law of the form

$$u_t + f(u)_x = 0, \tag{2.8}$$

where $f(u) = u(u - C)$, i.e. $f'(u) = 2u - C$. The characteristic curves of (2.8) satisfy

$$\hat{x}'(t) = f'(u(\hat{x}(t), t)).$$

Since

$$\begin{aligned}
\frac{d}{dt}u(\hat{x}(t), t) &= u_x\hat{x}' + u_t \\
&= u_x f'(u) + u_t \\
&= 0
\end{aligned}$$

for characteristics, we get $u(\hat{x}(t), t) = b = const$, hence $\hat{x}'(t) = f'(b)$ and thus

$$\hat{x}(t) = tf'(b) + \hat{x}(0). \tag{2.9}$$

Proposition 2.4.1 (Interval of existence and regularity.) *If the initial function $u_0 = u(0, \cdot)$ is at least once continuously differentiable, then solutions of system (2.5), (2.6) exist up to some strictly positive time $t_s > 0$. This time horizon depends only on*

$$\max_{x \in [0,l]} f'(u_0(x))$$

and becomes smaller with growing maximal derivative. Furthermore, the solution respects the bounds of u_0 and inherits its regularity, i.e. if $u_0 \in \mathcal{C}^1[0,l]$, then $u(t, \cdot) \in \mathcal{C}^1[0,l]$ for all $t \in [0, t_s)$. Finally, if u_0 is monotone, then so is $u(t, \cdot)$ for $0 \le t < t_s$.

Proof. Let us write the characteristic equations corresponding to (2.5) as

$$\begin{aligned}
\dot{t} &= 1, \\
\dot{x} &= 2u - C, \\
\dot{u} &= 0.
\end{aligned} \tag{2.10}$$
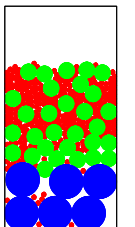
System (2.10) has solutions

$$t = s,$$
$$x = x_0 + (2u_0 - C)s,$$
$$u = u_0,$$

i.e. the characteristic lines are given by

$$x(t) = x_0 + (2u_0 - C)t, \tag{2.11}$$

where u_0 here denotes the value of the function $u_0(\cdot)$ at $x = x_0$. Denote by u_1, u_2 two values of the function $u_0(\cdot)$ at $x_1 < x_2$, respectively. Equation (2.11) yields

$$0 = x_2 - x_1 + 2(u_2 - u_1)t.$$

If $u_2 > u_1$, then these two characteristics do not intersect for $t \geq 0$. In case $u_2 < u_1$, they intersect at $t = (x_2 - x_1)/(2(u_1 - u_2)) > 0$. If T is a lower bound for the intersection time, then

$$\frac{u_1 - u_2}{x_2 - x_1} \leq \frac{1}{2T}. \tag{2.12}$$

Using the Mean Value Theorem of calculus for continuously differentiable initial functions $u_0(\cdot)$, we get the condition $-u_0' \leq 1/(2T)$. In other words, if the derivative u_0' is bounded, then there is a minimal intersection time t_s satisfying (2.12) for all $x_2 > x_1 \in [0, l]$.

With the behavior of the characteristics understood, it is clear that the latter only transport information (i.e. values of the solution of (2.5), (2.6)) from one point of the interval $[0, l]$ to another. In other words, the solution at some time $0 \leq t < t_s$ results as a mere diffeomorphic transformation of the domain $[0, l]$. As a consequence, the image of the function u never changes, as long as t stays below t_s, and hence the bounds as well as the monotonicity of the initial function are conserved. In order to see that the regularity is conserved as well, we choose $t \in [0, t_s)$, $x \in [0, l]$ and determine the value of u at the point (t, x). This value determined by the value of the initial function $u_0(\cdot)$ at some point x_0. In order to see that this correspondence is bijective, we write (2.11) as a continuously differentiable function of the unknown x_0,

$$F(x_0) := x_0 - x + (2u_0(x_0) - C)t = 0.$$

F can be reversed if its derivative is non-zero. But

$$F'(x_0) = 1 + 2tu_0'(x_0),$$

which is strictly positive whenever

$$u_0' > -\frac{1}{2t}. \tag{2.13}$$
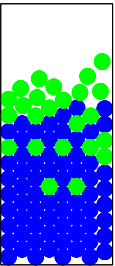
Note that (2.13) is exactly the non-intersection condition for the characteristics we derived previously. Hence, for $0 \leq t < t_s$, the function F is invertible and its inverse is again continuously differentiable. This proves proposition 2.4.1. $\square$.

As an example, let us choose the initial function to be $u_0(x) = C - Cx/l$ (see figure 2.2(a)). We see that at time $t = l/(2C)$, a shock develops at $x = l/2$.
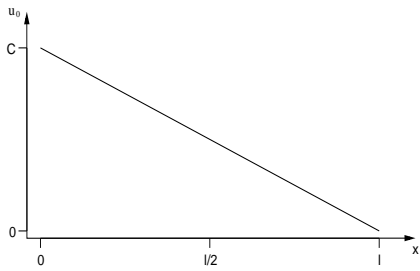
(a) Example of a linear initial condition.
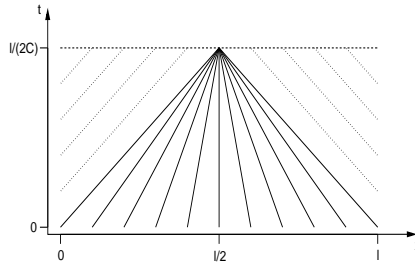
(b) The characteristics impinge on the shock.

Figure 2.2: Linear initial conditions and characteristics for the conservation law (2.5) with boundary condition (2.6).

Below this shock, u is equal to the cell capacity C. Above, $u = 0$. This is exactly the stationary solution we expect.

If the initial condition u_0 has not this particular form, the shock can form at an earlier time. For example, choose

$$u_0(x) = \begin{cases} C\left(1 + \cos\left(\frac{3}{2}\pi x\right)\right)/2 & 0 \leq x < 2C/3 \\ \\ 0 & 2C/3 \leq x \leq l \end{cases} \tag{2.14}$$

(figure 2.3(a)). This time, the shock occurs at an earlier time $t_s < l/(2C)$. The corresponding stationary solution is again given by (2.7).

In order to interpret functions with discontinuities like (2.7) as solutions of a conservation law of the form (2.5), (2.6), we consider *weak solutions*.

Definition 2.4.2 (Weak solutions.) *A weak solution of an equation of the form (2.8) with boundary condition $u(0, x) = u_0(x)$ is a function $u : I\!R^{2+} \longrightarrow I\!R^n$, such*

(a) A non-linear, monotone initial function.

(b) The shock develops at an earlier time $0 < t_s < l/(2C)$.
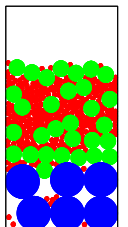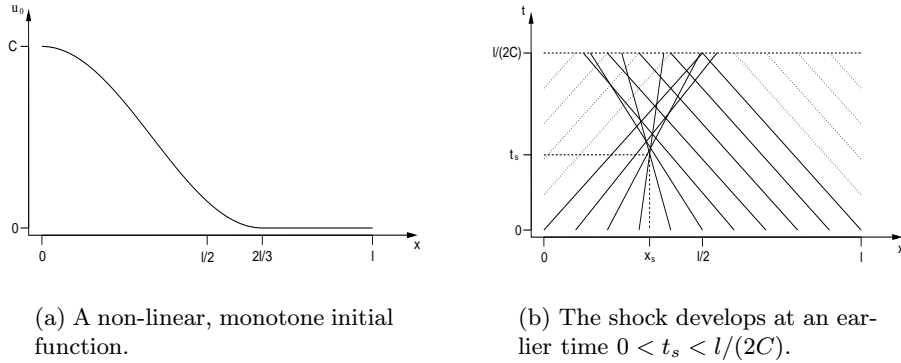
Figure 2.3: Example of a non-linear initial condition.

that

$$\int_0^\infty \int_{-\infty}^\infty \left[u(t,x)\Phi_t(t,x) + f(u(t,x))\Phi_x(t,x) \right] dxdt +$$

$$+ \int_{-\infty}^\infty u_0(x)\Phi(0,x)dx = 0$$

for every function $\Phi \in \mathcal{C}_0^1(I\!\!R^{2+})$, where $I\!\!R^{2+} = \{(t,x) : t \geq 0, x \in I\!\!R\}$ and $\mathcal{C}_0^1$ denotes the set of $\mathcal{C}^1$ functions with bounded support.

As the following proposition shows, this definition extends the concept of a *solution* to step functions of the form (2.7).

Proposition 2.4.3 (Step function as weak solution.) *The step function (2.7) is a weak solution of the conservation law (2.5) with boundary conditions (2.6).*

Proof. Let $\Phi \in \mathcal{C}_0^1(I\!\!R^{2+})$ with supp $\Phi \subset S_r$, where S_r is a ball in $I\!\!R^2$ with radius $r > \max\{l, C\}$. We have

$$\int_0^\infty \int_{-\infty}^\infty \left[u\Phi_t + f(u)\Phi_x \right] dxdt + \int_{-\infty}^\infty u_0\Phi_0 dx =$$

$$= \iint_S \left[u\Phi_t + f(u)\Phi_x \right] dxdt + \int_{-\infty}^\infty u_0\Phi_0 dx$$

$$= \iint_S \left[(u\Phi)_t + (f(u)\Phi)_x \right] dxdt + \int_{-\infty}^\infty u_0\Phi_0 dx,$$

since in $[0, l_0) \cup (l_0, l]$, u is a classical solution and thus

$$(u\Phi)_t + (f(u)\Phi)_x = (u_t + f(u)_x)\Phi + u\Phi_t + f(u)\Phi_x$$

$$= u\Phi_t + f(u)\Phi_x.$$
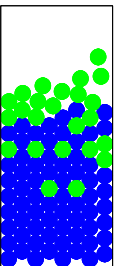
Using Green's Theorem and the fact that supp $\Phi \subset S_r$, we finally get

$$\int_0^\infty \int_{-\infty}^\infty \left[u\Phi_t + f(u)\Phi_x\right] dx dt + \int_{-\infty}^\infty u_0 \Phi_0 dx =$$
$$= \iint_{\partial S} -u\Phi dx + f(u)\Phi dt + \int_{-\infty}^\infty u_0 \Phi_0 dx$$
$$= -\int_0^l u_0 \Phi_0 dx + \int_0^l u_0 \Phi_0 dx$$
$$= 0,$$

i.e. u_0 is a weak solution. $\square$.

We can now follow solutions of (2.5), (2.6) beyond a single shock. If x_s is the locus of the shock developing at time $t = t_s$ and if we denote by u^r and u^l the value of u on the right and left side of the shock, respectively, and if s is the characteristic speed, i.e. the velocity at which the shock moves, then the Rankine-Hugoniot condition (see for example [Renardy93]) yields

$$s(u^r - u^l) = f(u^r) - f(u^l)$$
$$-Cs = 0,$$

i.e. the shock stays at x_s. With the Rankine-Hugoniot condition verified, we can apply the Lax shock condition (see again [Renardy93]), which in the case of a single shock states

$$f'(u^l) > s > f'(u^r)$$
$$2u^l - C > 0 > 2u^r - C$$
$$C > 0 > -C,$$

i.e. the characteristic speeds left and right of the shock are C and $-C$ respectively. Consequently, the characteristics impinge on the shock which stays at $x = x_s$ for all $t > t_s$ (see figure 2.4). This phenomenon is described as a *loss of information*. Note that, once a solution develops a shock, the stationary (weak) solution in general is not reached yet. In order to follow the solution beyond the shock, one has therefore to extend the concept of the solution yet again and allow functions with discontinuities. At this point, we will not go into any details concerning weak solutions in general. Instead, we refer to [Renardy93].

When hyperbolic partial differential equations, such as (2.5), are used to model granular material, we can imagine each individual particle moving on its characteristic curve in space and time. Hence, as long as the characteristics do not intersect, the grains cannot pass each other. An area in the vessel, which is already filled with material, cannot be penetrated by another particle. In shaking experiments, we expect the movement of the container to mix up the material and
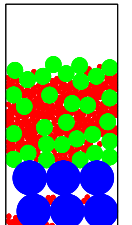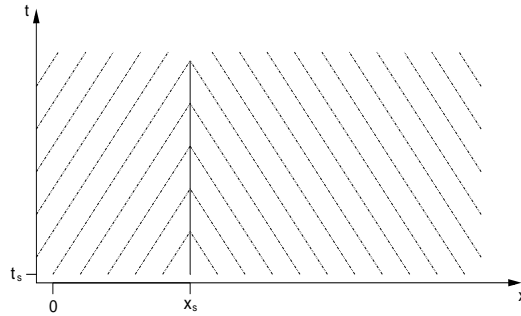
Figure 2.4: The characteristics impinge on the shock. At $x = l_0$ the characteristic line is vertical. The shock stays at l_0.

thus enable the grains to *diffuse*. Consequently, one of our next goals will be the analysis of parabolic equations including a diffusive term. Such equations are also used in order to identify physically relevant solutions, so-called *viscosity solutions*, among all the weak solutions of a hyperbolic problem.

2.5   The viscosity solution approach

As we have seen in proposition 2.3.1(iv), the physically realistic stationary solutions are at best weak solutions of the evolution equation (2.5), (2.6). Therefore we need a suitable selection principle for solutions. Such a principle is provided by the *viscosity* approach, where a small second order term $\epsilon\partial_x^2$ is added in order to make the equation parabolic. In terms of the physical model of a vertical vessel filled with granular matter, this term can be seen as representing small random perturbations of the particles' motion, which otherwise is governed by the conservation law. Thus, in the present context, the addition of the viscosity term is not merely a mathematical procedure to select certain solutions, but it also represents a physical phenomenon. Indeed, in the conservation law (2.5), before a shock occurs, particles travel on their particular characteristics and keep the order they had in the initial data. According to the model, particles cannot pass each other. Therefore the evolution of the density is performed by reshuffling the values of the initial data without changing their order. The viscosity term gives more flexibility, which can be interpreted as stochastic changes of the grains' positions. This stochastic effect can fill gaps and smooth humps.

Let ϵ be a small parameter. Consider the parabolic equation

$$u_t = Cu_x - (u^2)_x + \epsilon u_{xx} \tag{2.15}$$

with boundary condition

$$Cu - u^2 + \epsilon u_x = 0 \tag{2.16}$$
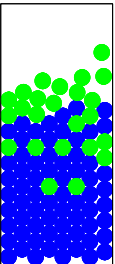
at $x = 0, l$. Notice that (2.16) implies

$$\frac{d}{dt}\int_0^l u\,dx = \left[Cu - u^2 + \epsilon u_x\right]_0^l = 0,$$

i.e. the total mass of the particles is conserved.

Before we continue with the investigation of the stationary solutions of (2.15), (2.16), we have to guarantee the existence of solutions.

Proposition 2.5.1 (Existence of solutions.) *System (2.15), (2.16) has a unique classical solution $u = u(t,x)$, which exists globally for all $t \geq 0$.*

Proof. The proof of existence of solutions is postponed to chapter 3, which we devote entirely to the study of parabolic equations. □.

Our goal is to find stationary solutions of the new system (2.15), (2.16) and then consider the limit of these solutions as the diffusion parameter ϵ tends to zero.

Setting u_t equal to zero and using the boundary condition, we find that stationary solutions satisfy

$$u' = \frac{1}{\epsilon}u(u - C), \tag{2.17}$$

where the prime indicates derivation with respect to the space variable. If we use Riccati's trick and introduce $v = v(t,x) = 1/u(t,x)$, equation (2.17) becomes

$$v' = \frac{1}{\epsilon}(Cv - 1),$$

the solution of which is $v(x) = 1/C + \kappa\exp\left(Cx/\epsilon\right)$, i.e.

$$u_\epsilon(x) = \frac{C}{1 + \kappa C e^{Cx/\epsilon}}. \tag{2.18}$$

The parameter κ in (2.18) is determined by the total mass M, where naturally $M \leq Cl$:

$$\begin{aligned}
M &= \int_0^l \frac{C}{1 + \kappa C e^{Cx/\epsilon}}\,dx \\
&= \epsilon\int_\kappa^{\kappa e^{lC/\epsilon}} \frac{1}{z(z+1)}\,dz \\
&= \epsilon\left[\ln\frac{z}{z+1}\right]_\kappa^{\kappa e^{lC/\epsilon}} \\
&= \epsilon\ln\frac{(\kappa+1)e^{lC/\epsilon}}{1 + \kappa e^{lC/\epsilon}},
\end{aligned}$$
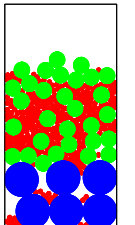
which yields

$$\kappa = \frac{e^{lc/\epsilon} - e^{M/\epsilon}}{e^{lC/\epsilon}\left(e^{M/\epsilon} - 1\right)}.$$

Hence the unique stationary solution with total mass M is given by

$$u_\epsilon(x) = \frac{Ce^{lC/\epsilon}\left(e^{M/\epsilon} - 1\right)}{Ce^{xC/\epsilon}\left(e^{lC/\epsilon} - e^{M/\epsilon}\right) + e^{lC/\epsilon}\left(e^{M/\epsilon} - 1\right)}. \qquad (2.19)$$

Finally, as ϵ tends to zero, we find

$$u_\epsilon(x) \xrightarrow[\epsilon \to 0]{} \begin{cases} C- & \text{for } x < M/C \\ \dfrac{C}{C+1} & \text{for } x = M/C \ , \\ 0+ & \text{for } x > M/C \end{cases}$$

i.e. the viscosity solution (2.7) is the desired step function (see figure 2.5).
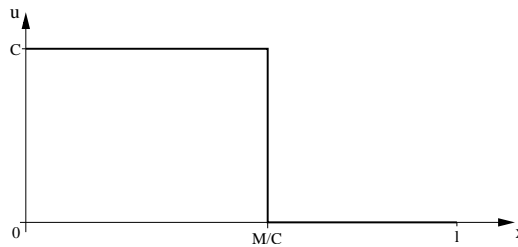
Figure 2.5: The step function (2.7) is the viscosity solution of system (2.15), (2.16).

2.6   Discrete models for n types of particles

In order to analyze the properties of mixtures of different grains varying in size and specific weight, we start again with one type of particles. For simplicity we think of spherical balls. If we neglect boundary effects, then the space filling properties are independent of the size of the balls. This relation follows from a simple scaling argument for any regular or statistical packing, in particular for the practically densest packing which appears when we shake granular material in an experiment. This mathematically obvious fact can be interpreted in practical terms as follows: On the one hand, the number of gaps left between individual grains is larger when we fill the volume with small balls. On the other hand, the gaps are smaller and these two effects balance each other.

The situation changes if we use two types of balls of distinctly different size, still having the same specific weight. Now the smaller balls can partially fill the gaps between big balls and thus reduce the empty space and increase the density of
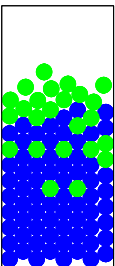
the packing. If such a mixture of two grain types is stirred for a short time, or if the container is tapped in order to make the grains slightly rearrange, one can achieve dense packings, in which the averaged mass density depends on the sizes of the two types of balls and their relative proportions in the mixture. We have imposed the condition that the material be stirred only for a short time for the following reason: If we shake the container rapidly and for a longer period of time and thus introduce more kinetic energy into the system than is done by mere stirring, the so-called *Brazil nut* or *muesli* effect can take over, i.e. space liberated by large particles at the bottom of the vessel can be occupied by small grains, while the motion of the small balls rarely leaves enough space for one big grain to fall down. As a result, the big particles will gradually move up in the mixture and finally settle towards the top.

If we consider a mixture of two kinds of balls of equal size but different specific weight, yet another effect appears. Any random mixture, however inhomogeneous, will remain stationary as long as gravitational forces do not overcome static friction. If the mixture is stirred, then friction becomes small and gravitation will cause buoyancy effects and the heavier grains will move to the bottom.

Finally, most real mixtures contain balls varying both in size and specific weight. In this case, depending on the situation, either the Brazil nut effect or the buoyancy effect will dominate. An overview of packing properties of various types of mixtures, including theoretical and experimental results concerning mixtures composed of two or more grain types, is given in [Aste00]. In the remainder of this chapter, we discuss the four previously described situations, the one with equal grains and with grains varying in size, weight or both, in a sequence of heuristic models. Our goal is to find a unified approach which explains all observed effects in terms of the potential energy of the mixture.

Now we have the following general problem: There are k species of grains numbered $i = 1, \ldots, k$. If V_i is the volume occupied by one grain of type i, and if we have a sample of u_i individual particles of that type, then the volume occupied by this sample is $U_i = u_i V_i$. We take samples from all species, each with volume U_i, and produce a homogeneous mixture with practically densest packing, then this packing leaves a volume of empty space which we call U_0. In an experimental setting, the number U_0 would be determined experimentally, for given grain sizes V_i, from the numbers u_i, i.e., as a function of the u_i.

Hence the total volume is given by $U = U_0 + U_1 + \cdots + U_k$. We repeat that the empty space U_0 is a function of the particle numbers u_i. Let us denote this function by Φ,

$$U_0 = \Phi(u_1, \ldots, u_k).$$

The function Φ is a *material parameter*. By definition, it is homogeneous of degree
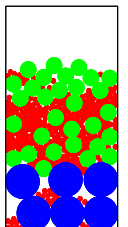
one, i.e.

$$\Phi(\alpha u_1, \ldots, \alpha u_k) = \alpha \Phi(u_1, \ldots, u_k)$$

for all $\alpha > 0$.

In order to describe the dynamics of such a system under the influence of gravity, we have to determine the conditions under which one individual particle can move into a cell already partly filled with grains. Let us therefore divide the container into N layers, each of height h, numbered $j = 1, \ldots, N$, and let u_i^j denote the number of grains of type i in the jth layer. Accordingly, let U_i^j be the volume occupied by grains of type i in the jth cell. In other words, each state of the system is described by an $N \times k$-matrix of the form

$$\begin{pmatrix} u_1^N & \ldots & u_k^N \\ \vdots & \ddots & \vdots \\ u_1^1 & \ldots & u_k^1 \end{pmatrix}.$$

Suppose each layer has a fixed cell volume denoted by C. If the cell at height j contains a mixture of grains $(u_1^j, \ldots, u_k^j)$, then the probability of another particle, say of type i, to fall down from the level $j + 1$ and enter the jth cell will depend on the number of available particles u_i^{j+1} on the upper level as well as on their volume V_i and the available space in cell j. The latter is determined as follows: We hypothetically add one particle of type i to the mixture in cell j and calculate the empty space left by this new mixture,

$$^i\tilde{U}_0^j = \Phi(u_1^j, \ldots, u_{i-1}^j, u_i^j + 1, u_{i+1}^j, \ldots, u_k^j). \tag{2.20}$$

Now, if the new occupied volume $^i\tilde{U}_0^j + \sum_{\nu=1}^k U_\nu^j + V_i$ is still smaller than the capacity C, then the particle can move from $j + 1$ down to j. Otherwise, it stays at $j + 1$ and the state vector $(u_1^j, \ldots, u_k^j)$ is unchanged. (For illustration see figure 2.6.) These considerations yield the following discrete-step equation governing the dynamics of the above two-species system:

$$\dot{u}_i^j = u_i^{j+1} \left(C - \sum_{\nu=1}^k U_\nu^j - {}^i\tilde{U}_0^j - V_i \right)_+ - \\ - u_i^j \left(C - \sum_{\nu=1}^k U_\nu^{j-1} - {}^i\tilde{U}_0^{j-1} - V_i \right)_+, \tag{2.21}$$

$j = 1, \ldots, N$, where $(\ )_+$ denotes the positive part. The parameter a denotes again the transition rate due to gravitation, the only driving force in the system. Again, as in section 2.3, equation (2.21) is the result of a continuous-time limit of a difference equation, while the space variable remains discretized. The function (2.21) is not differentiable at the point, where the terms in parentheses touch zero. For practical reasons, it seems more reasonable to approximate (2.21) by a $\mathcal{C}^1$

(a) An arbitrary, in general not optimally packed, mixture of grains.

(b) A rearrangement of the particles is sought, in which the new grain has enough space to enter.

(c) If the particle is small enough, there exists a packing including the new grain, which is dense enough to fit into one cell.
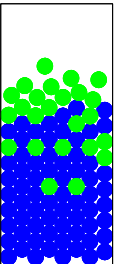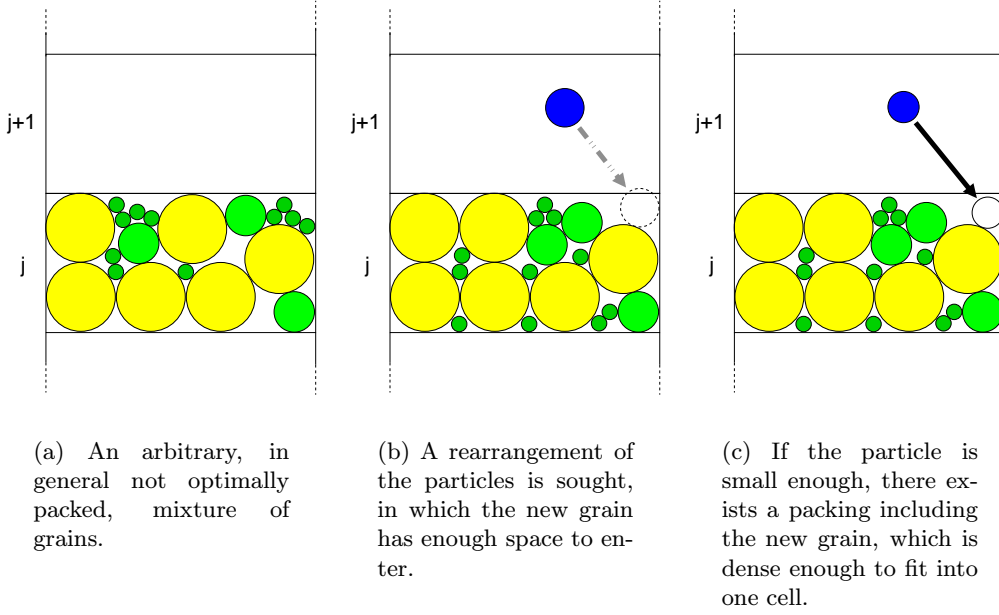
Figure 2.6: The method of determining available space for new particles to enter a cell. An arbitrary mixture (a) of grains in a cell j of the container is optimally rearranged in a way that a new particle can enter from the compartment $j+1$ above. Even though the actually occupied volume might be smaller than the cell capacity C, no such rearrangement might be found (b). In this case, the particle stays in cell $j+1$. Consequently, only small grains can enter and occupy gaps between larger particles (c).

function in the neighborhood of these critical points. Thus, if $F_i^j = F_i^f(u_1, \ldots, u_k)$, $i = 1, \ldots, k$, designates a suitable approximation of the function

$$\tilde{F}_i^j(u_1, \ldots, u_k) = \left(C - \sum_{\nu=1}^{k} U_\nu^j - {}^i\tilde{U}_0^j - V_i \right)_+, \qquad (2.22)$$

then equation (2.21) becomes

$$\dot{u}_i^j = u_i^{j+1} F_i^j - u_i^j F_i^{j-1}. \qquad (2.23)$$

In order to describe the physical idea correctly, we impose the boundary conditions

$$\begin{aligned} F_i^0 &= 0, \\ u_i^{N+1} &= 0 \end{aligned} \qquad (2.24)$$

for $i = 1, \ldots, k$. From a physical point of view, (2.24) guarantees that no particles can enter the vessel through the lid and that the bottom is solid (or already optimally filled with grains). Equations of the form (2.23) with boundary
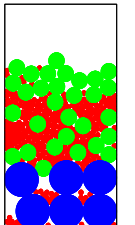
conditions (2.24) have been used in the past to model the way parking cars gradually fill up a parking lot of given dimensions. Since these dynamics are very similar to those observed in granular material during compaction, some of the ideas have been adapted in order to gain new insight (see for example [Krapivsky93], [Tarjus92] or [Wackenhut02]).

Since (2.23), (2.24) allows particle motion in downward direction only, we expect that the system is dissipative, i.e. particle constellations change only in the direction of diminishing potential energy.

Proposition 2.6.1 (Potential energy of the discrete model.) *Let ρ_i denote the specific density of the grains of type i and define the total potential energy of the system by*

$$G = \sum_{j=1}^{N} j \left(\sum_{i=1}^{k} U_i^j \rho_i \right).$$

Then, G can only decrease in time, i.e. its time derivative $\dot{G}$ is non-positive.

Proof. We write $G = \sum_i m_i \left(\sum_j j u_i^j \right)$, where $m_i = \rho_i V_i$ is the mass of an individual particle of type i. Then

$$\dot{G} = \sum_i m_i \left(\sum_j j \dot{u}_i^j \right)$$
$$= \sum_i m_i \left[\sum_j j \left(u_i^{j+1} F_i^j - u_i^j F_i^{j-1} \right) \right]$$
$$= - \sum_{\nu=1}^{N} u_i^\nu F_i^{\nu-1}$$
$$\leq 0,$$

hence the total potential energy cannot grow during the process of sedimentation.
□.

Notice that $\dot{G}$ vanishes only if for all $\nu = 1, \ldots, N$, $u_i^\nu = 0$ or $F_i^{\nu-1}$ vanishes. This does not necessarily mean that G tends to a global minimum. We will come back to this point in section 2.16 and again in section 8.3 of chapter 8.

2.7   Transition to a continuous model

As in section 2.3, we introduce the space variable x designating the height in the container and let $u_i = u_i(t, x)$ denote the number of grains of type i at time t in
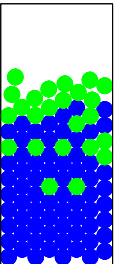
a compartment of fixed volume C occupying the section $[x, x + \Delta x]$. Expressed in terms of t and x, the original difference equation takes the form

$$\frac{1}{a}[u_i(t + \Delta t, x) - u_i(t, x)]\Delta x =$$

$$= \{u_i(t, x + \Delta x)F_i(u(t, x)) - u_i(t, x)F_i(u(t, x - \Delta x))\}\Delta t$$

$$= \{[u_i(t, x + \Delta x) - u_i(t, x)] F_i(u(t, x)) +$$

$$+ u_i(t, x) [F_i(u(t, x)) - F_i(u(t, x - \Delta x))]\}\Delta t \qquad (2.25)$$

$$= \{[\Delta x u_{ix}(t, x) + \mathcal{O}(\Delta x^2)] F_i(u(t, x)) -$$

$$- u_i(t, x) [\Delta x F_{ix}(u(t, x)) + \mathcal{O}(\Delta x^2)]\}\Delta t,$$

where u designates the vector $(u_1, \ldots, u_k)^T$. The function $F_i = F_i(u)$ in (2.25) is now some continuous analogon of F_i^j. In view of (2.22), the most manifest choice is a continuously differentiable approximation $F_i = F_i(u_1, \ldots, u_k)$ of

$$\tilde{F}_i = \tilde{F}_i(u) = \left(C - \sum_{\nu=1}^{k} U_\nu - {}^i\tilde{U}_0 - V_i\right)_+ .$$

Here, $U_\nu = U_\nu(x)$ is the relative volume occupied by grains of type ν at position x in the vessel, and ${}^i\tilde{U}_0 = {}^i\tilde{U}_0(x)$ is the continuous analogon of (2.20). Then, carrying (2.25) to the limit as $\Delta t, \Delta x \longrightarrow 0$, we end up with the conservation law

$$u_{it} = a(u_i F_i)_x \qquad (2.26)$$

with boundary condition

$$F_i(0) = 0,$$
$$u_i(l) = 0 \qquad (2.27)$$

for $i = 1, \ldots, k$, where l is now the height of the container.

Proposition 2.7.1 (Potential energy of the continuous model.) *System (2.26) with boundary conditions (2.27) is dissipative, i.e. the total energy*

$$H = \int_0^l x \sum_{i=1}^{k} U_i(x)\rho_i dx$$

decreases along trajectories.

Proof. Writing the total potential energy as

$$H = \sum_i m_i \int_0^l x u_i(x) dx,$$
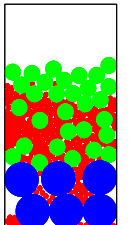
we get

$$\dot{H} = \sum_i m_i \int_0^l x \dot{u}_i(x) dx$$

$$= a \sum_i \int_0^l x(u_i F_i)_x dx$$

$$= -a \sum_i m_i \int_0^l u_i F_i dx,$$

which is always non-positive. $\square$.

2.8   An example with two types of spherical particles

Before proceeding to a model for the segregation of granular material, we illustrate some properties of the systems analyzed in sections 2.6 and 2.7 by means of a computer simulation. We will use the discrete system (2.23), (2.24) for the implementation.

Let us consider a two-dimensional vessel containing two-dimensional spherical particles of two different sizes. As figure 2.7 illustrates, the optimal fill level for a single grain type is approximately $\gamma_1 = 0.91$, regardless of the radius of the particles. Now we add a second type of grains with radius $r = (2 - \sqrt{3})R/\sqrt{3}$,
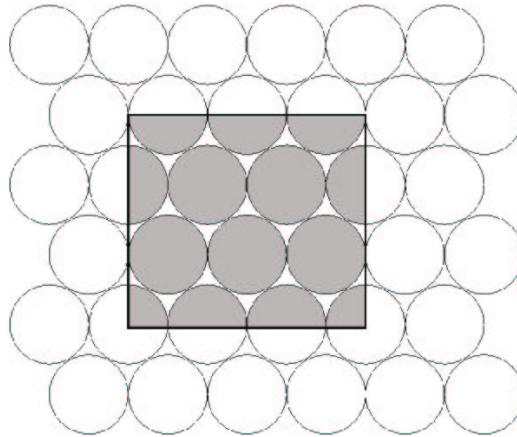
Figure 2.7: The fill level of an optimal packing with discs of the same radius R. We cut a rectangle out of a region which is optimally filled with spheres and count their number. In a box of length $6R$ and height $3\sqrt{3}R$ we find 9 balls. Hence, the fill level is $\gamma_1 = 9\pi R^2/(18\sqrt{3}R^2)$ or $\pi/(2\sqrt{3})$, which is approximately 91 percent.

chosen in such a way that the small balls fit exactly into the gaps between the large ones in the optimal one-particle packing of figure 2.7. It stands to reason
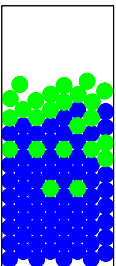
to assume that the the best filling using both grain types is illustrated in figure 2.8. Let one layer in the vessel have unit volume $C = 1$ and let the radius of
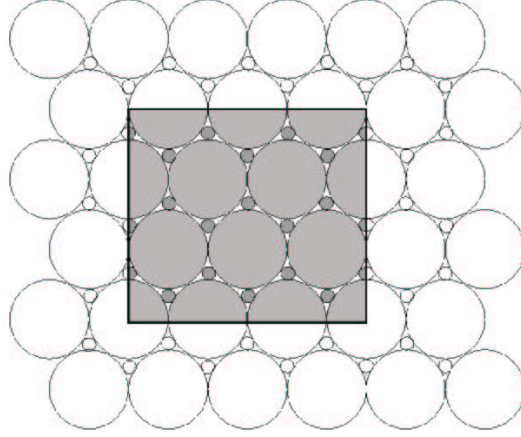
Figure 2.8: If the container is optimally filled with a mixture of two types of grains, the large ones with radius R, the small ones with $r = R(2 - \sqrt{3})/\sqrt{3}$, we count nine large spheres and eighteen small ones in the box. Hence, the fill level has increased to $\gamma_2 = (9R^2\pi + 18r^2\pi)/(18\sqrt{3}R^2)$ or $\pi(3 + 2(2 - \sqrt{3})^2)/(6\sqrt{3})$, which is approximately 95 percent.

the larger spheres be $R = 10^{-3}$. Thus, the optimal one-particle packings contain $u_1^{max} = 10^6\gamma_1/\pi$ and $u_2^{max} = 3 \cdot 10^6\gamma_1/(\pi(2 - \sqrt{3})^2)$ grains, respectively. In each layer j, the function F_1^j therefore becomes zero at $u_1 = u_1^{max} - 1$, $u_2 = 0$ and at approximately $u_1 = 0$, $u_2 = u_2^{max} - \gamma_1 R^2/r^2$, since about $\gamma_1 R^2/r^2$ small particles occupy the space of one big one. For $u_1 = u_2 = 0$, $F_1^j = 1 - V_1 = 1 - 10^{-6}\pi$. In the same way, F_2^j vanishes at $u_1 = u_1^{max}$, $u_2 = 0$ and at $u_1 = 0$, $u_2 = u_2^{max} - 1$ and has its maximal value $1 - V_2 = 1 - 10^{-6}\pi(2 - \sqrt{3})^2/3$ at $u_1 = u_2 = 0$. In order to keep calculations simple, we suppose that F_i^j are linear in between the designated points, hence their graphs have the shapes illustrated in figure 2.9. Assuming these functions for available space, we run a simulation. The result shows nicely how the two particle types settle towards the bottom of the container (figure 2.10).

Up to this point, we have developed a model for the interaction of particles of varying size during the process of compaction. Here, the differences in size are of great importance, since they lead to denser packings in comparison to mono-size material. Notice that we have not yet implemented any diffusive effects, which play a role in real systems. We will do so in the following, thus creating the possibility for the granular material to segregate under the influence of additional forces as periodic shaking or vibration.
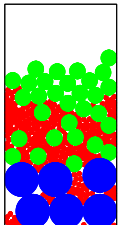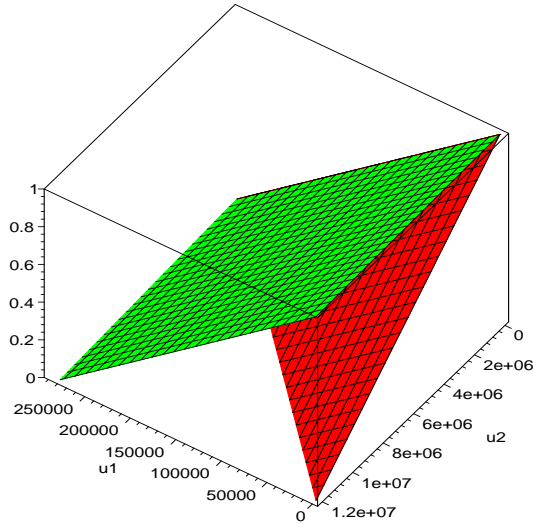
Figure 2.9: The graphs of the linearly interpolated available space functions F_1^j and F_2^j for the two grain types of figure 2.8.

2.9   A random walk model with drift term

In the present and following sections, we address the design of more realistic compaction and segregation models. As in the previous sections, we will derive partial differential equations from elementary random walk models describing the microscopic particle movement. Now, however, we add a random component to the transition rates, thus supplying the equations with a diffusive term. Starting with a random walk on a grid in continuous time and the limiting case of a diffusion equation, we step by step incorporate various effects which finally yield a system adequate to describe segregation in vertical direction. First we neglect gravity and suppose that the vessel of height l contains a certain number N_{tot} of particles. Dividing the vessel in small compartments, we denote by N_k the number of particles in the kth compartment. We assume that each particle is subject to a random walk, i.e. at any time and at any point in the vessel a particle has a certain constant rate of moving to the right or left. Then the change of the particle number in time will be given by

$$\frac{d}{dt}N_k = \tilde{\alpha}(N_{k+1} + N_{k-1} - 2N_k), \tag{2.28}$$

where $\tilde{\alpha}$ is the rate of moving to a neighboring site (see figure 2.11). Model (2.28) assumes constant rates and does not take into account interactions between the particles. We assume that the rate is inversely proportional to the square of the distance between compartments, i.e. $\tilde{\alpha}\Delta x^2 \equiv D$ is a constant. In the limit for small Δx, we get the diffusion equation

$$N_t = DN_{xx} \tag{2.29}$$
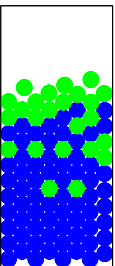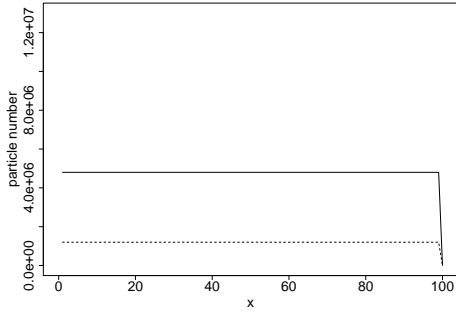
(a) Uniform initial distribution.
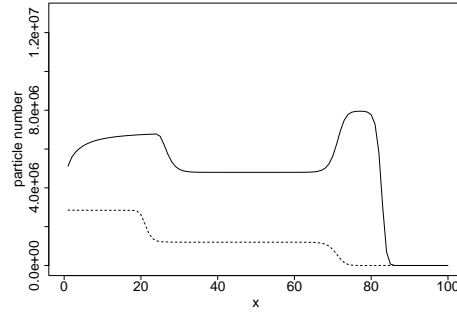
(b) The distribution at $t = 50$.
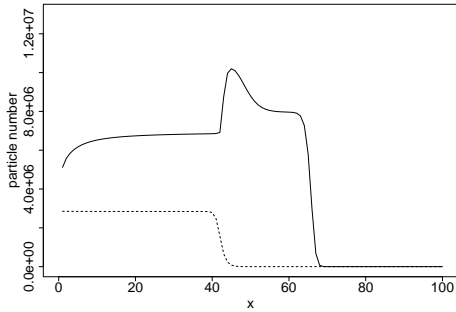
(c) The distribution at $t = 100$.
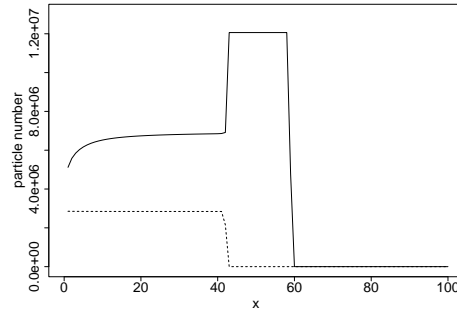
(d) The approximate stationary state, $t = 200$.

Figure 2.10: Simulation of (2.23), (2.24) with $C = 1$, $R = 10^{-3}$. We used the functions F_i^j represented in figure 2.9 and started with a homogeneous distribution. In each layer, we initially placed $1.2 \cdot 10^5$ large grains and $4.8 \cdot 10^6$ small ones. Due to gravitation, the particles move towards the bottom of the container. In the limit state, all the large particles have gathered at the bottom of the container and formed a densest packing. Small grains were able to fill up the gaps left in between up to a certain point. The surplus of small particles forms a single-particle-type layer on top of the mixture. For better visibility, the number of large grains (dashed lines) is scaled by a factor of 10.

with diffusion rate D.

If we supply equation (2.29) with the Neumann boundary condition

$$N_x = 0 \qquad\qquad (2.30)$$

at $x = 0, l$, saying that particles cannot enter or leave the vessel, then clearly all solutions of system (2.29), (2.30) converge to states with homogeneous distributions throughout the vessel, and the appearing concentration (or particle number per site) depends only on the total number of grains in the container.

(a) simple.   (b) volume filling.
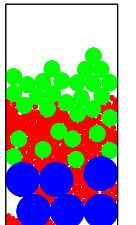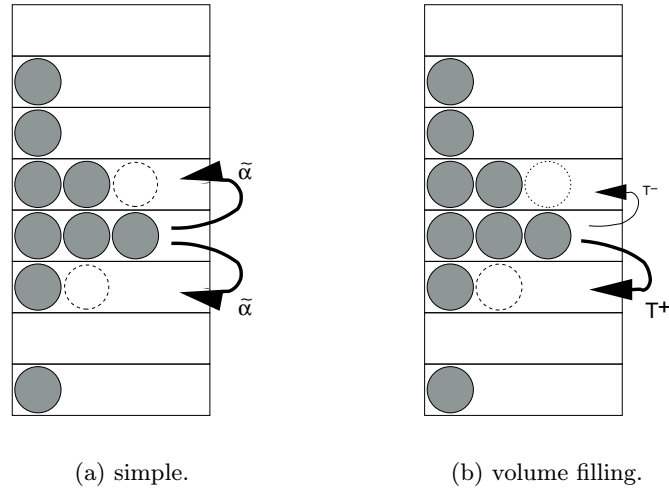
Figure 2.11: Random walk without gravity. The simplest particle transition rate is constant (subfigure (a)). Density-dependent rates (subfigure (b)) yield volume-filling functions. Here, a grain can only enter a neighboring cell, if the available space at the destination is sufficiently large.

In a first step towards a more general model, we suppose that gravity acts in the negative x-direction of the (vertical) vessel. Furthermore, we assume that the particle distributions are homogeneous at each height x, i.e. the grains can only move up or down. Thereby, we reduce the real three-dimensional physical setup to a one-dimensional model. Note that we do not want to treat here the case of a very thin vessel (like for instance a vertical tube), where boundary effects become important and the movement of the particles is limited by their ability to pass each other vertically. The simplification to one dimension can be justified since we are mainly interested in vertical segregation and compaction of granular material. Again, we consider a continuous-time, discrete-space random walk, and we restrict attention to one-step jumps. We point out that our main interest lies in treating mixtures of at least two types of particles in the vessel, where N and n then designate their respective numbers.

Denote by T_k^+ the rate for a particle of the first type in the cell k to move up to the position $k+1$, and by T_k^- its rate of jumping down (see figure 2.12). For the corresponding rates for particles of the second type we use lower case letters, t_k^-
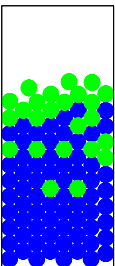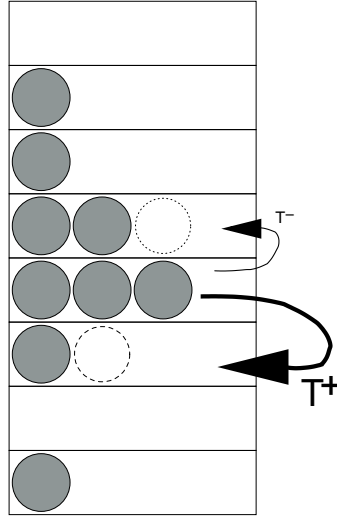
Figure 2.12: The influence of gravity adds a new component to the transition rates of the particles. Downward movement is favored.

and t_k^-. For a mixture of two species, the system of master equations then reads

$$
\frac{d}{dt}N_k = T_{k+1}^- N_{k+1} + T_{k-1}^+ N_{k-1} - N_k(T_k^+ + T_k^-),
$$
$$
\frac{d}{dt}n_k = t_{k+1}^- n_{k+1} + t_{k-1}^+ n_{k-1} - n_k(t_k^+ + t_k^-).
$$
(2.31)

If the rates are constants, then these equations describe independent random walks for two types of grains with possibly different rates.

2.10 Compaction of a single particle species

We modify the parameters in (2.31) and adapt it to different situations. First consider jumping rates of the form

$$
T_k^+ = \tilde{\alpha} - \tilde{\beta}G_k,
$$
$$
T_k^- = \tilde{\alpha} + \tilde{\beta}G_k,
$$
(2.32)

where $\tilde{\alpha}$ and $\tilde{\beta}$ are constant. Thus, in addition to the constant term $\tilde{\alpha}$ giving rise to a non-biased diffusion process as in section 2.9, we have a second term depending on the composition of the mixture in the kth cell. Typically, G_k specifies a drift due to gravitation. We assume $\tilde{\alpha} > \tilde{\beta}G_k$ in (2.32), which guarantees that the resulting jumping rates do not become negative. If we chose for example $G_k = Mg\Delta x$, where M is the mass of an individual particle, g the gravitational constant and
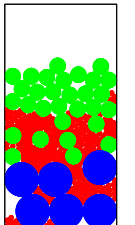
Δx the grid size, then

$$\begin{aligned}
\frac{d}{dt}N_k =&(\tilde{\alpha} + \tilde{\beta}Mg\Delta x)N_{k+1} + (\tilde{\alpha} - \tilde{\beta}Mg\Delta x)N_{k-1}- \\
&- N_k(\tilde{\alpha} + \tilde{\beta}Mg\Delta x + \tilde{\alpha} - \tilde{\beta}Mg\Delta x), \\
=&\tilde{\alpha}(N_{k+1} + N_{k-1} - 2N_k) + \tilde{\beta}Mg\Delta x(N_{k+1} - N_{k-1}).
\end{aligned} \tag{2.33}$$

The gravitational coefficient $G_k = Mg\Delta x$, as modeled above, has the form a potential energy. When the particle falls down from one cell to the one below, this potential energy is transformed into kinetic energy. For a given grid size, the drift term thus depends on the masses of the particles, which seems to be a reasonable approach. If now the rate $\tilde{\beta}$ scales as $\tilde{\beta} = \beta/(\Delta x^2)$, we get in the parabolic limit

$$N_t = DN_{xx} + 2\beta MgN_x. \tag{2.34}$$

Equation (2.34) is a diffusion-convection model for a single species with constant diffusion coefficient D and convection rate β. If we write (2.34) in divergence form,

$$N_t = -J_x, \tag{2.35}$$

then the flux $J = -DN_x - 2\beta MgN$ drives the particles towards the bottom of the container. We expect to see the grains aggregate at the bottom. This feature is verified by simulation (see figure 2.13). In view of (2.35), we impose that the
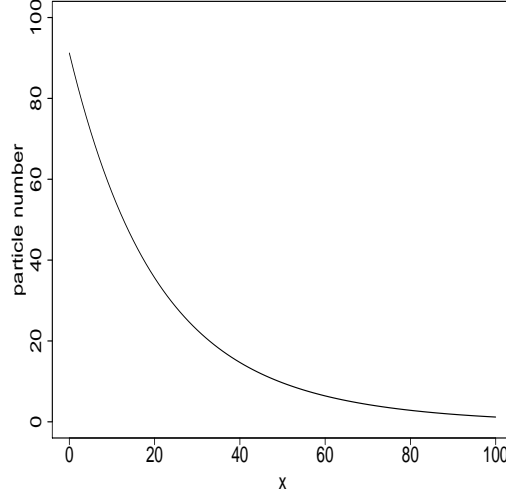
Figure 2.13: Sedimentation of particles of a single type under the influence of gravity. We used the set of master equations (2.33) with $M = 0.06$, $\tilde{\alpha} = 1$, $\tilde{\beta} = 0.4$ and a total number of $N_{tot} = 2020$ particles in a vertical vessel of height $l = 100$ divided into 101 cells.

flux vanishes at the boundary of the domain, i.e. the boundary condition reads

$$DN_x + 2\beta MgN = 0 \tag{2.36}$$
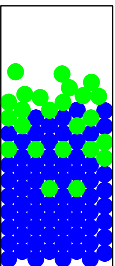
at $x = 0, l$.

Proposition 2.10.1 (Global solution.) *Equation (2.34) with boundary condition (2.36) has a unique classical solution, which exists for all positive times.*

Proof. Global existence of solutions to convection-diffusion equations is guaranteed, provided the convection function satisfies some growth conditions. For the proof of proposition 2.10.1, as well as the discussion on global existence of solutions to more complex systems developed later in the present chapter, we refer to chapter 3. $\square$.

The stationary solutions of (2.34), (2.36) are the solutions of the ordinary differential equation

$$N' = -2\frac{\beta}{D}MgN, \tag{2.37}$$

where the prime indicates differentiation with respect to the space variable. The solutions of (2.37) are

$$N(x) = \lambda e^{-2\beta Mgx/D},$$

where the parameter λ is determined by the total number $\bar{N}$ of grains in the vessel, i.e.

$$
\begin{aligned}
\bar{N} &= \int_0^l N(x)dx \\
&= \int_0^l \lambda e^{-2\beta Mgx/D} dx \\
&= \frac{\lambda}{2\beta Mg/D}\left(1 - e^{-2\beta Mgl/D}\right),
\end{aligned}
$$

hence

$$\lambda = 2\frac{\bar{N}\beta Mg/D}{1 - e^{-2\beta Mgl/D}}. \tag{2.38}$$

The random walk model discussed in this section assumes independent movement of the individual grains. In contrast to the models in sections 2.11 or 2.14, particles do not interact. They are all driven to the bottom of the container in the same way. In the light of the lacking competition between grains, the stable steady state in form of the strictly convex curve (2.38) is not surprising (figure 2.13). This behavior will change in section 2.11, where particle movement is limited by the available space per cell. Here, the typical sigmoid-shaped distributions appear as stable states. Of course, a model assuming independent motion does not describe the physical reality correctly and should be understood as a first step towards more realistic models.
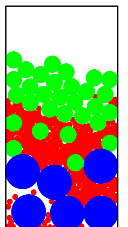
2.11   The volume filling model for a single species

We move one step ahead in the development of a random walk model simulating segregation. Some effects observed in shaken or vibrated granular material, such as the *Brazil nut* effect or effects similar to the *Rayleigh-Bénard* phenomenon in fluid dynamics (see also chapter 9), can be explained in terms of very basic particle properties, above all the size and mass of grains. Thus, the remainder of this chapter will be mainly dedicated to the study of so-called *volume filling* models. These are models in which the available space per cell determines, among other variables, the transition rates.

First we develop a model for only one particle species. We do not expect new phenomena besides the compaction already exhibited in section 2.10. Nevertheless, the analysis will be helpful in the development of more complicated models. We start with the same setup as in section 2.10, using transition rates of the form (2.32). This time, however, the gravitational term G_k will not only depend on the particle mass M, but also on the available space at the destination. Thus, when a cell k in the container is already filled with a large number of particles, the rate for yet another particle to move to that cell will decrease. In reality, this rate depends on all the details of the configuration of the particles located at the destination of the incoming particle. In [Wackenhut02], the situation is simplified insofar, as the author computes the available free volume for the site of the incoming particle (neglecting the locations of that volume and the relative position of the incoming particle). Here we further simplify and let the rate depend on the total available volume only. Thus, the microscopic effects of the shaking process, which generates space between the grains, are not taken into account. We therefore choose a gravitational term of the form $G_k = MgQ_k$ or, expressed in terms of the specific weight ρ_N of the material and the volume V_N of the particle,

$$G_k = \rho_N V_N g Q_k, \tag{2.39}$$

where $Q_k = Q_k(N_k)$ is a non-increasing function with $Q_k(0) = 1$. A discussion of different so-called *volume filling* functions Q_k is postponed to a later section.

As in section 2.9, we pass to the parabolic limit to find

$$N_t = DN_{xx} + 2\beta \rho_N V_N g(Q(N)N)_x \tag{2.40}$$

with Neumann condition

$$N_x = -2\frac{\beta}{D}\rho_N V_N g Q(N)N \tag{2.41}$$

at the boundary $x = 0, l$. We call the system (2.40), (2.41) the *Q-model*.

We compare our previous segregation model (2.34), (2.36) to the *Q*-model (2.40), (2.41) by means of a simulation (see figure 2.14). For the implementation, we use
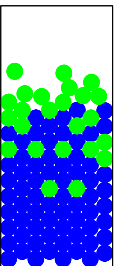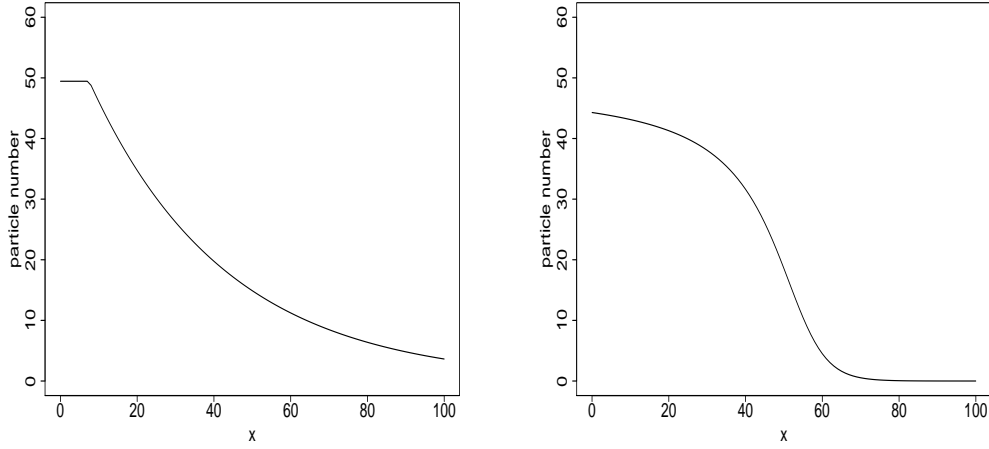
(a) Volume filling functions, which are merely continuous, in general yield continuous solutions.

(b) If we use differentiable volume filling functions, the stationary states are smooth as well.

Figure 2.14: Sedimentation of particles of a single type under the influence of gravity and the presence of a restricting volume filling function Q. We used again the set of master equations (2.31) with transition rates (2.32), (2.39). Subfigure (a) was generated using a volume filling function of the form (2.42), while (b) was produced with the help of (2.43). Parameter values are $\rho_N = 3$, $V_N = 0.02$, $\tilde{\alpha} = 1.7$, $\tilde{\beta} = 0.4$. A total number of $N_{tot} = 2020$ particles in a vertical vessel of height $l = 100$, divided into 101 cells, were initially (at time $t = 0$) distributed evenly all over the vessel.

the discrete model with a single equation of the form (2.31). The special choice for the function Q_k is

$$Q_k(N_k) = \begin{cases} 1 & \text{if } 0 \leq N_k \leq N^{\max} \\ 0 & \text{otherwise} \end{cases} . \qquad (2.42)$$

Here, $N^{\max}$ denotes the maximal number of particles fitting into one cell. We use again the particle volume V_N to write $N^{\max} = V^{\max}/V_n$, where $V^{\max}$ is the volume of one cell, or, in other words, the maximal available space at one discrete site of the vessel. Notice that, in contrast to figure 2.13, the steady state distribution in figure 2.14(a) exhibits a flat part at about 50 grains per cell at the bottom of the container. Evidently, this is the effect of the volume filling function Q_k, which limits the number of particles per site.

Alternatively, we use the continuously differentiable function

$$Q_k(N_k) = \begin{cases} (N_k - N^{\max})^2 & \text{if } 0 \leq N_k \leq N^{\max} \\ 0 & \text{otherwise} \end{cases} , \qquad (2.43)$$
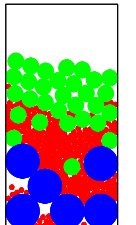
which yields a smooth stable distribution as shown in figure 2.14(b).

The stationary solutions of system (2.40), (2.41) are solutions of the ordinary differential equation

$$N' = -2\frac{\beta}{D}\rho_N V_N g Q(N)N, \qquad (2.44)$$

which are decreasing functions taking values between 0 and $N^{\max}$.

2.12   The Q-model for two types of particles

We return to two particle species, using again the system of equations (2.31). The transition rates of the form (2.32) with constant G_k are replaced by

$$\begin{aligned}
T_k^+ &= \tilde{\alpha} - \tilde{\beta}G_k, \quad T_k^- = \tilde{\alpha} + \tilde{\beta}G_k, \\
t_k^+ &= \tilde{\alpha} - \tilde{\beta}g_k, \quad t_k^- = \tilde{\alpha} + \tilde{\beta}g_k,
\end{aligned} \qquad (2.45)$$

where G_k, g_k are convection terms which depend on the location k of the particle in the vessel. The volume filling functions $Q_k = Q_k(N_k, n_k)$ and $q_k = q_k(N_k, n_k)$ have the following properties:
(a) $Q_k(0,0) = q_k(0,0) = 1$.
(b) Q_k and q_k are decreasing functions in both arguments.
(c) Q_k and q_k vanish if the total number of particles $N_k + n_k$ reaches a certain level and stay zero henceforth. Property (c) guarantees that, given the size of a cell, the number of particles cannot exceed a certain value. Of course, when there is no more space for a large particle, smaller grains may still enter. We now construct the transition rates using these volume filling functions. With $T^\pm$, $t^\pm$ as in (2.45), we choose

$$\begin{aligned}
G_k &= \rho_N V_N g Q_k, \\
g_k &= \rho_n V_n g q_k.
\end{aligned} \qquad (2.46)$$

Then, in the parabolic limit, system (2.31) becomes

$$\begin{aligned}
N_t &= [DN_x + 2\beta\rho_N V_N g Q(N,n)N]_x, \\
n_t &= [Dn_x + 2\beta\rho_n V_n g q(N,n)n]_x,
\end{aligned} \qquad (2.47)$$

The boundary conditions read

$$\begin{aligned}
DN_x + 2\beta\rho_N V_N g Q(N,n)N &= 0, \\
Dn_x + 2\beta\rho_n V_n g q(N,n)n &= 0
\end{aligned} \qquad (2.48)$$

at $x = 0, l$. The equations (2.47) are coupled convection-diffusion equations in divergence form. In view of the boundary conditions (2.48), the total masses of the two species are conserved.
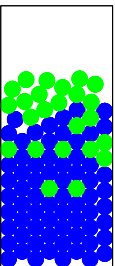
Next, we discuss the preservation of positivity and the boundedness of the solutions of (2.47), (2.48). Since N and n physically describe particle numbers, we would like them to be confined to the intervals $[0, N^{\max}]$ and $[0, n^{\max}]$ for the given positive constants $N^{\max}$ and $n^{\max}$, respectively. The following proposition establishes this property.

Proposition 2.12.1 (Boundedness of solutions.) *Let the initial data $N(0, x)$, $n(0, x)$ for the system (2.47), (2.48) be continuous, non-negative and bounded by the constants $N^{\max}$, $n^{\max}$, respectively. Then the solutions $(N(t, x), n(t, x))$ satisfy $0 \leq N(t, x) \leq N^{\max}$, $0 \leq n(t, x) \leq n^{\max}$ for all $t \geq 0$.*

Proof. For the proof of positivity, we refer to chapter 3, where we treat general equations of the form $u_t = (d(u)u_x)_x - f(u)_x$. In proposition 3.5.1 of section 3.5, we show that under certain, relatively weak conditions on the convection function f, positivity of the solutions is preserved. The conditions required apply to system (2.47), (2.48).

In order to show that upper bounds exist for N and n, we use a similar comparison argument. The proof is carried out for N, but it can be used for n without modification. Consider the auxiliary function

$$v(t, x) := N(t, x) - \epsilon e^t$$

for some constant ϵ to be specified later. Suppose N were to become larger than some value $\bar{N} > N^{\max}$ somewhere in the interval $[0, l]$. This is equivalent to saying that the function v touches $\bar{N}$ from below at some point x_0 for some $\epsilon > 0$ for the first time. Suppose $x_0 \in (0, l)$. At the touching point, we have $v_x = 0$, $v_{xx} \leq 0$ and

$$\begin{aligned} v_t &= N_t - \epsilon e^t \\ &= DN_{xx} + 2\beta \rho_N V_N g[Q(N, n)N]_x - \epsilon e^t. \end{aligned}$$

But for $N > N^{\max}$, Q is constantly equal to zero. Hence,

$$\begin{aligned} v_t &= DN_{xx} - \epsilon e^t \\ &= Dv_{xx} - \epsilon e^t \\ &< 0. \end{aligned}$$

This is a contradiction, since v was supposed to touch $\bar{N}$ from below. If the touching point is on the boundary, $x_0 = 0$ or $x_0 = l$, then the boundary condition (2.48) implies $N_x = 0$, and hence $N_{xx} \leq 0$. Again, $v_t < 0$, which is a contradiction. Consequently, N cannot exceed any value $\bar{N} > N^{\max}$ and must therefore be bounded by $N^{\max}$. $\square$
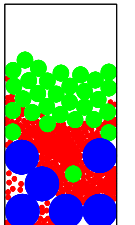
We close this section with a remark on the monotonicity of the stationary solutions of (2.47), (2.48), which are given by

$$N_x = -aQN,$$
$$n_x = -bqn. \tag{2.49}$$

Here, $a = 2\beta\rho_N V_N g/D$ and $b = 2\beta\rho_n V_n g/D$.

Proposition 2.12.2 (Monotonicity.)   *The solutions of (2.49) are all non-increasing for $x \in [0, l]$.*

Proof.   Since the constants a and b, as well as Q and q, are non-negative everywhere, monotonicity follows immediately. $\square$.

Since the stationary solutions of the system (2.47), (2.48) are monotone, (see figure 2.15), the system describes compaction effects only, while segregation does
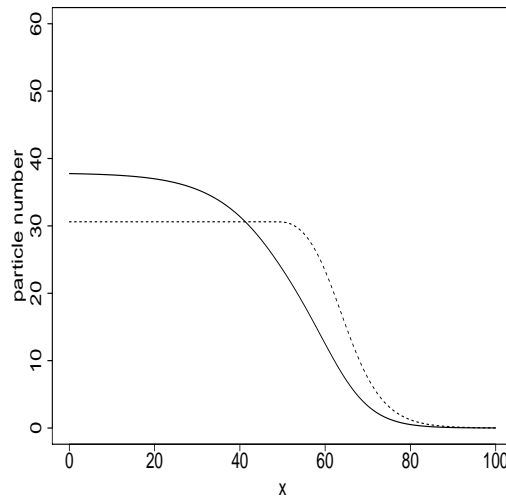
Figure 2.15: Compaction of particles simulated by a Q-model for two types of particles with gravitational terms (2.46). Parameter values are $V_N = 0.015$, $V_n = 0.01$, $\rho_N = 200/3$, $\rho_n = 100$, $\tilde{\alpha} = 2$, $\tilde{\beta} = 0.2$. A total number of $N^{tot} = n^{tot} = 2020$ particles is in the vessel. The solid line represents the small particles, while the number of large grains is given by the dashed line.

not take place.

2.13   A Q-model for two grain types exhibiting segregation

As we mentioned above, the model discussed in section 2.12 does not describe segregation of granular material. This is not surprising in view of the underly-

ing microscopic dynamics. The transition rates (2.45) with gravitational term (2.46) stipulate that, except for an undirected rate $\tilde{\alpha}$ giving rise to a diffusional component, all particles are equally driven towards the bottom of the container, independent of their type. Thus, we did not enable the larger or lighter particles to move towards the top and generate empty space for the smaller or heavier ones to fill up. Consequently, we update the model by adding a *shaking term* to (2.45), which continuously pushes all the grains up and lets them settle according to the dynamics described before. Consider
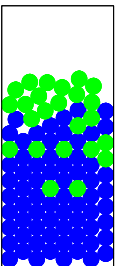
$$T_k^+ = \tilde{c} + \tilde{\alpha} - \tilde{\beta}G_k, \quad T_k^- = \tilde{\alpha} + \tilde{\beta}G_k,$$
$$t_k^+ = \tilde{c} + \tilde{\alpha} - \tilde{\beta}g_k, \quad t_k^- = \tilde{\alpha} + \tilde{\beta}g_k \tag{2.50}$$

with G_k, g_k as in (2.46), where $\tilde{c}$ is now the extra shaking rate acting only in positive x-direction. If $\tilde{c}$ scales as $\tilde{c}\Delta x^2 \equiv c$, then we get in the parabolic limit

$$N_t = [DN_x + (2\beta\rho_N V_N gQ(N,n) - c)N]_x,$$
$$n_t = [Dn_x + (2\beta\rho_n V_n gq(N,n) - c)n]_x, \tag{2.51}$$

with boundary condition

$$DN_x + (2\beta\rho_N V_N gQ - c)N = 0,$$
$$Dn_x + (2\beta\rho_n V_n gq - c)n = 0 \tag{2.52}$$

at $x = 0, l$.

We emphasize that the stationary states of (2.51), (2.52), given by the solutions of

$$N_x = \frac{c - 2\beta\rho_N V_N gQ}{D}N,$$
$$n_x = \frac{c - 2\beta\rho_n V_n gq}{D}n \tag{2.53}$$

in general are not monotone any more. In fact, if we choose a non-physical, very large shaking rate c,

$$\tilde{c} > 2\beta\max\{\rho_N, \rho_n\}\max\{V_N, V_n\}g,$$

all solutions will be strictly increasing. The upward momentum introduced into the system is then too large for the particles to settle at all. They accumulate at the top. As we know from shaking experiments (see also chapter 9), there is an optimal range, within which the shaking rate must be chosen to get visible segregation. While it has to be so small, that the grains can settle to the ground after each shake, it must be large enough for the interaction to take place in domains with very condensed material. The stationary states of the discrete system (2.31) with transition rates (2.50) are shown in figure 2.16 for different values of $\tilde{c}$. We used

(a) $\tilde{c} = 0.001$.

(b) $\tilde{c} = 0.02$.

(c) $\tilde{c} = 0.04$.

(d) $\tilde{c} = 0.2$.
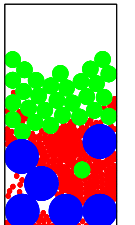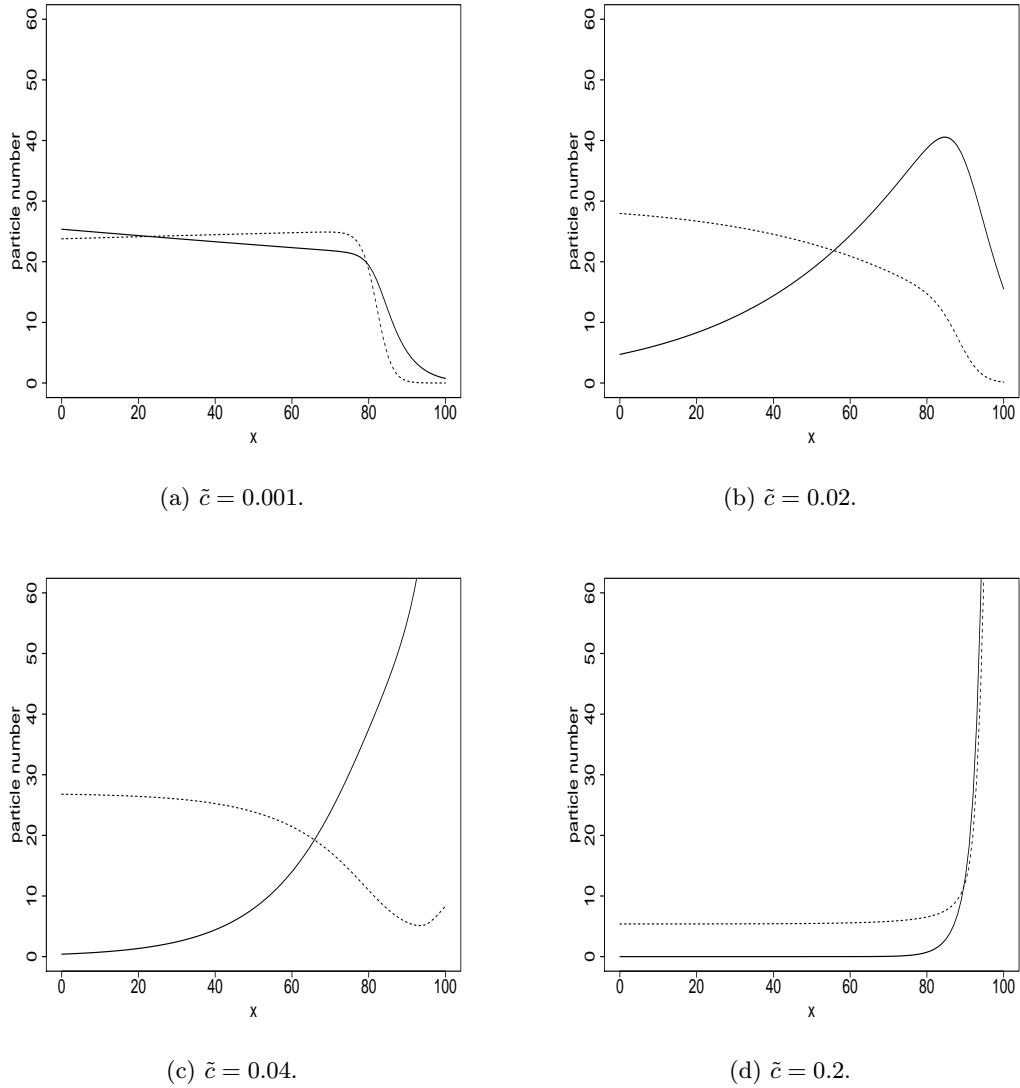
Figure 2.16: Stationary states for the Q-model, system (2.31) with the linearly decreasing volume filling functions Q, q given in (2.54), and different shaking constants $\tilde{c}$. Parameter values for all pictures are $V_N = 0.03$, $V_n = 0.01$, $\rho_N = \rho_n = 1$, $g = 10$, $\tilde{\alpha} = \tilde{\beta} = 0.4$. The solid line represents the small particles, the number of large grains is given by the dashed line.

the volume filling functions

$$
\begin{aligned}
Q(N,n) &= 1 - \frac{NV_N + nV_n}{1 - V_N}, \\
q(N,n) &= 1 - \frac{NV_N + nV_n}{1 - V_n},
\end{aligned}
\tag{2.54}
$$
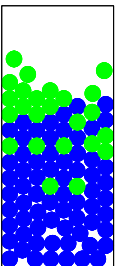
which are linearly decreasing in each argument. In fact, they represent crude linear interpolations. We will justify such volume filling functions below. As in the case $\tilde{c} = 0$, the time-dependent solutions stay non-negative:

Proposition 2.13.1 (Positivity of the Q-model.) *Consider system (2.51), (2.52) with initial functions satisfying $N(0,x), n(0,x) \geq 0$ for all $x \in [0,l]$. Then solutions stay non-negative for all time.*

Proof. Again, we refer to the proof of the general convection-diffusion problem, proposition 3.5.1, carried out in section 3.5 of chapter 3. $\square$

Finding upper bounds for N and n turns out to be more difficult. While lacking the natural upper bounds N^{max} and n^{max}, the model (2.51), (2.52) is not inconsistent. The shaking parameter $\tilde{c}$, as it appears in the equations, drives particles towards the top of the container independently of their local concentration. We therefore expect concentrations to become large especially on the right boundary $x = l$. If we assume that the upward transition rate at each location is limited by the available space above, e.g. if we replace $\tilde{c}$ by by $\tilde{c}Q_{k+1}$ and $\tilde{c}q_{k+1}$, respectively, then the resulting equations again preserve the upper bounds.

The volume filling function (2.54) giving rise to the above simulations is the result of a very crude approximation. Before we use our model to compare the behavior of different particle mixtures, we legitimate the use of linear functions Q, q. Imagine an optimal two-dimensional packing of mono-size balls with radius R (see figure 2.17(a)). While having a volume of only $R^2\pi$, each ball occupies the area of the surrounding regular hexagon, which equals $2\sqrt{3}R^2$, i.e. about $z := 1.1$ times as much. Of course, this ratio becomes larger for suboptimal packings. Suppose a cell of volume 1 were partly filled with a mixture of large balls with radius R and small balls with radius r. Then, for a large ball, the available space in the cell is

$$Q(N,n) := 1 - zNV_N - znV_n. \tag{2.55}$$

Since the small grains can also fill up the wedges between the large spheres, the available space for a small ball is

$$q(N,n) := 1 - NV_N - znV_n \tag{2.56}$$

(see also figure 2.17(b)). Hence linear functions Q and q are justified.

Within the framework of the segregation system (2.51), (2.52), we can now investigate the effects of different specific densities of the grains. We start with a bi-disperse mixture of balls with a volume ratio of $V_N/V_n = 1.5$. Both particle types have the same specific density, i.e. the mass ratio equals 1.5 as well. Using the volume filling functions (2.55), (2.56), the simulation in figure 2.18 nicely

(a) Available space for another large particle.   The triangular gaps between the grains cannot be filled.

(b) Small particles can take not only the space potentially occupied by another large particle, but also the triangular gaps left blank in between the big grains.
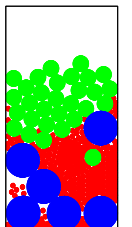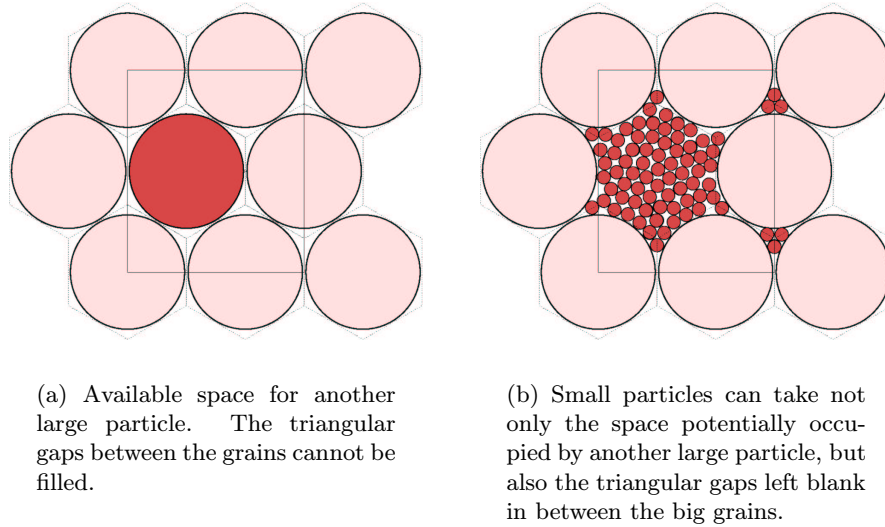
Figure 2.17: Volume filling properties of large and small particles.
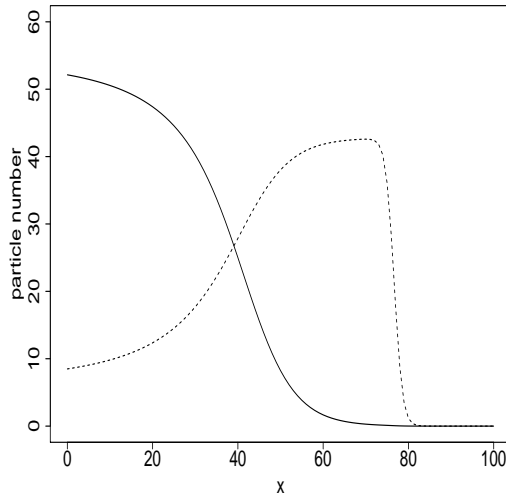
Figure 2.18: Segregation of two types of grains. We used the system of master equations (2.31) with transition rates (2.50), gravitational terms (2.46) and volume filling functions (2.55), (2.56). Parameter values are $\tilde{\alpha} = 1$, $\tilde{\beta} = 0.4$, $\tilde{c} = 0.1$, $M = 1.5$, $m = 1$, $V_N = 0.015$, $V_n = 0.01$ and $z = 10/7$. The solid line represents the small grains, while the number of the large particles is indicated by the dashed curve.

shows the compaction of the material as well as a relatively strict segregation due to the difference in size, driving the large balls to the top. If we now decrease the mass of the smaller grains, we expect that at some point the equilibrium is
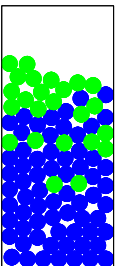
reversed and the larger, heavier particles move to the bottom. This phenomenon is shown in figure 2.19.
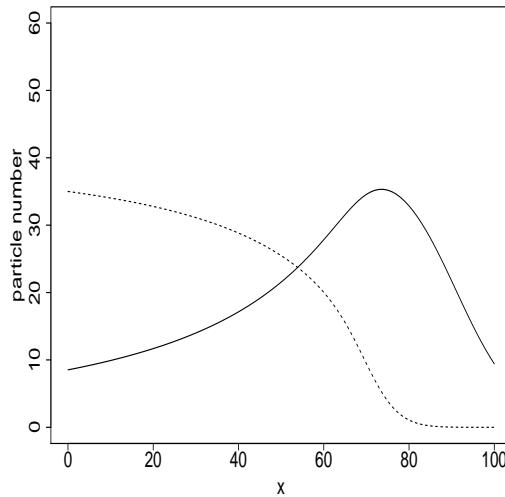
Figure 2.19: We used the same model and set of parameters as in figure 2.18, with the exception that the mass of the smaller particles was decreased from 1 to 0.3. This is enough for the segregation to reverse its direction. The larger, heavier particles (dashed line) now form the bottom layer, with the small grains (solid line) on top.

2.14   A random walk model with buoyancy effect

Before we set out to derive another model, which is apt to describe segregation of granular material without using volume filling functions as in section 2.13, we recall the physical laws governing the settling of particles in a liquid due to gravitation and buoyancy. Suppose a spherical particle of radius r made of a material with specific weight ρ is submerged in a container filled with fluid. If the fluid has a specific weight ρ_f then Stokes' settling velocity of the ball is

$$v_{\text{sett}} = \frac{2r^2 g(\rho - \rho_f)}{9\eta},$$

where g is the gravitational constant and η the viscosity of the fluid. We use the same idea in the case where the medium surrounding the spherical particle is not a fluid but a mixture of other particles of the same or other type. In this case, of course, the friction between the individual particles will prevent the grains from moving at all, unless we introduce some sort of shuffling or shaking that creates space between particles and thus enables fluctuation. Using again the basic master
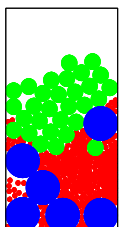
equations (2.31), we choose transition rates of the form

$$T_k^+ = \tilde{\alpha} - \tilde{\beta}G_k, \quad T_k^- = \tilde{\alpha} + \tilde{\beta}G_k,$$
$$t_k^+ = \tilde{\alpha} - \tilde{\beta}g_k, \quad t_k^- = \tilde{\alpha} + \tilde{\beta}g_k, \tag{2.57}$$

where now G_k and g_k depend on the difference in specific weight between the considered particle and the surrounding mixture of particles. Let

$$G_k = (\rho_N - \bar{\rho}_k)V_N gh,$$
$$g_k = (\rho_n - \bar{\rho}_k)V_n gh, \tag{2.58}$$

where ρ_N and ρ_n are the specific weights of the particles of type N and n, respectively. $\bar{\rho}_k$ is the mean specific weight of the N_k particles of type N and the n_k particles of type n in the kth cell. Thus, $\bar{\rho}_k = (N_k\rho_N V_N + n_k\rho_n V_n)/V^{\max}$, where $V^{\max}$ is the volume of one cell. If $\tilde{\alpha}$ and $\tilde{\beta}$ scale as $\tilde{\alpha}\Delta x^2 \equiv D$ and $\tilde{\beta}\Delta x^2 \equiv \beta$, respectively, then in the parabolic limit

$$N_t = [DN_x + 2\beta V_N gN(\rho_N - \bar{\rho})]_x,$$
$$n_t = [Dn_x + 2\beta V_n gn(\rho_n - \bar{\rho})]_x, \tag{2.59}$$

with $\bar{\rho} = (N\rho_N V_N + n\rho_n V_n)/V^{\max}$. The appropriate boundary conditions are

$$DN_x + 2\beta V_N gN(\rho_N - \bar{\rho}) = 0,$$
$$Dn_x + 2\beta V_n gn(\rho_n - \bar{\rho}) = 0 \tag{2.60}$$

at $x = 0, l$. While conservation of total mass for (2.59), (2.60) is straightforward due to the divergence form of the equations, the boundedness of the solutions requires attention. Since no physical upper bounds appear in the equations explicitly, we cannot give a priori estimates. Here, we prove the conservation of positivity.

Proposition 2.14.1 (Positivity of the buoyancy model.) *Consider the system of diffusion-convection equations (2.59) with boundary conditions (2.60). If the initial functions satisfy $N(0, x) \geq 0$, $n(0, x) \geq 0$, then the solutions stay nonnegative for all times.*

Proof. System (2.59), (2.60) is a special case of the general convection-diffusion model analyzed in chapter 3. We therefore refer to the proof of proposition 3.5.1 on page 67. $\square$.

In view of the boundary conditions (2.60), the equilibrium states of system (2.59) are solutions of

$$N' = -2\frac{\beta}{D}V_N gN(\rho_N - \bar{\rho}),$$
$$n' = -2\frac{\beta}{D}V_n gn(\rho_n - \bar{\rho}),$$
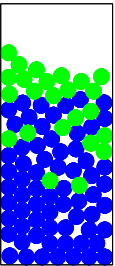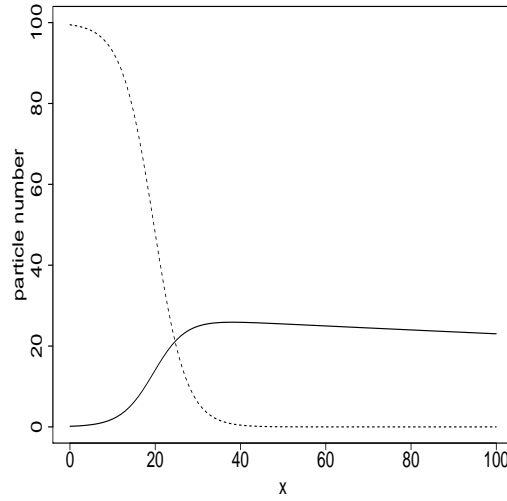
Figure 2.20: The stationary states of the discrete system (2.31) with transition rates (2.57) and gravitational terms (2.58). Parameter values are $\tilde{\alpha} = 0.3$, $\tilde{\beta} = 0.4$, $\rho_N = 1$, $\rho_n = 0.01$ and $V_N = V_n = 0.01$. Segregation due to the difference in specific weight takes place. The solid line represents the small particles, the dashed curve the large ones.

which are typically non-monotone functions of the shape shown in figure 2.20. Hence, the ρ-model discussed in this section, as the Q-model in section 2.13, exhibits segregation of granular material.

2.15 On competitive systems and stationary solutions

The stationary solutions of both the Q-model in section 2.13 and the buoyance model in section 2.14 are solutions of a system of ordinary differential equations of the form

$$\begin{aligned} \dot{u} &= u(\gamma - \beta_1 u - \beta_2 v), \\ \dot{v} &= v(\delta - \beta_1 u - \beta_2 v), \end{aligned} \tag{2.61}$$

where γ, δ, β_1 and β_2 are positive constants. The derivative is taken with respect to the variable x. The vector (N, n) designating particle numbers in sections 2.13 and 2.14 is replaced by the general notation (u, v). System (2.61) represents a Lotka-Volterra competition model (see for example [Murray93]). Its nullclines, given by $\beta_1 u + \beta_2 v = \gamma$ and $\beta_1 u + \beta_2 v = \delta$, respectively, are parallel straight lines (see figure 2.21), hence, the only equilibria lie on the axes. A coexistence point does not exist. In two dimensions, we can derive some interesting properties of the stationary states of the original segregation models, (2.51), (2.52) and (2.59), (2.60).
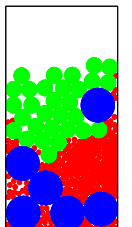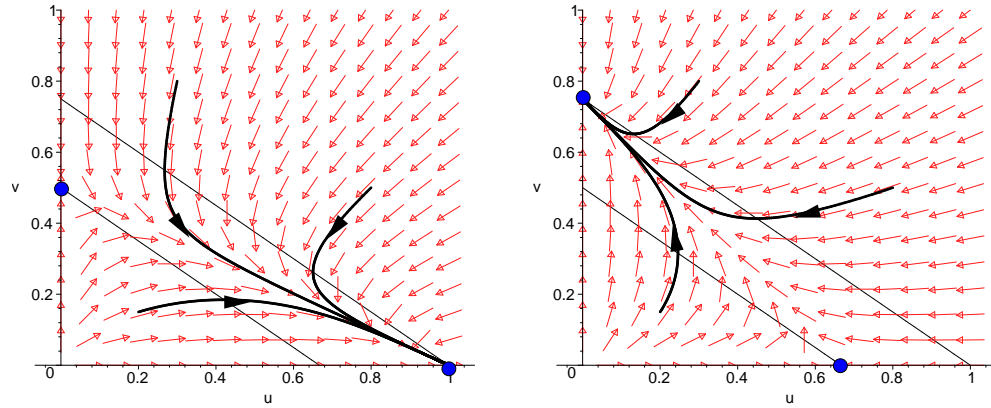
(a) The nullclines and some typical tra-
jectories of system (2.61) in the case
$\gamma > \delta$. Parameter values are $\gamma = 3$,
$\delta = 2$, $\beta_1 = 3$ and $\beta_2 = 4$.

(b) Nullclines and trajectories of the
same system, only this time with $\gamma = 2$
and $\delta = 3$.

Figure 2.21: Simulation of some typical solutions of system (2.61) for different sets of
parameters.

Proposition 2.15.1 (Invariance and monotonicity of competitive systems.)
*(I) The open positive cone $C := \{(u,v) \in I\!R^2 \mid u, v > 0\}$, as well as the two axes,
are invariant under solutions of system (2.61).*
*(II) Furthermore, any solution exhibits at most one sign change of the derivative.
In other words, only one of the following four cases is possible:*
(i) N and n are both strictly increasing.
(ii) N and n are both strictly decreasing.
*(iii) One of the two components is strictly increasing, the other one strictly de-
creasing.*
*(iv) One of the two components is strictly monotone (increasing or decreasing),
the other one exhibits exactly one local extremum in the open interval $(0, l)$.*

We point out that case (i) is unphysical when the solutions describe particle
concentrations in a vertical container. The interesting case is (iv), since it
describes segregation.

Proof. (I) The invariance of the axes and the cone C is straightforward due to
the form of the equations.
(II) If we restrict to the open set C, the Jacobian

$$
J = \begin{pmatrix} \gamma - 2\beta_1 u - \beta_2 v & -\beta_2 u \\ -\beta_1 v & \delta - 2\beta_1 u - \beta_2 v \end{pmatrix}
$$
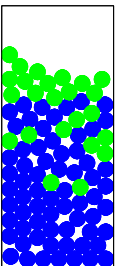
is a competitive matrix, since its off-diagonal entries are both strictly negative. (For an overview on cooperative and competitive systems, we refer to [Smith95].) Part (II) thus follows from [Smith95], proposition 2.1 on page 34. □.

In the following, we discuss the existence of stationary solutions of the Q-model and of the buoyancy model, i.e. solutions of (2.61), for a given total mass proportion of the two species. Therefore, write the system (2.61) as

$$\dot{z}(t) = g(z(t)),$$

and let G be the solution operator,

$$\frac{d}{dt}G(t,z) = g(G(t,z)),$$
$$G(0,z) = z,$$

for $z = (u,v)^T \in \bar{C}$, $t \geq 0$. The vector of relative total masses $\bar{z}$ is then defined by

$$\int_0^l G(t,z)dt = \bar{z}l$$

for a given container height l. Define the total mass operator $H : [0,\infty) \times \mathbb{R}^2 \longrightarrow \mathbb{R}^2$ by

$$H(l,z) := \frac{1}{l}\int_0^l G(s,z)ds, \qquad (2.62)$$
$$H(0,z) := z.$$

H is continuous and maps $[0,\infty) \times \bar{C}$ into $\bar{C}$, where the axes are again invariant due to proposition 2.15.1, part (I). Note that $H(0,\cdot)$ is the identity. In chapter 3, we will show that in the case of a slightly different system of convection-diffusion equations, stationary solutions exist for any given container height and for any given vector $\bar{z}$ of relative total masses (see theorem 3.5.2 in section 3.5). In the present case, i.e. for systems (2.51), (2.52) and (2.59), (2.60), this is not true in general.

Proposition 2.15.2 (Non-existence of stationary states.)
(I) Let $\bar{z} \in C$ be given. Then there exists a container height l^*, for which $H(l^*,z) \neq \bar{z}$ for all $z \in \bar{C}$.
(II) Let a container height $l > 0$ be given. Then there exists a vector $\bar{z}$ of relative total masses, which is not realized by $H(l,\cdot)$. In other words, $H(l,z) \neq \bar{z}$ for all $z \in \bar{C}$.

Proof. (I) For any set of parameters, system (2.61) has exactly one stable equilibrium E on one of the two axes, and its domain of attraction is all of C (see [Murray93], section 3.5, page 80/81). Let $\bar{z} \in C$ and choose a small open ball B_r
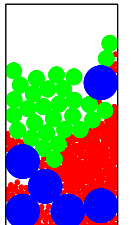
of radius $r > 0$ around E, such that $\bar{z} \notin B_r$. Denote by $B_{r/2}$ the ball of radius $r/2$ around E. Let $z \in C$. Since E attracts all trajectories, there is a $t_1 > 0$ such that $G(t, z) \in B_{r/2}$ for all $t > t_1$. Choose $t_2 > 2t_1 |\|z\| - r|/r$, where $\| \cdot \|$ designates the Euclidean norm in $\mathbb{R}^2$. Then $t_1\|z\| + t_2 r/2 < r(t_1 + t_2)$, i.e. for $l^* := \max\{t_1 + t_2, 1\}$, we have $\|H(t^*, z)\| < r$. Hence, the vector $\bar{z}$ is not realized by $H(l^*, \cdot)$. This proves part (I).

(II) We first argue on one of the axes and then carry forward the argument to the interior C by continuity. Without loss of generality, let $\bar{z}$ be on the u-axis. Since $H(l, C) \subseteq C$ and both axes are invariant respectively, we have to look for a point z on the u-axis such that $H(l, z) = \bar{z}$. Since $v = 0$ in $\bar{z}$, system (2.61) reduces to

$$\dot{u} = u(\gamma - \beta_1 u), \tag{2.63}$$

the solution of which is

$$u(x) = \frac{1}{\left(\frac{1}{u_0} - \frac{\beta_1}{\gamma}\right)e^{-\gamma x} + \frac{\beta_1}{\gamma}}. \tag{2.64}$$

In case the trajectory starts below the equilibrium, i.e. if $u_0 < \gamma/\beta_1$, the function (2.64) is defined for all positive and negative values of x. However, if $u_0 > \gamma/\beta_1$, then (2.64) explodes at $x^* := \ln\left(1 - \gamma/(\beta_1 u_0)\right)/\gamma < 0$. Note that $x^* \longrightarrow 0$ for $u_0 \longrightarrow \infty$. For the given container height $l > 0$, choose $\bar{u}$ such that $|x^*| < l/2$. Then, the solution (2.64) of (2.63) can only be traced backward in x over an interval of length less than half the container height for any starting point $u_0 > \bar{u}$. This is equivalent to saying, that every solution of system (2.61) starting at a point $z = (u_0, 0)^T$ on the u-axis spends more than half the time below $\bar{u}$, and hence, the first component of $H(l, z)$ is less than $\bar{u}$. We have thus proven part (II) of proposition 2.15.2 for $\bar{z} = (\bar{u}, 0)^T$ on the u-axis. Since H is continuous in particular with respect to its second argument z, we can generalize the result to points $\bar{z} \in C$ close to the axis. This completes the proof of proposition 2.15.2. $\square$.

We point out, that the previous proof crucially depends on the fact that the local particle concentrations are not a priori bounded from above. In particular, they do not always add up to a constant. In chapter 3, we will analyze a system of convection-diffusion equations, for which concentrations always add up to one. This is equivalent to saying, that one species is designated the role of a *medium*, like a fluid or air, in which the other species move and which fills up all the gaps in between the grains. In that case, we are able to show, that stationary states exist for any given total mass distribution.

Even though solutions of system (2.61) do not exist for any given total mass distribution, as shown in proposition 2.15.2, the solutions are unique when they exist:
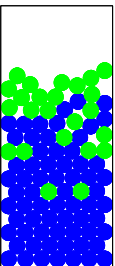
Theorem 2.15.3 (Uniqueness of stationary states.) *Let the competitive Lotka-Volterra system (2.61) with strictly positive constants γ, δ, β_1 and β_2 be given, and consider the total mass operator $H : [0,\infty) \times I\!R^2 \longrightarrow I\!R^2$ defined in (2.62). If for a given container height $l > 0$ and a given vector $\bar{z}$ in the positive cone C, the equation*

$$H(l, z) = \bar{z} \tag{2.65}$$

has a solution $z \in C$, then this solution is unique. In other words, for a given total mass distribution, there is at most one corresponding stationary state.

Proof. In order to prove uniqueness, we give the explicit solution of (2.61) and use the monotonicity of the mapping H. Verify that

$$
\begin{aligned}
u(x) &= u_0 e^{\gamma x} \frac{\delta \gamma}{Z(x)}, \\
v(x) &= v_0 e^{\delta x} \frac{\delta \gamma}{Z(x)}
\end{aligned}
\tag{2.66}
$$

solves system (2.61) for

$$Z(x) = v_0 \gamma \beta_2 \left(e^{\delta x} - 1 \right) + u_o \delta \beta_1 \left(e^{\gamma x} - 1 \right) + \delta \gamma,$$

where (u_0, v_0) designates the initial point, i.e. in terms of the particle models of sections 2.13 and 2.14 the vector of concentrations at the bottom of the vessel. Now, with $z := (u_0, v_0)$, the two components of H have the form

$$
\begin{aligned}
H_1(l, z) &= \frac{1}{l} \int_0^l u_0 e^{\gamma x} \frac{\delta \gamma}{Z(x)} dx, \\
H_2(l, z) &= \frac{1}{l} \int_0^l v_0 e^{\delta x} \frac{\delta \gamma}{Z(x)} dx
\end{aligned}
$$

for $l > 0$. For $l > 0$, the derivatives of H are

$$
\begin{aligned}
\frac{\partial}{\partial u_0} H_1 &= \frac{\delta \gamma^2}{u_0^2 l} \int_0^l \frac{e^{\gamma x}}{Z^2} \left[\beta_2 v_0 \left(e^{\delta x} - 1 \right) + d \right] dx, \\
\frac{\partial}{\partial u_0} H_2 &= \frac{\delta \gamma^2 v_0}{u_0^3 l} \int_0^l \frac{e^{\delta x}}{Z^2} \left[\beta_2 v_0 \left(e^{\delta x} - 1 \right) + d \right] dx - \frac{\delta \gamma v_0}{u_0^2 l} \int_0^l \frac{e^{\delta x}}{Z} dx \\
&= -\frac{\delta \gamma v_0}{u_0^2 l} \int_0^l \frac{e^{\delta x}}{Z^2} \left[\delta \beta_1 \left(e^{\gamma x} - 1 \right) + \frac{\delta \gamma}{u_0} \right] dx, \\
\frac{\partial}{\partial v_0} H_1 &= -\frac{\delta \gamma^2 \beta_2}{u_0 l} \int_0^l \frac{e^{\gamma x}}{Z^2} \left(e^{\delta x} - 1 \right) dx, \\
\frac{\partial}{\partial v_0} H_2 &= \frac{\delta \gamma}{u_0 l} \int_0^l \frac{e^{\delta x}}{Z} dx - \frac{\delta \gamma^2 \beta_2 v_0}{u_0^2 l} \int_0^l \frac{e^{\delta x}}{Z^2} \left(e^{\delta x} - 1 \right) dx \\
&= \frac{\delta^2 \gamma}{u_0 l} \int_0^l \frac{e^{\delta x}}{Z^2} \left[\beta_1 \left(e^{\gamma x} - 1 \right) + \gamma \right] dx,
\end{aligned}
$$
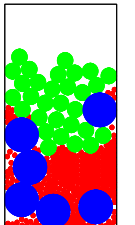
i.e. the Jacobian has positive diagonal and negative off-diagonal elements. Straightforward calculation yields the Jacobian determinant

$$
\begin{aligned}
\det J_H = & \frac{\delta^4 \gamma^3 \beta_1}{u_0^3 l^2} \left(\int_0^l \frac{e^{\gamma x}}{Z^2} \right) \left(\int_0^l \frac{e^{\delta x} \left(e^{\gamma x} - 1 \right)}{Z^2} \right) + \\
& + \frac{\delta^4 \gamma^4}{u_0^4 l^2} \left(\int_0^l \frac{e^{\gamma x}}{Z^2} \right) \left(\int_0^l \frac{e^{\delta x}}{Z^2} \right) + \\
& + \frac{\delta^3 \gamma^4 \beta_2 v_0}{u_0^4 l^2} \left(\int_0^l \frac{e^{\delta x}}{Z^2} \right) \left(\int_0^l \frac{e^{\gamma x} \left(e^{\delta x} - 1 \right)}{Z^2} \right).
\end{aligned}
$$

For $l > 0$, this expression is always strictly positive. Hence, all principal minors of J_H are strictly positive, and the Jacobian is a so-called *P-matrix* (see e.g. [Gale65]). Suppose for some given $l > 0$ and a given vector $\bar{z} \in C$ of relative total masses, the equation (2.65) has two distinct solutions $z_1 \neq z_2 \in C$. Choose a rectangular region $R \ni z_1, z_2$, the sides of which are parallel to the u- and v-axis, respectively. On such a rectangle, the P-matrix J_H is univalent (see theorem 4 of [Gale65]), which is a contradiction. This completes the proof of theorem 2.15.3. □.

2.16   The potential energy and the shaking process

Reconsider the basic model (2.34) describing the compaction for a single particle type. From a heuristic point of view, it is evident that the compaction process gradually reduces the potential energy of the particles in the vessel up to a certain experimental minimum (even though the theoretical optimal packing can never be reached in practice; see also [Aste00], [deLarrard99]). Surprisingly, the situation is different in the case of several mixing particle types. Imagine a material composed of small and big grains of the same (for example spherical) shape. If the specific weight of both grain types is the same, we observe that during the shaking process, the large particles tend to move up and form a uniform layer on top of the small grains. This *Brazil nut* effect is reproduced by our particle simulations in chapter 8 and the experiments described in chapter 9. Figure 2.22 shows two different levels of compaction for the same material composition. Clearly, the fill level in subfigure (a), which represents the completely segregated limit state, is higher, and thus the overall potential energy is larger than in the mixed state in subfigure (b). Now, we gradually increase the specific weight of the large balls. At some point, we will have reached a situation in which the two effects, the buoyancy driving large grains up and the gravitation favoring a downward movement of heavy particles, balance each other. Before we reach this equilibrium configuration, we can make heavy grains move up by shaking the container. This energy paradox could be explained as follows: The Brazil nut effect is commonly explained by the fact that the gaps between large particles can be filled by small ones, while small grains rarely create gaps big enough for a big grain to fit in. In a polydisperse particle
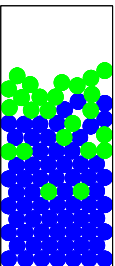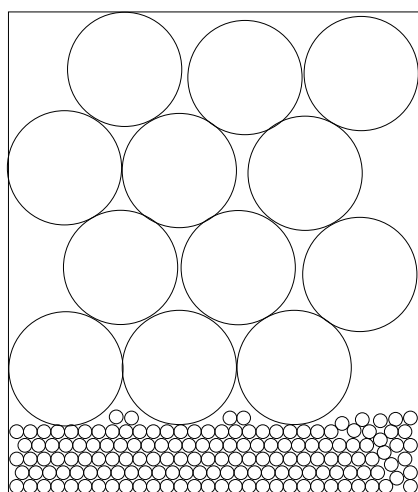
(a) Complete segregation, the theoretical equilibrium state of a shaking experiment.
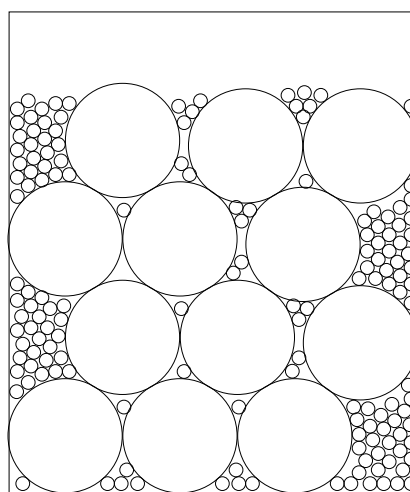
(b) Mixed states are much denser and energetically favorable. The fill level is lower.

Figure 2.22: Sketch of two energetically different limit states.

mixture, this disparity creates a *ratchet* effect. The energy introduced by the shaking lifts the heavy, large grains onto a higher level, while their way down is blocked. In chapter 8, we illustrate this ratchet effect by simulations tracking the overall potential energy of the system along trajectories.
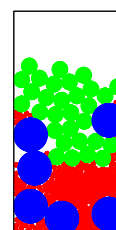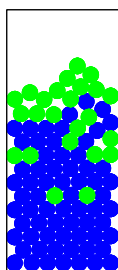
Chapter 3

Segregation of granular material by diffusion and convection

Summary. We use a convection-diffusion equation to model segregation within a mixture of particles of different size, shape or surface structure in a vertical vessel. Convection describes competition between species on a vertical scale, whereas random noise (shaking) allows particles to exchange positions. For two species, it is shown that the solutions converge to a unique distribution along the vertical scale. For more than two species, at least one equilibrium distribution exists (there are examples with multiple equilibria). For a class of models with simple competition laws, uniqueness of the equilibrium is shown for any number of species.

3.1 Introduction

The Brazil nut effect is a well-known phenomenon in granular media: A mixture of two kinds of grains which differ in size is filled into a vertical (glass) cylinder and then stirred or shaken. The bigger grains tend to move up. In some sense the smaller particles fall between the gaps of the bigger ones. If the grains differ also in specific weight, shape, coarseness of the surface etc., or if more than two kinds of grains are used, then the behavior may become more complex. It seems that there are not too many experimental results on segregation with more than two kinds or a continuous distribution of grain sizes.

However, the case of two types of particles has been studied by several authors. In [Hong01], [Lätzel00], [Luding96.1], [Luding97], [Luding98], [Luding99] and [Luding01], the particles are modeled as hard spheres. In [Lätzel00] and [Luding97] qualitative features of the material are derived from laws for the
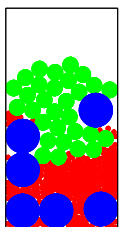
contacts between individual particles. In [Luding98] and [Luding99] a cooling process is used to describe segregation, whereas in [Luding96.1] pattern formation caused by vibration is investigated. [Hong01] and [Luding01] analyze percolation and condensation effects in granular material with both varying size and specific density. In [Rosato87] an adaptation of the Monte Carlo cooling method is used to analyze size segregation that occurs by shaking mixtures of two types of grains. Cellular automaton models are used in [Anderson93], [Cizeau99], [Makse97.2] and [Makse98.1] to study stratification and pattern formation in poured mixtures. In [Boutreux99], [Gray98], [Makse97.1], [Makse97.3] and [Makse99.1] continuum models are used to explain segregation in surface flows and flowing avalanches, i.e. so-called *kinetic sieving*. In [Karolyi98] experiments and theory are compared with respect to surface flows in 2D silos, and in [Makse98.2], stratification is studied experimentally. [Gray97], [Makse99.2] and [Ristow99] deal with segregation and pattern formation in rotating drums. Finally, [Duran93], [Farkas02], [Pöschel95] and [Wambaugh02] study microscopic phenomena, such as the so-called *ratchet* effect, the formation of convection cells in vibrating mixtures and local disruptions in the structure of granular material giving rise to global effects, which favor or accelerate segregation.

Since the details of the interactions between several kinds of particles will differ widely and are also not generally known, we propose a heuristic model based on *diffusion* and *convection*, i.e. the model has the form of a convection-diffusion system. The idea is that the different species *compete* with each other for an appropriate position on a vertical scale via different convection rates and that random noise gives sufficient freedom for grains to pass between other grains.

The model studied in this chapter is unrealistic insofar as we assume that the proportion of empty space is constant throughout the vessel independently of the composition of the material. Hence we do not allow for compaction. Thus, the system should be seen as our first attempt towards a general model for segregation.

In section 3.2 we describe the model system and we introduce the necessary invariance and conservation properties. In section 3.3 we show, that in the case of two species, there is a unique stationary distribution of grains which depends only on the initial total masses of the two species. This stationary solution is globally stable, i.e. for any initial distribution within the vessel (given the total masses) the solution of the convection-diffusion system will approach this equilibrium. In section 3.5 the case of more than two species is studied. We show that for any set of total masses there is at least one equilibrium solution. Simple examples with three species show that the equilibrium may not be unique. In section 3.8, we study a special model for n species with a simple competition law, the so-called *replicator equation* with linear fitness. Here we can prove uniqueness. Section 3.9 treats a more general type of replicator equations, for which uniqueness does not necessarily hold. Model refinements and particle simulations are deferred to
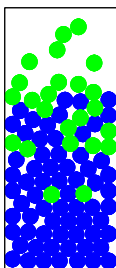
sections 3.10 and 3.11, respectively.

3.2 The model

Following the simple experimental setup described in chapter 2, we consider a vessel in the form of a vertical cylinder of height l. Assuming that the distribution of the material is homogeneous in horizontal direction, we simplify the physical setup to a one-dimensional model. Hence, the container is represented by the interval $\Omega := [0, l]$, where $x = 0$ corresponds to the bottom and $x = l$ to the top. We assume there are n types or species of particles numbered $i = 1, \ldots, n$. Let $u_i(t, x)$ be the density of the ith species at level x and time t. We collect these into a vector $u = (u_1, ..., u_n)^T$. Here u is a column vector, the symbol ^{T} means transpose. We assume that the motion of particles in vertical direction, caused by shaking and the influence of gravity, can be described by diffusion and convection. Diffusion is a random (*Brownian*) undirected motion, convection is directed and depends strongly on the types of interacting particles and their relative frequencies. We understand the model in such a way, that the diffusion term accounts for the random effects of shaking that provides space for convective motion. The convection term incorporates effects of friction of grains and of small grains falling into the gaps between large grains ([Gray98], [Barker90]). Hence the model assumes the general form of a system of convection-diffusion equations. We underline that this is a standard form of model that should be applied when a more detailed description (transport equation, Boltzmann equation, particle model) is not available or not applicable for lack of estimates for experimental parameters. In fact, for many macroscopic models, convection-diffusion equations occur as limiting cases for rapid microscopic motion and frequent changes of direction. The model must be written in divergence form because of conservation of mass.

Our final equation governing the changes in relative particle densities thus assumes the general form
$$u_{it} = (D_i(u)u_{ix} - f_i(u))_x$$
for $i = 1, \ldots, n$. We assume that the functions D_i and f_i are twice continuously differentiable. We collect the diffusion coefficients into a diagonal matrix $D(u) = (D_i(u)\delta_{ij})$ and we interpret the functions $f_i(u)$ as components of a vector field $f(u) = (f_i(u))$. We also will use later the vector of all 1's, $e^T = (1, \ldots, 1)$. In vector notation the system assumes the form

$$u_t = (D(u)u_x - f(u))_x. \tag{3.1}$$

The model does not account for empty space between grains. It is tacitly assumed that the grains fill the volume completely or, equivalently, that empty space is evenly distributed throughout the vessel whatever the distribution of species is.
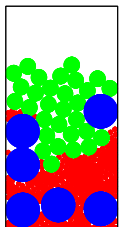
Although this assumption is not realistic, the model is a first step in the study of mixtures. More complex models would allow for variable distributions of empty space and hence also for compaction effects.

At first glance, one might try to give one of the n species forming the granular material the role of the suspension medium or the empty space, thus granting it essentially the same qualities as the other ones, which are composed of actual particles. But this straightforward approach is not very realistic. Since the medium has to be able to fill the gaps in between the grains, whatever their size is, we would have to assume that the imaginary *particles* composing the medium are infinitely small. But this contradicts the fact that the medium is displaced step by step by the real particles moving down in the cylinder during the sedimentation process. Very small grains, on the contrary, would seep through the granular material and gather at the bottom of the container.

In order to face the problem of this special role of the medium, we will follow two different approaches in chapter 5, thus interpreting the particle densities or settling velocities as being measured relative to those of the surrounding medium.

At this point, we would like to emphasize the general nature of equation (3.1). Besides the physical context described above, a biological interpretation could be of some importance, when it comes to modeling interaction between living species. Instead of considering small grains driven by gravitation and *competing* for the most *privileged* space in the topmost layers of the granular material, we imagine biological species being in competition with each other for some vital quality. The latter could be a food source, a desirable temperature or a favored habitat, but also light in the case of submerged algae (see for example [Wörz-Busekros76] or [Radach74]). The species adapt more or less efficiently to the environmental situation and other competing species or predators. The term *competition*, widely used to describe interaction between species in general, finds its original meaning in this biological interpretation. Here, the function f in equation (3.1) incorporates all interactions between the populations, while $D = D(u)$ is again a diffusion matrix allowing for random movement of the individuals.

The system (3.1) must be supplied with boundary conditions. As we shall see in a moment, the requirement of conservation of total mass for each species determines the boundary condition uniquely. We require

$$D(u)u_x - f(u) = 0 \tag{3.2}$$

at $x = 0, l$. In order for the model to be realistic, we have to impose two further requirements.
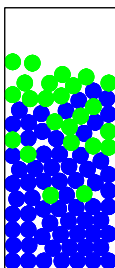
(i) The particle densities u_i are non-negative.

(ii) At each space point x and time t the particle densities add up to 1.

For these requirements to be fulfilled, the following assumptions on the diffusion rates and the vector field are sufficient and also necessary.

(a) The diffusion rates (which may depend on the vector u of densities) are the same for all species, i.e. the diffusion matrix $D(u)$ is a multiple $d(u)I$ of the identity matrix.

(b) The diffusion rate is positive, $d(u) > 0$.

(c) $e^T f(u) = \sum_{i=1}^n f_i(u) \equiv 0$.

(d) $u_i = 0$ implies $f_i(u) = 0$.

(e) $\partial f_i / \partial u_j|_{u_i=0} = 0$ for $i \neq j$.

With these hypotheses the system and the boundary condition read

$$u_t = (d(u)u_x - f(u))_x \,, \tag{3.3}$$

$$d(u)u_x - f(u) = 0 \tag{3.4}$$

at $x = 0, l$. The positivity of the diffusion coefficient (condition (b)) is just the standard condition which ensures that diffusion is not degenerate.

Proposition 3.2.1 (Conservation of total mass and constant sum.) *All solutions of system (3.3), (3.4) conserve the total mass of each one of the species in the vessel. Furthermore, condition (c) above guarantees that the particle densities add up to one at every point x.*

Proof. From the differential equation (3.3) and the boundary condition (3.4) we get

$$\begin{aligned} \frac{d}{dt} \int_0^l u\,dx &= \int_0^l [D(u)u_x - f(u)]_x \, dx \\ &= [D(u)u_x - f(u)]|_0^l \\ &= 0. \end{aligned} \tag{3.5}$$

Hence total mass is preserved.

Next, in view of (3.3), (3.4) and hypothesis (c), the scalar function $e^T u$ satisfies the diffusion equation

$$(e^T u)_t = e^T u_t = \left(d(u)(e^T u)_x\right)_x \tag{3.6}$$

and the boundary condition

$$(e^T u)_x(0) = (e^T u)_x(l) = 0. \tag{3.7}$$
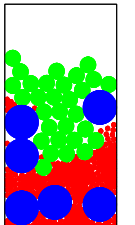
We have $e^T u^0(x) \equiv 1$. Hence, both the given function u and the function which is uniformly equal to one satisfy the differential equation and the boundary condition, and therefore they are identical, $e^T u(t, x) \equiv 1$. This shows that everywhere masses add up to one. $\square$.

We close this section with the subject of global existence of solutions.

Theorem 3.2.2 (Global existence of the time-dependent solution.) *Under the hypotheses stated above, i.e. in particular if f is at least twice continuously differentiable and if the diffusion matrix $D(u) = (D_i(u)\delta_{ij})$ is diagonal, then the solutions of system (3.1) with boundary condition (3.2) exist globally in time.*

Proof. The spadework for our proof was done by H. Amann, who intensively studied the conditions for local and global existence of solutions to quasi-linear parabolic systems. We refer to [Amann89], theorem 3, and show in the following that the necessary conditions are satisfied. First of all, with $a_{jk}(\cdot, t, u) = D(u)$ in definition (0.9) of Amann's paper being a diagonal matrix, and for $b_0(\cdot, t, u) = \text{diag}(f_1(u), \ldots, f_n(u))$ and $\delta = 1$ in definition (0.10), system (3.1), (3.2) qualifies as a *normally elliptic boundary value problem* in the sense of [Amann89]. The triangularity conditions (0.16) through (0.18) simply reduce to the diagonality of $D(u)$, since the domain Ω is one-dimensional in our case, i.e. since $m = 1$ in theorem 3 of [Amann89]. In condition (0.20), we can choose $\lambda = 1$ and $d(z) := \max\{\|f'(u)\|, 1\}$, where $\|\cdot\|$ designates the spectral norm of the matrix. Finally, the solution u is trivially bounded away from $\partial \mathcal{G}$, since f is defined globally. With the boundedness of the solutions guaranteed by proposition 3.5.1 in section 3.5, the global existence follows. $\square$

3.3   The case of two species

In the case of two species we can, in view of $e^T u = 1$, put $u_1 = u$, $u_2 = 1 - u$ and $f_1(u_1, u_2) = f_1(u, 1 - u) = f(u)$. Then we get the scalar convection-diffusion equation

$$u_t = (d(u)u_x - f(u))_x \tag{3.8}$$

with the boundary condition

$$d(u)u_x - f(u) = 0 \tag{3.9}$$

at $x = 0, l$. As in the general case, we require conditions (a) through (e) above. In the case $n = 2$ these assume the following simpler form:

(a),(b) $d(u) > 0$.
(c) says that $f_2 = -f_1$, hence becomes redundant.
(d) $f(0) = f(1) = 0$.
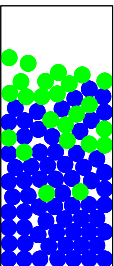
(e) is a consequence of (d) for $n = 2$.

Besides the conservation of the total mass of the grains in the container stated in proposition 3.2.1, the positivity of the solutions is a desirable property of systems modeling the variation of physical densities. The following proposition establishes this fact for scalar equations of the form (3.8) with boundary conditions (3.9).

Proposition 3.3.1 (Positivity in the scalar case.) *Consider system (3.8), (3.9). If the initial density distribution satisfies $u(0, x) \geq 0$ for all $x \in [0, l]$, then positivity is preserved for all time.*

There is a well-developed machinery for maximum and comparison theorems for parabolic equations and for getting strict inequalities from weak inequalities by using comparison functions (see [Walter70], [Prottere84] or [Friedman64]). It appears that the results in these monographs apply only to standard Dirichlet or Neumann conditions or to boundary conditions of the third kind with strong monotonicity properties. For our type of boundary condition, we have to use a specially designed comparison function and some local estimates.

Proof. Let D be a positive constant which will be specified later and define $b := f'(0)/D - 1$, $a := 1/l$. Then $b + 1 = f'(0)/D = 2al + b - 1$ holds. Furthermore, define the function
$$\rho(x) = e^{ax^2 + bx}.$$
Then $\rho'(x) = (2ax + b)\rho(x)$ and $\rho''(x) = \rho(x)[2a + (2ax + b)^2]$. It is straightforward to check that
$$\frac{f'(0)}{D}\rho(0) - \rho'(0) = \frac{f'(0)}{D} - b = 1 \tag{3.10}$$
and
$$-\frac{f'(0)}{D}\rho(l) + \rho'(l) = e^{al^2 + bl}. \tag{3.11}$$

Consider a time horizon $T > 0$. Since we investigate the solution u in the neighborhood of zero, we may restrict to small absolute values without loss of generality. Thus, we define
$$M := \sup_{\xi \in (-1, 1)} |f''(\xi)|.$$
Let u be a fixed solution of problem (3.8), (3.9) and choose κ be so large, that
$$|d(u)\rho''(x)| \leq \frac{1}{4}\kappa\rho(x), \tag{3.12}$$
$$|f'(u)\rho'(x)| \leq \frac{1}{4}\kappa\rho(x). \tag{3.13}$$

This is possible, if we again restrict u to take values in the interval $(-1, 1)$. Now choose $\epsilon > 0$ so small, that
$$\epsilon|d'(u)\rho'^2(x)e^{\kappa T}| \leq \frac{1}{4}\kappa\rho(x), \tag{3.14}$$
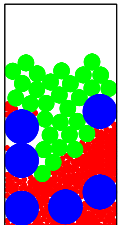
$$\epsilon < \frac{1}{M} e^{-\kappa T - 2al^2 - 2bl}. \tag{3.15}$$

Define the family of functions (with parameters κ and ϵ) $v(t,x) := -\epsilon\rho(x)e^{\kappa t}$ with derivatives $v_t(t,x) = -\epsilon\kappa\rho(x)e^{\kappa t}$, $v_x(t,x) = -\epsilon\rho'(x)e^{\kappa t}$ and $v_{xx}(t,x) = -\epsilon\rho''(x)e^{\kappa t}$. Assume $u - v$ reaches zero from above at (t_0, x_0) for some positive ϵ, κ. Suppose $x_0 \in (0, l)$. At this point, we have $(u - v)_x = 0$, $(u - v)_{xx} \geq 0$ and $(u - v)_t \leq 0$. The latter is due to the fact that $u - v$ has strictly negative time-derivative in some neighborhood around (t_0, x_0) (otherwise $u - v$ would not have touched zero). Then,

$$\begin{aligned}
0 &\geq (u - v)_t \\
&= d'(u)u_x^2 + d(u)u_{xx} - f'(u)u_x + \epsilon\kappa\rho(x)e^{\kappa t} \\
&= d'(u)v_x^2 + d(u)u_{xx} - f'(u)v_x + \epsilon\kappa\rho(x)e^{\kappa t} \\
&\geq d'(u)v_x^2 + d(u)v_{xx} - f'(u)v_x + \epsilon\kappa\rho(x)e^{\kappa t} \\
&= d'(u)\epsilon^2\rho'^2(x)e^{2\kappa t} - d(u)\epsilon\rho''(x)e^{\kappa t} + f'(u)\epsilon\rho'(x)e^{\kappa t} + \epsilon\kappa\rho(x)e^{\kappa t} \\
&= \epsilon e^{\kappa t}[d'(u)\epsilon\rho'^2(x)e^{\kappa t} - d(u)\rho''(x) + f'(u)\rho'(x) + \kappa\rho(x)] \\
&\geq \epsilon e^{\kappa t}(\kappa\rho(x)/4) \\
&> 0,
\end{aligned}$$

which is a contradiction. Assume $x_0 = 0$ or $x_0 = l$. There, we have

$$\begin{aligned}
(u - v)_x &= \frac{f(u)}{d(u)} + \epsilon\rho'(x)e^{\kappa t} \\
&= \frac{1}{d(u)}f(-\epsilon\rho(x)e^{\kappa t}) + \epsilon\rho'(x)e^{\kappa t} \\
&= \epsilon e^{\kappa t}\left[\frac{1}{d(u)}\left(-f'(0)\rho(x) + \frac{\epsilon}{2}\rho^2(x)e^{\kappa t}f''(\xi_{x_0})\right) + \rho'(x)\right],
\end{aligned}$$

where ξ_{x_0} is a constant depending on whether $x_0 = 0$ or $x_0 = l$ (Taylor formula). Here, we use $u = v$ at x_0. At this point, the choice of the constant D enters. First consider the case $x_0 = 0$. Let $D := d(u(t_0, 0))$. Thus, according to the preliminary definitions, $f'(0)\rho(0)/D - \rho'(0) = 1$ and therefore, if ϵ is small enough then $(u - v)_x < 0$. Again, we have a contradiction since if $u - v$ is zero for the first time then we must have $(u - v)_x(0) \geq 0$. Now let $x_0 = l$. If we choose $D := d(u(t_0, l))$ then $-f'(0)\rho(l)/D + \rho'(l) = e^{al^2 + bl}$ and thus

$$(u - v)_x = \epsilon e^{\kappa t}\left[e^{al^2 + bl} + \frac{\epsilon}{2D}\rho^2(l)e^{\kappa t}f''(\xi_l)\right].$$

The first term in brackets is greater than 1, whereas the absolute value of the second term is at most $\rho^2(l)e^{-2al^2 - 2bl}/2$, i.e. always less than $1/2$. This means $(u - v)_x(l) > 0$, which is a contradiction since $u - v$ is zero for the first time on the right boundary $x = l$. Consequently, $u - v$ cannot drop down to zero for any $\epsilon, \kappa > 0$, and hence, u itself cannot become negative. This proves proposition 3.3.1. $\square$.
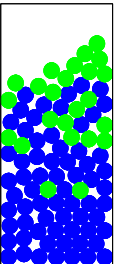
3.4 Stationary solutions in the scalar case

Let us look for stationary solutions of system (3.8), (3.9). From (3.8), we get $(d(u)u_x - f(u))_x = 0$. Hence, $d(u)u_x - f(u)$ is a constant which vanishes in view of the boundary condition (3.9). Thus, stationary solutions correspond to solutions of the ordinary differential equation

$$\frac{d}{dx}u = g(u) \tag{3.16}$$

where

$$g(u) = f(u)/d(u). \tag{3.17}$$

Of course we have

$$g(0) = g(1) = 0 \tag{3.18}$$

by condition (d).

Proposition 3.4.1 (Monotonicity of equilibria in the scalar case.) *All stationary solutions of the one-dimensional equation (3.8) with boundary condition (3.9) are monotone functions (increasing, decreasing, or constant) on the interval $[0, l]$.*

Proof. Solutions of scalar autonomous ordinary differential equations are always monotone. □.

Before investigating the qualitative behavior of the model, we discuss what we can expect. For larger numbers of species and complicated interactions, we cannot rule out complicated (e.g. oscillatory) behavior. But in the case of only two species, i.e. in the case of one scalar differential equation, we expect that the process of reshuffling by convection and diffusion leads to a stationary distribution. However, since we can think of many different initial distributions with different proportions of species, there must be many stationary solutions. Nevertheless, we can show that for any given proportion of total masses of the two species there is exactly one equilibrium. This fact is expressed in the following proposition.

Proposition 3.4.2 (Existence and uniqueness in the scalar case.) *Let $\bar{u}$ be the relative total mass of the first species, such that*

$$\int_0^l u(x)dx = \bar{u}l \tag{3.19}$$

is the absolute total amount in the vessel. For any number $\bar{u} \in [0, 1]$, the differential equation (3.16) has exactly one solution satisfying condition (3.19).

Proof. We note that condition (3.18) ensures that every solution $u(x)$ of equation (3.16) with initial condition $u^0 = u(0) \in M = [0, 1]$ never leaves M. By the existence and uniqueness theorem for ordinary differential equations, (3.16) has exactly one solution for each $u^0 \in M$. By the same argument solution curves
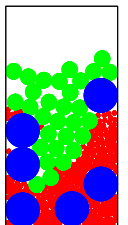
cannot intersect and thus lie one above each other in the way indicated in figure 3.1. In other words, the mapping $F : u^0 \longmapsto \bar{u}$ is strictly monotone and therefore one-to-one. Furthermore, the solutions of (3.16) depend continuously on the initial data u^0 and we have $F(0) = 0$, $F(1) = l$ in view of (3.18). As a consequence, the mapping F is onto. $\square$.

Figure 3.1 shows the typical behavior of the species distribution for the function $f(u) = u(1 - u)$ which corresponds to $f_1(u_1, u_2) = -f_2(u_1, u_2) = u_1 u_2$. Solutions for very small and very large proportions of u_1 are convex or concave, respectively, intermediate solutions show sigmoid behavior. The figure shows clearly that the solutions of the ordinary differential equation can be parametrized either by their initial data, i.e. their values at $x = 0$, or by the total mass $\bar{u}$. One can imagine, that for $n \geq 3$ and more complicated dynamics, where solutions can be still parametrized by their initial data (as ensured by the existence and uniqueness theorem for ordinary differential equations), there may be several or perhaps no solutions for a given vector of proportions of total masses. Next we discuss the
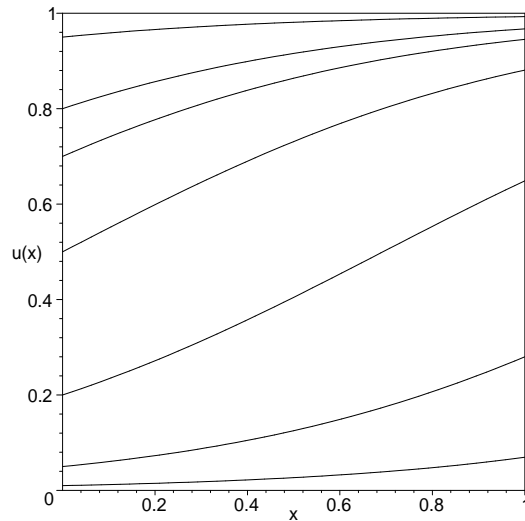
Figure 3.1: The layers of stationary solutions for $f(u) = u(1 - u)$, $d(u) \equiv 1$, and $l = 1$. Each curve represents the local proportion of the first one of two species as a function of the height $x \in [0, 1]$ in the vessel. The family of curves is parametrized either by the initial value or by the total mass.

behavior of the time-dependent problem (3.8), (3.9). We have the following result:

Proposition 3.4.3 (Convergence to equilibrium in the scalar case.) *For any initial distribution $u_0 \in \mathcal{C}^3([0, l])$ of species 1, the time-dependent solution of (3.8), (3.9) converges to the unique equilibrium distribution characterized by the total mass proportion $\bar{u}$.*
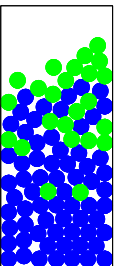
Proof. As stated in section 3.2, f is assumed to be at least twice continuously differentiable. Define the function of two variables

$$v(t, x) = d(u(t, x))u_x(t, x) - f(u(t, x)).$$

Then

$$v_t = d'(u)u_t u_x + d(u)u_{xt} - f'(u)u_t,$$
$$v_x = u_t,$$

and thus

$$v_t = a(t, x)v_{xx} + b(t, x)v_x \tag{3.20}$$

with $a(t, x) = d(u(t, x))$, $b(t, x) = d'(u)u_x - f'(u)$. The coefficients a and b are bounded. Clearly, v vanishes on the boundary $x = 0, l$ in view of (3.9). With the smoothness conditions requested, the solution v goes to zero together with its space derivative (see [Friedman64], p. 158, theorem 1). $\square$

We point out the following fact: The function $v = d(u)u_x - f(u)$ satisfies equation (3.20). Suppose at time $t = 0$,

$$d(u)u_x \geq f(u) \tag{3.21}$$

(or $d(u)u_x \leq f(u)$, respectively). Then by the comparison principle, the same inequality holds for all positive t. If, for example, f is non-negative (see the example section 3.3) and (3.21) holds initially, then u will be monotone in x for all time.

As an example we choose $f(u) = u(1 - u)$, $d(u) = D = const$. Then the ordinary differential equation (3.16)

$$u' = \frac{1}{D}u(1 - u) \tag{3.22}$$

is a Riccati equation. The solution for the initial value $u^0 \in [0, 1]$ is

$$u(x) = \frac{u^0}{(1 - u^0)e^{-x/D} + u^0}$$

which is represented in figure 3.2. We observe that in the stationary solution the first substance u_1 is concentrated at the bottom of the vessel whereas u_2 has its maximum concentration at the top. We give the exact expression for the total mass of species $u = u_1$ as a function of the initial value u^0 as

$$\int_0^l u(x)dx = \int_0^l \frac{u^0}{(1 - u^0)e^{-x/D} + u^0}dx$$
$$= D \cdot \ln\left[(1 - u^0) + u^0 e^{l/D}\right]. \tag{3.23}$$
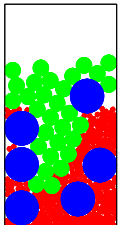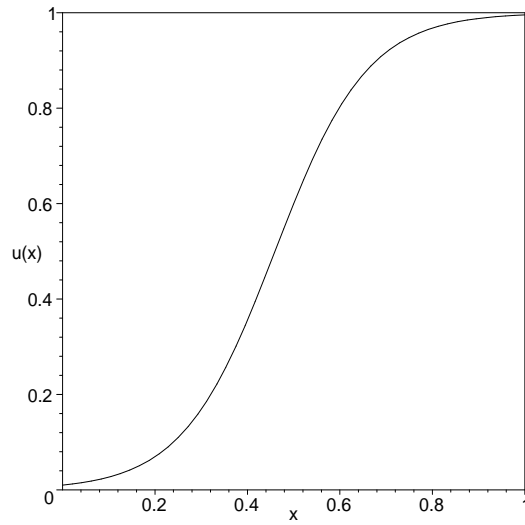
Figure 3.2: Segregation of two types of particles due to diffusion and convection. A stationary state of system (3.8) with $d(u) \equiv D = 0.1$ and $u(0) = 0.01$. The graph shows the concentration of the first species in the vessel.
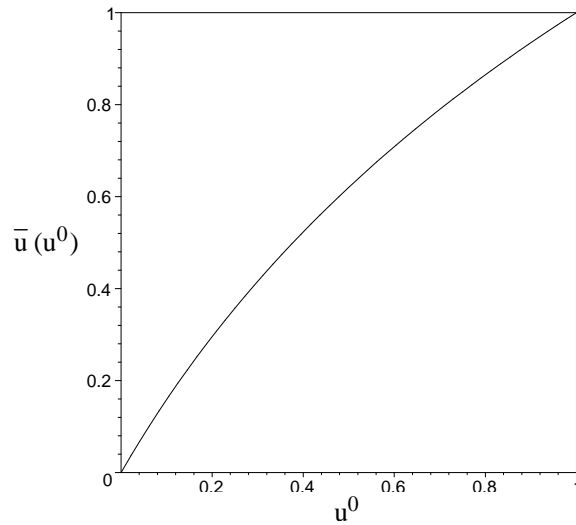
Figure 3.3: The normed total mass $\bar{u}$ of species u as a function of the initial value u^0. Parameter values are $D = 1$ and $l = 1$. The resulting map is a bijection of the interval $[0, 1]$.

Hence, we have an explicit formula connecting the initial data at $x = 0$ and the total mass, namely

$$u^0 = \frac{e^{\bar{u}l/D} - 1}{e^{l/D} - 1}.$$
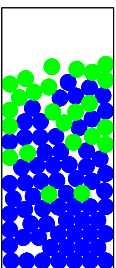
The dependence of $\bar{u}$ on u^0 is shown in figure 3.3. We emphasize, that the example discussed in this section characterizes the qualitative behavior of *any* system of the form (3.8). In a general situation some profiles may be increasing, some decreasing, but they always form a set of nonintersecting layers.

3.5 The general case of n species

If we treat the case of more than two species, our convection-diffusion equation becomes the vector equation

$$u_t = (d(u)u_x - f(u))_x \tag{3.24}$$

with boundary condition

$$d(u)u_x = f(u) \tag{3.25}$$

or, component-wise,

$$u_{it} = \langle d'(u) \cdot u_x \rangle u_{ix} + d(u)u_{ixx} - \langle f'_i(u) \cdot u_x \rangle, \tag{3.26}$$
$$d(u)u_{ix} = f_i(u)$$

for $i = 1, \ldots, n$, where $\langle \, \cdot \, \rangle$ denotes the scalar product. As in the case of two particle species, where the equations reduce to one dimension, positivity is also conserved in the multi-dimensional case.

Proposition 3.5.1 (Positivity in the multi-dimensional case.) *If the initial (vector-valued) function $u^0(x) = u(0, x)$ of problem (3.24) satisfies $u_i^0(x) \geq 0$ for all $i = 1, \ldots, n$ and $x \in [0, l]$ then the components of the solution $u = u(t, x)$ stay non-negative for all positive t.*

Recall the component notation (3.26) of system (3.24), and suppose that at time $t = \bar{t}$ the ith component u_i vanishes for the first time at $x = \bar{x} \in [0, l]$. First assume $0 < \bar{x} < l$. Then $u_{ix}(\bar{t}, \bar{x}) = 0$, $u_{it}(\bar{t}, \bar{x}) \leq 0$, $u_{ixx}(\bar{t}, \bar{x}) \geq 0$. Hence at this point,

$$u_{it} = d(u)u_{ixx} - \sum_{j \neq i} \frac{\partial f_i}{\partial u_j} \frac{\partial u_j}{\partial x}.$$

The left hand side is non-positive, the first term on the right hand side is non-negative, and the second term on the right hand vanishes in view of property (e). Hence we would have a contradiction if one of the inequalities were strict. This argument shows how property (e) enters. Next assume $\bar{x} = 0$ (or $\bar{x} = l$). Then $u(\bar{t}, x)$ goes to zero from positive values, and so does $u_x(t, x)$ in view of the boundary condition. It seems that it is *unlikely* that u and u_x pass through zero at the same time.

Proof. In order to prove the proposition, we proceed similarly to the scalar case in section 3.3. We define the vector b component-wise by $b_i := (\partial f_i / \partial u_i(\bar{u}_0))/D - 1$,
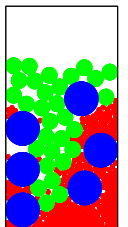
where the constant D will be specified later. Take $a := 1/l$ and define the vector-valued function ρ by $\rho_i(x) := e^{ax^2 + b_i x}$. Then we get $(\partial f_i/\partial u_i(\bar{u_0}))\rho_i(0)/D - \rho_i'(0) = 1$ and $(\partial f_i/\partial u_i(\bar{u_0}))\rho_i(l)/D - \rho_i'(l) = e^{al^2 + b_i l}$. In the sequel, we will assume that the concentration u_i of species i takes a small negative value and derive a contradiction. Therefore, we can restrict to values u_i in the neighborhood of zero. Without loss of generality, assume $u_i \in (-1, 1)$. Under this assumption, and in view of $f \in \mathcal{C}^2$, the definition

$$M := \max_{i,j,k} \sup_{\chi} \left| \frac{\partial^2 f_i}{\partial u_j \partial u_k}(\chi) \right| \tag{3.27}$$

makes perfect sense, when the supremum is taken over all $\chi \in (-1, 1)$. Consider a time horizon T for problem (3.24), (3.25) and define the vector-valued function $v = v(t, x)$ component-wise by $v_i(t, x) := -\epsilon \rho_i(x) e^{\kappa t}$ and consider the function $u - v$ with initial data $u_i(0, x) - v_i(0, x) = u_i^0(x) + \epsilon \rho_i(x) e^{\kappa t}$ and boundary condition $(u - v)_{ix} = f_i(u)/d(u) + \epsilon \rho_i' e^{\kappa t}$ for some $\epsilon, \kappa > 0$ to be specified later. Assume $u - v$ becomes zero for the first time in component i at (t_0, x_0), i.e. the vector of concentrations is given by $u = \bar{u} := (u_0, \ldots, u_{i-1}, v_i, u_{i+1}, \ldots, u_n)$. First, let $x_0 \in (0, l)$. At (t_0, x_0), we have $(u_i - v_i)_x = 0$, $(u_i - v_i)_{xx} \geq 0$ and $(u_i - v_i)_t \leq 0$. In view of $d(u) > 0$, we get

$$
\begin{aligned}
0 \geq (u_i - v_i)_t &\\
&= \langle d'(\bar{u}) \cdot u_x \rangle u_{ix} + d(\bar{u}) u_{ixx} - \langle f_i'(\bar{u}) \cdot u_x \rangle + \epsilon \kappa \rho_i(x) e^{\kappa t} \\
&\geq \langle d'(\bar{u}) \cdot u_x \rangle v_{ix} + d(\bar{u}) v_{ixx} - \langle f_i'(\bar{u} \cdot u_x) \rangle + \epsilon \kappa \rho_i(x) e^{\kappa t} \\
&= \langle d'(\bar{u}) \cdot u_x \rangle (-\epsilon \rho_i'(x) e^{\kappa t}) - d(\bar{u}) \epsilon \rho_i''(x) e^{\kappa t} - \langle f_i'(\bar{u}) \cdot u_x \rangle + \epsilon \kappa \rho_i(x) e^{\kappa t}.
\end{aligned}
\tag{3.28}
$$

In order to estimate the term $(f_i'(\bar{u}) \cdot u_x)$, we use Taylor's formula. For $i \neq k$, we have

$$\left. \frac{\partial f_i}{\partial u_k} \right|_{u_i = 0} = 0$$

by assumption (e), and thus

$$
\begin{aligned}
\frac{\partial f_i}{\partial u_k}(u) = \frac{\partial f_i}{\partial u_k}(\bar{u}) &= \frac{\partial f_i}{\partial u_k}(\bar{u_0}) + \left\langle (\bar{u} - \bar{u_0}) \cdot \mathrm{grad}\left(\frac{\partial f_i}{\partial u_k} \right)(\xi_k) \right\rangle \\
&= v_i \frac{\partial}{\partial u_i}\left(\frac{\partial f_i}{\partial u_k} \right)(\xi_k),
\end{aligned}
$$

where ξ_k is a constant vector (Taylor formula). In view of (3.27), we can find a positive constant N, such that

$$\left| \frac{\partial}{\partial u_i}\left(\frac{\partial f_i}{\partial u_k} \right)(\xi_k) \right| \leq N.$$

Since the solution u of (3.24), (3.25) exists and is at least $\mathcal{C}^2$ for all positive times (see theorem 3.2.2 in section 3.2), there exists a positive constant P, such that
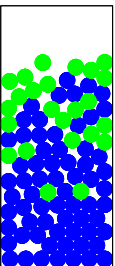
$|u_{kx}| \leq P$ for all $k = 1, \ldots, n$. Hence,

$$
\begin{aligned}
\left| \langle f_i'(\bar{u}) \cdot u_x \rangle \right| &= \left| \sum_k \frac{\partial f_i}{\partial u_k}(\bar{u}) u_{kx} \right| \\
&\leq \left| \frac{\partial f_i}{\partial u_i}(\bar{u}) v_{ix} + (n-1)NP v_i \right| \\
&= \left| -\frac{\partial f_i}{\partial u_i}(\bar{u}) \epsilon \rho_i'(x) e^{\kappa t} + \epsilon (n-1) NP \rho_i'(x) e^{\kappa t} \right|.
\end{aligned}
$$

Choose the parameter κ so large, that at (t_0, x_0),

$$
\begin{aligned}
|d(\bar{u}) \rho_i''(x)| &\leq \kappa \rho_i(x)/5, \\
|\langle d'(\bar{u}) \cdot u_x \rangle \rho_i'(x)| &\leq \kappa \rho_i(x)/5, \\
\left| \frac{\partial f_i}{\partial u_i}(\bar{u}) \rho_i'(x) \right| &\leq \kappa \rho_i(x)/5, \\
\left| (n-1)NP \rho_i'(x) \right| &\leq \kappa \rho_i(x)/5.
\end{aligned} \tag{3.29}
$$

Then, by (3.28),

$$
\begin{aligned}
0 &\geq \epsilon e^{\kappa t} [-\langle d'(u) \cdot u_x \rangle \rho_i'(x) - d(u) \rho_i''(x) + \kappa \rho_i(x)] - \langle f_i'(u) \cdot u_x \rangle \\
&\geq \epsilon e^{\kappa t} \kappa \rho_i(x)/5 \\
&> 0,
\end{aligned}
$$

for any strictly positive ϵ, which is a contradiction. On the boundary $x_0 = 0$ or $x_0 = l$, we have

$$
(u_i - v_i)_x = \frac{f_i(\bar{u})}{d(\bar{u})} + \epsilon \rho_i'(x) e^{\kappa t}
$$

in view of the boundary condition (3.25). By Taylor's formula,

$$
f_i(\bar{u}) = f_i(\bar{u_0}) + \langle \operatorname{grad} f_i(\bar{u_0}) \cdot (\bar{u} - \bar{u_0}) \rangle + \frac{1}{2} \left((\bar{u} - \bar{u_0})^T \operatorname{Hess}_{f_i}(\chi_{x_0})(\bar{u} - \bar{u_0}) \right),
$$

where χ_{x_0} is a constant depending on whether $x_0 = 0$ or $x_0 = l$. $\operatorname{Hess}_{f_i}$ is the Hessian of the component f_i. In view of $(\bar{u} - \bar{u_0})^T = (0, \ldots, 0, v_i, 0, \ldots, 0)$ and assumption (d) of section 3.2, the equation for $(u_i - v_i)_x$ becomes

$$
\begin{aligned}
(u_i - v_i)_x &= \frac{1}{d(\bar{u})} \left[\frac{\partial f_i}{\partial u_i}(\bar{u_0}) v_i + v_i^2 \frac{\partial^2 f_i}{\partial u_i^2}(\chi_{x_0}) \right] + \epsilon \rho_i'(x) e^{\kappa t} \\
&= \frac{1}{d(\bar{u})} \left[\frac{\partial f_i}{\partial u_i}(\bar{u_0})(-\epsilon \rho_i(x) e^{\kappa t}) + \epsilon^2 \rho_i^2(x) e^{2\kappa t} \frac{\partial^2 f_i}{\partial u_i^2}(\chi_{x_0}) \right] + \epsilon \rho_i'(x) e^{\kappa t} \\
&= \epsilon e^{\kappa t} \left\{ \frac{1}{d(\bar{u})} \left[-\frac{\partial f_i}{\partial u_i}(\bar{u_0}) \rho_i(x) + \epsilon \rho_i^2(x) e^{\kappa t} \frac{\partial^2 f_i}{\partial u_i^2}(\chi_{x_0}) \right] + \rho_i'(x) \right\}.
\end{aligned}
$$
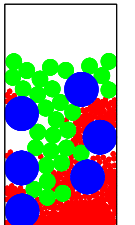
Consider the case $x_0 = 0$. Let $D := d(u(t_0, 0))$. Using our preliminary definitions, we see that $(u_i - v_i)_x < 0$ if we choose ϵ small enough. This is a contradiction. Now let $x_0 = l$ and $D := d(\bar{u})$. Then

$$-\frac{1}{D}\frac{\partial f_i}{\partial u_i}(\bar{u})\rho_i(l) + \rho_i'(l) = e^{al^2 + bl},$$

and thus

$$(u_i - v_i)_x = \epsilon e^{\kappa t}\left\{e^{al^2 + bl} + \frac{\epsilon}{D}\rho_i^2(l)e^{\kappa t}\frac{\partial^2 f_i}{\partial u_i^2}(\chi_l)\right\}.$$

The first term in brackets is always greater than one, whereas the absolute value of the second term is at most equal to

$$\frac{1}{2}\rho_i^2(l)e^{-2al^2 - 2bl},$$

i.e. less than $1/2$. This is a contradiction. Consequently, $u - v$ can never reach zero from above, and hence, u itself cannot become strictly negative. This proves proposition 3.5.1. $\square$

The stationary solutions of system (3.24) with boundary conditions (3.25) are solutions of the system of ordinary differential equations

$$\dot{u} = g(u) \tag{3.30}$$

where $g(u) = f(u)/d(u)$. Let G be the solution operator of (3.30), i.e.

$$\begin{aligned}\frac{d}{dt}G(t, u) &= g(G(t, u)) \\ G(0, u) &= u.\end{aligned}$$

From hypotheses (c) and (d), it follows that the function g satisfies

$$u_i = 0 \Rightarrow g_i(u) = 0, \tag{3.31}$$

$$e^T g(u) \equiv 0. \tag{3.32}$$

Define the simplex (generalized triangle or tetrahedron) of probability vectors

$$S = \{u \in \mathbb{R}^n \,|u_i \geq 0, \, i = 1, \ldots, n, \, \sum_{i=1}^{n} u_i = 1\},$$

The set S is the set of local distributions of the n species. The conditions (3.31), (3.32) ensure that solutions of (3.30) starting in S remain in S for all times t (positive or negative). Hence S is invariant with respect to the flow of (3.30). If $G(t, u)$, $0 \leq t \leq l$, is the solution of (3.30) starting from $u(0) = u$, then

$$\int_0^l G(t, u)dt = \bar{u}l. \tag{3.33}$$
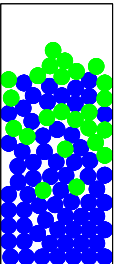
defines the normed vector $\bar{u}$ of total masses of the n species (the actual total mass is given by $\bar{u}l$). The next theorem shows that for any distribution $\bar{u} \in S$ of total masses there is *at least one* stationary solution (exactly one in the case $n = 2$ by Proposition 3.4.2).

Theorem 3.5.2 (Existence of equilibria in the multi-dimensional case.) *Assume (3.31), (3.32). For every $\bar{u} \in S$, there is at least one $u \in S$, such that (3.33) holds.*

Proof. Under the hypotheses of section 3.2 the system lives on the simplex S. In the following argument we use the topological degree (see [Ortega70]). Let L be some positive number (the largest height of the vessel we are interested in). Define the function $H : [0, L] \times \mathbb{R}^n \longrightarrow \mathbb{R}^n$ by

$$H(l, u) = \frac{1}{l} \int_0^l G(s, u) ds \quad \text{for} \quad l > 0, \tag{3.34}$$

$$H(0, u) = u. \tag{3.35}$$

The function H is continuous, and it maps $[0, L] \times S$ into S, $H(0, \cdot)$ is the identity. Let $u \in \partial S$, i.e. $u_i = 0$ for some i. Then $G_i(l, u) = 0$ for the same i and hence also $H_i(l, u) = 0$. Conversely, let $H(l, u) \in \partial S$ for some l and u. Then $H_i(l, u) = 0$ for some i and hence $\int_0^l G_i(t, u) dt = 0$ or, equivalently, $\int_0^l G_i(t, u) dt = 0$. Then $u_i = 0$ which means $u \in \partial S$.
In short, $H(l, \cdot)$ maps the interior S° of S into the interior and the boundary ∂S into itself. Also each lower-dimensional face of the boundary is mapped into itself.
Now let $\bar{u} \in S^\circ$. Then $H(l, u) \neq \bar{u}$ for all $u \in \partial S$. Thus, H defines a homotopy of S and the degree $\deg(H(l, \cdot), S, \bar{u})$ is well-defined for all $l \in [0, L]$. Since $\deg(H(0, \cdot), S, \bar{u}) = 1$, we have $\deg(H(l, \cdot), S, \bar{u}) = 1$ for all $l \in [0, L]$ and hence the equation $H(l, u) = \bar{u}$ has at least one solution in $u \in S$ for all $l \in [0, L]$.
Now assume $\bar{u} \in \partial S$. Then $\bar{u}_i = 0$ for some i. Then, in the above argument, replace S by the face of S corresponding to the positive components of $\bar{u}$. $\square$

In general, there will be more than one stationary solution for a given mass distribution. This can be seen from the following argument. Assume the system (3.30) has a non-constant periodic solution with minimal period $\omega > 0$. Choose $l = \omega$. Then for all points u on the periodic orbit we get the same value $\bar{u}$. In this example we can extend the function from $[0, l]$ periodically to the whole real axis to get an infinitely high vessel with a periodic distribution of species. Then the phase of this distribution can be chosen arbitrarily. We do not claim that such choice of the function f or g is realistic. In section 3.6 we give an example illustrating the above argument.

We reformulate the above result in terms of boundary value problems of second order systems of ordinary differential equations. Theorem 3.5.2 says that the
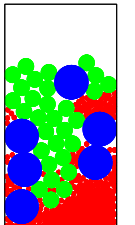
boundary value problem

$$\ddot{v} = g(\dot{v}) \tag{3.36}$$

with boundary values

$$\begin{aligned}
v(0) &= 0 \\
v(l) &= \bar{u}l
\end{aligned} \tag{3.37}$$

has at least one solution in S for every $\bar{u} \in S$.

3.6   Non-unique stationary states

At this point we briefly interrupt the general discussion of conditions for unique stationary solutions and give a counter-example exhibiting different equilibria with the same total mass distribution. Consider system (3.24) with boundary condition (3.25), where $d(u) \equiv D = 1/\sqrt{3}$, and the three-dimensional convection function is given by

$$\begin{aligned}
f_1(u) &= u_1(1 - u_1 - 2u_2), \\
f_2(u) &= u_2(-1 + u_2 + 2u_1), \\
f_3(u) &= -f_1(u) - f_2(u).
\end{aligned} \tag{3.38}$$

Conditions (a) through (e) in section 3.2 are satisfied, and, denoting the vector $u = (x, y, z)^T$, the stationary solutions are solutions of the system of ordinary differential equations

$$\begin{aligned}
\dot{x} &= \sqrt{3}x(1 - x - 2y), \\
\dot{y} &= \sqrt{3}y(-1 + y + 2x).
\end{aligned} \tag{3.39}$$

Due to the fact that concentrations always add up to one, we may omit the third equation

$$\dot{z} = -\dot{x} - \dot{y} = \sqrt{3}x(x - 1) - \sqrt{3}y(y - 1) \tag{3.40}$$

governing the change in z. The solutions of (3.39) are represented in figure 3.4(a). The three-dimensional system (3.39), (3.40) lives on the simplex $\mathcal{S} = \{(x, y, z) : x + y + z = 1\} \subset \mathbb{R}^3$. It has stationary points in the three corners of $\mathcal{S}$ and a coexistence point at $P := (\frac{1}{3}, \frac{1}{3}, \frac{1}{3})$. The boundary of $\mathcal{S}$ and the orbits of system (3.39), (3.40) are represented in figure 3.4(b).

Linearization of (3.39) yields a system with matrix

$$J_P = \frac{1}{\sqrt{3}} \begin{pmatrix} -1 & -2 \\ 2 & 1 \end{pmatrix},$$

the eigenvalues of which are $\pm i$. The two-dimensional system $\dot{X} = J_P X$ is a center, its trajectories are the ellipses sketched in figure 3.5(a). The two successive

(a) planar center

(b) center on the three-dimensional simplex
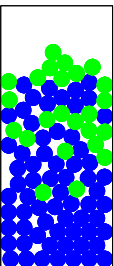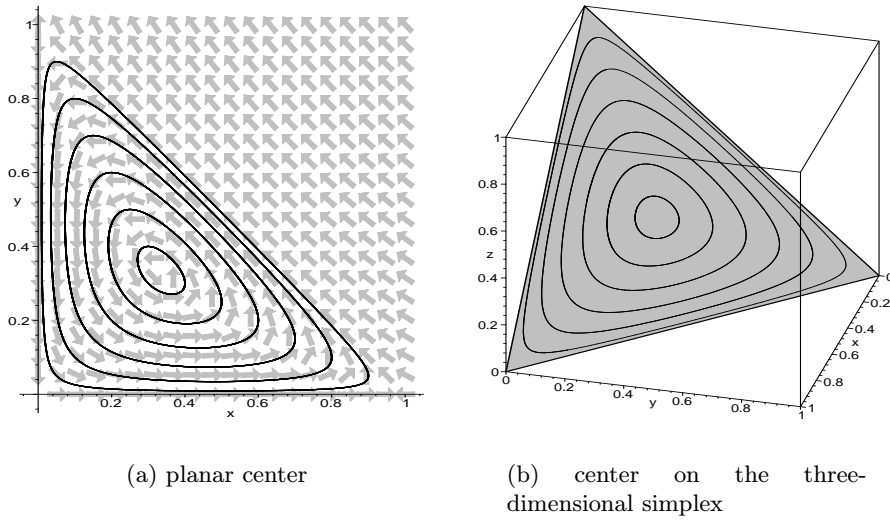
Figure 3.4: The center of system (3.39) and its projection onto the three-dimensional simplex, system (3.39), (3.40).

(a) The linear system described by J_P.

(b) Orbits after rotation of the variables.

(c) Orbits after rescaling of x.
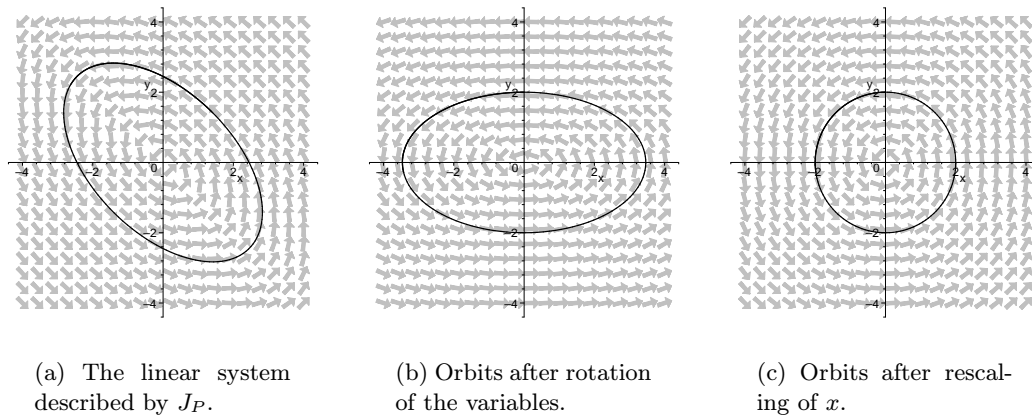
Figure 3.5: The orbits of the linear system described by the matrix J_P, and the corresponding flows after the variable transformations (3.41) and (3.42).

variable transformations

$$
\begin{aligned}
x &\mapsto \sqrt{3}(x - y), \\
y &\mapsto x + y
\end{aligned}
\tag{3.41}
$$

and
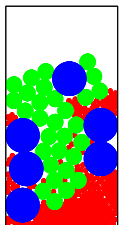
$$x \mapsto \sqrt{3}x$$
$$y \mapsto y \tag{3.42}$$

yield the orbits sketched in figures 3.5(b) and 3.5(c), respectively. They do not change the period. The resulting system is the center $\dot{x} = -y$, $\dot{y} = x$, which is known to have period $T = 2\pi$. As a result, the linear system described by J_P also has period equal to 2π. Thus, the closed orbits of system (3.39), (3.40) around the point P have periods assuming all values in the interval $[2\pi, \infty)$, depending on the starting point $(x_0, y_0, z_0) \in \mathcal{S}$. In fact, there could even be periods of length smaller than 2π. The more trajectories approach one of the three stationary points in the corners of $\mathcal{S}$, the longer the corresponding period becomes.

The above argument shows, that for any container height $l > 2\pi$, there is at least one closed orbit of (3.39), (3.40) with period equal to l. Each starting point on this cycle yields a different stationary state with the same total mass distribution. Figures 3.6 and 3.7 show two sequences taken from computer simulations, illustrating the fact that different stationary solutions exist and are locally stable. In both cases, we used system (3.24) with boundary condition (3.25), where $d(u) \equiv D = 1/\sqrt{3}$, and the three-dimensional convection function is given component-wise by (3.38). The container height equals 10 units of length, and the total masses of the three species were chosen to be 3.2, 3.2 and 3.4 units of mass, respectively. The two runs differ only in the initial mass distribution in the container (see figure parts 3.6(a) and 3.7(a)).

3.7   Monotonicity and convergence

Before we approach the problem of convergence of the solutions, let us touch the issue of monotonicity of the stationary states. Clearly, the equilibria of (3.24), (3.25) in general need not be monotone any more, even though the corresponding ordinary differential equation (3.30) is autonomous. In chapter 5, where we apply the theory developed in the present chapter to the analysis of sedimentation processes, we will encounter a special case, in which all components of the convection function f are strictly negative everywhere. Of course, this guarantees monotonously decreasing equilibria.

Once we know that stationary solutions exist for problem (3.36) with boundary condition (3.37), we naturally ask the question of convergence to these steady states as time progresses. Define

$$v := d(u)u_x - f(u). \tag{3.43}$$

It is straightforward to check that v satisfies

$$v_t = d(u)v_{xx} + Av_x, \tag{3.44}$$

(a) Initial distribution.

(b) At $t = 0.1$ units of time.

(c) At $t = 0.5$ units of time.

(d) At $t = 3$ units of time.

(e) At $t = 5$ units of time.

(f) At $t = 30$ units of time.
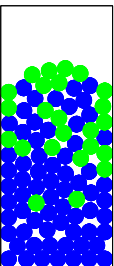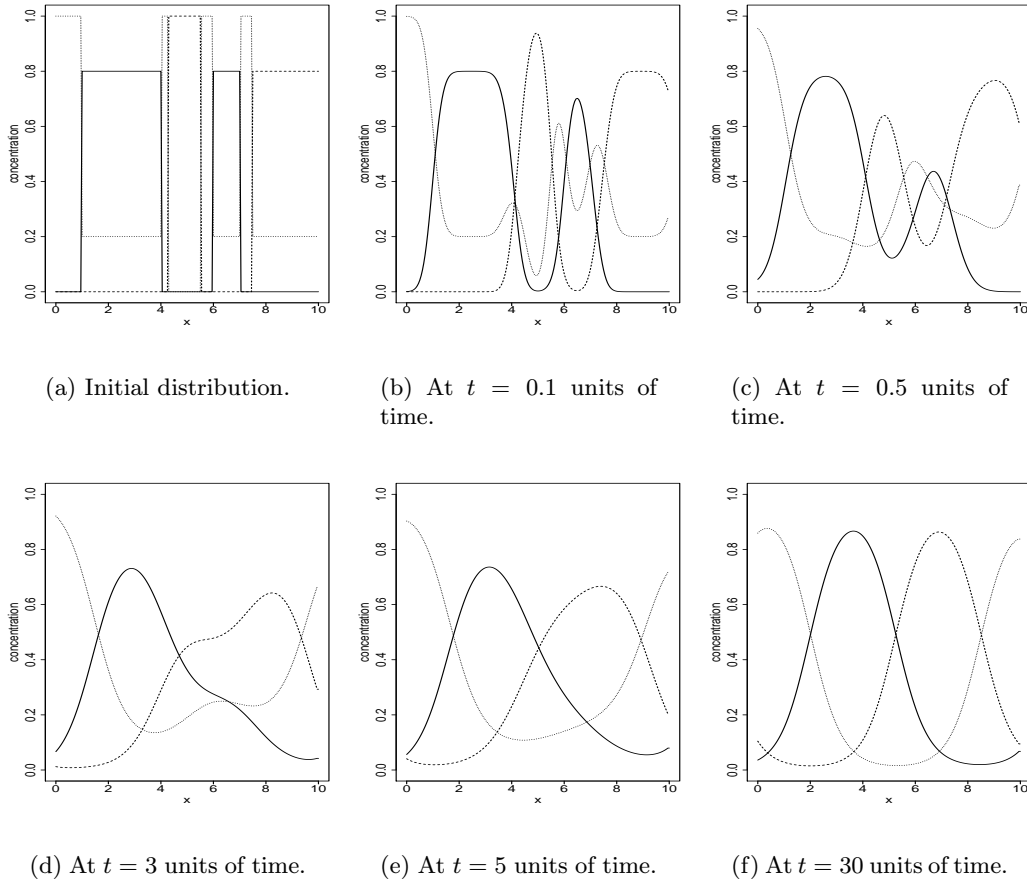
Figure 3.6: Sequence in the simulation of system (3.24) with boundary condition (3.25) and convection function (3.38), where $d(u) \equiv D = 1/\sqrt{3}$ and $l = 10$. The concentrations of the three types of grains are drawn in solid, dashed and dotted lines, respectively.

where A is the matrix $u_x d'(u)^T - f'(u)$ and f' the Jacobian of f. Furthermore, v satisfies $v(0) = v(l) = 0$. As the following theorem states, we can now realize the convergence of the solutions of (3.24), (3.25) to a stationary state with the same total mass distribution in a container with fixed height l, given that the norm of the Jacobian of f does not exceed a certain value. In other words, if the container height is too large, we cannot guarantee globally stable equilibria any more. In this case, one could imagine the formation of steady waves or similar periodic phenomena, disturbing the appearance of stationary states.

Theorem 3.7.1 (Convergence to equilibrium in the multi-dimensional case.) *Denote by A the Jacobian of the function f,*

$$A(t, x) := f'(u(t, x)),$$

(a) Initial distribution.

(b) At $t = 0.1$ units of time.

(c) At $t = 0.5$ units of time.

(d) At $t = 3$ units of time.

(e) At $t = 5$ units of time.

(f) At $t = 30$ units of time.
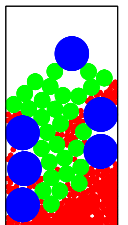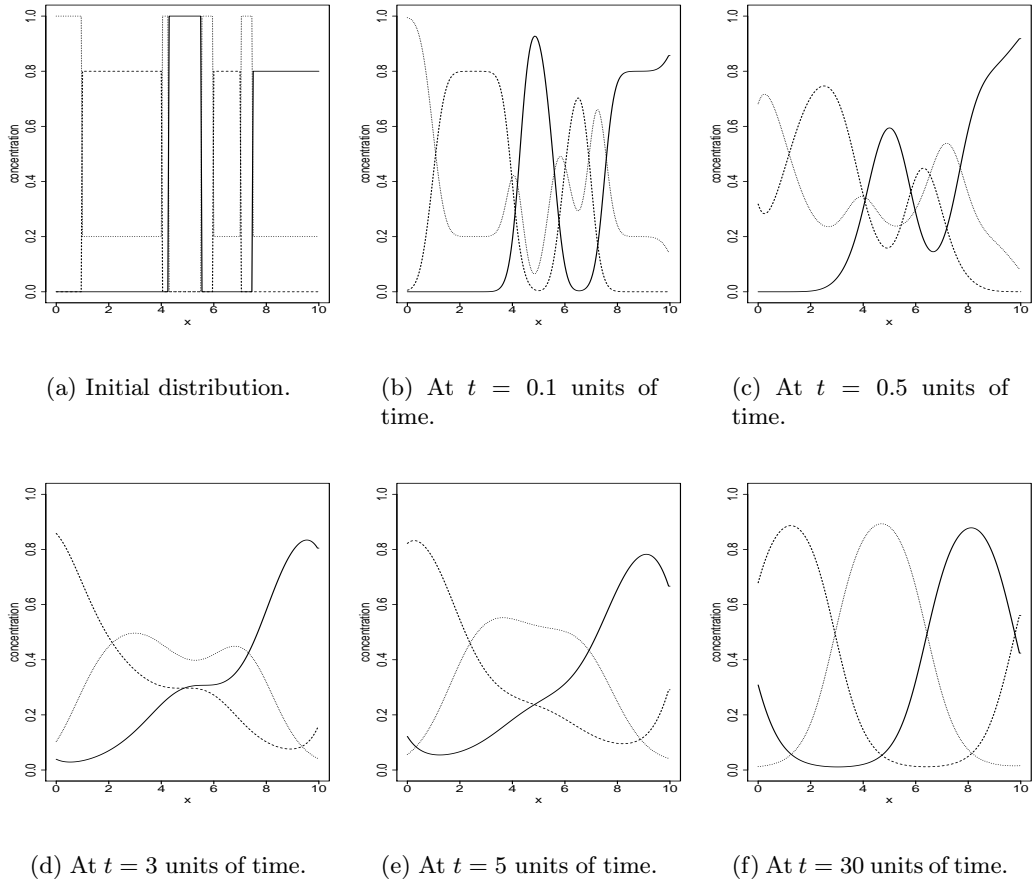
Figure 3.7: Sequence in the simulation of the same system used to obtain figure 3.6, this time with a different initial mass distribution. The stationary state, which is approximately that illustrated in part (f), shows layers of the same type, but with interchanged roles of the three species.

and define

$$m := \sup_{t \geq 0} \max_{0 \leq x \leq l} \|A(t,x)\|.$$

If $l < \sqrt{2}\pi/m$, then the function v defined in (3.43) tends to zero uniformly on the interval $[0, l]$ as $t \to \infty$. Consequently, every solution u of (3.24), (3.25) approaches equilibrium.

Proof. The function $\langle v \cdot v \rangle = \langle v \cdot v \rangle(t, x)$ (scalar product) satisfies $\langle v \cdot v \rangle_t = 2\langle v \cdot v_{xx} \rangle - 2\langle v \cdot A v_x \rangle$, $\langle v \cdot v \rangle_x = 2\langle v \cdot v_x \rangle$ and $\langle v \cdot v \rangle_{xx} = 2\langle v_x \cdot v_x \rangle + 2\langle v \cdot v_{xx} \rangle$, and thus solves the Dirichlet problem

$$\langle v \cdot v \rangle_t = \langle v \cdot v \rangle_{xx} - 2\langle v_x \cdot v_x \rangle - 2\langle v \cdot A v_x \rangle \tag{3.45}$$
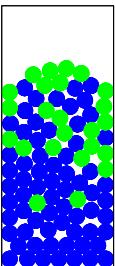
with boundary condition

$$\langle v \cdot v \rangle(0) = \langle v \cdot v \rangle(l) = 0. \tag{3.46}$$

We rewrite (3.45) as

$$\langle v \cdot v \rangle_t = \langle v \cdot v \rangle_{xx} - 2 \left[\langle v_x \cdot v_x \rangle + \langle v \cdot Av_x \rangle + \kappa \langle v \cdot v \rangle \right] + 2\kappa \langle v \cdot v \rangle \tag{3.47}$$

with the parameter $\kappa > 0$ to be specified later. The form giving rise to the term in brackets on the right hand side, $Y := [\langle v_x \cdot v_x \rangle + \langle v \cdot Av_x \rangle + \kappa \langle v \cdot v \rangle]$, is defined by the matrix

$$P := \begin{pmatrix} 1 & \frac{1}{2}A \\ \frac{1}{2}A^T & \kappa \end{pmatrix},$$

in the sense that

$$\langle v_x \cdot v \rangle P \langle v_x \cdot v \rangle^T = Y.$$

We will choose κ as small as possible, but still large enough for Y to be non-positive, thereby giving an upper estimate for $\langle v \cdot v \rangle_t$. The symmetric matrix P is negative definite if and only if its determinant is positive. We therefore choose $\kappa = m^2/4$. With this choice made, equation (3.47) becomes the inequality

$$\langle v \cdot v \rangle_t \leq \langle v \cdot v \rangle_{xx} + \frac{m^2}{2} \langle v \cdot v \rangle, \tag{3.48}$$

which, in combination with the boundary condition (3.46), is a Dirichlet problem with constant coefficient $m^2/2$. Rescale $x \mapsto x\sqrt{m^2/2}$, $t \mapsto tm^2/2$. Relation (3.48) becomes

$$\langle v \cdot v \rangle_t \leq \langle v \cdot v \rangle_{xx} + \langle v \cdot v \rangle. \tag{3.49}$$

It is known (see for example [Britton], p. 50, theorem 4.40) that (3.49) has a critical patch width equal to π, i.e. if l lies below this value, the trivial solution is stable and $\langle v \cdot v \rangle$ tends to zero uniformly. In our case, we have to rescale this patch width. The resulting condition for the uniform convergence to the trivial state is thus $l < \sqrt{2}\pi/m$. Using [Friedman64], theorem 1, p. 158, we conclude that u tends to zero as well. This completes the proof of theorem 3.7.1. $\square$

3.8 A replicator type competition law with constant fitness

There is one choice of the vector field f, for which we can show uniqueness of the stationary state in any dimension n. We choose $D = const.$ and

$$f(u) = Mu - (e^T Mu)u \tag{3.50}$$
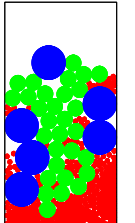
where $M = (m_i \delta_{ij})$ is a diagonal matrix of order n and the m_i are strictly positive constants. Without loss of generality we assume $m_1 > m_2 > ... > m_n$. In coordinate notation the ordinary differential equation (3.30) reads

$$\frac{d}{dx}u_i = \frac{1}{D}\left[m_i u_i - \left(\sum_{k=1}^{n} m_k u_k\right) u_i \right]. \tag{3.51}$$

This equation is just a renormalization of the linear system $\dot{u} = Mu$. In theoretical ecology, this type of system has been called *replicator equation* (see for example [Hofbauer98]). Here, the coefficient m_i is the (constant) fitness of species i in the population. The evolutionary success of the species, i.e. its relative rate of increase $\dot{u}_i/u_i$, is expressed as the difference between m_i and the average fitness $\bar{m} = \sum u_k m_k$ of the population. In section 3.9, we discuss the general replicator system. There, the individual fitnesses will be linear functions of the state vector u.

The solution of (3.51) can be explicitly given as

$$u_i(x) = \frac{e^{m_i x/D}u_i(0)}{\sum_{j=1}^{n} e^{m_j x/D}u_j(0)}. \tag{3.52}$$

Then the equation

$$\int_0^l \frac{e^{m_i x/D}u_i}{\sum_{j=1}^{n} e^{m_j x/D}u_j(0)}dx = l\bar{u}_i \tag{3.53}$$

establishes the connection between stationary solutions and total masses.

Theorem 3.8.1 (Uniqueness of equilibria for replicator models.) *Consider the system (3.1) with boundary condition (3.2), where the nonlinearity is given by (3.50). For any choice $\bar{u} \in S$ of total masses, there is exactly one stationary solution.*

Proof. Existence of solutions has been shown in theorem 3.5.2 of section 3.5. We can assume $D = 1$. In this case the function $H(l, \cdot)$, for $l > 0$, is given component-wise by

$$H_i(l, u) = \frac{1}{l}\int_0^l \frac{e^{m_i x}u_i}{\sum_{j=1}^{n} e^{m_j x}u_j}dx. \tag{3.54}$$

$H(l, \cdot)$ maps S onto S (as shown in the proof of theorem 3.5.2). Of course $H(0, u) = u$ on S as before. Now we want to compute the Jacobian of $H(l, \cdot)$ at a point $u \in S$. For that purpose, we interpret (3.54) as a mapping from $\mathbb{R}^n \to \mathbb{R}^n$ and later restrict to the set S. The Jacobian J has elements

$$\frac{\partial H_i}{\partial u_i} = \frac{1}{l}\int_0^l \frac{1}{\left(\sum_{k=1}^{n} e^{m_k x}u_k\right)^2}e^{m_i x}\left(\sum_{k \neq i} e^{m_k x}u_k\right)dx > 0,$$

$$\frac{\partial H_i}{\partial u_j} = -\frac{1}{l}\int_0^l \frac{e^{(m_i+m_j)x}u_i}{\left(\sum_{k=1}^{n} e^{m_k x}u_k\right)^2}dx < 0 \tag{3.55}$$
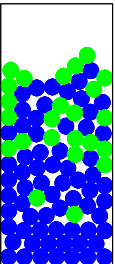
for $i \neq j$. Thus, J has strictly positive diagonal elements and strictly negative off-diagonal entries. Let us now restrict to solutions $G = G(t, u)$ starting on the simplex S, i.e. with $u \in S$. Along those trajectories, $e^T G(t, u) = e^T u$ for all t, and hence

$$
\begin{aligned}
e^T H(l, u) &= \frac{1}{l} \int_0^l e^T G(t, u) dt \\
&= e^T \frac{1}{l} \int_0^l G(t, u) dt \\
&= e^T \bar{u}
\end{aligned}
$$

is a constant. Consequently, $e^T J = 0$ for the system restricted to S, i.e. the Jacobian of H has a zero eigenvalue, and the corresponding eigenvector is the normal of S. Consider $-J$, which is a matrix with negative diagonal and positive off-diagonal elements. The Perron-Frobenius theorem (e.g. [Gantmacher59]) implies, that all eigenvalue of $-J$ have non-positive real parts, and that zero is a single eigenvalue. For the Jacobian J itself, this means that the restriction of the system to the simplex S has only eigenvalues with strictly positive real part. Its determinant is therefore strictly positive as well. Consequently, the degree $\deg(H(l, \cdot), S, \bar{u})$ (see for example [Ortega70]), which is the sum of the indices of all solutions of the equation

$$ H(l, u) = \bar{u}, \tag{3.56} $$

equals the number of these solutions. Since $H(l, \cdot)$ is homotopically equivalent to the identity $H(0, \cdot)$ on S and since (3.56) has no solutions on ∂S (see the proof of theorem 3.5.2 in section 3.5), the degree is equal to one. Hence, uniqueness follows. This proves theorem 3.8.1. $\square$.

In section 3.11 we compare the stationary states of a replicator type convection-diffusion system with convection term (3.50) with those of a particle simulation. An illustration of the corresponding density distributions is given is figure 3.12.

3.9 The general replicator equation with linear fitness

At present, we generalize the constant fitness model discussed in section 3.8 and let the fitness m_i of species i depend linearly on the state vector u (see again [Hofbauer98]). Thus, we choose $m_i = m_i(u) = (Au)_i$, where $A = (a_{ij})$ is the $n \times n$ fitness matrix. If we normalize the diffusion constant to $D = 1$, and if $U = (\delta_{ij} u_i)$ is the diagonal state matrix, then the convection-diffusion equation reads

$$ u_t = u_{xx} - \left[UAu - u(u^T Au) \right]_x, \tag{3.57} $$

or, in component notation,

$$ u_{it} = u_{ixx} - \left[u_i \left(\sum_{j=1}^n a_{ij} u_j - \sum_{j,k=1}^n a_{jk} u_j u_k \right) \right]_x $$
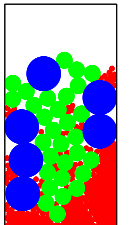
for $i = 1, \ldots n$. As supplied before, we impose the boundary condition

$$u_x = UAu - u(u^T Au) \tag{3.58}$$

at $x = 0, l$. Verify, that conditions (a) through (e) in section 3.2 are fulfilled for equation (3.57). Positivity and upper bounds are preserved for all positive times, and the concentrations of the species always add up to one. Hence, the replicator model with linear fitness, system (3.57), (3.58), qualifies as a granular matter model in the context of the present chapter. In some sense, the underlying physical idea is similar to the buoyancy effect (see also the discussion in section 2.14 of chapter 2). Here, the fitness of the species is just its capability to move up in the container during the shaking process. Whether a species prevails is determined by its own fitness in relation to the average fitness of the population. Hence, the use of equation (3.57) in segregation models is justified.

Consider the stationary solutions of system (3.57) with boundary condition (3.58), i.e. the solutions of

$$u_x = f(u) = UAu - u(u^T Au). \tag{3.59}$$

As before, let G be the solution operator corresponding to (3.59), and define the total mass operator $H : \mathbb{R} \times \mathbb{R}^n \longrightarrow \mathbb{R}^n$ by

$$H(l, u) = \frac{1}{l} \int_0^l G(t, u) dt, \tag{3.60}$$
$$H(0, u) = u$$

for $l > 0$. As a consequence of theorem 3.5.2 in section 3.5, we have existence of equilibria:

Corollary 3.9.1 (Existence of equilibria for linear fitness.)   *Assume (3.57), (3.58). For every $\bar{u} \in S$ and for every $l \geq 0$, there is at least one $u \in S$, such that*

$$H(l, u) = \bar{u} \tag{3.61}$$

holds. $\square$.

Uniqueness of the solutions of (3.61) does not hold in general. The famous *rock-scissors-paper* game, for example, has the fitness matrix

$$A = \begin{pmatrix} 0 & 1 & -1 \\ -1 & 0 & 1 \\ 1 & -1 & 0 \end{pmatrix},$$

and the solutions of the corresponding stationary state equation (3.59) are periodic orbits (see [Hofbauer98]). We showed in section 3.6, that such a center violates the uniqueness property for large container heights l.
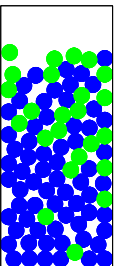
3.10 Model refinements

In this section, we propose several refinements of the original model (3.1), (3.2). In particular, we will be concerned with compaction effects in granular material and the issue of optimal particle packings. To simplify matters, we choose the diffusion matrix to be constant, $D(u) \equiv D$.

3.10.1 The maximal total density

The basic assumption underlying model (3.1), (3.2) is, that the grains composing the mixture in the vessel can fill the available space completely, as a fluid would be able to do. This analogy, of course, is generally false for granular material. In all practical situations, the particles leave gaps, and the maximal packing density u^{max} lies below one. While the density of a theoretically optimal packing of mono-size, two-dimensional balls for example is $\pi/(2\sqrt{3})$, or about 91%, experimental packings only reach values between 60% and 70% (see also the discussion in section 2.8 of chapter 2 and [Aste00]). Thus, given the system (3.1), (3.2), we can meet these concerns by directly limiting the convective flux f. For example, we can multiply f by a function $\Phi = \Phi(u)$ of the form

$$\Phi(u) = \left(1 - \frac{u^{\mathrm{tot}}}{u^{\mathrm{max}}}\right)^p, \qquad (3.62)$$

for some $p \geq 1$, where $u^{\mathrm{tot}} = u_1 + \cdots + u_n$ is the total particle concentration. The convection-diffusion law then reads

$$u_t = Du_{xx} - [f(u)\Phi(u)]_x$$

with boundary condition

$$Du_x = f(u)\Phi(u).$$

In the case of a bi-disperse mixture, i.e. if $n = 1$, we end up with a one-dimensional equation (see also section 3.3). Figure 3.8 shows the convection function $f\Phi$ for $f(u) = u(1-u)$ and $u^{\mathrm{max}} = 0.8$, as well as the corresponding stationary solutions of (3.1), (3.2).

3.10.2 The special role of the medium

In the introduction to the present chapter (section 3.1), we mentioned the problem we encountered with modeling the empty space between the particles. When considering multi-disperse material, we tacitly assumed that this empty space (or the sedimentation medium) is evenly distributed throughout the vessel. In reality, of course, the packing density in the stationary state decreases with growing height in the container. Consequently, the volumetric fraction occupied by the medium is an increasing function of x. If compaction takes place, the upper layer will eventually contain no particles at all (see also figure 3.9). Assigning one of
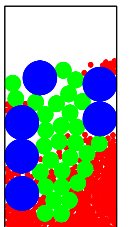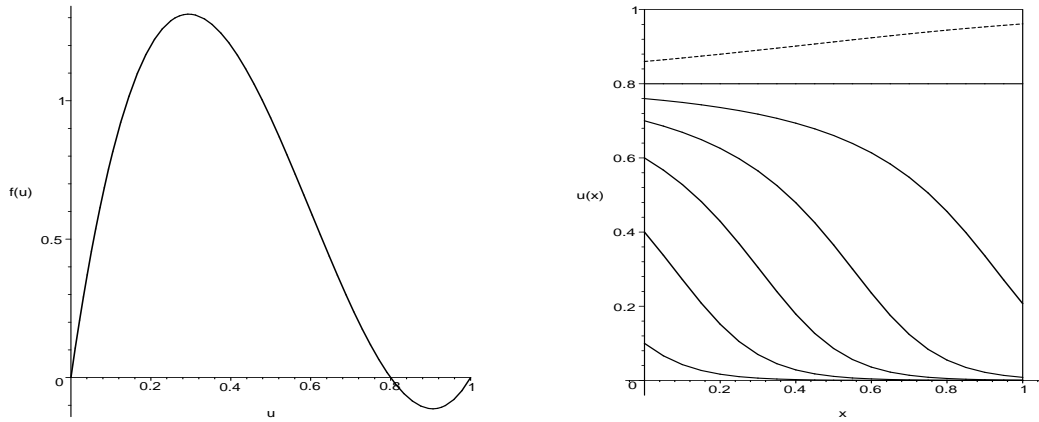
(a) Sketch of the new convection function $f\Phi$ with Φ of the form (3.62) for $p = 1$ and $u^{max} = 0.8$.

(b) The corresponding stationary solutions show saturation at $u = 0.8$. Beyond (dotted line), solutions become increasing functions of x and fail to describe the physical reality of compaction.

Figure 3.8: Convection functions of the form $f\Phi$ with $f(u) = u(1-u)$, $u^{\max} = 0.8$ and Φ of the form (3.62) impose an upper bound for the particle density. Stationary solutions with initial values below this bound are feasible stable states for the physical system.
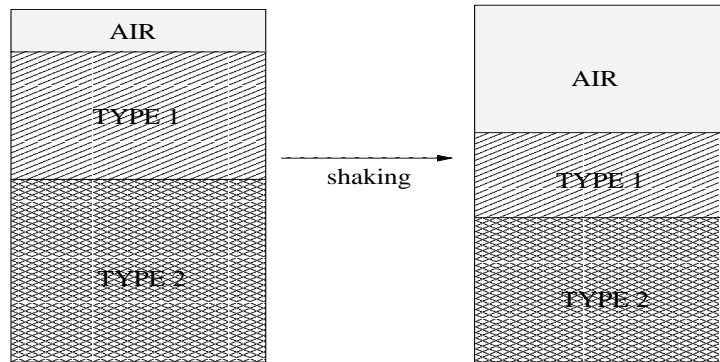
Figure 3.9: The vessel containing two types of particles as well as air. Shaking makes the particles move closer together, and the mixture ends up occupying a smaller volume. This compaction takes place in most practical situations.

the n species the role of the medium does not solve the problem, either. If we imagine it as being composed of very small grains, it would not form the top layer in the equilibrium state, while large particles certainly do not have the ability to fill the small gaps in a densely packed mixture.
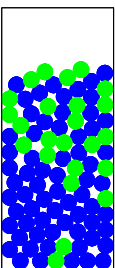
Instead of describing the fluctuation of the medium concentration directly, one could consider the movement of the particles *relative* to that of the medium. The convection term $f_i(u) = u_i v_i$, where v_i is the absolute velocity of the grains of type i, is then replaced by the equation

$$f_i = u_i \left(w_i - \sum_{j=1}^{n} u_j w_j \right),$$

in which $w_i = v_i - v_{medium}$ is the relative velocity of the grains. This approach is due to J. H. Masliyah (see [Masliyah79] and [Bürger00.1], [Bürger00.2]). In chapter 5, which is devoted to the study of sedimentation processes, we generalize these ideas and link them to our basic model (3.1), (3.2).

3.10.3   More complicated convection functions

The convection functions we have used so far originate from very simple reaction kinetics. The *law of mass action* (see for example chapter 5 of [Murray93] or the original work on reaction kinetics by L. Michaelis and M. I. Menten, [Michaelis13]) states that the reaction rate is proportional to the product of the concentrations of the reactants. When dealing with two species with concentrations u_1 and u_2, this yields $f(u_1, u_2) = u_1 u_2$, or, when reduced to one dimension, $f(u) = u(1 - u)$. In subsection 3.10.1, we took a first step towards more complex kinetics. Figure 3.10 represents an example of another (fictitious) type of convection function.

3.11   Particle model simulations

The system of convection-diffusion equations used in the present chapter to describe segregation of granular material looks relatively simple. All the particle properties, such as size, weight and surface constitution, and all effects of inter-particle collisions and rebounds from the container walls are resumed in the convection function f. Such a basic model obviously entails the advantage of variability and the possibility of analytical solutions. Nevertheless, one would assume that precise predictions are impossible. Especially the Brazil nut effect, which has, up to date, only been explained heuristically, and which certainly incorporates numerous processes on a microscopic level, seems to be reflected only roughly by the general model. If we want to compare the latter's predictions to real experiments or multi-particle simulations, the crucial point will be to find a convection function comprising all these effects in a balanced manner.

In the present section, we use a particle simulation in order to compare its stationary states to those of our convection-diffusion model. We postpone a detailed description of the algorithm used, as well as several other related particle simulations, to chapter 8. Reconsider the replicator type convection-diffusion system
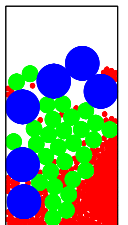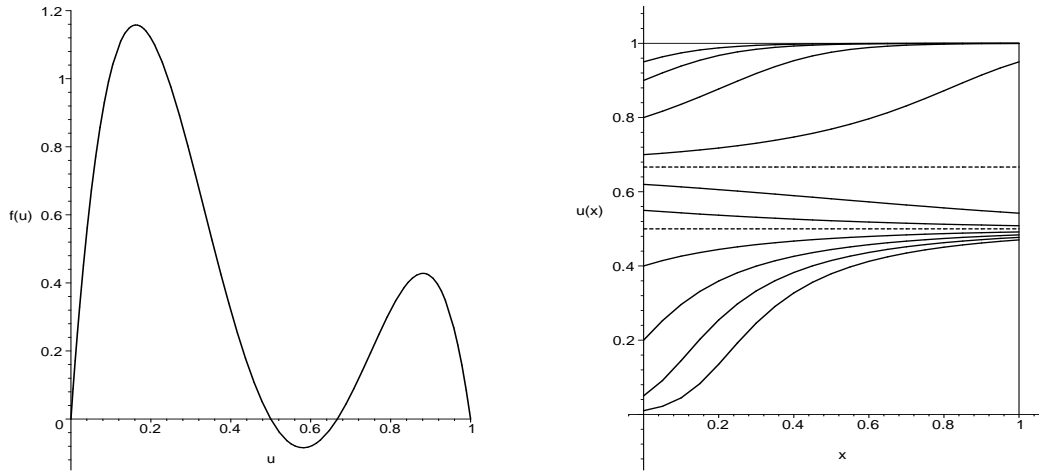
(a) The function $f(u) = 50u(1-u)(\frac{1}{2} - u)(\frac{2}{3} - u)$ as an example of a non-standard convection function.

(b) The corresponding stationary solutions exhibit layers of increasing and decreasing states.

Figure 3.10: More complex convection functions.

with convection function (3.50) for three species, i.e.

$$
\begin{aligned}
u_{1t} &= u_{1xx} + \left(m_1 - \sum_{i=1}^{3} m_i u_i \right) u_1, \\
u_{2t} &= u_{2xx} + \left(m_2 - \sum_{i=1}^{3} m_i u_i \right) u_2, \\
u_{3t} &= u_{3xx} + \left(m_3 - \sum_{i=1}^{3} m_i u_i \right) u_3.
\end{aligned} \tag{3.63}
$$

We interpret the replicator coefficients m_i as *masses*, i.e. with growing m_i the species have higher tendency to move down in the vessel. If we attribute the highest mass to species u_1 and the lowest one to u_3, we expect the species to segregate according to this mass distribution. Since u_3 forms the top layer, we can (with the restrictions explained in subsection 3.10.2) interpret it as the suspension medium. Thus, we reduce the situation to two segregating particle species in fluid or air. Figure 3.11 shows the stationary state of a particle model simulating the sedimentation and segregation of two grain types under the influence of gravity and forced by periodic shaking of the container. In figure 3.12, we compare the density diagrams of the particle model and the replicator equation. Even though the absolute values differ largely, the similarity cannot be dismissed.
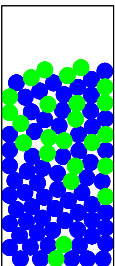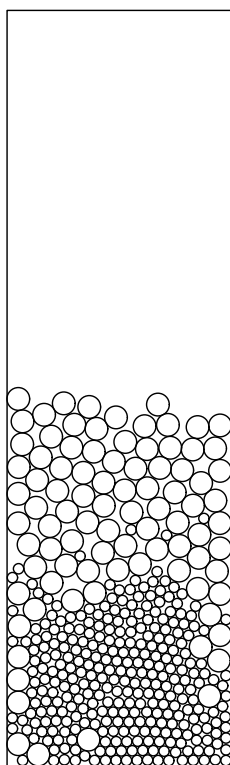
Figure 3.11: Simulation of the segregation of two types of particles under the influence of gravity, forced by periodic shaking of the container holding the granular mixture. We modeled a vessel of height 1 and width 0.3, containing 300 grains of radius $7.5 \cdot 10^{-3}$ and 90 grains of radius $1.5 \cdot 10^{-2}$.

(a) Replicator equation.

(b) Particle simulation.
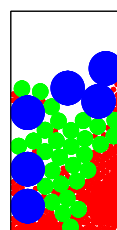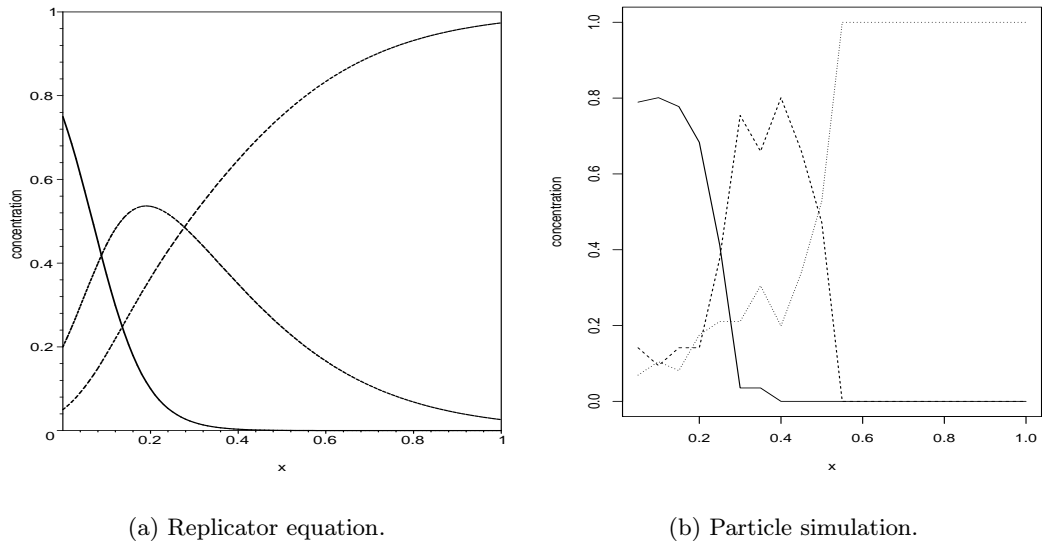
Figure 3.12: Comparison of the stationary states of the replicator equation (a) and the particle simulation (b). The solid and dashed lines represent the first and second grain type, respectively, while the concentration of the medium is the dotted line. Both results agree qualitatively.
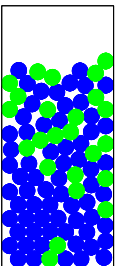
Chapter 4

The two-point boundary value problem

Summary. A two-point boundary value diffusion-convection equation is used to model the segregation and mixing properties of granular material or fluids in a (vertical) container. We prescribe fixed concentrations at both ends of the vessel. Diffusion is due to random *Brownian* motion, caused for example by simple shaking of the vessel. Convection describes the interaction of the species, i.e. the competition between particles or fluids of different type. For convection functions depending only on the concentrations of the species, we show, that the time-dependent solution in the scalar case converges to the unique stationary solution. In the vector-valued case, and for more general convection functions, we prove the existence of stationary solutions.

4.1 Introduction

In chapter 3, we analyzed a diffusion-convection equation with a convection function f depending only on the concentrations of the species. The model was supplied with Neumann boundary conditions, guaranteeing that no matter can enter or leave the vessel through its boundary. In the present chapter, we focus on the corresponding two-point boundary value problem and prescribe constant boundary conditions (sections 4.2 and 4.4). While we treat the special class of convection functions $f = f(u)$ depending only on the concentration u in sections 4.2 through 4.5, our main goal is the generalization to convection functions $f = f(x, u(x))$, depending on the position x in the vessel as well (section 4.7). The corresponding stationary solutions solve boundary value problems of nonlinear ordinary differential equations of second order. H. Epheser (see for example [Epheser55]) gives necessary conditions in terms of Lipschitz bounds on the function. P. Cubiotti and B. Di Bella (see [Cubiotti01]) show existence of stationary solutions under relatively strong conditions on f. Their result is generalized to functions satisfying certain global Lipschitz bounds in [DiBella02]. In section 4.7, we prove existence
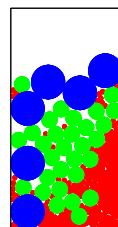
of the solution for continuous, globally bounded f, using a different approach. As in the case $f = f(u)$, our proof can be generalized to functions with Lipschitz bounds for small containers. Uniqueness follows in section 4.8 for the scalar case.

4.2   The model

As in chapter 3, we consider a (vertical) vessel containing a mixture of fluids or particles with different physical properties. Instead of closing the vessel at both ends, we imagine it to be connected to two large reservoirs, so-called wash vessels, which contain given constant concentrations. Instead of using static reservoirs, the ends of the container could be washed with a medium of constant concentration (see figure 4.1). A similar situation naturally occurs
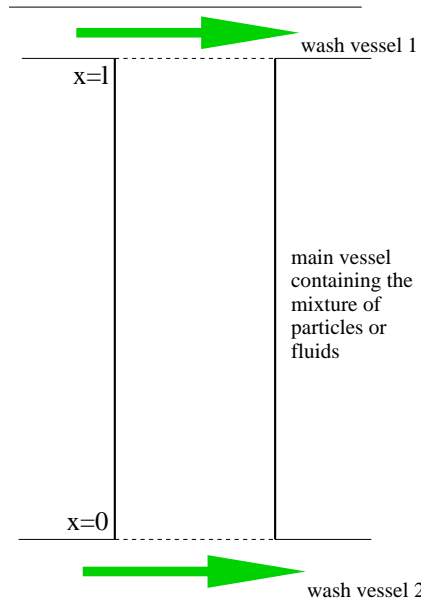
Figure 4.1: Two wash vessels are connected to the top and bottom of the main vessel containing the particle mixture.

for example in rivers, when rocks or artificially inserted walls separate certain compartments from the rest of the river bed. In these areas, the current becomes very small, which gives small fish the possibility to spawn, while the water flux at both ends of the separated compartment provides fresh water and nutrient.

In a first step, let us assume one single species in the vessel. The general case of more than one species will be treated in section 4.6, and again, for a more general convection function, in section 4.7. Under the above assumptions, the concentrations at the boundary of the main vessel will be equal to the concentrations
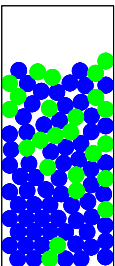
of the respective wash media for all time. As in chapter 3, we reduce the three-dimensional vessel to one dimension and study the problem on the interval $[0, l]$. Hence, we impose the boundary condition

$$u(t, 0) = a, \quad u(t, l) = b, \tag{4.1}$$

where a and b are constant vectors. We use a convection function f of the same type as in chapter 3, i.e. we assume, that $f \in \mathcal{C}^2(\mathbb{R})$ satisfies conditions (c) through (e) in section 3.2. If we further restrict to constant diffusion $d(u) \equiv 1$, then our model takes the form

$$u_t = u_{xx} - f(u)_x \tag{4.2}$$

with the Dirichlet boundary condition (4.1). Here, $u = u(t, x)$ is the n-dimensional concentration vector, defined for $x \in [0, l]$ for some positive container height l. It is obvious, that problem (4.2), (4.1) does not preserve the total mass of the species, since material will leave (or enter) the main vessel according to the concentration gradients across the two ends. In the case of two interacting species, we can eliminate one equation via $u_2 = 1 - u_1$ and obtain a scalar model. This special case will be treated in sections 4.4, 4.5 and 4.8.

4.3 Positivity and upper bounds

As in the case with Neumann boundary condition treated in chapter 3, the time-dependent solutions of the two-point problem are bounded:

Proposition 4.3.1 (Positivity and boundedness.) *Consider system (4.2) with Dirichlet boundary condition (4.1).*
(i) Suppose the n concentrations add up to one at $t = 0$, i.e. $e^T u(0, x) = 1$ for all $x \in [0, l]$, where $e = (1, \ldots, 1)^T$. If the boundary condition also satisfies $e^T a = e^T b = 1$, then this property is preserved for all positive times.
(ii) Furthermore, $u_i(t, x) \in [0, 1]$, $i = 1, \ldots, n$, for all $t > 0$ and for all $x \in [0, l]$, if the components $u_i(0, x)$ of the initial function are bounded in between zero and one, and if the boundary condition satisfies $a_i, b_i \in [0, 1]$, $i = 1, \ldots, n$.

Proof. Property (i) follows from assumption (c). Positivity can be proven similarly to the granular matter case with Neumann boundary condition, model (3.1), (3.2) in section 3.2 of chapter 3. Here, we need assumptions (d) and (e). Finally, boundedness from above follows from the positivity and from (i). For details, we refer to the proofs of proposition 3.2.1 in section 3.2 and proposition 3.5.1 in section 3.5. $\square$.

In the scalar case $n = 1$, we can prove a somewhat stronger result.
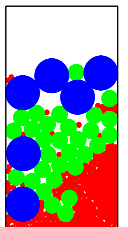
Proposition 4.3.2 (Local extrema.)   *The solutions of the scalar model (4.2), (4.1) do not develop local extrema away from the boundary $x = 0, l$. In other words, if the initial function $u^0 = u(0, \cdot)$ is monotone, then monotonicity is preserved for all times.*

Proof. Define the family of functions $v(t) := -\epsilon e^t$ with parameter $\epsilon > 0$, and consider the difference $u - v$. Suppose $u - v$ touches a value $\gamma \in \mathbb{R}$ from above for the first time at $t = t_0 > 0, x = x_0 \in (0, l)$. Then, u is strictly less than γ in some neighborhood around x_0, since $v < 0$. At (t_0, x_0), we have

$$
\begin{aligned}
0 \geq (u - v)_t \\
= u_{xx} - f'(u)u_x + \epsilon e^t \\
> 0,
\end{aligned}
$$

since $v_x \equiv 0$ and hence $u_{xx}(t_0, x_0) \geq 0$, $u_x(t_0, x_0) = 0$. This is a contradiction. Since the above argument goes through for any $\epsilon > 0$, the concentration u cannot drop below γ locally at an interior point, i.e. u cannot develop local minima. Using the same argument with $v(t) := \epsilon e^t$, we deduce, that the solution cannot form local maxima, either. This proves proposition 4.3.2. $\square$.

Proposition 4.3.2 in particular yields positivity for $\gamma = 0$. Furthermore, we educe, that the time-dependent solution satisfies the lower and upper bounds assumed by the initial distribution. In other words, if

$$
\begin{aligned}
\underline{u} := \min_{x \in [0,l]} \{u^0(x)\}, \\
\overline{u} := \max_{x \in [0,l]} \{u^0(x)\},
\end{aligned}
$$

then $u(t, x) \in [\underline{u}, \overline{u}]$ for all $t \geq 0$, $x \in [0, l]$.

4.4   Existence and uniqueness of stationary solutions in the scalar case

The stationary problem corresponding to the scalar equation (4.2) in integrated form is

$$
u_x = f(u) + \lambda, \tag{4.3}
$$

with simultaneous consideration of (4.1). As the following proposition shows, the stationary solutions of (4.3) with boundary condition (4.1) always exist and are unique.

Proposition 4.4.1 (Existence and uniqueness.)   *Under the assumption $f \in \mathcal{C}^2(\mathbb{R})$ made in section 4.2, the boundary value problem (4.3), (4.1) has a unique solution for every height $l > 0$ of the vessel.*
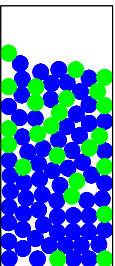
Proof. First assume $a < b$. Differentiation of (4.3) yields $u_{xx} = f'(u)u_x$, i.e. with $v := u_x$,

$$u_x = v,$$
$$v_x = f'(u)v. \tag{4.4}$$

The points $(u, 0)$ are the only stationary points of the planar system (4.4). For $v \neq 0$, we can rescale the x-variable in order to get

$$u_x = 1,$$
$$v_x = f'(u). \tag{4.5}$$

This does not change the trajectories of the system away from the axis $v = 0$. These trajectories satisfy $dv/du = f'(u)$, and are thus given by the one-parameter family

$$v = f(u) + \lambda. \tag{4.6}$$

Note that we are only interested in solutions of (4.5), for which $v \neq 0$ for all x, since the original system (4.4) otherwise reduces to $u_x = v_x = 0$ and does not have a solution for $a \neq b$. For $a < b$, we seek solutions with $v > 0$ for all x. Put

$$\lambda_0 := -\min_{a \leq u \leq b} f(u).$$

If $\lambda > \lambda_0$, then $f(u) + \lambda > 0$ for $a \leq u \leq b$, and the piece of trajectory

$$\Gamma_{ab} := \{(u, v) | a \leq u \leq b, v = f(u) + \lambda\}$$

connecting $\{u = a\}$ to $\{u = b\}$ remains entirely in the half-space $v > 0$. Hence, it yields a solution of (4.3), (4.1) for some $l > 0$ (see figure 4.2). Consider the equation

$$l = \int_0^l dx = \int_a^b \frac{dx}{du} du = \int_a^b \frac{du}{f(u) + \lambda}. \tag{4.7}$$

We interrupt the proof of proposition 4.4.1 for an auxiliary lemma.

Lemma 4.4.2 (Bijection.) *Equation (4.7) gives us a one-to-one correspondence between values $l > 0$ and the solutions of (4.3), (4.1), determined by the parameter λ with $\lambda_0 < \lambda < \infty$. In other words, the following hold:*
(a) l is a strictly decreasing function of λ.
(b) $l = l(\lambda)$ tends to zero as $\lambda \longrightarrow \infty$.
(c) $l \longrightarrow \infty$ as $\lambda \longrightarrow \lambda_0+$.

Proof. (a) follows directly from (4.7). For large $\lambda > \lambda_0$, the denominator $f(u) + \lambda$ becomes large, hence (b). For the proof of (c), we proceed in two steps. Since we assumed $a < b$, we know that $f(u) + \lambda_0 \geq 0$ in $[a, b]$. First suppose $f(a) + \lambda_0 = 0$ or $f(b) + \lambda_0 = 0$. Without loss of generality, we can assume the former. Denote
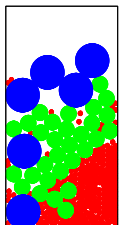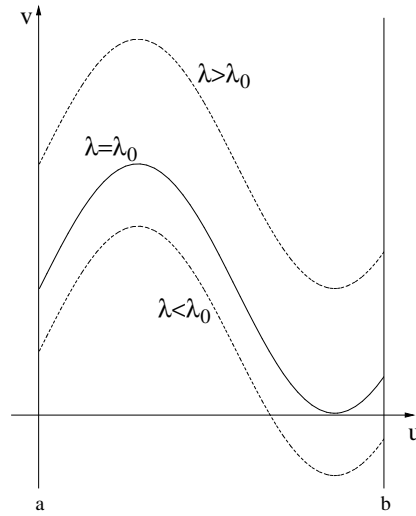
Figure 4.2: Sketch of the one-parameter family of solutions of (4.3).

$S := f'(a) < \infty$. Then, under the assumption of continuous differentiability of f, we have

$$f(u) + \lambda_0 < (S+1)(u-a)$$

in $[a, a+\epsilon)$ for some $\epsilon > 0$. Hence,

$$\int_a^{a+\epsilon} \frac{du}{f(u)+\lambda} > \int_a^{a+\epsilon} \frac{du}{(S+1)(u-a)+\lambda-\lambda_0},$$

which tends to infinity as $\lambda \longrightarrow \lambda_0+$. Now suppose $f(z) = 0$ for some $z \in (a, b)$. Since $f(u) \geq 0$ for all $u \in [a, b]$, we must have $f'(z) = 0$, i.e. for all $S > 0$, there is a positive ϵ, such that $f(u) < S(u-z)$ for all $u \in (z, z+\epsilon)$. Consequently,

$$\int_z^{z+\epsilon} \frac{du}{f(u)+\lambda} > \int_z^{z+\epsilon} \frac{du}{S(u-z)+\lambda-\lambda_0},$$

which grows infinitely large as $\lambda \longrightarrow \lambda_0+$. This proves lemma 4.4.2. $\square$.

For $a > b$, the above argument goes through in the same way with $f(u) + \lambda < 0$. Finally, $a = b$ yields the stationary solution $u \equiv a$ for any $l > 0$. This proves proposition 4.4.1. $\square$.

4.5   Dynamics of the scalar equation

Now that we have shown the existence and uniqueness of stationary solutions of (4.2), (4.1) in the scalar case, we are naturally interested in the question of global stability of these equilibria.
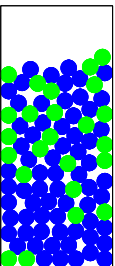
Proposition 4.5.1 (Convergence for the scalar equation.) *Every solution of the scalar two-point problem (4.2), (4.1) converges to a stationary solution as $t \to \infty$.*

Proof. In case $a = b$, we define $w = w(t, x) := u(t, x) - a$. This function satisfies $w_t = u_t$, $w_x = u_x$ and $w_{xx} = u_{xx}$, i.e. w solves the equation

$$w_t = w_{xx} - f'(u)w_x \tag{4.8}$$

with boundary condition $w(0) = w(l) = 0$. Problem (4.8) has a unique solution which tends to zero uniformly on the interval $[0, l]$ as $t \to \infty$ ([Friedman64], p. 158, theorem 1). Thus u tends to a uniformly as $t \to \infty$.

In the general case $a, b \in [0, 1]$, the situation is more complicated, and a simple subtraction of the straight line $s(x) := a + (b-a)x/l$ does not solve the problem. In [Brunovsky92], the authors prove a more general result concerning the convergence of solutions of one-dimensional, non-autonomous equations with both the diffusion matrix and the convection function being periodic in time. Instead of reproducing their proof for our case of autonomous equations, we refer to their article, as well as to previous work by H. Matano (see [Matano78], [Matano88]). $\square$

4.6 Stationary solutions of the vector-valued equation

In the general vector-valued case, we admit a mixture of $n \geq 3$ species in the vessel. Even though we can not expect the stationary solutions of system (4.2), (4.1), i.e. solutions of

$$u_{xx} = f(u)_x \tag{4.9}$$

with boundary condition

$$\begin{aligned} u(0) &= a, \\ u(l) &= b, \end{aligned} \tag{4.10}$$

to be unique, the latter always exist if the convection function f is bounded:

Theorem 4.6.1 (Existence of equilibria in the multi-dimensional case.) *Suppose $\|f(u)\| \leq M$ for all $u \in \mathbb{R}^n$ for some positive constant M, where $\|\cdot\|$ denotes the Euclidean norm in $\mathbb{R}^n$. Then, system (4.9), (4.10) has a (not necessarily unique) solution for any given vectors a and b.*

Proof. We will use a degree argument. Problem (4.9) is equivalent to

$$u_x = f(u) + \lambda, \tag{4.11}$$

in consideration of (4.3), for any constant vector λ. Thus, let a container length $l > 0$ and vectors $a, b \in \mathbb{R}^n$ be given. In order to solve (4.11), we have to find a
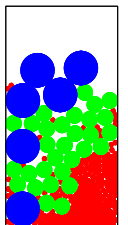
vector λ, such that

$$u(l) = u(0) + \int_0^l f(u(x))dx + \int_0^l \lambda dx$$

$$= a + \int_0^l f(u(x))dx + l\lambda$$

$$= b$$

holds, where $u(x)$ satisfies $u_x = f(u) + \lambda$. We can assume $a = 0$ without loss of generality. For $0 \leq \epsilon \leq 1$, define the mapping $F_\epsilon : \mathbb{R}^n \longrightarrow \mathbb{R}^n$ by

$$F_\epsilon(\lambda) = \epsilon \int_0^l f(u(x))dx + l\lambda - b. \qquad (4.12)$$

F_ϵ is continuous for every $0 \leq \epsilon \leq 1$ and depends continuously on the parameter ϵ. Solving (4.9), (4.10) is equivalent to finding a zero of F_1 in $\mathbb{R}^n$. In the sequel, we determine an adequate domain for the mapping F_ϵ. The equation $F_\epsilon(\lambda) = 0$ is equivalent to

$$l\lambda = b - \epsilon \int_0^l f(u(x))dx,$$

and thus, since f is assumed to be globally bounded by M,

$$\|\lambda\| \leq \frac{\|b\|}{l} + \epsilon M.$$

Define the domain $\mathcal{B} \subset \mathbb{R}^n$ as

$$\mathcal{B} := \left\{\lambda \ : \ \|\lambda\| \leq \frac{\|b\|}{l} + M + \delta\right\}$$

for some fixed small value $\delta > 0$. We interrupt the proof of theorem 4.6.1 to state an auxiliary lemma.

Lemma 4.6.2 (Zeros on the boundary.) *The mapping F_ϵ has no zero on the boundary $\partial\mathcal{B}$ of $\mathcal{B}$ for $0 \leq \epsilon \leq 1$.*

Proof. Let $\lambda \in \partial\mathcal{B}$. From

$$u(l) = \epsilon \int_0^l f(u(x))dx + l\lambda,$$

we get the estimate

$$\|u(l)\| + \epsilon \int_0^l \|f(u(x))\|dx \geq l\|\lambda\|,$$
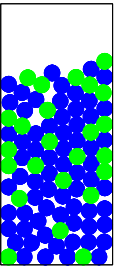
and hence,

$$\begin{aligned}
\|u(l)\| &\geq l\|\lambda\| - \epsilon lM \\
&\geq l\|\lambda\| + lM + l\delta - \epsilon lM \\
&> \|b\|
\end{aligned}$$

for $0 \leq \epsilon \leq 1$. This proves lemma 4.6.2. $\square$

We resume the proof of theorem 4.6.1. By lemma 4.6.2, F_ϵ is a homotopy. For $\epsilon = 0$, the problem $F_\epsilon(\lambda) = F_0(\lambda) = 0$ always has a solution, namely $\lambda = b/l$. In view of lemma 4.6.2 and with the help of the homotopy invariance theorem, we conclude the existence of a zero of F_1, and hence the existence of a stationary solution of system (4.2), (4.1). This proves theorem 4.6.1. $\square$

Under somewhat weaker growth conditions on the function f, we can prove the existence of stationary solutions for small containers. Again, we assume $a = 0$ without loss of generality.

Theorem 4.6.3 (Existence of equilibria for small containers.) *Suppose f satisfies $\|f(u)\| \leq \alpha + \beta\|u\|$ for some non-negative constants α and β. If the container height l is less than $1/(2\beta)$, then a stationary solution of system (4.2), (4.1) always exists.*

Proof. We proceed as in the case of theorem 4.6.1 and define a homotopy F_ϵ by (4.12) for $0 \leq \epsilon \leq 1$. From $F_\epsilon(\lambda) = 0$, we get

$$\|\lambda\|l \leq \|b\| + \epsilon l(\alpha + \beta m),$$

where $m \geq 0$ is the maximal norm the solution u of (4.11) can assume when x runs from 0 to l. In the worst case $\epsilon = 1$, hence

$$\|\lambda\|l \leq \|b\| + l(\alpha + \beta m). \tag{4.13}$$

Using

$$u(l) = \epsilon \int_0^l f(u(x))dx + \lambda l,$$

we can give an upper bound for m. We have

$$m \leq l(\alpha + \beta m + \|\lambda\|),$$

hence

$$m \leq \frac{(\alpha + \|\lambda\|)l}{1 - \beta l},$$

and therefore, by (4.13),

$$\|\lambda\|l \leq \|b\| + l\left(\alpha + \beta\frac{(\alpha + \|\lambda\|)l}{1 - \beta l}\right),$$
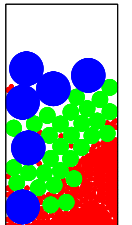
or

$$\|\lambda\| l \left(1 - \frac{\beta l}{1 - \beta l}\right) \le \|b\| + l \left(\alpha + \beta \frac{\alpha l}{1 - \beta l}\right). \qquad (4.14)$$

For $\beta l < 1/2$, the term $1 - \beta l/(1 - \beta l)$ on the left-hand side of equation (4.14) is strictly positive, and hence

$$\|\lambda\| l \le \frac{\|b\|(1 - \beta l) + \alpha l}{1 - 2\beta l}.$$

Define the domain $\mathcal{D} \subset \mathbb{R}^n$ by

$$\mathcal{D} := \left\{\lambda \ : \ \|\lambda\| \le \frac{\|b\|(1 - \beta l) + \alpha l}{(1 - 2\beta l)l} + \delta\right\}$$

for some small $\delta > 0$. Then, F_ϵ has no zero on $\partial \mathcal{D}$ for $0 \le \epsilon \le 1$. $F_0(\lambda) = 0$ has the trivial solution $\lambda = b/l$. Hence, F_1 has at least one zero. This proves theorem 4.6.3. $\square$.

4.7   Existence for general convection functions

We now generalize problem (4.2), (4.1) to a wider class of convection functions $f = f(x, u(x))$, depending on the concentrations as well as on the position in the vessel. In the present section, we prove a result similar to [DiBella02], using a different approach. This will pave the way for the proof of uniqueness in the scalar case in section 4.8.

Theorem 4.7.1 (Global existence of the time-dependent solution.)   *Let the vector-valued function $f = f(x, u(x))$ be defined on $[0, l] \times \mathbb{R}^n$ (as in section 4.2, we assume $f \in \mathcal{C}^2$), and consider the two-point problem*

$$u_t = u_{xx} - f(x, u(x))_x \qquad (4.15)$$

with boundary values

$$\begin{aligned} u(0) &= a, \\ u(l) &= b, \end{aligned} \qquad (4.16)$$

where a and b are constant concentration vectors. If f is globally bounded, i.e. if $\|f(x, u)\| \le M \ \forall x \in [0, l] \ \forall u \in \mathbb{R}^n$ for some $M \ge 0$, then (4.15), (4.16) has a stationary solution.

Problem (4.15) is of the form

$$u_t = u_{xx} - g(x, u, u_x). \qquad (4.17)$$

In the case, where g actually depends on x, (4.15), (4.16) takes a somewhat simpler form. Introducing $v = v(t,x) := u(t,x) - [a + x(b-a)/l]$, we find $v_x = u_x - (b-a)/l$ and $v_{xx} = u_{xx}$. Thus, v satisfies a similar equation, namely

$$v_t = v_{xx} - g\left(x, v + a + x\frac{b-a}{l}, v_x + \frac{b-a}{l}\right) \qquad (4.18)$$

with boundary condition

$$v(0) = v(l) = 0. \qquad (4.19)$$
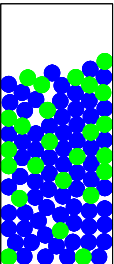
This argument shows, that if g depends on x explicitly, then we can assume (4.19) instead of (4.16) without loss of generality.

Historically, there are two standard approaches to solving (4.17), (4.16), the contraction principle and the degree argument. The contraction approach was initiated by Picard (see for example [Picard08] and [Picard30]), the sharpest results, in terms of Lipschitz bounds on g, were obtained by H. Epheser ([Epheser55]) and later by P. Cubiotti and B. Di Bella (see [Cubiotti01] and [DiBella02]).

Stationary solutions of (4.15) correspond to solutions of

$$u_x = f(x, u) + \lambda, \qquad (4.20)$$

which is the stationary equation in integrated form. It is important to notice that, given $\lambda \in \mathbb{R}$, solutions of (4.20), (4.16) do not always exist for all positive x. A simple counter-example in the one-dimensional case is the equation $u_x = u^2 + \lambda$ with initial value $u(0) = a > 0$. The situation is even worse. If we merely assume continuity of f, solutions of (4.20), (4.16) may not exist for any λ, even in the scalar case. [DiBella02] gives a counter-example and shows, that solutions of (4.20) with zero boundary condition in one dimension exist for any λ, if there are constants $p > 0$ and $q \geq 0$ such that $|f(x,u)| \leq p + q|u|$.

Proof. In order to prove theorem 4.7.1, we use the invariance of the so-called *Leray-Schauder degree* of a certain operator under homotopies, i.e. we adapt the proof of theorem 4.6.1 in section 4.6 to the general convection function. Introduce a new parameter $\epsilon \in [0, 1]$, and consider the family of boundary value problems

$$u_x = \epsilon f(x, u) + \lambda \qquad (4.21)$$

with boundary condition (4.16). For $\epsilon = 0$, the solution of (4.21), (4.16) is straightforward:

Lemma 4.7.2 (Trivial solution.) *Let $\epsilon = 0$. Problem (4.21) then takes the simple form $u_x = \lambda$. Thus, given the boundary values (4.16), $\lambda = (b-a)/l$, and the unique solution is given by $u(x) = a + x(b-a)/l$.* $\square$
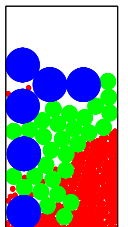
In the general case $\epsilon \in [0, 1]$, integration of (4.21) yields

$$u(x) = \epsilon \int_0^x f(s, u(s))ds + \lambda x + a, \qquad (4.22)$$

and thus

$$u(l) = b = \epsilon \int_0^l f(s, u(s))ds + \lambda l + a. \qquad (4.23)$$

With the boundedness assumption on f, we find

$$\|\lambda\|_\infty \leq \left\|\frac{b-a}{l}\right\|_\infty + \epsilon M, \qquad (4.24)$$

where $\|\cdot\|$ denotes the maximum norm of a vector. We now give an estimate for u. From (4.22), we obtain

$$\|u(x)\| \leq \|a\|_\infty + \|\lambda x + \epsilon \int_0^x f(s, u(s))ds\|_\infty$$

$$\leq \|a\|_\infty + \left\|\left(\left\|\frac{b-a}{l}\right\|_\infty + \epsilon M\right) x + \epsilon x M\right\|_\infty$$

$$\leq \|a\|_\infty + \left\|\frac{b-a}{l}\right\|_\infty l + 2\epsilon M l$$

using (4.24), and thus

$$\|u(x)\|_\infty \leq 2 \left(\max\left\{\|a\|_\infty, \|b\|_\infty\right\} + \epsilon M l\right). \qquad (4.25)$$

For some small $\delta > 0$, define the set

$$\mathcal{B} := \{(u, \lambda) : \|u\|_\infty \leq 2\left(max\{\|a\|_\infty, \|b\|_\infty\} + \epsilon M l\right) + \delta,$$

$$\|\lambda\|_\infty \leq \left\|\frac{b-a}{l}\right\|_\infty + \epsilon M + \delta\},$$

which is a closed box in $(\mathcal{C}[0, 1])^n \times \mathbb{R}^n$. If u is a solution of (4.21), (4.16) for any given $\epsilon \in [0, 1]$ with corresponding λ, then $(u, \lambda) \in \mathcal{B} \setminus \partial\mathcal{B}$. For $\epsilon \in [0, 1]$, define a vector field $T_\epsilon : (\mathcal{C}[0, l])^n \times \mathbb{R}^n \to (\mathcal{C}[0, l])^n \times \mathbb{R}^n$ by

$$T_\epsilon \begin{pmatrix} u \\ \lambda \end{pmatrix}(x) := \begin{pmatrix} u(x) - a - \lambda x - \epsilon \int_0^x f(s, u(s))ds \\ \lambda - \frac{b-a}{l} + \frac{\epsilon}{l} \int_0^l f(s, u(s))ds \end{pmatrix} \qquad (4.26)$$

for $x \in [0, l]$.

Lemma 4.7.3 (Homotopy.) *Let $\epsilon \in [0, 1]$. Then T_ϵ is a homotopy on $\mathcal{B}$, and $0 \notin T_\epsilon(\partial\mathcal{B})$.*
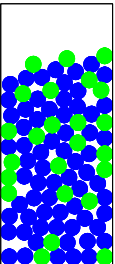
Proof. The statement follows from (4.24) and (4.25). □.

We use the *Leray-Schauder degree* of the homotopy $T_\epsilon : \mathcal{B} \to \mathcal{B}$ in order to prove existence of solutions of problem (4.20), (4.16). (For a detailed introduction to the Leray-Schauder degree see for example [Deimling74].) This degree can be defined for operators of the form $T = I - K$, where I is the identity and K is compact. Compactness is established by the following lemma:

Lemma 4.7.4 (Compact operator.) *The vector field T_ϵ defined by (4.26) is of the form $I - K$ with compact K.*

Proof. We have to show that $K := I - T_\epsilon$ is compact for every $\epsilon \in [0,1]$. K is defined by

$$K \begin{pmatrix} u \\ \lambda \end{pmatrix} (x) = \begin{pmatrix} a + \lambda x + \epsilon \int_0^x f(s, u(s)) ds \\ \frac{b-a}{l} - \frac{\epsilon}{l} \int_0^l f(s, u(s)) ds \end{pmatrix}.$$

Let us first consider the operator $P : u \mapsto \int_0^x f(s, u(s)) ds$.
Uniform boundedness: Since f is continuous and thus bounded on $C := [0,l] \times ([0,1])^n$, there is a positive constant R, such that $\|f\|_\infty \leq R$. Thus, $\|Pu\|_\infty \leq Rl$, i.e. P is uniformly bounded on C.
Equi-continuity: Let $\xi > 0$ and $|x - x'| < \xi$. Then

$$\|(Pu)(x) - (Pu)(x')\|_\infty = \left\| \int_0^x f(s, u(x)) ds - \int_0^{x'} f(s, u(s)) ds \right\|_\infty$$
$$= \left\| \int_{x'}^x f(s, u(x)) ds \right\|_\infty$$
$$\leq |x - x'| R$$
$$< \xi R$$

for any integrable function u with values in $([0,1])^n$, i.e. the functions $P(u)$ are equi-continuous.
Using the Arzelà-Ascoli theorem, we conclude that P is compact. The rest is straightforward. Since a and b are constant vectors and the term λx is linear in x, the operator K is compact as well. This proves lemma 4.7.4. □.

We now have all the tools, which are necessary to establish the existence of solutions of the original problem (4.20), (4.16). If S is the set of solutions of problem (4.21), (4.16), then $S \subset \mathcal{B}$, and furthermore $T_\epsilon(S) = 0$. Since T_ϵ is of the form $I - K$ with compact K, we can define the Leray-Schauder degree $D(T_\epsilon, \mathcal{B}, 0)$. Since T_ϵ is a homotopy with parameter ϵ, and since $D(T_0, \mathcal{B}, 0) = 1$, we also have $D(T_1, \mathcal{B}, 0) = 1$, i.e. problem (4.20), (4.16) has at least one solution. This proves theorem 4.7.1. □.
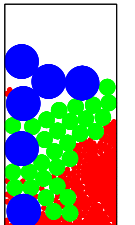
Note that we can generalize the statement of theorem 4.7.1 to convection functions satisfying global Lipschitz bounds, as we have done in 4.6.3 for the special case $f = f(u)$:

Theorem 4.7.5 (Existence of equilibria for small containers for general f.) *Suppose f is continuous and satisfies $\|f(x, u)\| \leq \alpha + \beta u$ for positive constants α and β. If $l < 1/(2\beta)$, then problem (4.15), (4.16) has at least one stationary solution.*

Proof. We refer to the proof of theorem 4.6.3. $\square$.

4.8   Uniqueness of stationary solutions in the scalar case

The approach developed in section 4.7 can be used to prove the uniqueness of stationary solutions in the scalar case:

Theorem 4.8.1 (Uniqueness of equilibria in the scalar case.) *Under the assumptions made in theorem 4.7.1, problem (4.15), (4.16) has a unique stationary solution in the scalar case.*

Proof. We fall back on the operator T_ϵ defined in (4.26).

Lemma 4.8.2 (Non-positive eigenvalues.) *For every $\epsilon \in [0, 1]$, the linear part of T_ϵ always has two non-positive real eigenvalues or none at all.*

Proof. If L_ϵ is the linearization of T_ϵ around $(u, \lambda) \in \mathcal{B}$, then small perturbations (ν, μ) satisfy

$$L_\epsilon \begin{pmatrix} \nu \\ \mu \end{pmatrix} (x) = \begin{pmatrix} \nu(x) - \mu x - \epsilon \int_0^x f_u(s, u(x))\nu(s)ds \\ \mu + \frac{\epsilon}{l} \int_0^l f_u(s, u(s))\nu(s)ds \end{pmatrix}. \tag{4.27}$$

Here, f_u is the derivative of f with respect to the scalar u. The eigenvalue equation for L_ϵ takes the form $L_\epsilon(\nu, \mu)^T = \gamma(\nu, \mu)^T$, i.e.

$$\gamma\nu(x) = \nu(x) - \mu x - \epsilon \int_0^x f_u(s, u(s))\nu(s)ds, \tag{4.28}$$

$$\gamma\mu = \mu + \frac{\epsilon}{l} \int_0^l f_u(s, u(s))\nu(s)ds. \tag{4.29}$$

Differentiation of (4.28) for $\gamma = neq1$ yields

$$\nu'(x) = \frac{\mu}{1 - \gamma} + \frac{\epsilon}{1 - \gamma} f_u(x, u(x))\nu(x),$$

the solution of which is given by

$$\nu(x) = \frac{\mu}{1 - \gamma} \int_0^x \left(e^{\int_s^x \frac{\epsilon}{1-\gamma} f_u(\tau, u(\tau))d\tau} \right) ds + \nu_0 e^{\int_0^x \frac{\epsilon}{1-\gamma} f_u(\tau, u(\tau))d\tau} \tag{4.30}$$
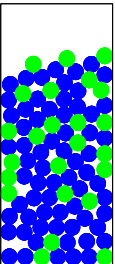
(variation of constants). Using (4.28), we get $\nu(0)(\gamma - 1) = 0$, i.e. $\nu(0) = \nu_0 = 0$ for $\gamma \neq 1$. (4.28) also implies

$$\nu(l)(\gamma - 1) = -\mu l - \epsilon \int_0^l f_u(s, u(s))\nu(s)ds,$$

and, in combination with (4.29), we find

$$\nu(l) = \frac{\gamma}{1 - \gamma}\mu l. \tag{4.31}$$

First consider the case $\gamma \neq 1$, i.e. $\nu_0 = 0$. Setting $x = l$ in (4.30) and comparing to (4.31), we get

$$\gamma = \frac{1}{l} \int_0^l \left(e^{\frac{\epsilon}{1-\gamma} \int_s^l f_u(\tau, u(\tau))d\tau} \right) ds > 0 \tag{4.32}$$

Therefore, the real solutions of (4.28), (4.29) are strictly positive if they exist. The case $\gamma = 1$ does not alter this result. This proves lemma 4.8.2. $\square$.

Using theorem 4.7 on page 136 of [Krasnosel'skii64], we conclude that the index of every potential zero of T_ϵ is one. Using lemma 4.7.3 in section 4.7, theorem 4.8.1 follows by the homotopy invariance theorem. $\square$.
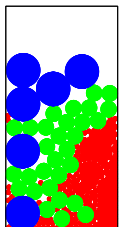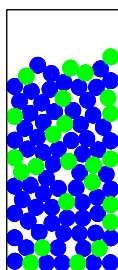
Chapter 5

Sedimentation

Summary. In the present section, we interpret the general diffusion-convection equation developed and analyzed in chapter 3 in the context of sedimentation. We recall earlier sedimentation models and try to carry over the basic mechanisms leading to sedimentation of granular material in liquid suspension and identify the corresponding parameters in our model.

5.1   Introduction

Sedimentation is by definition the process of depositing matter suspended in a fluid as a result of gravitation and interaction of particles with the fluid and possibly between particles. Most often, the deposited material consists of solid particles suspended in water. Sedimentation is widely observed in nature, for example in the formation of rocks, the formation of ore deposits or the deposition of biological material at the bottom of lakes. It also has great industrial importance, especially in the chemical or biochemical industry. The priming period in the process of biofilm formation and the treatment of wastewater are two areas of application. Another example is the flotation of ore. This is a process of physical separation, whereby an ore is ground with water to produce a pulp. Fine bubbles of air introduced into this pulp attach to the precious minerals, which have been liberated from the rest during the grinding process, and rise to the surface. The froth containing the minerals can then effectively be removed from the mixture. Instead of air bubbles, other chemicals are often used. Last but not least, the principle of sedimentation in a wider sense is used in the various chromatography and electrophoresis techniques, without which modern biological research is unimaginable. Chromatography is a physical method used to separate and analyze complex mixtures. The components to be separated are distributed between two phases, the *stationary bed* and the *mobile phase*, which percolates through the bed. The different rates of migration of the components as the mixture moves over adsorptive materials provide separation. The great importance of this segregation technique arises from the precision with which mixtures can be
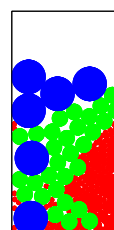
separated and purified, a quality which is indispensable in any chemical or bio-processing industry. Electrophoresis embra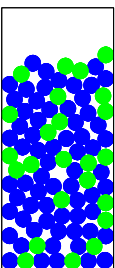ces similar physical principles in order to separate components of mixtures. The technique is based on the movement of analytes through a conductive medium in response to an applied electrical field.

Sedimentation and settling of polydisperse suspensions has been studied in various fields, such as biology, chemistry or geology. In [Batchelor82.1], a relatively simple model describing the settling of a system of spherical particles in suspension is analyzed, while numerical simulations are carried out in [Bürger00.1] and [Bürger00.2]. Finally, [Bustos99] gives a summary of various approaches to sedimentation.

We start by giving a purely heuristic approach to the phenomenon of sedimentation in section 5.2, thus illustrating the dependence of the effect on particle density and specific weight of the material and the surrounding medium. In 1851, G. G. Stokes (see [Stokes51]) formulated his equation governing the limiting settling velocity of spherical particles in a fluid, thus initiating a more and more elaborate discussion on sedimentation processes. We recall the basic idea of his approach in section 5.3. In section 5.4, we develop a general diffusion-convection model for sedimentation and bridge to the analysis carried out in chapter 3. Sections 5.5 and 5.6 link our approach to the well-known Batchelor and Kynch models, respectively. We try to establish parallels between these models and ours and identify the parameters in our equations. In section 5.7, we discuss a new sedimentation approach using non-constant diffusion coefficients. Finally, numerical solutions are illustrated in section 5.8.

5.2   Heuristic approach

Following chapters 3 and 4, we consider a vertical cylinder of height l, represented by $\Omega = [0, l]$ and containing a mixture of grains of different size, density and surface structure. Contrary to the setup we previously had in mind, we now imagine the granular mixture in a liquid suspension. The species of grains are subject to convectional movement (due to the gravitational force) as well as diffusion (random, Brownian motion), the interaction of which we expect to lead to sedimentation of the grains in combination with possible segregation of the different species into more or less distinct layers (see figure 5.1). Depending on the size of the particles and especially their individual shape (spherical or flattened), the friction of the fluid will play a more or less important role. While hydrodynamically favorable shapes experience relatively low frictional forces, grains with leaf structures, which are encountered frequently in the context of sedimentation in geological or biological processes, are subject to much higher forces. In some cases, the sedimentation process may even come to a complete rest, and the particles stay in suspension. An illustrative example taken from the culinary

(a) The initial state: A random mixture of particles in suspension.

(b) An advanced state in the sedimentation process: Sedimentation and segregation are clearly visible.
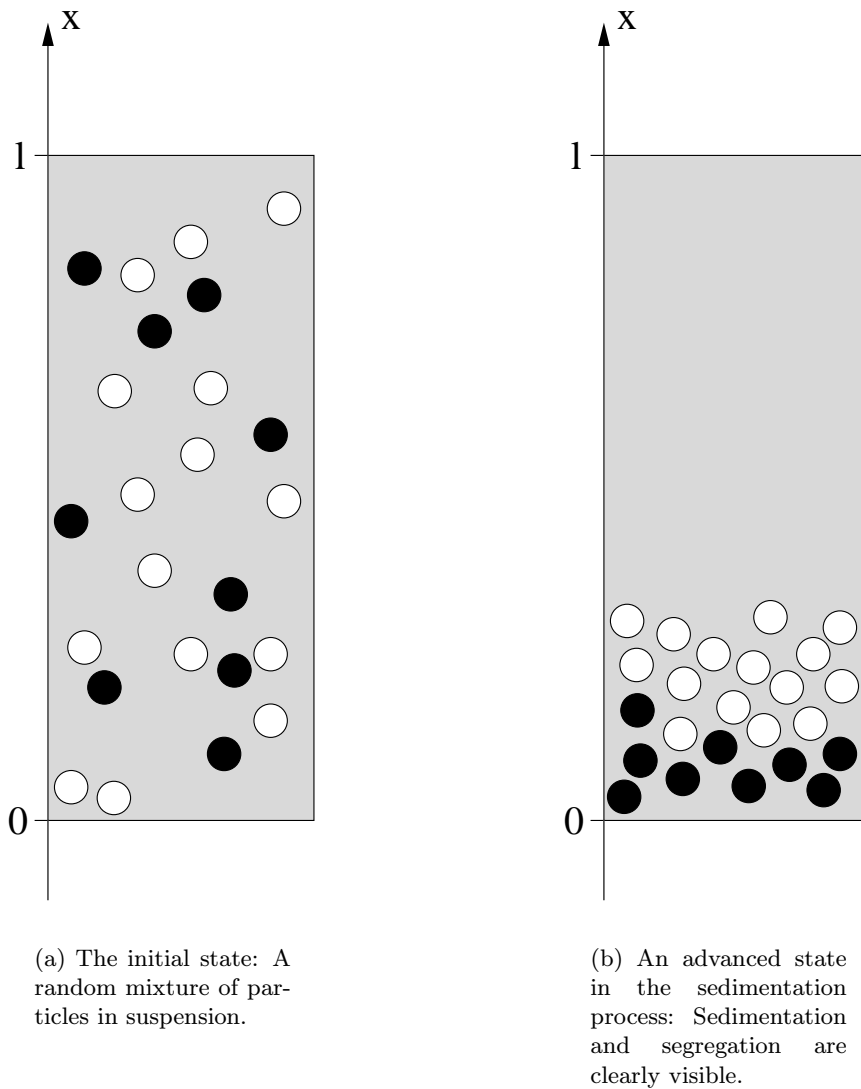
Figure 5.1: Heuristic illustration of the process of sedimentation. Two types of particles (or biological species), represented by spheres, in liquid suspension, subject to gravity and diffusion.

world is the so-called *Danziger Goldwasser*, a liqueur flavored with caraway seed, orange peel and spices. Its name, which translates from German as *gold water*, comes from the fact that it has minuscule flecks of gold leaf suspended in it.

Let $u = u(t, x)$ with $t \geq 0$, $x \in \Omega$ be the density (fraction of the total particle mass) of a granular material in fluid suspension. In general, we consider a mixture of n different species in the container, i.e. u is a vector of dimension n. As in chapter
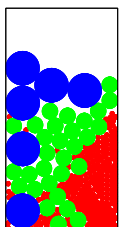
3, let

$$u_t = (u_x - F(u))_x \tag{5.1}$$

be the equation governing the change in concentration of the species. Then, $F(u)$ must have the dimension of a velocity. If we presume further, that F has the form $F(u) = uf(u)$, then f is a velocity as well. We interpret it as the settling velocity of the particles.

Suppose that the density u is relatively high, i.e. that the distance between neighboring particles is about of the order of their diameter. In this case, the particle-particle interactions play an important role in the sedimentation process. We speak of so-called *hindered settling*, as opposed to *free settling*, where the effects of mutual interference may be disregarded. Under these conditions, the particles in suspension have more or less free space to move, depending on whether the density u is high or low (see figure 5.2). From this consideration, we deduce that

(a)   Densely   packed   (b) Moderately dense   (c) Little density; high
balls; velocity zero.   packing; small velocity.   velocity.
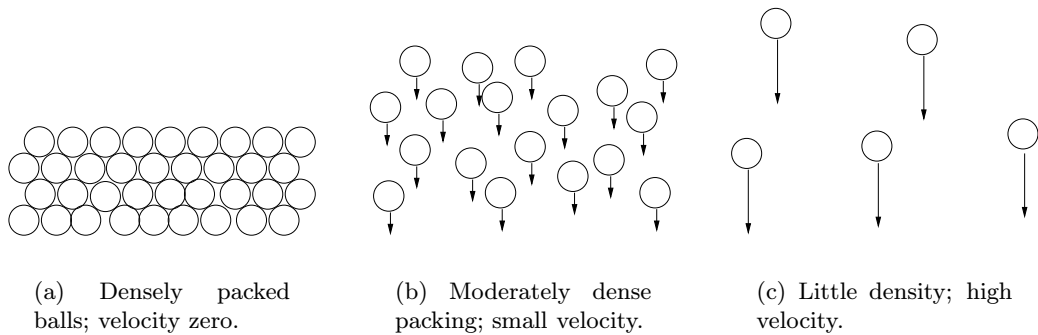
Figure 5.2: The velocity of the particles in the granular material depending on the package density.

their mean settling velocity f decreases with growing u, for example as

$$f(u) = f_{\max} (\bar{u} - u), \tag{5.2}$$

where $f_{\max}$ is the maximal settling velocity and $\bar{u}$ designates the highest packing density (figure 5.3(a)). Finally, $F(u) = uf(u)$ is of logistic type (see figure 5.3(b)). The linear relation (5.2) is only a first approximation, the actual dependence of the velocity on the particle density is of more complicated nature. An example of the resulting model (5.1) has been discussed and simulated in the context of segregation in chapter 3. We point out the particular nature of the diffusive component in equation (5.1). As opposed to the granular matter model, where it enables the particle interaction by creating gaps (due to the shaking of the container, for example), diffusion in the present context describes small perturbations in the movement of the grains due to differences in shape or surface structure, particle

(a) Shape of the function $f = f(u)$.

(b) The logistical function $F(u) = u f(u)$.
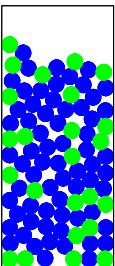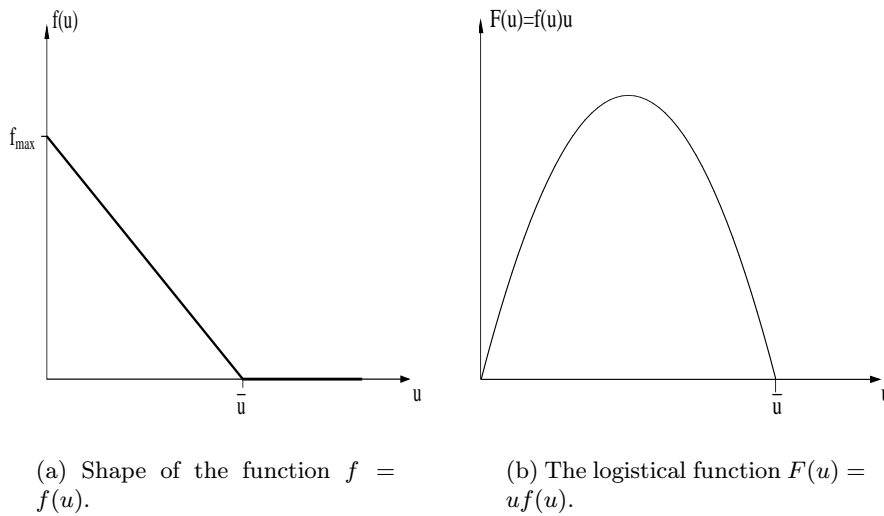
Figure 5.3: The (hypothetically) linear degression of the hindered settling velocity for relatively high concentrations of the species and the resulting convection function of logistic type.

collisions or turbulences in the flow of the fluid. Small diffusion coefficients yield distinct segregation and thus represent the result of an experiment conducted in a very high vessel, while large coefficients lead to less segregated material observed in short containers. This issue will be of importance in section 5.7, where we use diffusion coefficients depending on the concentrations of the particles.

5.3 A simple sedimentation model

Consider a mixture of small spherical particles of two different types, with specific densities ρ_1, ρ_2 and volumes V_1, V_2, respectively. We will carry out the derivation of a simple convection-diffusion equation governing sedimentation in the case of these two types of particles, but the theory can be extended to the general case of n interacting species.

Before we investigate the influence of the fluid surrounding the sedimenting grains more closely in sections 5.4, 5.5 and 5.6, we oversimplify the situation in the present section and neglect the effects of the fluid medium. Thus, we assume that the grains fill up the space completely, without leaving gaps. Since we usually act on the assumption, that these gaps are necessary to enable particle movement at all, we have to attribute the grains a certain fluid quality. Of course, this assumption is incorrect, when we deal with solid particles. Let us focus attention on one of the two species, say the first one, with spheres of radius r_1, volume
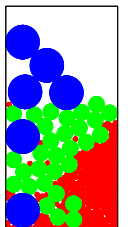
$V_1 = 4\pi r_1^3/3$ and specific weight ρ_1. Pick one of these spheres and denote it by S. It is suspended in a medium composed of species of both types (see figure 5.4). If the species of type i are all spheres with the same density ρ_i, then the medium
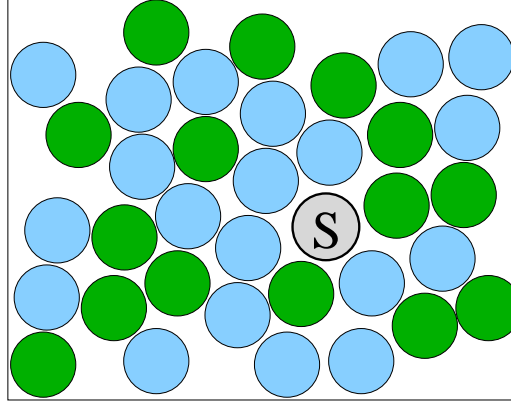
Figure 5.4: A spherical particle denoted by S, suspended in a mixture of different particles.

surrounding S has an average density of

$$\bar{\rho} = \frac{n_1 \rho_1 V_1 + n_2 \rho_2 V_2}{n_1 V_1 + n_2 V_2}, \tag{5.3}$$

where n_i is the total number of grains of type i in the surrounding mixture. Here, + we tacitly assumed that the mixture is homogeneous and, what is even more problematic, that the grains fill up the whole space without leaving gaps in between them. If we further assume, that all particles have the same size, then (5.3) reduces to

$$\bar{\rho} = \sum_i u_i \rho_i. \tag{5.4}$$

Hence, if we interpret the surrounding particle mixture now as a fluid medium, then S will descend (or rise, depending on the difference between ρ_1 and $\bar{\rho}$) at a constant velocity, thus equalizing Stokes' friction and gravitational force. (The theoretical approach to this phenomenon was originally developed in [Stokes51].) The so-called *settling velocity* is given by

$$v^{stok} = -\frac{2r_1^2 g(\rho_1 - \bar{\rho})}{9\eta}, \tag{5.5}$$

where g is the gravitational constant and η the viscosity of the surrounding medium. The negative sign indicates, that the particles experience a downward movement. Let u_i be the relative density of species i (fraction of species i in the mixture of two species). Then the flux of the first species is given by $J_1 = vu_1$. Using equation (5.5) we get

$$J_1 = u_1 c_1 (\rho_1 - \bar{\rho})$$
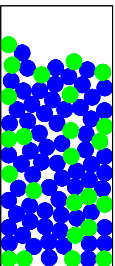
where c_1 is a constant depending on r_1, g and η,

$$c_1 = -\frac{2r_1^2 g}{9\eta},$$

and $\bar{\rho}$ is given by (5.4). Since the relative densities u_i add up to one, it suffices to set up only one equation, for example the one governing the change in u_1, in order to determine the behavior of the system. We have

$$
\begin{aligned}
J_1 &= c_1 u_1 \left(\rho_1 - \sum_i u_i \rho_i \right) \\
&= c_1 u_1 \left(\rho_1(1 - u_1) - \rho_2(1 - u_1) \right) \\
&= c_1 u_1 (1 - u_1)(\rho_1 - \rho_2) \\
&= c_1 \Delta\rho\, u_1 (1 - u_1),
\end{aligned}
$$

where $\Delta\rho = (\rho_1 - \rho_2)$. If this flux is the only factor determining the variation in particle concentrations, we end up with an equation of the form

$$\frac{\partial}{\partial t} u_1 = -\frac{\partial}{\partial x} J_1 = -c_1 \Delta\rho \frac{\partial}{\partial x} F(u_1) \tag{5.6}$$

governing the change in u_1, where the function F is again of logistic type as in section 5.2. Of course, solutions of equation (5.6) must satisfy boundary conditions imposed at the ends of the vessel. To be precise, particles can neither enter nor leave the top or bottom during the interaction, and thus

$$J_1 = c_1 \Delta\rho F = 0 \tag{5.7}$$

at $x = 0, l$. Since c_1 and $\Delta\rho$ are constants, the boundary condition (5.7) reduces to $F = 0$, i.e. $u_1 = 0$ or $u_1 = 1$ at $x = 0, l$.

Proposition 5.3.1 (Conservation of total mass.) *Equation (5.6) with boundary condition (5.7) conserves the total mass of species u_1, and hence also of u_2, for all positive times.*

Proof. Equations of similar convergence form were shown in chapter 2 to conserve total mass. $\square$

We emphasize that the convection-diffusion equations used to model segregation in chapter 3 in fact describe simple sedimentation of a single species in the case of a one-dimensional equation. As we mentioned before, the interpretation of a mixture of solid particles as a fluid bares difficulties. In the following, we will incorporate the influence of a separate fluid medium, usually water, with fundamentally different properties than the solid particles. It will be attributed a special role in the sedimentation process, the equation governing its change of concentration will be of a different nature.
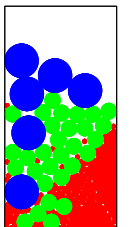
5.4   A convection approach to sedimentation

Consider a suspension of n species, modeled by spheres with different radii but with the same specific density ρ_s (a model, in which the particles may have different material densities as well will be discussed below), in a fluid with specific density ρ_f, contained in a vertical vessel of height l. We neglect effects in horizontal direction, thus restricting to one space dimension. Let $u_i = u_i(t, x)$ be the volumetric concentration of species i and $v_i = v_i(t, x)$ its velocity. Finally, let u_{n+1} and v_{n+1} be the volumetric concentration and the velocity of the fluid, respectively.

We have to consider two different effects. The first one is diffusion (random motion of the particles or biological species), the second one takes into account convectional movement due to gravitation and interaction of the species. The convectional flux of the ith species is given by $J_i^c = u_i v_i$ whereas the diffusional flux is $J_i^d = -D_i u_{ix}$. The total flux $J_i^{\text{tot}} = J_i^c + J_i^d$ yields

$$u_t = D u_{xx} - f(u)_x \tag{5.8}$$

where f is given by $f_i(u) = u_i v_i$. Furthermore, we impose that the total flux vanish at the boundary of the vessel, i.e.

$$D u_x = f(u) \tag{5.9}$$

at $x = 0, l$. Note that we have recovered a system of the same form used in chapter 3, where it described interaction of individual particles in general. In the following, we would like to compare our model to work done previously in this field.

At this point, we recall one of the major drawbacks of system (5.8), (5.9) in the context of sedimentation. We already mentioned in chapter 3 the special role of the suspension medium, the air or fluid surrounding the grains. One could interpret the air as a granular material composed of infinitely small particles, but this approach raises difficulties when it comes to interpreting the result: Small grains were shown to move down in the process of shaking, a quality air or any other *light* suspension medium does not have. In most of the remainder of this chapter, we follow and compare two different approaches to the theory of sedimentation. Both original models do not treat the medium explicitly, and both lack a diffusion term. The first one, due to G. K. Batchelor (see for example [Batchelor82.1] or [Bürger00.2]), emanates from the assumption of absolute sedimentation velocities of each one of the n particle types. The second approach has been followed by J. H. Masliyah and G. J. Kynch (see [Masliyah79], [Kynch52]) and yields a system of equations known as the Kynch model. Here, the settling velocities of the n grain types are taken relative to that of the suspension medium, but an equation governing the medium itself does not exist. We will use ideas of both approaches in our segregation model (5.8), (5.9).
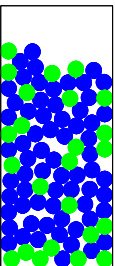
Before we go into further details of the above sedimentation approaches, we briefly touch the hyperbolic problem corresponding to system (5.8), (5.9).

5.5   Batchelor's approach

Consider one single sphere of radius r and density ρ_s, suspended in a fluid of density ρ_f and viscosity η. The sphere then moves at a constant velocity, namely Stokes' settling velocity (5.5). Let us now investigate the situation, in which a mixture of spheres differing in size and specific weight is in dilute suspension. If we subdivide the mixture in n types and denote by r_i and ρ_i the radius and specific density of a particle of type i, respectively, then, according to G. K. Batchelor (see [Batchelor82.1], [Batchelor82.2] and [Bürger00.2]), the velocities of the spheres are

$$v_i = v_i(u) = v_i^{stok}\left(1 + \sum_{j=1}^{n} S_{ij}u_j\right). \tag{5.10}$$

Here, v_i^{stok} is Stokes' settling velocity for a grain of type i. The interaction coefficients S_{ij} appearing in (5.10) generally depend on the particles' radii and specific densities and vary largely. While [Batchelor82.1] and [Batchelor82.2] give several theoretical limiting approximations, a fit of experimental data is used in [Bürger00.2] in order to derive the formula

$$S_{ij} = -3.52 - 1.04\frac{r_j}{r_i} - 1.03\frac{r_j^2}{r_i^2} \tag{5.11}$$

for $i, j = 1, \ldots, n$. Strictly speaking, the sedimentation coefficients S_{ij} depend not only on the size ratio of the particles, but also on their specific densities. Expression (5.11) is obtained for equal densities. Equation (5.10) was used in [Bürger00.2] in a conservation law with zero flux boundary condition. We will extend the idea to general diffusion-convection equations of the type discussed in chapter 3.

Note that a negative sign of v_i means, that particles experience a downward movement. Equation (5.11) is a crude approximation and is valid only if Brownian motion of the individual grains is neglected and if the particle concentrations are small (see [Batchelor82.2]). The latter in particular poses problems when it comes to describing the final stage of the sedimentation process, in which the material forms denser and denser packings and inter-particle effects come into play. We will produce relief by introducing a saturation term, thus limiting the particle concentration to a prescribed fixed value in the first place (see below). For a single sedimenting grain type u, equation (5.10) becomes

$$v_i = v_i^{stok}(1 - 5.59u),$$
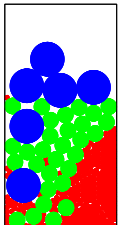
i.e. the settling velocity is constant and has the same value for all particles.

As we mentioned above, equation (5.10) describes the velocities of the spheres correctly up to the order of u_i but does not take into account the particles' lack of free space to move once the total volume density $u^{\text{tot}} = \sum u_i$ reaches a certain value u^{max}. In order to avoid this problem, we can introduce a factor of $(1 - u^{\text{tot}}/u^{\text{max}})$, or, as it is done in [Bürger00.2], of $(1 - u^{\text{tot}}/u^{\text{max}})^2$. For reasons of numerical stability, we only use the left branch of this volume limiting term and extend it by zero into values beyond $u^{\text{tot}} = u^{\text{max}}$. At the same time, we do not want to alter the behavior of v_i with respect to the concentrations u_i in the neighborhood of $u = 0$. Thus, we replace (5.10) by

$$v_i = v_i^{stok}\exp\left(\sum_{j=1}^{n} S_{ij}u_j + 2\frac{u^{\text{tot}}}{u^{\text{max}}}\right)\left(1 - \frac{u^{\text{tot}}}{u^{\text{max}}}\right)^2 \qquad (5.12)$$

for $i = 1, \ldots, n$ and $u^{\text{tot}} \leq u^{\text{max}}$. The extension $v_i = 0$ for $u^{\text{tot}} > u^{\text{max}}$ guarantees stability of the densest state and does not change the continuity of the first derivatives of v_i. We use the exponential function in (5.12) in order to avoid a change of sign for larger concentrations u_i. Note that both the value and the first derivatives of v_i agree for (5.10) and (5.12).

In order to use Batchelor's equation in our general sedimentation model of section 5.4, we define the components of the convection function f using the velocities given in (5.12). Thus, we end up with an $n + 1$-dimensional system of the form (5.8), where the n first components of the convection function f are given by

$$f_i(u) = u_i v_i^{stok}\exp\left(\sum_{j=1}^{n} S_{ij}u_j + 2\frac{u^{\text{tot}}}{u^{\text{max}}}\right)\left(1 - \frac{u^{\text{tot}}}{u^{\text{max}}}\right)^2 \qquad (5.13)$$

for $i = 1, \ldots, n$ and $u^{\text{tot}} \leq u^{\text{max}}$. We extend (5.13) by $v_i = 0$ for $u^{\text{tot}} > u^{\text{max}}$. Finally, we define the $(n + 1)$st component of f (governing the change in the volumetric density of the fluid) by

$$f_{n+1} = -\sum_{i=1}^{n} f_i. \qquad (5.14)$$

Corollary 5.5.1 (Boundedness and convergence.) *Consider system (5.8) with boundary condition (5.9) in section 5.4 for some positive diffusion constant $D > 0$. Let the function f be defined by (5.13) and (5.14). Then, the solutions $u = u(t, x)$ of (5.8), (5.9) conserve positivity and total mass. All $n + 1$ concentrations always add up to one, and stationary solutions always exist (even though they are not necessarily unique). Finally, for small container heights l, the time-dependent solutions converge to an equilibrium state.*
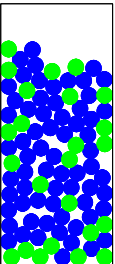
Proof. Due to the definition (5.14) of the last component of the convection function, condition (c) in section 3.2 of chapter 3 is satisfied. This ensures the conservation of the total mass in the vessel. It is straightforward to verify, that conditions (d) and (e) hold as well, hence positivity is conserved and particle densities add up to one. Finally, theorem 3.7.1 in section 3.7 of chapter 3 guarantees convergence to stationary solutions for small l. If fact, If $A = A(t, x)$ is the Jacobian of the function f defined in (5.13), (5.14), then the solutions converge if $l \leq \pi\sqrt{2}/m$, where

$$m = \sup_{t \geq 0} \max_{0 \leq x \leq l} \|A(t, x)\|.$$

This completes the proof of corollary 5.5.1. $\square$.

Proposition 5.5.2 (Monotonicity of stationary states.) *Consider the sedimentation model (5.8) with boundary condition (5.9) and a convection function (5.13), (5.14), where the settling velocity is given by (5.12). Then, the first n components of all equilibrium states are monotonously decreasing functions.*

Proof. Stationary solutions of (5.8), (5.9) are solutions of the ordinary differential equation

$$Du_x = f(u)$$

with boundary condition (5.9). Since the first n components of the vector-valued function f are all strictly negative, proposition 5.5.2 follows directly. $\square$

The example of an equilibrium state in the case of three sedimenting particle types is shown in figure 5.5. Here, we used a maximal particle concentration of $u^{\max} = 0.95$, which is approximately the volume fraction filled by an optimal mixture of three types of of the given sizes.

## 5.6   Masliyah's equation and the Kynch model

Historically, G. J. Kynch was one of the first ones to develop a rigorous theory for the sedimentation of particles dispersed in a fluid. In his treatise published in 1952 (see [Kynch52]), he formulated the conservation law

$$u_t = S_x, \tag{5.15}$$

where u is the volumetric particle concentration and $S = uv$ the particle flux, with $v = v^{stok}(1 - \alpha u)$ being the speed of fall in the fluid. In case the grains are all hard spheres of the same size and weight, the parameter α takes a value of approximately 2.5. Under these assumptions, equation (5.15) reads

$$u_t = v^{stok}\tilde{f}(u)_x, \tag{5.16}$$

where $\tilde{f}(u) = u(1 - \alpha u)$. The hyperbolic equation (5.16) is of the form we deduced heuristically in sections 5.2 and 5.3. Following Kynch's work, the equation has
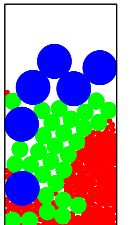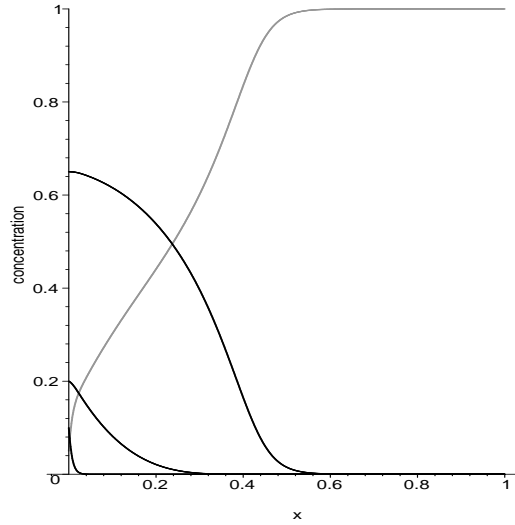
Figure 5.5: The stationary state of the sedimentation model (5.8), (5.9) for $D = 5$, $\rho_s = 2650\text{kg}/\text{m}^3$, $\rho_f = 1027\text{kg}/\text{m}^3$. The radii of the three grain types are $r_1 = 2.5 \cdot 10^{-4}$, $r_2 = 5 \cdot 10^{-4}$ and $r_3 = 1.5 \cdot 10^{-3}$, their specific weights all equal $\rho_s = 2650\text{kg}/\text{m}^3$. We used a dynamic fluid viscosity of $\eta = 1.36 \cdot 10^{-6}\text{m}^2/\text{s}$ and set the gravitational constant equal to $g = 9.806\text{m}/\text{s}^2$. The illustration shows monotone particle concentrations in the sedimented equilibrium state (black curves). The empty space is plotted in gray.

been extended and modified, among others by J. H. Masliyah (see for example [Masliyah79]), in order to incorporate the interaction between the individual particles in a more accurate way and allow mixtures of grains of different physical properties. We will discuss Masliyah's contribution here and establish the relationship to the model we used in chapter 3 to describe segregation. As before, our aim is to derive an expression for the convectional particle flux J^c and to determine the convection function f in equation (5.8) governing the dynamics of the sedimentation process (see the approach in section 5.4). In contrast to section 5.5, we consider the movement of the particles relative to that of the fluid and thus do without setting up an equation for the change in fluid concentration.

In the vessel, the total particle concentration $u^{\text{tot}} = \sum_{i=1}^{n} u_i$ can take values between zero and $u^{\max}$, where in general $u^{\max} < 1$. Let $u_{n+1} = u_f = 1 - u^{\text{tot}}$ be the volumetric fluid concentration and denote by $v_{n+1} = v_f$ the velocity of the fluid. v_f can be defined by

$$\left(1 - u^{tot}\right) v_f + \sum_{i=1}^{n} u_i v_i = 0, \tag{5.17}$$

which is another way of saying that the volume-averaged velocity vanishes at every height in the vessel. Let us rewrite (5.17) in terms of the n relative velocities
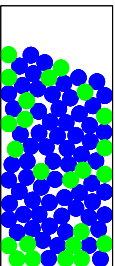
$w_i := v_i - v_{n+1}$, $i = 1, \ldots, n$. We get $v_f = -\sum_{i=1}^{n} u_i w_i$ and, since $f_i = u_i v_i = u_i(w_i + v_{n+1})$,

$$f_i = u_i \left[w_i - \sum_{j=1}^{n} u_j w_j \right] \tag{5.18}$$

for $i = 1, \ldots, n$. In order to describe the physical realities correctly, we impose boundary conditions. At the top and bottom of the vessel, all velocities vanish and we have

$$Du_x = f(u)$$

at $x = 0, l$. For the relative velocities w_i appearing in the convection function (5.18), J. H. Masliyah (see [Masliyah79]) derived the relation

$$w_i = w_i^{stok} V(u^{\text{tot}}),$$

where w_i^{stok} is Stokes' settling velocity of one single spherical particle in a medium of *averaged* density $\rho = u^{\text{tot}} \rho_s + (1 - u^{\text{tot}})\rho_f$, given by

$$w_i^{stok} = -\frac{2}{9} \frac{(1 - u^{\text{tot}})\Delta \rho g r_i^2}{\nu}$$

(see section 5.5) and $V(u^{\text{tot}})$ is one of the *hindered settling* functions, for example $V(u^{\text{tot}}) = (1 - u^{\text{tot}})^p$ for some $p > 1$ (see [Richardson54]). Equation (5.18) then yields for $i = 1, \ldots, n$

$$f_i(u) = V\left(u^{tot}\right) u_i \left[w_i^{stok} - \sum_{j=1}^{n} u_j w_j^{stok} \right]. \tag{5.19}$$

It is interesting to observe, that (5.19) has, aside from the factor $V(u^{tot})$, the outer form of a replicator competition law with constant fitnesses $m_i = w_i^{stok}$ (see equation (3.50) and the discussion in section 3.8 of chapter 3). Only this time, the system does not live on the n-simplex S, since particle concentrations do not necessarily add up to one. Nevertheless, one can show, that if $u = u(t)$ is a solution of (5.8) with convection function (5.19), then $u(t)\phi(t)$ lies on S for some positive function ϕ. Furthermore, the factor V can be eliminated after rescaling of time. Hence, the qualitative behavior of our sedimentation model is rendered by the replicator equation. Figure 5.6 shows the stationary state of the system. We used the same initial conditions as in section 5.5. The graph shows, that the stationary solutions need not be monotone any more.

5.7 Variable diffusion

The hyperbolic sedimentation model of the form used originally in the approaches due to G. J. Kynch, G. K. Batchelor and J. H. Masliyah (see also our compaction
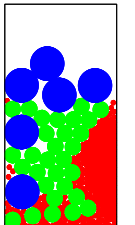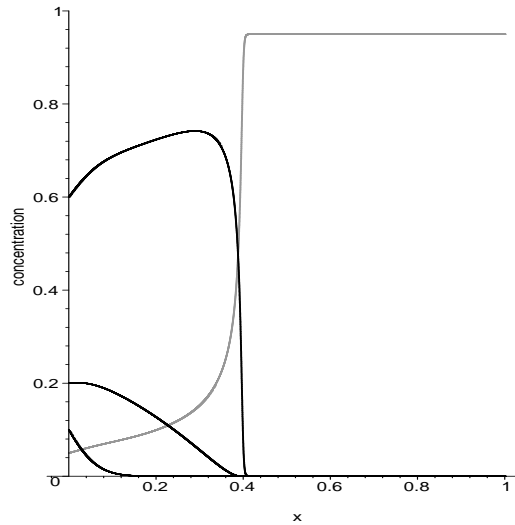
Figure 5.6: In contrast to figure 5.5, the stationary solutions of system (5.8), (5.9) with convection function (5.19) are non-monotone in general. The particle concentrations are plotted in black, the empty space is represented by the gray line.

and segregation models in the first half of chapter 2) usually develops shocks, which are difficult to handle both mathematically and numerically. While the parabolic equations derived in sections 5.5 and 5.6 avoid this problem by adding a diffusive term to the conservation law, they also pose new difficulties. As we mentioned before, these equations are designed to describe segregation processes (see chapter 3). Even though sedimentation in some parts follows the same rules, one important issue is not taken into account: The (stable) equilibrium state does not depend on the height of the vessel and thereby on the time the sedimenting material has to segregate, a phenomenon which contradicts all experimental observations. On the contrary, it is the diffusion term, which constantly smears the sharp layer boundaries and pushes the segregation, even though the material has already settled to the bottom of the container.

We will try to produce relief by considering variable diffusion and convection terms, both depending on the total particle density. To be more precise, let us consider the vector equation

$$u_t = [D(u)u_x + \gamma(u)u]_x \tag{5.20}$$

with boundary condition

$$D(u)u_x = -\gamma(u)u \tag{5.21}$$

at $x = 0, l$, where u is the n-dimensional concentration vector and both D and γ are matrices. Intuitively, one would assume that D and γ are in some sense decreasing functions of u, and that $D(u) = \gamma(u) = 0$ if the total particle density $u^{\text{tot}} = \sum u_i$ exceeds a certain maximal value u^{max}, namely that of the densest
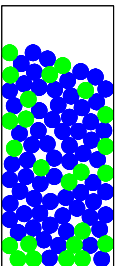
packing. Nevertheless, this reasoning does not necessarily hold for models derived from simple random walk processes. In particular, we will see that in the case of a single grain type, it stands to reason to assume that the diffusion function D is in fact independent of the total density.

In order to gain some more insight, let us derive a one-dimensional sedimentation model again from an elementary random walk process in the style of chapter 2. Consider a one-dimensional grid and denote by u_k the particle concentration at position k. If $\tilde{\alpha}$ is the diffusive transmission rate from one position to a neighboring one, and if $\tilde{\beta}$ designates the rate of convective particle transmission, then the standard continuous time discrete space random walk process reads

$$\dot{u}_k = \tilde{\alpha}\left[u_{k+1} + u_{k-1} - 2u_k\right] + \tilde{\beta}\left[u_{k+1} - u_k\right], \tag{5.22}$$

where Δx designates again the space increment, i.e. the vertical distance between two compartments. If now α and β are the positive diffusion and convection coefficients, respectively, and if $\tilde{\alpha}\Delta x^2 \equiv \alpha$, $\tilde{\beta}\Delta x \equiv \beta$, then (5.22) yields in the limit for $\Delta x \to 0$ the diffusion-convection equation

$$u_t = \alpha u_{xx} + \beta u_x.$$

Now let us leave the idea of constant particle transmission coefficients $\tilde{\alpha}$ and $\tilde{\beta}$ and suppose the transmission rates are proportional to the concentration u and to the available space $u^{\max} - u$ at the destination site. Then
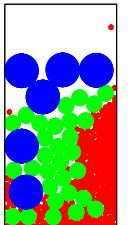
$$\begin{aligned}
\dot{u}_k =& \tilde{\alpha}\left[u_{k+1}(u^{\max} - u_k) + u_{k-1}(u^{\max} - u_k) - u_k(u^{\max} - u_{k+1}) - u_k(u^{\max} - u_{k-1})\right] + \\
&+ \tilde{\beta}\left[u_{k+1}(u^{\max} - u_k) - u_k(u^{\max} - u_{k-1})\right] \\
=& \tilde{\alpha}u^{\max}\left[u_{k+1} + u_{k-1} - 2u_k\right] + \\
&+ \tilde{\beta}\left[u^{\max}(u_{k+1} - u_k) - u_k(u_{k+1} - u_{k-1})\right],
\end{aligned}$$

and hence, in the parabolic limit,

$$u_t = \alpha u^{\max} u_{xx} + \beta\left[u(u^{\max} - u)\right]_x.$$

It is interesting to observe, that this modification of the transmission rate does not alter the resulting diffusion constant D, but that it changes the convection function. Thus, in the above terminology, $\gamma(u) = u^{\max} - u$, but still $D(u) \equiv \alpha$. At this point, let us take a brief look back at the heuristic considerations in sections 5.2 and 5.3. Note that we recovered the same convection function $\gamma(u) = u^{\max} - u$, which is just the free length of path of the grains' fall, or, in other words, the concentration of the suspension medium. In the light of this interpretation, the monotonicity assumption on γ makes perfect sense.

The actual interesting situation is the sedimentation of a mixture of different particles. Let us treat a bi-disperse material as an example. As before, consider

a one-dimensional grid and denote the concentrations of the two components at position k by u_k^1 and u_k^2, respectively. The corresponding random walk process under the influence of gravitation is then described by

$$\dot{u}_k^i = \tilde{\alpha} \left[u_{k+1}^i (u^{\max} - u_k^1 - u_k^2) + u_{k-1}^i (u^{\max} - u_k^1 - u_k^2) - \right.$$
$$- u_k^i (u^{\max} - u_{k+1}^1 - u_{k+1}^2) - u_k^i (u^{\max} - u_{k-1}^1 - u_{k-1}^2) \right] +$$
$$+ \tilde{\beta} \left[u_{k+1}^i (u^{\max} - u_k^1 - u_k^2) - u_k^i (u^{\max} - u_{k-1}^1 - u_{k-1}^2) \right]$$

for $i = 1, 2$, which yields

$$u_t^1 = \alpha \left(u^{max} u_{xx}^1 + u^1 u_{xx}^2 - u^2 u_{xx}^1 \right) + \beta \left[u^1 (u^{\max} - u^{\mathrm{tot}}) \right]_x,$$
$$u_t^2 = \alpha \left(u^{max} u_{xx}^2 + u^2 u_{xx}^1 - u^1 u_{xx}^2 \right) + \beta \left[u^2 (u^{\max} - u^{\mathrm{tot}}) \right]_x \tag{5.23}$$

in the parabolic limit. Here, u^{tot} is the total particle concentration, $u^{\mathrm{tot}} = u^1 + u^2$ and $u^{\max}$ is its maximal value. Hence, the diffusion-convection system is of the form (5.20) with diffusion matrix

$$D(u) = \alpha \begin{pmatrix} u^{\max} - u^2 & u^1 \\ u^2 & u^{\max} - u^1 \end{pmatrix} \tag{5.24}$$

and a scalar convection function

$$\gamma(u) = \beta \left(u^{\max} - u^{\mathrm{tot}} \right). \tag{5.25}$$

The adequate boundary condition is again

$$D(u) u_x = -\beta u (u^{\max} - u^{\mathrm{tot}}) \tag{5.26}$$

at $x = 0, l$.

The merits of the variable diffusion approach show up, when we look at stationary solutions of (5.20), (5.21). Let us again use the example of two species with diffusion term (5.24) and convection function (5.25). We are particularly interested in the saturation property of the diffusion term $D(u)u$. If the total particle density has reached its maximal value, for example in an advanced sedimentation stadium at the container bottom, then the diffusion matrix D reduces to

$$D(u) = \begin{pmatrix} u^1 & u^1 \\ u^{\max} - u^1 & u^{\max} - u^1 \end{pmatrix},$$

and hence, $[D(u)u_x]_x = 0$, since $(u_1 + u_2)_x = (u_1 + u_2)_{xx} = 0$. Consequently, no diffusion takes place. This, however, does not imply that arbitrary dense packings are stationary states, as the following proposition shows.

Proposition 5.7.1 (Monotonicity of equilibria for variable diffusion.) *The stationary states of (5.20), (5.21) with diffusion matrix (5.24) and convection function (5.25) are all strictly decreasing functions, unless the whole container is already optimally filled with material.*
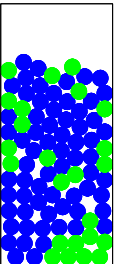
Proof. The equilibria of system (5.20), (5.21) are solutions of

$$D(u)u_x + \gamma(u)u = 0. \tag{5.27}$$

If we denote by $w = u^1 + u^2$ the total particle concentration, then (5.27) yields

$$w_x = \frac{1}{u^{\max}}w^2 - w,$$

the solution of which is

$$w(x) = \frac{u^{\max}w_0}{(u^{\max} - w_0)e^x + w_0}. \tag{5.28}$$

As long as the total particle concentration stays below $u^{\max}$, w is thus strictly decreasing. From (5.27), we also derive

$$u^1_x = -\frac{u^1}{u^{\max}}(u^{\max} - u^1 - u^2),$$

$$u^2_x = -\frac{u^2}{u^{\max}}(u^{\max} - u^1 - u^2).$$

Hence, strict monotonicity holds for each one of the two concentrations as well as long as $u^{\max} > u^1 + u^2$. This proves proposition 5.7.1. $\square$.

Let us now return to the original idea of system (5.20), (5.21) with D and γ both tending to zero as the total concentration approaches $u^{\max}$. In case of a single particle type, the behavior of the equilibria at the left boundary is resumed in the following proposition.

Proposition 5.7.2 (Slope of stationary states.) *Suppose γ and D are both strictly decreasing functions on the interval $[0, u^{\max}]$ with $\gamma(0) = \gamma_0 > 0$ and $D(0) = D_0 > 0$. Assume further, that $\gamma(u^{\max}) = D(u^{\max}) = 0$. We distinguish two cases:*
(a) If $b := \lim\limits_{u \to u^{\max}} \frac{\gamma(u)}{D(u)} < \infty$, then the stationary solution of system (5.20), (5.21) starts out with a slope equal to $-b$ at $u = 0$.
*(b) If $b = \infty$, the stationary solution has infinite slope at $u = 0$.*
In any case, the stationary solution is a decreasing function.

Proof. Since γ and D are both non-negative and become zero only at $u = u^{\max}$, the monotonicity of the stationary solutions follows from (5.29). Due to the boundary condition, the stationary solutions of (5.20), (5.21) are solutions of

$$u_x = -\frac{\gamma(u)}{D(u)} \tag{5.29}$$

wherever $D(u) \neq 0$. The crucial point is now the behavior of the ratio $\gamma(u)/D(u)$ in the limit as $u \to u^{\max}$, i.e. in other words the ratio of the derivatives of γ and D at $u = u^{\max}$ in case both functions are $\mathcal{C}^1$. The behavior at zero can thus be
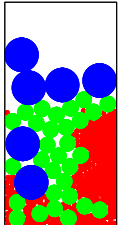
characterized by either (a) or (b). □.

Before we close this section on variable diffusion, we would like to illustrate the behavior of the stationary solutions to problem (5.20), (5.21) in the general case of several interacting species by means of an example. In order to avoid the peculiarities of case (b) in proposition 5.7.2, we choose

$$\gamma(u) = (u^{\max} - u^1 - u^2) \tag{5.30}$$

and

$$D(u) = \epsilon\gamma(u) \tag{5.31}$$

for some $\epsilon > 0$. Thus, stationary solutions start off with a slope equal to $-1/\epsilon$ at $x = 0$ and satisfy

$$\epsilon(u^{\max} - u^1 - u^2)u_x = -(u^{\max} - u^1 - u^2)u,$$

i.e. either $u^{\max} = u^1 + u^2$ or $u_x = -u/\epsilon$. The latter yields solutions of the form $u^i(x) = \lambda_i e^{-x/\epsilon}$, while the former condition just characterizes dense packings. Hence, the general variable diffusion approach fulfills the stipulated requirements: Once a layer of dense material has formed at the bottom of the vessel, its local composition is invariant. Above this dense layer, the concentrations decay exponentially. On the boundary between these two deposits, we necessarily have a discontinuity of the slope u_x.

The question is now, which ones of the above equilibria are stable. As the simulations in figures 5.7 and 5.8 show, the same total mass relation between the two particle types can yield different stable states, depending on the initial distribution. In the first simulation, we introduced a layer of composite material into the bottom half of the container. Hence, sedimentation only had a relatively short time to segregate the two species, before the mixture gathered at the ground. In comparison, a second simulation was conducted, in which the material had more time to segregate. The resulting layers are more distinct.

5.8   Simulation of a particle sedimentation model

In order to judge the quality of the two models introduced in sections 5.5 and 5.6, we compare their predictions with the simulation of a particle model.

We imagine a suspension of spherical particles of varying size and specific weight. During the sedimentation process, three different forces act constantly on each individual particle. On the one hand, the gravitational force F_G, which is proportional to the particle's mass, acts in vertical, downward direction and accelerates the fall. On the other hand, the particle experiences a buoyancy force F_B, directed upward. It depends on the volume of the grain, as well as on the specific
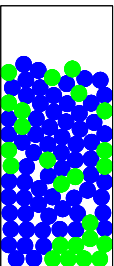
densities of the sedimenting material and the fluid. Finally, the particle is slowed down by the flow resistance F_D. It generally depends on the particle's shape and its velocity. Hence, the total acting force is given as the sum of the three forces, respecting their respective signs,

$$F = -F_G + F_B + F_D.$$

Consider one sediment particle with radius r and specific weight ρ_s, and denote by ρ_f the specific weight of the suspension medium. Then

$$-F_G + F_B = -\frac{4}{3}\pi r^3 g \left(\rho_s - \rho_f\right),$$

where g is the gravitational constant. Furthermore, if we assume that the suspension fluid is at rest, the flow resistance acting on the sediment particle is given by
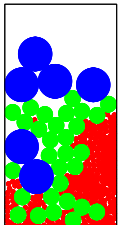
$$-\frac{1}{2}c_D\rho_f w|w|\pi r^2,$$

where c_D is the drag coefficient and w the vertical component of the velocity of the grain. A. J. Raudkivi (see [Raudkivi76]) has derived the following dependency of c_D on the particle's Reynolds' number Re, which is given by $\mathrm{Re} = 2|w|r/\nu$:

$$c_D = \begin{cases} \dfrac{24}{\mathrm{Re}}\left(1 + 0.15\mathrm{Re}^{\,0.678}\right) & \text{for } \mathrm{Re} \leq \mathrm{Re}^{\,crit}, \\ c_D^\infty & \text{for } \mathrm{Re} > \mathrm{Re}^{\,crit}. \end{cases}$$

Here, ν is the fluids dynamic viscosity, $c_D^\infty \approx 0.424$ is the limiting drag coefficient for high particle velocities and $\mathrm{Re}^{\,crit}$ is the critical Reynolds' number, $\mathrm{Re}^{\,crit} \approx 10^3$.

For the simulation, we placed a total number of 1580 spherical particles of three different sizes in an aqueous suspension and recorded the composition of the granular material after total sedimentation at the bottom of the container. The result is shown in figures 5.9 and 5.10.

(a) Initial distribution.

(b) 10^4 iterations.

(c) $2 \cdot 10^5$ iterations.

(d) $4 \cdot 10^5$ iterations.

(e) $6 \cdot 10^5$ iterations.

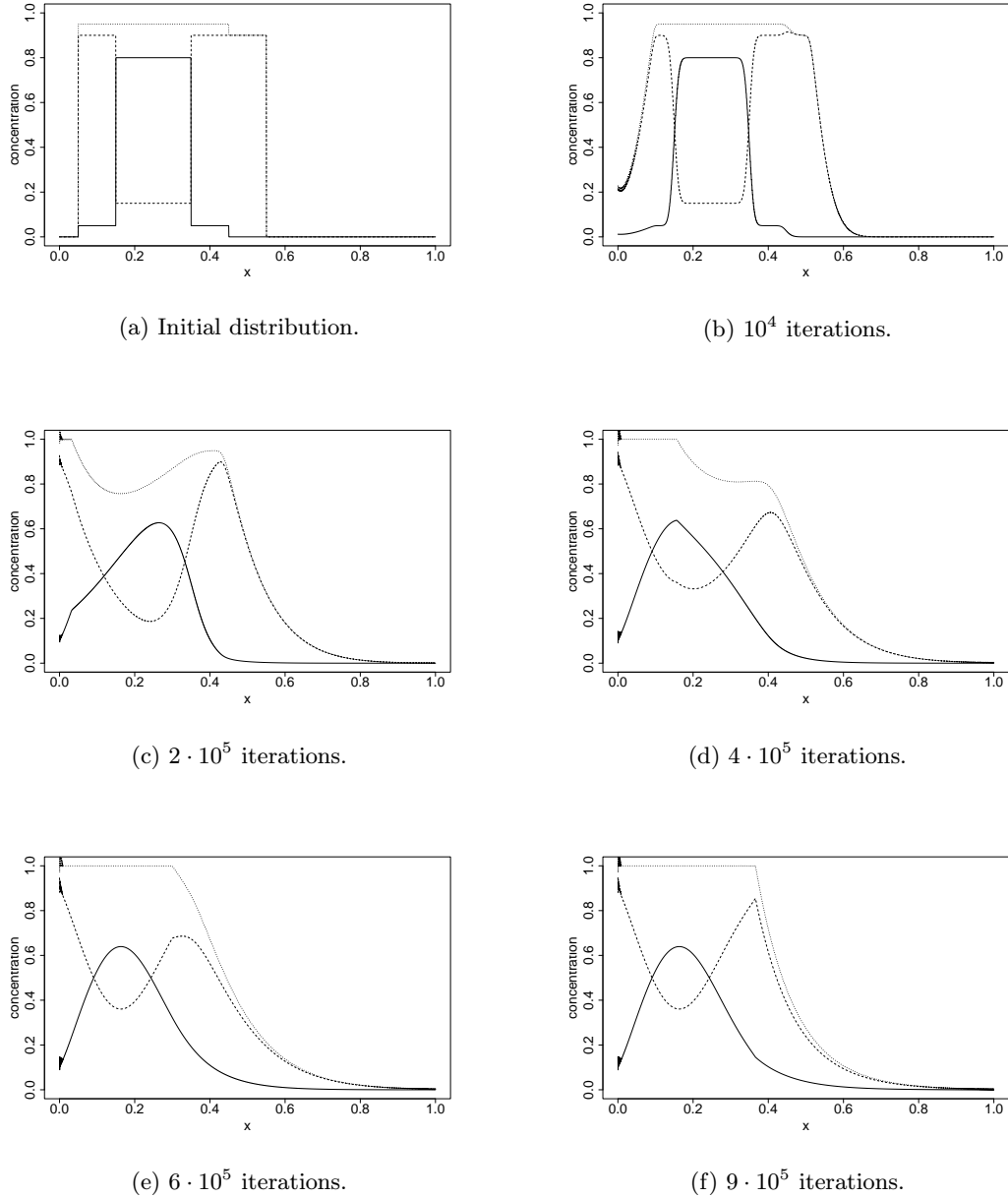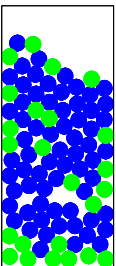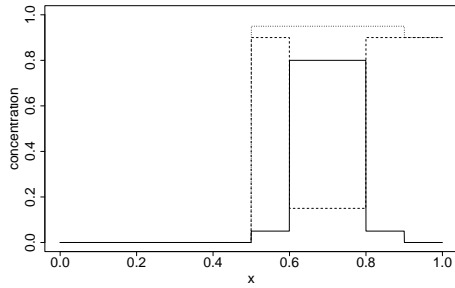

(f) $9 \cdot 10^5$ iterations.

Figure 5.7: Simulation of the time-dependent solution of system (5.20) with boundary condition (5.21). The solid and dashed lines represent the concentrations of the first and second particle species, respectively, while the dotted line gives the total density. We used the diffusion function (5.31) and a convection function of the form (5.30) with $\epsilon = 0.1$, the maximal particle concentrations was chosen to be $u^{\max} = 1$. We initially introduced an inhomogeneous layer of material into the bottom half of the container (see (a)). The simulation indicates, that the non-monotone distribution shown in (f) is an equilibrium.
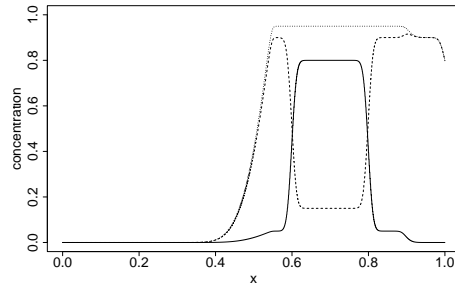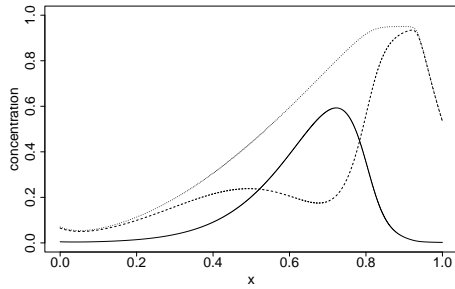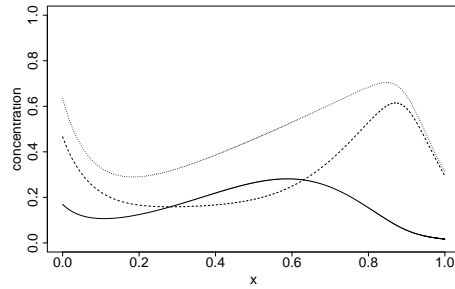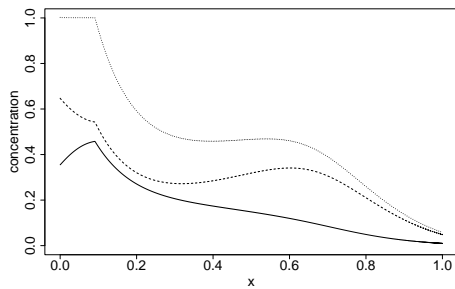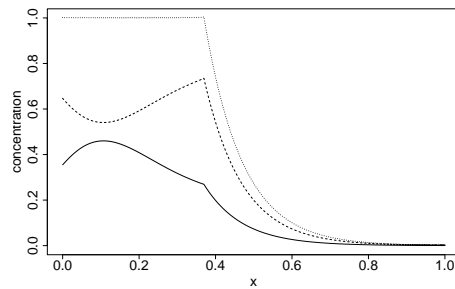
(a) Initial distribution.

(b) 10^4 iterations.

(c) $2 \cdot 10^5$ iterations.

(d) $5 \cdot 10^5$ iterations.

(e) 10^6 iterations.

(f) $3 \cdot 10^6$ iterations.

Figure 5.8: Simulation of the time-dependent solution of system (5.20) with boundary condition (5.21). As in figure 5.7, we used the diffusion (5.31) and a convection function of the form (5.30) with $\epsilon = 0.1$. Only this time, the material was initially introduced into the top of the vessel. Thus, the grains had more time to segregate during the sedimentation.
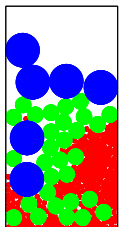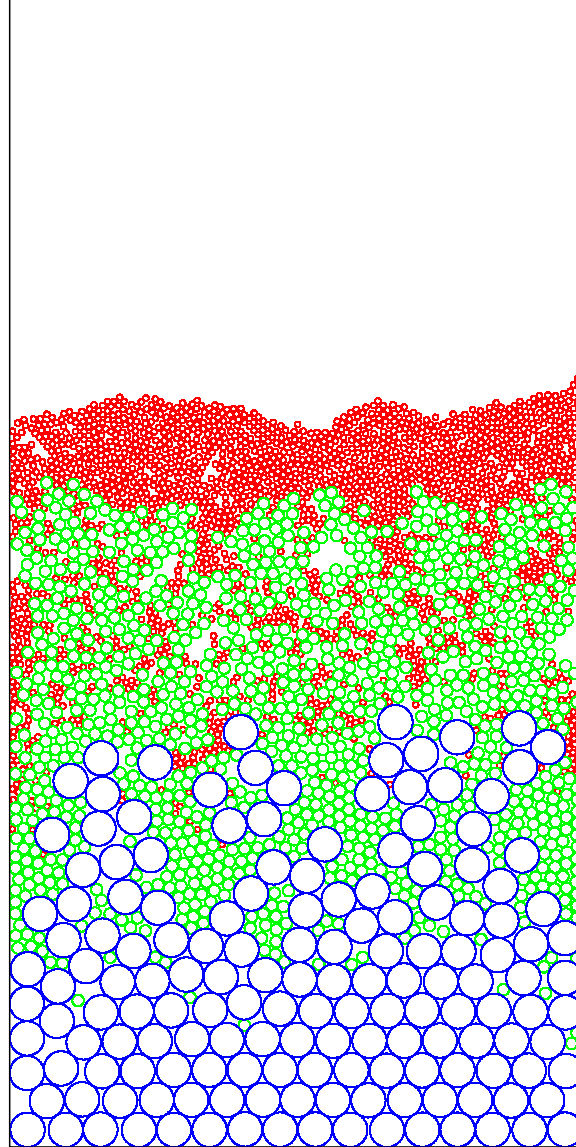
Figure 5.9: Sedimentation of a total number of 1580 spherical particles in aqueous suspension of specific density $\rho_f = 1027\text{kg}/\text{m}^3$. The radii of the three grain types are $r_1 = 2.5 \cdot 10^{-4}$, $r_2 = 5 \cdot 10^{-4}$ and $r_3 = 1.5 \cdot 10^{-3}$, their specific weights all equal $\rho_s = 2650\text{kg}/\text{m}^3$. We used a dynamic fluid viscosity of $\nu = 1.36 \cdot 10^{-6}\text{m}^2/\text{s}$ and set the gravitational constant equal to $g = 9.806\text{m}/\text{s}^2$. The illustration shows the sedimented material at the bottom of the container at $t = 1.6 \cdot 10^4$. The compaction is not complete, some gaps are still visible.
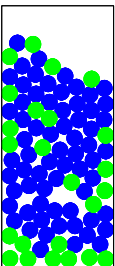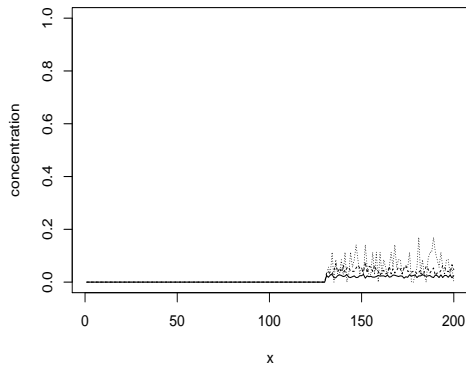
(a) Arbitrary initial distribution.
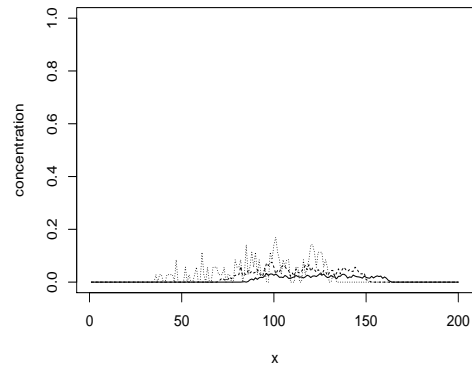
(b) Time $t = 4 \cdot 10^3$.
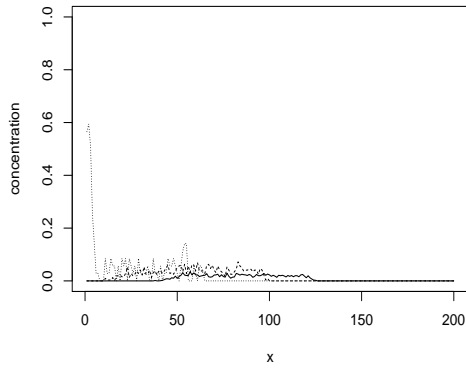
(c) $t = 8 \cdot 10^3$.
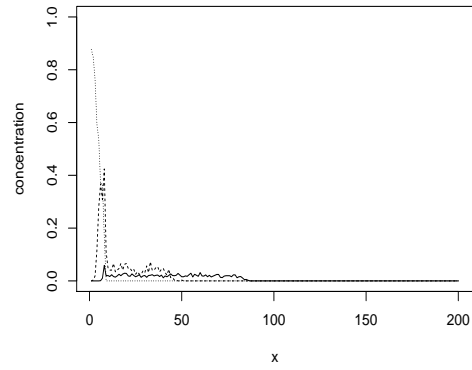
(d) $t = 1.2 \cdot 10^4$.
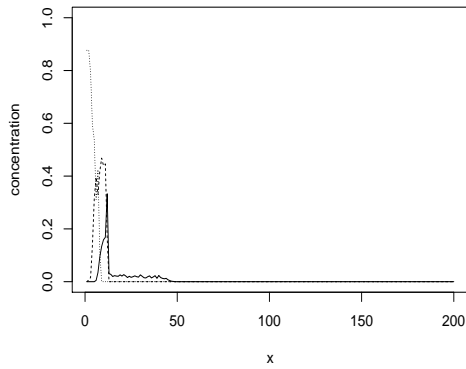
(e) $t = 1.6 \cdot 10^4$.
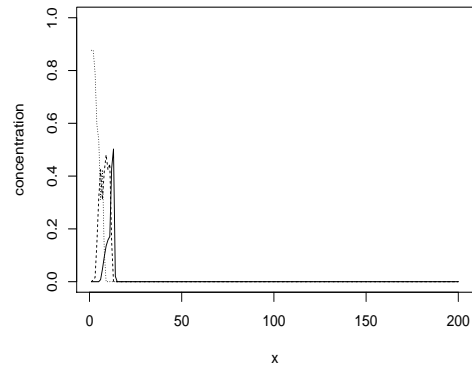
(f) $t = 2 \cdot 10^4$.

Figure 5.10: The density plots generated according to the particle simulation illustrated in figure 5.9. The dotted line gives the concentration of the largest grains, the dashed curve represents the intermediate grains, and the solid line the small particles.
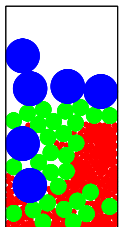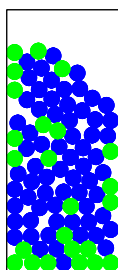
Chapter 6

The chemostat with non-constant washout rates

Summary. The classical chemostat system describes the behavior of two species competing for one substrate. The substrate is renewed at a constant rate, both the species and the substrate are washed out at possibly distinct washout rates. For this system, the competitive exclusion principle holds. We allow washout rates depending on the densities and show that coexistence is possible.

6.1 Introduction

The chemostat consists of a vessel, the so-called *growing chamber*, containing a certain number of biological (or chemical) species in a fluid medium. The species interact indirectly in the sense that they compete for a limited resource (*substrate*) which is diluted in the medium, and that they have more or less ability to adapt to their environment in order to utilize the supply at the best possible rate. The chamber is fed by a supply of *fresh* resource solution, while an outflow disposes of *used* nutrient and maintains a certain fill level in the vessel. The inhabiting species are gradually washed out together with the medium. We will in particular focus on these washout rates and, in contrast to previous work by G. J. Butler (see for example [Butler87], [Butler86] or [Butler85.1]), S. B. Hsu (see [Hsu94.1], [Hsu94.2]) or S. K. Wolkowicz (see [Wolkowicz96] or [Wolkowicz95]), allow the species to colonize and thus persist within the growing chamber. Once their number becomes large, more and more individuals drop out of the colonies and are washed out as well. Hence, the *death rates* or *washout rates* are not constant. One could imagine, for example, a mussel bed with variable ability of the individual animals to hold on to rocks or artificially inserted grilles (as it is done in industrial mussel cultivation), or a competitive relationship between animals with different ability to attach to the walls of their habitat (for an application to the microflora in the guts of mammals see for example [Stemmons00]). Another important field of application is the cultivation of so-called biofilms, thin layers
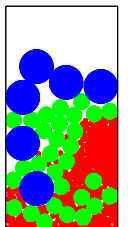
of organic material formed under controlled conditions in the biofilm growing chamber.

In section 6.2 we present a general model describing the competition of two species with distinct, non-linear growth rates and mortalities and correlate the individual terms to the biological setup in mind. The purpose of section 6.3 is to locate the equilibrium states of the general system and analyze their local stability. Section 6.4 is a first step towards global stability analysis. We determine invariant sets and discuss the boundedness of solutions. The proof of global stability of the coexistence state is achieved in section 6.5 for a certain class of uptake functions. An example for the coexistence point is analyzed in section 6.6, and the biological implications are explained. Finally, section 6.7 presents a computer simulation of the model for the case of linear uptake and washout functions.

6.2   The model

Consider the case of two species with concentrations x_i, $i = 1, 2$, competing for a single limited resource s. Let $D \geq 0$ be the rate of substrate inflow into the vessel (equal to the outflow rate). The washout rates of the species x_i are modeled by functions $D_i = D_i(x_i)$, $i = 1, 2$. Let $f_i = f_i(s)$, $i = 1, 2$, be the nutrient uptake functions of the two species. They are at the same time responsible for the overall growth of the population. These considerations yield the following model:

$$\begin{aligned}
\dot{s} &= D(1 - s) - x_1 f_1(s) - x_2 f_2(s), \\
\dot{x_1} &= x_1(f_1(s) - D_1(x_1)), \\
\dot{x_2} &= x_2(f_2(s) - D_2(x_2)).
\end{aligned} \tag{6.1}$$

We make the following assumptions:

(a) Let f_i and D_i be sufficiently smooth: $f_i, D_i \in \mathcal{C}^1[0, \infty)$.
(b) $D_i^0 := D_i(0) > 0$, $D_i'(x) > 0$ and $D_i(\infty) = D_i^* \in (D_i^0, \infty)$.
(c) Let $f_i(0) = 0$, $f_i'(s) > 0$.

Biologically speaking, condition (c) includes the case of infinitely growing uptake rates f_i, which means that the nutrient consumption of the species can grow infinitely large if sufficient concentrations are supplied. This seems to contradict biological facts, since real species have a level of saturation and hence experimentally observable uptake always has a finite limit. Condition (b) models strictly monotone washout rates, thus meeting our demands. The somewhat weaker condition $D_i'(x) \geq 0$ would allow to treat the often considered case of constant mortalities as a special case, but for analytical purposes we explicitly restrict to strict monotonicity. Notice that the number of deaths per time unit, $x_i D_i(x_i)$, has a positive derivative at $x_i = 0$. This ensures a certain washout speed for small
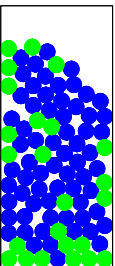
concentrations. When writing the first equation of system (6.1), we tacitly assume a maximal substrate concentration of one. In the following discussion, we therefore restrict to initial values $s(0) \leq 1$. Note that if s were to be larger than one hypothetically, then $\dot{s} < 0$ and the concentration would drop back below this saturation level.

Lemma 6.2.1 (Extinction.) *Suppose conditions (a) through (c) above hold for system (6.1). If in addition $f_i(1) < D_i^*$ for some i, then this species will die out and does not persist in the system.*

Proof. It is clear from (6.1) that under the additional hypothesis of lemma 6.2.1, $\dot{x}_i$ is always strictly negative. This proves lemma 6.2.1. $\square$.

In most of the following discussion, we will therefore assume $f_i(1) > D_i^0$ for $i = 1, 2$. If we define $\underline{s}_i$ by $f_i(\underline{s}_i) = D_i(0)$, this condition reads

(d) $\underline{s}_i < 1$, $i = 1, 2$.

6.3   Stationary points and their stability

Let us define G_i as the inverse function of D_i (here we need strict monotonicity of D_i) and the values $\overline{s}_i$ and $\underline{s}$ by $f_i(\overline{s}_i) = D_i^*$ and $\underline{s} = \max\{\underline{s}_i\}$, respectively. Note that G_i is only defined on the finite interval $[D_i^0, D_i^*]$ if $D_i^* < \infty$. This will be important for the existence of the coexistence equilibrium (see proposition 6.3.3). In order to find stationary points of the system (6.1) we draw the nullclines. Besides the trivial *substrate-only* equilibrium $S = (1, 0, 0)$, there can be two different *one-consumer* equilibria, denoted by $E_1 = (s^1, x_1^1, 0)$ and $E_2 = (s^2, 0, x_2^2)$, at which in each case the other species is extinct. With the above notation, the derivatives $\dot{x}_i$, $i = 1, 2$, vanish for non-trivial x_i if and only if $x_i = G_i(f_i(s))$ (see figure 6.1). Thus, by the first equation of (6.1) the substrate concentration at a one-consumer equilibrium E_i for species i is given by the equation

$$D(1 - s) = G_i(f_i(s))f_i(s), \tag{6.2}$$

if E_i exists. Finally, system (6.1) might have a *coexistence equilibrium*, which we denote by $E = (s^*, x_1^*, x_2^*)$. If E exists, the substrate concentration s^* at this stationary state solves the equation

$$D(1 - s) = \sum_{i=1}^{2} G_i(f_i(s))f_i(s). \tag{6.3}$$

These are all possible equilibria. We will discuss conditions for the existence and the stability of the above stationary states after giving two examples for the uptake functions f_i and the washout rates D_i.
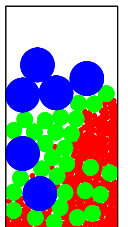
Besides the case of constant uptake and mortality functions (which is not included in (b), (c)), the simplest situation is the one with linear functions f_i and D_i. Let

$$f_i(s) = a_i s,$$
$$D_i(x_i) = D_i^0 + k_i x_i, \tag{6.4}$$

where $a_i, k_i > 0$ (see figure 6.1). In this case, the inverse G_i of D_i is given by
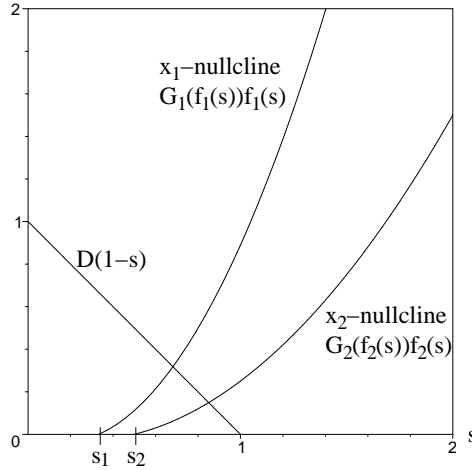
Figure 6.1: The nullclines of system (6.1) for the linear functions $f_1(s) = s$, $f_2(s) = 2s$, $D_1(x_1) = 1/2 + 2x_1$, $D_2(x_2) = 2/3 + 3x_2$ and $D = 1$.

$G_i(y_i) = (y_i - D_i^0)/k_i$. It is defined on the half-open interval $[D_i^0, \infty)$. The chemostat model (6.1) then becomes

$$\dot{s} = D(1 - s) - x_1 a_1 s - x_2 a_2 s,$$
$$\dot{x_1} = x_1(a_1 s - k_1 x_1 - D_1^0), \tag{6.5}$$
$$\dot{x_2} = x_2(a_2 s - k_2 x_2 - D_2^0).$$

A nonlinear example is represented in figure 6.2. Here the parameter functions take the form

$$f_i(s) = \frac{a_i s}{1 + b_i s},$$
$$D_i(x_i) = D_i^0 + k_i(1 - e^{-c_i x_i}), \tag{6.6}$$

where a_i, b_i and c_i, $i = 1, 2$, are all strictly positive constants. Nutrient uptake functions of such form are frequently used in biological modeling and describe so-called *Michaelis-Menten* reaction kinetics. The inverse function G_i of D_i in the case (6.6) is given by

$$G_i(y_i) = \frac{1}{c_i} \log\left(1 - \frac{y_i - D_i^0}{k_i}\right),$$
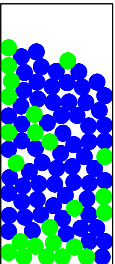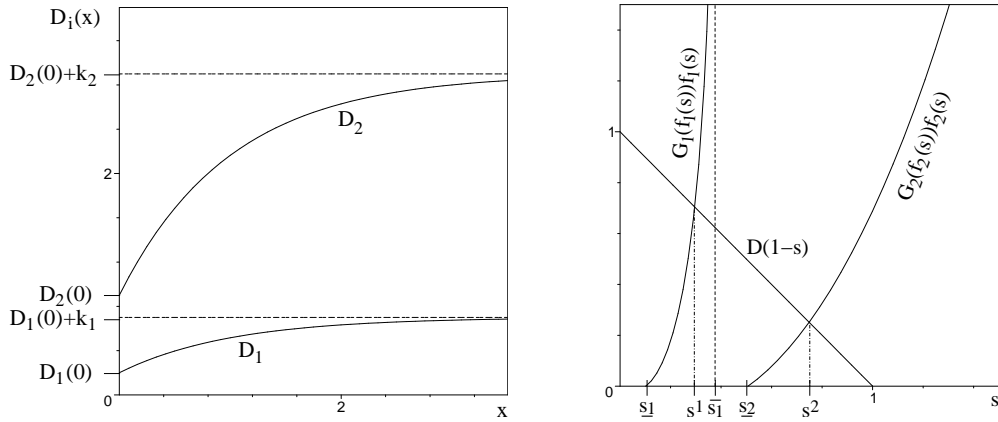
(a) The functions D_i of the form given in (6.6) for the parameter values $D_1(0) = 0.2$, $D_2(0) = 0.9$, $k_1 = 0.5$, $k_2 = 2$, $c_1 = c_2 = 1$.

(b) Nullclines of the system with nonlinear functions f_i and D_i.

Figure 6.2: The non-linear case.

its domain is the finite interval $[D_i^0, D_i^0 + k_i]$.

In order to determine the stability of the equilibria E_i and E we consider the Jacobian J. In general, the matrix J has the form

$$\begin{pmatrix} -D - x_1 f_1'(s) - x_2 f_2'(s) & -f_1(s) & -f_2(s) \\ x_1 f_1'(s) & f_1(s) - D_1(x_1) - x_1 D_1'(x_1) & 0 \\ x_2 f_2'(s) & 0 & f_2(s) - D_2(x_2) - x_2 D_2'(x_2) \end{pmatrix}.$$

First, we take a closer look at the substrate-only equilibrium $S = (1, 0, 0)$. A few properties are collected in the following proposition.

Proposition 6.3.1 (Trivial stationary state and stability.) *The trivial stationary point S always exists. Under the assumption (d) made in section 6.2, it is always locally unstable both in x_1 and x_2 direction.*

Proof. At the substrate-only equilibrium S, the Jacobian J takes the form

$$J_0 = \begin{pmatrix} -D & -f_1(1) & -f_2(1) \\ 0 & f_1(1) - D_1(0) & 0 \\ 0 & 0 & f_2(1) - D_2(0) \end{pmatrix}. \tag{6.7}$$

Assumption (d) in section 6.2 implies that two of the eigenvalues of J_0 are strictly positive. Consequently, S is locally unstable. This proves proposition 6.3.1. $\square$
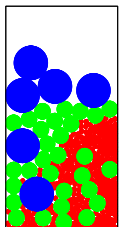
In a biological context, inequality (d) guarantees that S is unstable against invasion of x_1 and x_2. In other words, either species can immigrate into the system, once a small number of individuals is introduced, if only the concentration of the other species is low.

Next, let us analyze existence and stability of the one-consumer equilibria.

Proposition 6.3.2 (One-consumer equilibria and stability.) *Under the assumption (d) in section 6.2, both one-consumer equilibria E_i exist and are globally stable in the positive quadrant of the $(s, x_i)-$plane. E_i is locally stable in a three-dimensional neighborhood (i.e., in addition, stable against the invasion of the other species x_{3-i}), if and only if*

$$f_{3-i}(s^i) < D_{3-i}^0, \tag{6.8}$$

where s^i is the value of s at E_i.

Proof. At the one-consumer equilibria E_i, the respective Jacobian matrices J_i have the form

$$J_1 = \begin{pmatrix} -D - x_1^1 f_1'(s^1) & -f_1(s^1) & -f_2(s^1) \\ x_1^1 f_1'(s^1) & -x_1^1 D_1'(x_1^1) & 0 \\ 0 & 0 & f_2(s^1) - D_2^0 \end{pmatrix}$$

at $E_1 = (s^1, x_1^1, 0)$ and

$$J_2 = \begin{pmatrix} -D - x_2^2 f_2'(s^2) & -f_1(s^2) & -f_2(s^2) \\ 0 & f_1(s^2) - D_1^0 & 0 \\ x_2^2 f_2'(s^2) & 0 & -x_2^2 D_2'(x_2^2) \end{pmatrix}$$

at $E_2 = (s^2, 0, x_2^2)$. We will carry out the proof for E_1, the second equilibrium E_2 is treated in exactly the same way. Following (6.1) and using the strict monotonicity assumptions (b) and (c), the stationary state E_1 exists if and only if $\underline{s_1} < 1$. The stability of E_1 in the $(s, x_1)-$plane is determined by the 2x2 Jacobian

$$\tilde{J}_1 = \begin{pmatrix} -D - x_1^1 f_1'(s^1) & -f_1(s^1) \\ x_1^1 f_1'(s^1) & -x_1^1 D_1'(x_1^1) \end{pmatrix}.$$

It is straightforward to check that the eigenvalues of $\tilde{J}_1$ always have strictly negative real part. Hence, E_1 is locally stable in the $(s, x_1)-$plane. For the global stability in the plane we use a Bendixson argument. For $x_2 = 0$, system (6.1) reads

$$\begin{aligned} \dot{s} &= D(1 - s) - x_1 f_1(s), \\ \dot{x_1} &= x_1 \left(f_1(s) - D_1(x_1) \right). \end{aligned} \tag{6.9}$$

By rescaling the time variable, we can transform (6.9) into

$$\begin{aligned} \dot{s} &= \frac{D(1 - s)}{x_1} - f_1(s), \\ \dot{x_1} &= f_1(s) - D_1(x_1), \end{aligned} \tag{6.10}$$
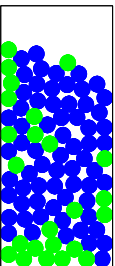
the Jacobian of which is

$$J_{trans} = \begin{pmatrix} -\frac{D}{x_1} - f_1'(s) & -\frac{D(1-s)}{x_1^2} \\ f_1'(s) & -D_1'(x_1) \end{pmatrix}.$$

The divergence $\operatorname{tr} J_{trans}$ of (6.10) is strictly negative everywhere. Hence, by Bendixson's negative criterion (e.g. [Perko96]), system (6.9) has no periodic orbits. Furthermore, it is straightforward to check, that the simplex

$$\mathcal{E} := \left\{ (s, x_1) \in \mathbb{R}_+^2 : s \geq 0, x_1 \geq 0, s + x_1 \leq \frac{D}{\min\{D, D_1^0\}} \right\}$$

is positively invariant and globally attracting (see also proposition 6.4.2 in section 6.4). Hence, the equilibrium E_1 (which is unique in $\mathbb{R}_+^2$) is globally stable in the positive two-dimensional cone. Finally, E_1 is also locally stable in an open three-dimensional neighborhood if the third eigenvalue $f_2(s^1) - D_2^0$ of J_1 is strictly negative. This completes the proof of proposition 6.3.2. $\square$

In order to get a better picture of the situation, let us recall: The coexistence equilibrium E_i exists if and only if $\underline{s_i} < 1$, i.e. if and only if the function f_i reaches the value D_i^0 below $s = 1$. But this is the same as saying that $f_i(1) > D_i^0$, which means that the corresponding eigenvalue of J_0 is strictly positive and the trivial substrate-only stationary state becomes unstable against invasion of the species x_i. Consequently, E_i and S can exist at the same time, but they cannot be both locally stable. This point will be illustrated with the help of simulations in section 6.7. Furthermore, note that the conditions (6.8) for the local stability of E_i are equivalent to $s^i < \underline{s_i}$. Obviously, $s^1 < \underline{s_2} \Rightarrow \underline{s_1} < s^2$ and $s^2 < \underline{s_1} \Rightarrow \underline{s_1} < s^2$ (see figure 6.2(b)). Hence, E_1 and E_2 cannot be both locally stable. In the following, we discuss the situation of two locally unstable one-consumer equilibria. To this end, we try to find conditions for the existence of the coexistence equilibrium E:

Proposition 6.3.3 (Coexistence equilibrium and stability.) *The coexistence equilibrium E exists if and only if all of the three following conditions hold:*
(i) $\underline{s_1} < 1$ and $\underline{s_2} < 1$, i.e. both E_1, E_2 exist,
(ii) $\underline{s} < \min\{\overline{s_1}, \overline{s_2}\}$,
(iii) $D > D^*$, where

$$D^* := \frac{\sum_{i=1}^2 G_i(f_i(\underline{s})) f_i(\underline{s})}{1 - \underline{s}}. \tag{6.11}$$

Whenever E exists, it is also locally stable.

Note that the critical value D^* in (6.11) is defined only if condition (ii) in proposition 6.3.3 holds.
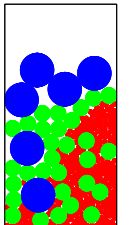
Proof. Clearly, a necessary condition for the existence of E is that $\dot{x}_i$ vanishes for $i = 1, 2$ in (6.1) for non-trivial x_i. In addition, the equation

$$D(1 - s) = \sum_{i=1}^{2} G_i(f_i(s))f_i(s). \tag{6.12}$$

must be satisfied for some $s \in (0, 1)$, hence we need $D > D^*$ with D^* as in (6.11).

In order to determine the stability of the coexistence point E we use the Routh-Hurwitz criterion (see for example [Gantmacher59]). The characteristic polynomial of the Jacobian at E is

$$\lambda^3 + A\lambda^2 + B\lambda + C \tag{6.13}$$

where the constants A, B and C are given by

$$
\begin{aligned}
A =\ & D + x_1^*[f_1'(s^*)D_1'(x_1^*)] + x_2^*[f_2'(s^*) + D_2'(x_2^*)] \\
B =\ & x_1^* x_2^* D_1'(x_1^*)D_2'(x_2^*) + \\
& + [D + x_1^* f_1'(s^*) + x_2^* f_2'(s^*)][x_1^* D_1'(x_1^*) + x_2^* D_2'(x_2^*)] + \\
& + x_1^* f_1(s^*)f_1'(s^*) + x_2^* f_2(s^*)f_2'(s^*) \\
C =\ & x_1^* x_2^* D_1'(x_1^*)D_2'(x_2^*)[D + x_1^* f_1'(s^*) + x_2^* f_2'(s^*)] + \\
& + x_1^* x_2^*[D_1'(x_1^*)f_2(s^*)f_2'(s^*) + D_2'(x_2^*)f_1(s^*)f_1'(s^*)].
\end{aligned}
\tag{6.14}
$$

By assumption, the constant D is non-negative and the derivatives of the functions f_i and D_i are both strictly positive. Thus A, B and C are strictly positive as well. Furthermore

$$\det \begin{pmatrix} A & 1 \\ C & B \end{pmatrix} = AB - C.$$

Straightforward calculation shows that

$$
\begin{aligned}
AB - C =\ & (D + x_1^* f_1'(s^*) + x_1^* D_1'(x_1^*) + x_2^* f_2'(s^*) + x_2^* D_2'(x_2^*)) \cdot \\
& \cdot [x_1^* x_2^* D_1'(x_1^*)D_2'(x_2^*) + \\
& + (D + x_1^* f_1'(s^*) + x_2^* f_2'(s^*))(x_1^* D_1'(x_1^*) + x_2^* D_2'(x_2^*)) + \\
& + x_1^* f_1(s^*)f_1'(s^*) + x_2^* f_2(s^*)f_2'(s^*)] - \\
& - x_1^* x_2^* D_1'(x_1^*)D_2'(x_2^*)(D + x_1^* f_1'(s^*) + x_2^* f_2'(s^*)) - \\
& - x_1^* x_2^*(D_1'(x_1^*)f_2(s^*)f_2'(s^*) + D_2'(x_2^*)f_1(s^*)f_1'(s^*)) \\
=\ & (D + x_1^* f_1'(s^*) + x_1^* D_1'(x_1^*) + x_2^* f_2'(s^*) + x_2^* D_2'(x_2^*)) \cdot \\
& \cdot (D + x_1^* f_1'(s^*) + x_2^* f_2'(s^*))(x_1^* D_1'(x_1^*) + x_2^* D_2'(x_2^*)) + \\
& + (x_1^* D_1'(x_1^*) + x_2^* D_2'(x_2^*))x_1^* x_2^* D_1'(x_1^*)D_2'(x_2^*) + \\
& + (D + x_1^* f_1'(s^*) + x_2^* f_2'(s^*))(x_1^* f_1(s^*)f_1'(s^*) + x_2^* f_2(s^*)f_2'(s^*)) \\
> &\ 0,
\end{aligned}
$$
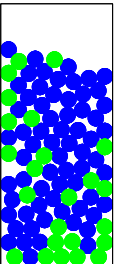
since by assumption all terms are strictly positive. Finally,

$$\det \begin{pmatrix} A & 1 & 0 \\ C & B & A \\ 0 & 0 & C \end{pmatrix} = (AB - C)C > 0,$$

since $C > 0$. Hence, the conditions of the Routh-Hurwitz criterion are satisfied and the coexistence equilibrium E is stable whenever it exists. This proves proposition 6.3.3. $\square$.

We observe that D^* does not depend on D. Thus, for any given value of D^* we can always choose $D > D^*$ (under the assumption that condition (ii) in proposition 6.3.3 is satisfied). Biologically speaking, one can always design a system with coexistence equilibrium by increasing the rate D of nutrient input into the chamber. In terms of the two one-consumer equilibria, the condition for the existence of the coexistence point can be formulated as follows: Condition (i) in proposition 6.3.3 guarantees the existence of two globally (in $\mathbb{R}_+^2$) stable stationary states E_i, $i = 1, 2$. Suppose condition (ii) holds, but $D < D^*$, i.e. E does not exist. Without loss of generality, let E_1 be the equilibrium, which is locally stable in the open three-dimensional cone R_+^3. If we now increase the parameter D, the new stationary state E emerges from E_1 and moves into R_+^3. This bifurcation occurs when D passes the critical value D^*. At the same time, E_1 loses its stability and E attracts all trajectories in the open cone. Figure 6.3 illustrates a sequence of different positions of the coexistence point for varying D in the case of linear uptake and washout rates. Figure 6.4 shows the nullclines and the substrate concentration at the coexistence equilibrium in the case of linear functions f_i and D_i. Note that system (6.1) with the non-linear functions (6.6) represents an example, in which the coexistence point does not exist because condition (ii) in proposition 6.3.3 is violated (see also figure 6.2(b)).

6.4 Invariant sets and boundedness of the solutions

From the structure of the equations of the general system (6.1) it is evident that the positive orthant $\mathbb{R}_3^+$ is positively invariant. Similarly, it follows that the set $\{(s, x_1, x_3) \in \mathbb{R}_3^+ : s \leq 1\}$ is positively invariant as well, i.e. the positivity of the concentrations is conserved. Furthermore, the following positively invariant and globally attracting bounded sets exist for the system with linear uptake and washout rates and the general system, respectively:

Proposition 6.4.1 (Linear rates.) *Consider system (6.5), i.e. the nutrient uptake functions as well as the washout rates are supposed to be linearly dependent on the concentrations of the species. Then the box shaped set*

$$\mathcal{A} = \left\{ (s, x_1, x_2) \in \mathcal{R}_+^3 : 0 \leq s \leq 1, 0 \leq x_i \leq a_i/k_i \right\}$$

is positively invariant and globally attracting in $\mathbb{R}_+^3$.
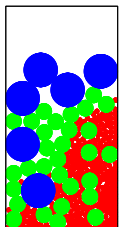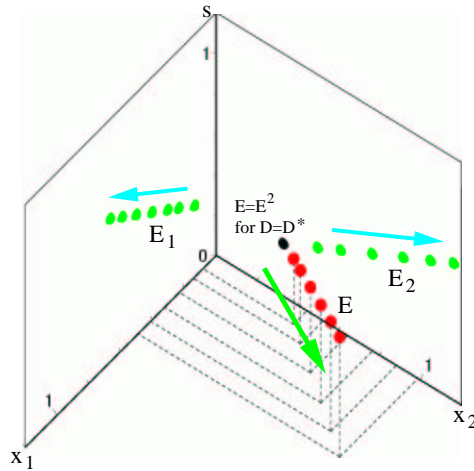
Figure 6.3: Sequence of coexistence equilibria emerging from the locally stable one-consumer stationary point E_2 in the case of linear functions $f_1(s) = 2s$, $f_2(s) = 3s$, $D_1(x_1) = 0.2 + x_1$ and $D_2(x_2) = 0.8 + 2x_2$. For $D = D^* \approx 0.24$, the coexistence point coincides with E_2. The values of the parameter D generating the sequence of coexistence points are $D = 0.54, 0.84, 1.44, 2.34, 3.54, 5.04$. With varying D, the positions of E_1 and E_2 move as well in their respective plane.
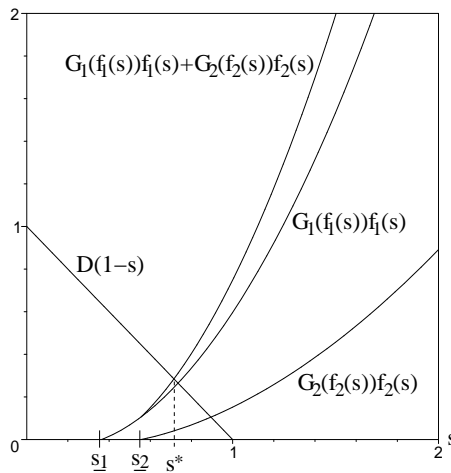
Figure 6.4: In the case of linear functions $f_1(s) = 2s$, $f_2(s) = 3s$, $D_1(x_1) = 0.2 + x_1$, $D_2(x_2) = 0.2 + 2x_2$ and $D = 1$, condition (6.11) is satisfied. The coexistence substrate concentration s^* is the solution of (6.3).

Proof. Conservation of positivity and the upper bound for s have been shown for solutions of the general system (6.1). From (6.5) it is evident that $\dot{x}_i$ becomes negative if $x_i > a_i/k_i$. This proves proposition 6.4.1. $\square$
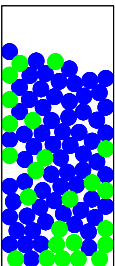
For the general system, upper bounds can only be given in terms of the parameters:

Proposition 6.4.2 (General system.) *The simplex*

$$\mathcal{B} = \big\{ (s, x_1, x_2) \in \mathcal{R}_+^3 :$$
$$s \geq 0, x_1 \geq 0, x_2 \geq 0, s + x_1 + x_2 \leq D/\min\{D, D_1^0, D_2^0\} \big\}$$

is positively invariant and globally attracting for system (6.1).

Proof. In view of

$$\dot{s} + \dot{x}_1 + \dot{x}_2 = D(1-s) - x_1 D_1(x_1) - x_2 D_2(x_2)$$
$$\leq D - \big[Ds + D_1^0 x_1 + D_2^0 x_2 \big] \tag{6.15}$$
$$\leq D - (s + x_1 + x_2)\min\{D, D_1^0, D_2^0\}.$$

we have $\dot{s} + \dot{x}_1 + \dot{x}_2 < 0$ whenever $s + x_1 + x_2 \geq D/min\{D, D_1^0, D_2^0\}$. $\square$

6.5 Convergence to stationary solutions

Consider the set M defined by

$$M = \{(s, x_1, x_2) | s \geq 0, x_1 \geq 0, x_2 \geq 0, s + x_1 + x_2 \leq D/D^*\}.$$

It is easy to show that M is a positively invariant set for the general system (6.1). The aim of this section is to find a suitable Lyapunov function in the case of a coexistence equilibrium. Once we know that such a function exists, we deduce that every trajectory of system (6.1) approaches equilibrium. Let us start with the case where one of the two species has disappeared from the system, thus leaving a single species with concentration x_1, uptake function $f_1 = f_1(s)$ and mortality $D_1 = D_1(x_1)$. The method of constructing a Lyapunov function will later be generalized to the three-dimensional model (6.1). Denote by $E_1 = (s^1, x_1^1)$ the one-consumer equilibrium, i.e. $D(1 - s^1) = x_1^1 f_1(s^1)$, $f_1(s^1) = D_1(x_1^1)$, and define a function $V : \mathcal{R}_+^2 \longrightarrow \mathcal{R}$ by

$$V(s, x_1) = \int_{s^1}^{s} \frac{f_1(\xi) - f_1(s^1)}{f_1(\xi)} d\xi + \left[x_1 - x_i^1 \left(1 + \log \frac{x_1}{x_1^1} \right) \right] \tag{6.16}$$

for $s, x_1 > 0$. Note that each one of the two terms in (6.16) is non-negative everywhere and vanishes only at (s^1, x_1^1). The first condition for Lyapunov functions is satisfied. Furthermore, with $\partial V/\partial s = (f_1(s) - f_1(s^1))/f_1(s)$ and $\partial V/\partial x_1 = (x_1 - x_1^1)/x_1$ we get

$$\dot{V} = \frac{\partial V}{\partial s} \dot{s} + \frac{\partial V}{\partial x_1} \dot{x}_1$$
$$= \left[\frac{f_1(s) - f_1(s^1)}{f_1(s)} \right] \dot{s} + \left[\frac{x_1 - x_1^1}{x_1} \right] \dot{x}_1 \tag{6.17}$$
$$= \left[\frac{f_1(s) - f_1(s^1)}{f_1(s)} \right] (D(1-s) - x_1 f_1(s)) + \left[x_1 - x_1^1 \right] (f_1(s) - D_1(x_1)).$$
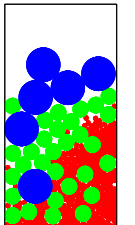
Next, we split $\dot{V}$ into one part depending only on s and a second one depending depending only on x_1. Write

$$\dot{V} = \left[\frac{f_1(s) - f_1(s^1)}{f_1(s)} \right] \left(D(1-s) - x_1^1 f_1(s) \right) + \left[x_1 - x_1^1 \right] \left(f_1(s^1) - D_1(x_1) \right). \tag{6.18}$$

Both terms on the right hand side of (6.18) are strictly concave functions of s and x_1, respectively, and both have their absolute maximum at (s^1, x_1^1). Thus, V represents a Lyapunov function for the two-dimensional system and the one-consumer equilibrium E_1 is globally stable. (This, we already know from proposition 6.3.2.)

The general, three-dimensional system (6.1) is more complicated, even though the same technique may be applied. We prove the following convergence result:

Theorem 6.5.1 (Global stability of the coexistence point.)   *Consider system (6.1) with general, monotone uptake and mortality functions f_i and D_i satisfying conditions (a) through (c) in section 6.2. Suppose that $\underline{s_1} < 1$, $\underline{s_2} < 1$ and $D > D^*$, where $\underline{s_1}$, $\underline{s_2}$, D^* are defined in section 6.3. If we impose in addition that $f_2(s) = a f_1(s)$ for some constant $a > 0$ and for all $s \geq 0$, then the existing coexistence equilibrium E is globally stable.*

Proof. In order to prove theorem 6.5.1, we define a function $W : \mathcal{R}_+^3 \longrightarrow \mathcal{R}$ by

$$W(s, x_1, x_2) = \sum_{i=1}^{2} \left\{ \frac{1}{2} \int_{s^*}^{s} \frac{f_i(\xi) - f_i(s^*)}{f_i(\xi)} d\xi + \left[x_i - x_i^* \left(1 + \log \frac{x_i}{x_{i^*}} \right) \right] \right\} \tag{6.19}$$

for $s, x_i > 0$.

Lemma 6.5.2 (Lyapunov function.)   *Under the hypotheses of theorem 6.5.1, the function (6.19) is a Lyapunov function for system (6.1).*

Proof. Note that each one of the four terms in the above sum is always greater than or equal to zero and that all four vanish only at the coexistence point $E = (s^*, x_1^*, x_2^*)$. Thus the first condition for Lyapunov functions is satisfied. We now calculate the derivative of W along the solution curves.

$$\begin{aligned} \dot{W} =& \frac{\partial W}{\partial s} \dot{s} + \frac{\partial W}{\partial x_1} \dot{x_1} + \frac{\partial W}{\partial x_2} \dot{x_2} \\ =& \left[\frac{1}{2} \sum_{i=1}^{2} \frac{f_i(s) - f_i(s^*)}{f_i(s)} \right] \dot{s} + \sum_{i=1}^{2} \left[\frac{x_i - x_i^*}{x_i} \right] \dot{x_i} \\ =& \frac{f_1(s) - f_1(s^*)}{f_1(s)} \left[D(1-s) - x_1^* f_1(s) - x_2^* a f_1(s) \right] + \\ & + (x_1 - x_1^*)(f_1(s^*) - D_1(x_1)) + \\ & + (x_2 - x_2^*)(a f_1(s^*) - D_2(x_2)), \end{aligned} \tag{6.20}$$
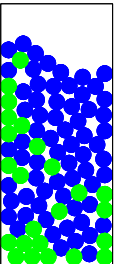
where $\dot{s}$ and $\dot{x}_i$ are defined by equations (6.1). Due to the fact that $\dot{s}$ and $\dot{x}_i$ vanish at $E = (s^*, x_1^*, x_2^*)$, the first term in the last row of equation (6.20) is always non-positive and becomes zero for $s = s^*$. The second and third terms are non-positive as well. They vanish for $x_1 = x_1^*$ and $x_2 = x_2^*$, respectively. Hence, $\dot{W}$ is strictly negative everywhere but in E. It is straightforward to check that the function W itself is strictly positive in $\mathbb{R}^3 \backslash E$ and vanishes only at the equilibrium. This proves lemma 6.5.2 and hence theorem 6.5.1. $\square$. $\square$.

6.6 Example of a coexistence equilibrium

We consider in this section linear uptake and mortality functions of the form (6.4). We will be interested in the quality of the coexistence equilibrium and in the problem of extinction and persistence of the two species. Suppose we have two one-consumer equilibria E_1 and E_2 where the latter is stable. We mentioned above that in this case the other point E_1 cannot be stable as well. These conditions can be expressed as follows:

$$0 < \frac{D_2(0)}{a_2} \leq \frac{D_1(0)}{a_1} \leq 1 \tag{6.21}$$

or, in terms of $\underline{s}_i$,

$$0 < \underline{s_1} \leq \underline{s_2} \leq 1.$$

Under which conditions can the species x_1 establish itself in the system, i.e. under which conditions can we transform the stable equilibrium E_2 into either a stable point E_1 or a coexistence equilibrium E (which is always stable)? The answer to this question can be given by looking at the condition for the existence of E, namely equation (6.11) which takes the form

$$D > D^* = \frac{D_1(0)[D_1(0) - D_2(0)]}{k_2[a_1 - D_1(0)]}. \tag{6.22}$$

Case 1. The species x_1 can *try* to invert equation (6.21) either by increasing a_2 or by decreasing $D_2(0)$. We will then have E_2 instable and E_1 stable.

Case 2. Species x_1 also has the possibility to reach coexistence. This can be done in two different ways. As we mentioned before, E can always be *generated* or *created* by increasing the input rate D over the limit level D^*. Biologically speaking this means that the input of nutrient s is high enough for each one of the two competing species to have sufficient food supply and competition cannot lead to the extinction of the *weaker* one of the two any more.

The other possibility is much more interesting. Suppose we increase the mortality coefficients k_i of the two species. This will decrease D^* as can be seen in equation (6.22). For any given input rate D the value of D^* will eventually become smaller
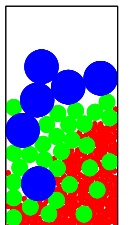
than D, and we have the situation of stable coexistence. The increase of mortality of the two species can be thought of as being the effect of an increasing predation of a hypothetical third species which is not considered in our model and which feeds on the two species x_i. If the number of individuals of this predator species is held constant (or if it is always high enough such that predation can take place at its maximum) then the mortality of x_i will be proportional to x_i and will not depend on the number of predators any longer. This additional predation will diminish the competing species in a way that only a relatively small number of them will survive. As a result, competition will drop to a minimum since the amount of substrate will not be a limiting factor any more.

6.7   Simulations

In order to illustrate the long-time behavior of system (6.1), we simulate some typical trajectories in the case of linear uptake and mortality functions of the form (6.4) (see figure 6.5). The resulting coexistence equilibrium is globally stable in the open positive octant.
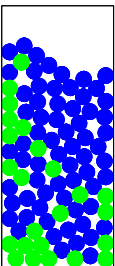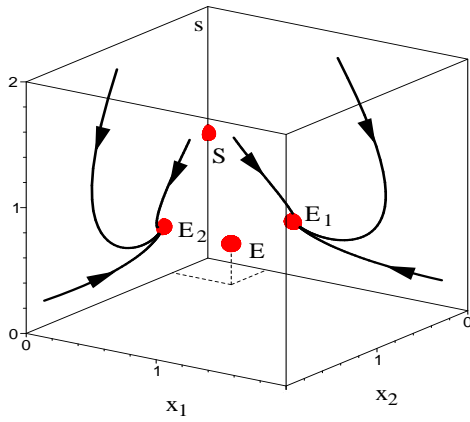
(a) Trajectories starting in the (s, x_i)-plane approach the corresponding one-consumer equilibria E_1 and E_2, respectively. We chose the sets of initial values $(0, 1.8, 0.2)$, $(0, 1, 1.8)$, $(0, 0.2, 1)$ and $(1.8, 0, 0.2)$, $(1, 0, 1.8)$, $(0.2, 0, 1)$.
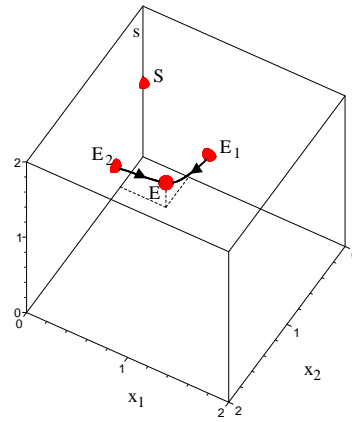
(b) The heteroclinic orbits connecting E_i to E.
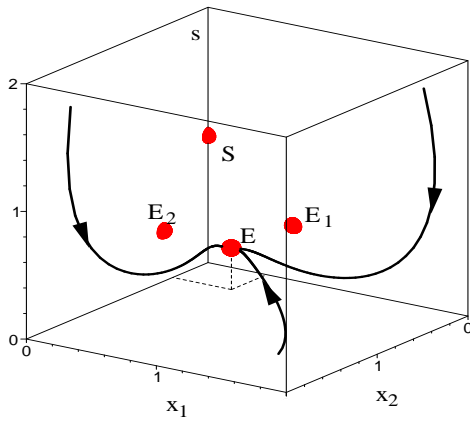
(c) Trajectories starting in the open positive cone approach the coexistence equilibrium. The starting points for the three orbits were $(1.8, 1.8, 0.2)$, $(0.2, 1.8, 1.8)$ and $(1.8, 0.2, 1.8)$.
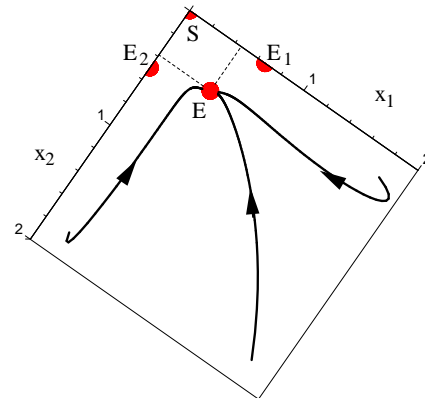
(d) Projection onto the (x_1, x_2)-plane, showing the same orbits as in (c).

Figure 6.5: Simulation of system (6.1) with $f_1(s) = 2s$, $f_2(s) = 3s$, $D_1(x_1) = 0.2 + x_1$, $D_2(x_2) = 0.2 + 2x_2$ and $D = 1$. The coexistence equilibrium E is globally attracting in the positive cone, while E_1 and E_2 are stable in the (s, x_1)- and (s, x_2)-planes, respectively.
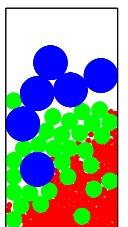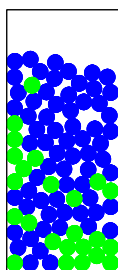
Chapter 7

The chemostat with diffusion

Summary. A chemostat model of the type discussed in chapter 6 is generalized in order to describe concentrations varying in space and time. Here, we focus on solutions exhibiting traveling wave fronts.

7.1 Introduction

In the present chapter we generalize a chemostat model of the type analyzed in chapter 6 for a single consumer species u. Instead of assuming homogeneous concentrations throughout the vessel, we now consider very long growing chambers and allow, that the concentrations of the consumer as well as the nutrient may depend on the position in the container. We restrict to one space dimension. It turns out that under certain parameter restrictions and with certain initial conditions, the concentrations propagate in form of traveling waves. Traveling wave fronts have been studied frequently in the context of Lotka-Volterra type predator-prey systems (see for example [Dunbar83], [Dunbar84] or [Dunbar86]) or the propagation of nerve signals (see [Feroe83] and [Feroe86]). The importance of traveling waves in ecological problems is discussed in [Okubo80]. In [Fife79], the formation and propagation of waves in the more general setting of reaction-diffusion systems is analyzed, while [Smoller83] provides a very detailed discussion of shock waves of various types. Finally, [Bosch90], [Lewis02.1], [Lewis02.2] and [Weinberger82] study the propagation velocities of wave fronts especially in diffusion models of ecological interest and seek out conditions under which minimal feasible wave speeds are attained. Special cases of diffusive chemostat models for two competing consumers were analyzed in [Hsu93] and [So91]. The authors studied the asymptotic behavior of solutions in the case of *Michaelis-Menten* type uptake functions and constant consumer mortalities, as well as the existence of inertial manifolds. A model for a single species in an unstirred chemostat is analyzed in [Dung99].

In section 7.2, we recall some properties of the simple, *stirred* chemostat model
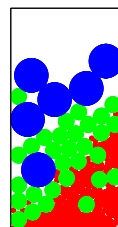
exhibiting a single consumer species and motivate the generalization to a system of partial differential equations describing consumer and substrate concentrations which vary in space and time. In the case of a bounded domain and equal diffusion coefficients, we can prove the convergence of the time-dependent solutions. Section 7.3 presents a heuristic approach to the propagation of traveling wave fronts. Here, we suggest different types of waves and discuss the conditions, under which they may occur. The traveling wave approach transforms the original two-dimensional system back to a three-dimensional ODE system, the solutions of which yield the shapes of possible wave fronts. The aim of section 7.4 is to locate possible equilibria of the ODE system, which are at the same time boundary values for the traveling wave. Sections 7.4.1 and 7.4.2 discuss the existence and stability of the substrate-only equilibrium and the non-trivial stationary state respectively. A mathematically and biologically interesting situation occurs, when the in- and outflow of nutrient solution is stopped and the consumer depends on the substrate present in the system (see section 7.5). In this so-called *epidemic* case, the system exhibits a two-dimensional invariant of motion, and yet another type of traveling waves can be observed. The conditions under which the minimal feasible wave speed is attained are consistent with the ones predicted by the so-called *linear conjecture* (see for example [Lewis02.1] and [Lewis02.2]). Two examples of the above reduction are given in section 7.6. Finally, section 7.7 gives a brief outlook to multi-consumer chemostat models incorporating diffusion.

7.2   The model for the chemostat with diffusion

Let us recall the so-called *stirred* chemostat with a single species u and a substrate s,

$$
\begin{aligned}
\dot{s} &= D_0(1-s) - uf(s), \\
\dot{u} &= u(f(s) - D_1).
\end{aligned}
\tag{7.1}
$$

Here, $D_0 \geq 0$ is the nutrient input and washout rate. Throughout the first part of this chapter, we will assume that D_0 is strictly positive, i.e. the system is constantly supplied with fresh nutrient solution. Only in the discussion of the so-called *epidemic case* in section 7.5, we set the washout rate equal to zero. The constant *mortality* or washout rate of the species u is denoted by D_1. We suppose $D_1 > 0$. Finally, we impose $f(0) = 0$, and we restrict to strictly monotone nutrient uptake functions, $f'(s) > 0$ for all s.

The basic properties of system (7.1) are collected in the following proposition.

Proposition 7.2.1 (The simple chemostat.) *Under the above assumptions on the uptake function f and the parameters D_0 and D_1, the following hold for (7.1):*
(i) Positivity of both s and u is preserved for all times.
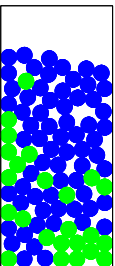
(ii) The substrate-only equilibrium $(s, u) = (1, 0)$ always exists. It is locally asymptotically stable if and only if $f(s) = D_1$ for some positive $s < 1$, which, in view of the monotonicity condition on f, is equivalent to $f(1) > D_1$.

(iii) System (7.1) exhibits a non-trivial stationary state $(s, u) = (\bar{s}, \bar{u})$ if and only if $f(1) < D_1$, i.e. if and only if the trivial equilibrium is not locally stable. The values $\bar{s}$ and $\bar{u}$ are then given by $f(\bar{s}) = D_1$ and $\bar{u} = D_0(1 - \bar{s})/f(\bar{s})$. This non-trivial equilibrium is also globally stable.

Proof. We refer to the corresponding proofs for the general three-dimensional system discussed in chapter 6. □.

In the above model, one implicitly assumes that the concentrations of each of the two reactants are constant all over the chemostat chamber. Now suppose we have a one-dimensional vessel and concentrations vary in time as well as in space. Then, u and s are subject to diffusion as well, and the resulting model is the system of partial differential equations

$$
\begin{aligned}
s_t &= D_0(1 - s) - uf(s) + \delta_s s_{xx}, \\
u_t &= u(f(s) - D_1) + \delta_u u_{xx},
\end{aligned}
\tag{7.2}
$$

where $u = u(t, x)$ and $s = s(t, x)$ both depend on time t and space x, and where δ_s and δ_u are the (constant) diffusion coefficients for s and u, respectively. Let us first consider a short vessel, represented by the finite interval $[0, l]$ for some $l > 0$. At the ends of this vessel, we impose the no-flux boundary conditions

$$
s_x = u_x = 0,
\tag{7.3}
$$

$x = 0, l$. Following the idea of section 6.5 in chapter 6, we can prove convergence of solutions of system (7.2) with boundary conditions (7.3) in the case of equal diffusion rates:

Proposition 7.2.2 (Convergence of solutions to the diffusive chemostat.) *Consider the diffusive chemostat, system (7.2), (7.3) for equal diffusion rates $\delta_s = \delta_u =: \delta$. Then, the equilibrium $s \equiv \bar{s}$, $u \equiv \bar{u}$ is globally stable.*

Proof. We define a function $Y = Y(s, u)$ on the solutions $(s, u) = (s(t), u(t))$ of (7.2), (7.3) by

$$
Y := \int_{\bar{s}}^{s} \frac{f(\xi) - f(\bar{s})}{f(\xi)} d\xi + \left[u - \bar{u} \left(1 + \log \frac{u}{\bar{u}} \right) \right],
$$

where $s = s(t, x)$, $u = u(t, x)$. Then, $Y \geq 0$ for all $s, u \geq 0$, and $Y = 0$ if and only
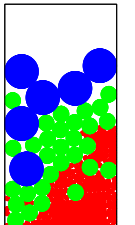
if $s = \bar{s}$, $u = \bar{u}$. Furthermore,

$$
\begin{aligned}
Y_t =& Y_s s_t + Y_u u + t \\
=& \frac{f(s) - f(\bar{s})}{f(s)} \left[D_0(1 - s) - u f(s) \right] + \delta s_{xx} \frac{f(s) - f(\bar{s})}{f(s)} + \\
& + (u - \bar{u}) \left[f(s) - D_1 \right] + \delta u_{xx} \frac{u - \bar{u}}{u} \\
=& \frac{f(s) - f(\bar{s})}{f(s)} \left[D_0(1 - s) - \bar{u} f(s) \right] + (u - \bar{u}) \left[f(\bar{s}) - D_1 \right] + \\
& + \delta \left[s_{xx} \frac{f(s) - f(\bar{s})}{f(s)} + u_{xx} \frac{u - \bar{u}}{u} \right].
\end{aligned}
$$

With

$$
Y_x = \frac{f(s) - f(\bar{s})}{f(s)} s_x + \frac{u - \bar{u}}{u} u_x
$$

and

$$
Y_{xx} = \frac{f'(s) f(\bar{s})}{f^2(s)} s_x^2 + \frac{\bar{u}}{u^2} u_x^2 + \frac{f(s) - f(\bar{s})}{f(s)} s_{xx} + \frac{u - \bar{u}}{u} u_{xx},
$$

we therefore get

$$
\begin{aligned}
Y_t =& \frac{f(s) - f(\bar{s})}{f(s)} \left[D_0(1 - s) - \bar{u} f(s) \right] + (u - \bar{u}) \left[f(\bar{s}) - D_1 \right] + \\
& + \delta Y_{xx} - \delta \left[\frac{f'(s) f(\bar{s})}{f^2(s)} s_x^2 + \frac{\bar{u}}{u^2} u_x^2 \right].
\end{aligned}
$$

The boundary condition (7.3) implies

$$
Y_x = 0. \tag{7.4}
$$

Define a function $V = V(s, u)$ on the solution space of (7.2), (7.3) by

$$
V := \int_0^l Y(s(t, x), u(t, x)) dx.
$$

Then

$$
\begin{aligned}
V_t = \int_0^l \Bigg\{ & \frac{f(s) - f(\bar{s})}{f(s)} \left[D_0(1 - s) - \bar{u} f(s) \right] + (u - \bar{u}) \left[f(\bar{s}) - D_1 \right] - \\
& - \delta \left[\frac{f'(s) f(\bar{s})}{f^2(s)} s_x^2 + \frac{\bar{u}}{u^2} u_x^2 \right] \Bigg\} \leq 0
\end{aligned}
$$

due to (7.4), and $V_t = 0$ only at the homogeneous equilibrium $s \equiv \bar{s}$, $u \equiv \bar{u}$. Hence, V is a Lyapunov function for system (7.2), (7.3). This proves proposition 7.2.2. $\square$

Figure (7.1) shows a sequence of a simulation of system (7.2), (7.3). The result confirms the theoretical prediction: The time-dependent solution converges to
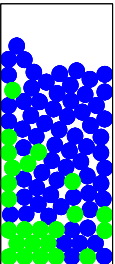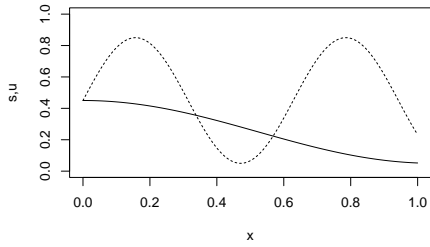
(a) Arbitrary initial function $s(0, x)$, $u(0, x)$.
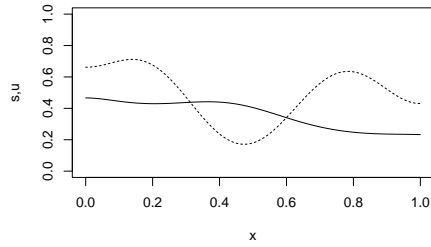
(b) The solution at $t = 0.4$.
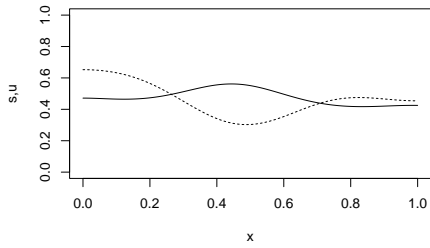
(c) The solution at $t = 1.2$.
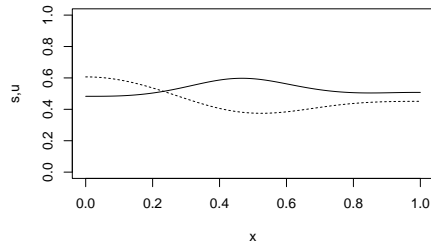
(d) The solution at $t = 2$.
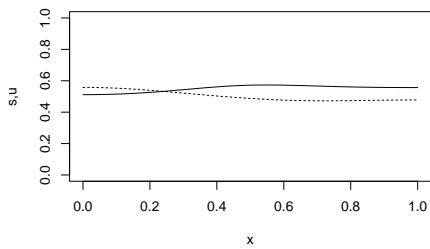
(e) The solution at $t = 4$.
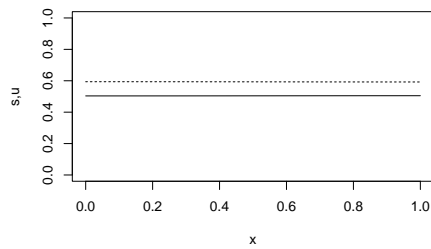
(f) The solution at $t = 12$.

Figure 7.1: Solution of system (7.2), (7.3) for $D_0 = 0.6$, $D_1 = 0.5$, $\delta_u = 0.01$ and $f(s) = s$ on an interval of length $l = 1$. The solid line represents the substrate concentration s, the dotted line is the consumer concentration u. The simulation reproduces the theoretical result: The time-dependent solution converges to the equilibrium $s \equiv \bar{s} = 0.5$, $u \equiv \bar{u} = 0.6$.
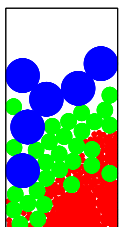
the equilibrium state with homogeneous concentrations.

For the following discussion, we consider a very long vessel (theoretically, it has infinite length), i.e. since we allow $x \in \mathbb{R}$, we do not impose boundary conditions. In order to reduce the complexity of system (7.2) we set $\delta_s = 0$. This restriction corresponds to a situation in which the substrate (or the prey species in the context of predator-prey models) diffuses much more slowly than the consumer (the predator). One could imagine, for example, a plant species being consumed by a relatively mobile animal. This assumption will reduce the dimensionality of the system from four to three, thus making the analysis considerably simpler. Rescaling of the variable u then yields

$$
\begin{aligned}
s_t &= D_0(1 - s) - u f(s), \\
u_t &= u(f(s) - D_1) + u_{xx}.
\end{aligned}
\tag{7.5}
$$

7.3   Traveling waves

In order to explain the formation of traveling wave fronts in reaction-diffusion systems of the type (7.5), we go back to the stirred chemostat model (7.1). As we have seen in section 7.2, this system exhibits two stationary states, the stability of which depends on the parameters and on the uptake function f. Suppose the parameters are chosen in a way that the non-trivial equilibrium $(s, u) = (\bar{s}, \bar{u})$ is locally (and hence globally) stable, i.e. suppose $f(1) < D_1$. In this case, we distinguish three types of orbits (see figure 7.2). The heteroclinic orbit of type (3)
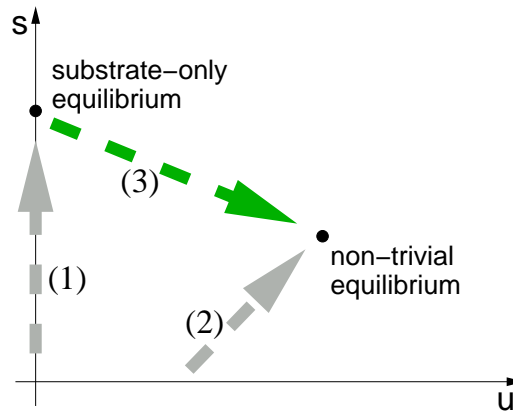
Figure 7.2: The non-trivial stationary state and typical trajectories. The heteroclinic orbit (3) connecting the trivial state $(1, 0)$ to the equilibrium $(\bar{s}, \bar{u})$ gives rise to a traveling wave front.

is the only trajectory able to generate traveling wave fronts as solutions of system (7.5), since it is the only one connecting two stationary points. If we impose the boundary values $(s, u) \to (\bar{s}, \bar{u})$ for $x \to -\infty$ and $(s, u) \to (1, 0)$ for $x \to \infty$, we
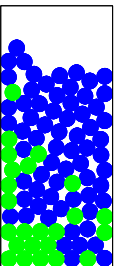
expect the formation of a wave front between these two values moving at a certain, as yet undetermined, wave speed c. Figure 7.3 illustrates such a wave. Here, we
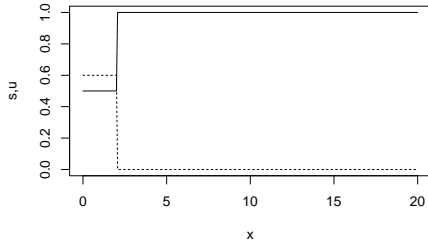
(a) The initial function $u(0, x)$ is a step function.
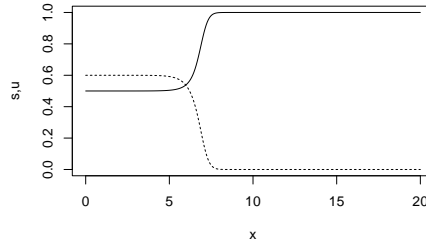
(b) The solution at $t = 40$.
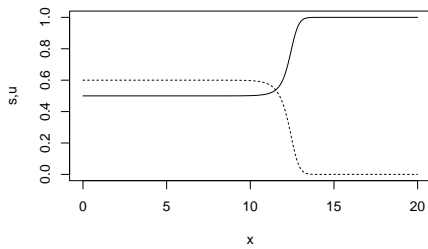
(c) The solution at $t = 80$.
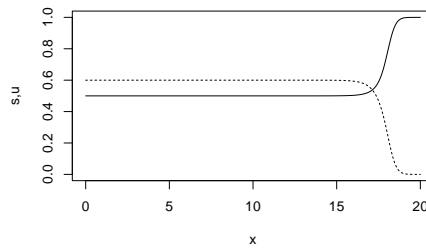
(d) The solution at $t = 120$.

Figure 7.3: Solution of system (7.5) with the same parameter values as in figure 7.1: $D_0 = 0.6$, $D_1 = 0.5$, $\delta_u = 0.01$ and $f(s) = s$. The solid line represents the substrate concentration s, the dotted line is the consumer concentration u. The (theoretically infinitely) long vessel is represented by the interval $[0, 20]$. We observe a traveling wave front, which corresponds to the heteroclinic orbit of system (7.1) connecting the substrate-only equilibrium $(s, u) = (1, 0)$ to the stationary state $(s, u) = (\bar{s}, \bar{u}) = (1/2, 3/5)$. Accordingly, the boundary values are $s(-\infty) = \bar{s} = 0.5$, $u(-\infty) = \bar{u} = 0.6$, and $s(\infty) = s_0 = 1$, $u(\infty) = u_0 = 0$.

chose $D_0 = 0.6$, $D_1 = 0.5$, $\delta_u = 0.01$ and $f(s) = s$. Hence, the corresponding non-trivial equilibrium $(s, u) = (1/2, 3/5)$ of system (7.1) is asymptotically stable.
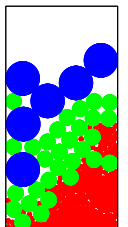
7.4   Analysis of the stationary states

We check for a traveling wave solution $s(t,x) = S(x - ct)$, $u(t,x) = U(x - ct)$, where c denotes the velocity of the wave. System (7.5) yields

$$-c\dot{s} = D_0(1 - s) - uf(s),$$
$$-c\dot{u} = u(f(s) - D_1) + \ddot{u}.$$
(7.6)

Note that we use again the notation s, u for the stationary wave concentrations previously denoted by S, U. Both depend on the single new space variable $X = x - ct$. The dots in system (7.6) thus denotes derivatives with respect to X. If we introduce the new variable $v = \dot{u}$, (7.6) becomes the first-order system

$$\dot{s} = -(D_0(1 - s) - uf(s))/c,$$
$$\dot{u} = v,$$
$$\dot{v} = -cv - u(f(s) - D_1).$$
(7.7)

Proposition 7.4.1 (Stationary states.) *System (7.7) has two possible stationary states. The trivial substrate-only equilibrium $S = (s,u,v) = (1,0,0)$ always exists. The coexistence point $E = (s,u,v) = (\bar{s}, \bar{u}, 0)$ exists if and only if $f(s) = D_1$ for some positive $s < 1$. The values $\bar{s}$ and $\bar{u}$ are then defined by $f(\bar{s}) = D_1$, $\bar{u} = D_0(1 - \bar{s})/f(\bar{s})$.*

Proof. Under the hypotheses of section 7.2, proposition 7.4.1 follows immediately. $\square$.

In the following, we analyze the stability of the two stationary states. We will be particularly interested in the so-called *epidemic case*, in which the nutrient input and washout rate D_0 drops to zero.

The general Jacobian

$$J = \begin{pmatrix} (uf'(s) + D_0)/c & f(s)/c & 0 \\ 0 & 0 & 1 \\ -uf'(s) & D_1 - f(s) & -c \end{pmatrix}$$
(7.8)

of system (7.7) yields the characteristic polynomial

$$\begin{aligned} \chi =\lambda^3 + \\ + \lambda^2 \left[c - (uf'(s) + D_0)/c \right] + \\ + \lambda \left[f(s) - D_1 - uf'(s) - D_0 \right] + \\ + \left[(uf'(s) + D_0)(D_1 - f(s)) + uf(s)f'(s) \right]/c. \end{aligned}$$
(7.9)
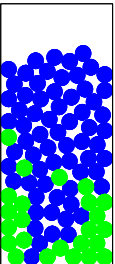
7.4.1 The substrate-only equilibrium

The qualitative behavior of trajectories in the neighborhood of S is resumed in the following proposition:

Proposition 7.4.2 (Substrate-only equilibrium.) *The substrate-only stationary state is always a saddle point in $\mathbb{R}^3$, having a two-dimensional stable manifold M_s and a one-dimensional unstable manifold M_u. If we reduce system (7.7) to M_s in S, the latter can be a node or a focus, depending on the wave speed c.*

Proof. At the substrate-only equilibrium $S = (1, 0, 0)$ the characteristic polynomial χ reduces to

$$\chi_S(\lambda) = \left(\lambda - \frac{D_0}{c} \right) (\lambda(\lambda + c) + f(1) - D_1). \qquad (7.10)$$

The eigenvalues of system (7.7) are thus $\lambda_0 = D_0/c$ and

$$\lambda_{1,2} = -c/2 \pm 1/2\sqrt{c^2 - 4(f(1) - D_1)}.$$

For $0 < c^2 < 4(f(1) - D_1)$, the eigenvalues $\lambda_{1,2}$ are complex with negative real part. The stationary state is a three-dimensional saddle point, its reduction to the stable manifold M_s a stable focus. In case $c^2 > 4(f(1) - D_1)$, $\lambda_{1,2}$ are negative real numbers, the equilibrium point is again a saddle. This time, S reduces to a stable node on M_s. □

7.4.2 The non-trivial stationary state

Proposition 7.4.3 (Non-trivial equilibrium.) *The non-trivial equilibrium E is a saddle point with a two-dimensional unstable manifold.*

Proof. At the non-trivial equilibrium point $E = (\bar{s}, \bar{u}, 0)$, the term $f(s) - D_1$ in (7.9) vanishes and the characteristic polynomial becomes

$$\begin{aligned}
\chi_E(\lambda) = & \lambda^3 + \\
& + \lambda^2 \left[c - (\bar{u}f'(\bar{s}) + D_0)/c \right] + \\
& + \lambda \left[-\bar{u}f'(\bar{s}) - D_0 \right] + \\
& + \bar{u}D_1 f'(\bar{s})/c.
\end{aligned} \qquad (7.11)$$

Clearly, χ_E always has one negative real zero, since for $\lambda = 0$, $\chi_E = \bar{u}D_1 f'(\bar{s})/c$ is strictly positive. As for the other two eigenvalues, we can at least determine the sign of their real part:

Lemma 7.4.4 (Roots of the characteristic polynomial.) *Aside from the negative real zero, χ_E has two roots in the positive complex half-plane.*
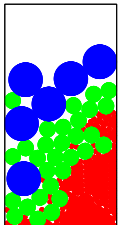
Proof. In order to prove lemma 7.4.4, we use the Routh-Hurwitz theorem (see for example [Gantmacher59], theorem 2, p. 213). Writing the characteristic polynomial as $\chi_E = a_0\lambda^3 + b_0\lambda^2 + a_1\lambda + b_1$ with coefficients

$$a_0 = 1,$$
$$b_0 = c - (\bar{u}f'(\bar{s}) + D_0)/c,$$
$$a_1 = -\bar{u}f'(\bar{s}) - D_0,$$
$$b_1 = \bar{u}D_1 f'(\bar{s})/c,$$

the *Routh scheme* is

$$a_0 = 1 \qquad\qquad\qquad a_1 = -\bar{u}f'(\bar{s}) - D_0$$
$$b_0 = c - \frac{\bar{u}f'(\bar{s}) + D_0}{c} \qquad b_1 = \frac{\bar{u}D_1 f'(\bar{s})}{c}$$
$$c_0 = -\bar{u}f'(\bar{s}) - D_0 -$$
$$\qquad - \frac{\bar{u}D_1 f'(\bar{s})}{c^2 - \bar{u}f'(\bar{s}) - D_0}$$
$$d_0 = \frac{\bar{u}D_1 f'(\bar{s})}{c}.$$

According to Routh's theorem, the number of zeros of χ_E lying in the positive complex half-plane equals the number of sign changes in the sequence (a_0, b_0, c_0, d_0). Clearly, a_0 and d_0 are both strictly positive under the hypotheses in section 7.2. Furthermore, straightforward calculation yields that $c_0 < 0$ whenever $b_0 > 0$. If $b_0 < 0$, then c_0 can be both positive or negative. In any case, the above sequence always has exactly two sign changes. This proves lemma 7.4.4 and hence proposition 7.4.3. $\square$. $\square$.

We conclude this section with a remark on possible wave speeds. According to the so-called *linear conjecture* (see conjecture 7.5.4 in section 7.5, as well as [Weinberger82], [Lewis02.1] or [Lewis02.2]), the minimal feasible wave speed for system (7.5) is

$$c^* = 2\sqrt{f(\zeta) - D_1},\tag{7.12}$$

where ζ is the concentration of the substrate at the (unstable) trivial equilibrium, $\zeta = 1$. Relation (7.12) is plausible if we recall the situation: A traveling wave of high consumer concentration moves into an area of maximal substrate concentration $s = 1$ (see figure 7.4). As in the example at the end of section 7.4, we imagine a plant species s being consumed by an animal u. The animal is relatively mobile, hence its diffusion rate is positive, while the plant species is immobile. The higher the reproduction rate f of u, the faster the animal can feed through the plant population. At the same time, a high mortality D_1 reduces the wave speed, which drops to zero for $f(1) = D_1$.
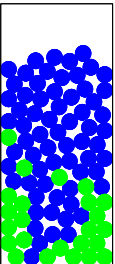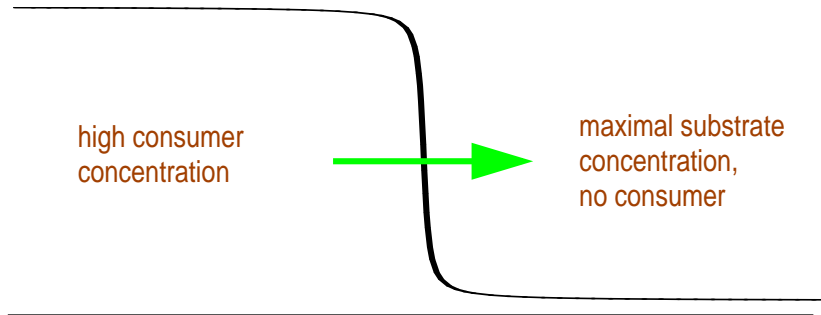
Figure 7.4: Illustration of a traveling wave feeding through the substrate, moving into the area of maximal substrate concentration.

7.5 The epidemic case

In the so-called *epidemic case* the substrate solution is consumed in the chemostat chamber without being reproduced. At the same time, the nutrient input is zero, and species u can feed only on the amount of substrate initially inserted into the vessel. We put $D_0 = 0$, thus reducing the chemostat system (7.1) to

$$\dot{s} = -uf(s),$$
$$\dot{u} = u(f(s) - D_1). \tag{7.13}$$

If we choose $f(s) = s$, (7.13) is just the well-known *Kermack-McKendrick* model describing the spread of epidemic diseases. For the original work see [Kermack27], an overview on variations of the model is given in [Hethcote94]. The stationary points of (7.13) are all the points on the s-axis, $(s, u) = \xi(1, 0)$ for $\xi \in \mathbb{R}$. Furthermore, the trajectories can be calculated explicitly. The two equations (7.13) yield

$$\frac{du}{ds} = \frac{D_1}{f(s)} - 1. \tag{7.14}$$

In order to integrate (7.14), we use a new function G, defined by

$$G(s) = \int_{s_0}^{s} \frac{1}{f(\tau)} d\tau. \tag{7.15}$$

Then, the solution curves of (7.13) are given by

$$u(s) = D_1 G(s) - s + s_0 + u_0,$$

where (s_0, u_0) is the initial value. If we choose f to be the identity, $f(s) = s$, then $G(s) = \ln s - \ln s_0$, and hence, the equation for the invariant of motion becomes

$$u(s) = D_1(\ln s - \ln s_0) - s + s_0 + u_0. \tag{7.16}$$
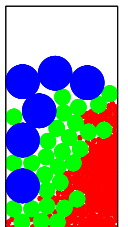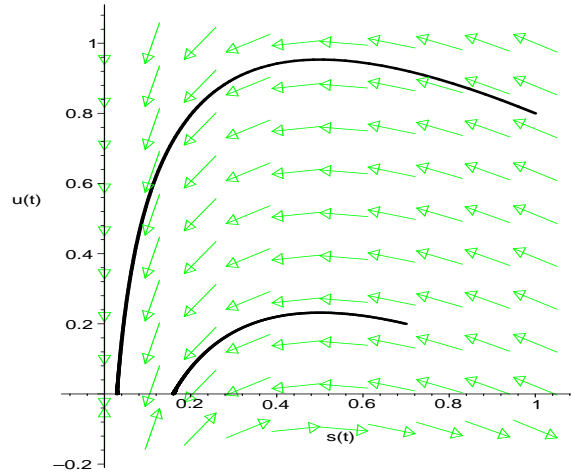
Figure 7.5: Solutions of the trivial chemostat in the epidemic case, system (7.13), for initial values $s(0) = 0.7$, $u(0) = 0.2$ and $s(0) = 1$, $u(0) = 0.8$. The value of the parameter is $D_1 = 0.5$, the uptake function f is given by $f(s) = s$. Here, the stability of the stationary states $(s, u) = \xi(1, 0)$ changes at $\xi = 0.5$.

An example of (7.16) is represented in figure 7.5. As the trajectories show, the stationary states change their local stability as ξ varies. Besides the trivial eigenvalue $\lambda_0 = 0$ we have a second eigenvalue λ_1, which changes its sign depending on whether $f(\xi) > D_1$ or $f(\xi) < D_1$. If we suppose $D_0 = 0$, the partial differential equation (7.5) describing the propagation of the concentrations in space becomes

$$\begin{aligned} s_t &= -uf(s), \\ u_t &= u(f(s) - D_1) + u_{xx}. \end{aligned} \tag{7.17}$$

As the simulation in figure 7.6 suggests, it makes sense to look for traveling wave solutions of system (7.17) as well. Using the traveling wave approach as in section 7.4, we end up with the system

$$\begin{aligned} \dot{s} &= uf(s)/c, \\ \dot{u} &= v, \\ \dot{v} &= -cv - u(f(s) - D_1). \end{aligned} \tag{7.18}$$

In order to integrate system (7.18), we again use the function G defined in (7.15). As we will see in the remainder of this section, the dynamics of system (7.18) is relatively simple, even for general uptake functions f.

Proposition 7.5.1 (Invariant of motion.) *System (7.18) has an invariant of motion M_κ, given by the zero set of*

$$V_\kappa = v - c(D_1 G(s) - s - u) - \kappa,$$
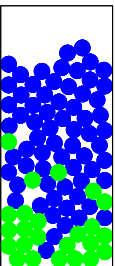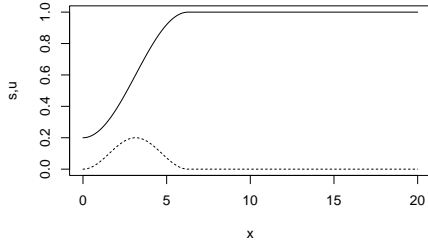
(a) The initial distribution shows a locally concentrated consumer u.
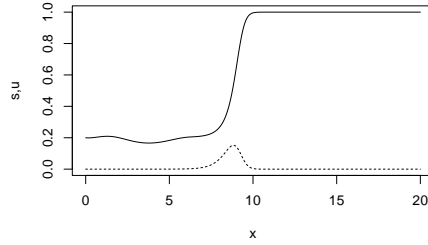
(b) The solution at $t = 30000 \cdot 10^{-3}$.
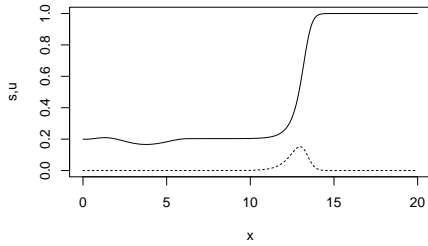
(c) The solution at $t = 60000 \cdot 10^{-3}$.
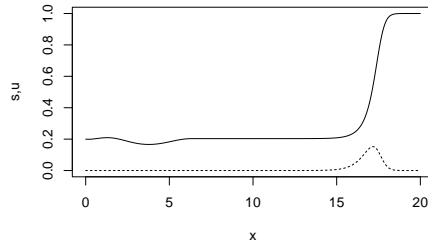
(d) The solution at $t = 90000 \cdot 10^{-3}$.

Figure 7.6: Solution of system (7.17) for $D_1 = 0.5$, $\delta_u = 0.01$ and $f(s) = s$. The solid line represents the substrate concentration s, the dotted line is the consumer concentration u. We find again a traveling wave moving in positive direction.

where κ is determined by the initial conditions, $\kappa = c(s_0 + u_0) + v_0$. In particular, for the initial value $(s_0, u_0, v_0) = (1, 0, 0)$, the parameter κ equals c and the invariant manifold $M_\kappa = M_c$ is given by

$$v = c(D_1 G(s) - s - u + 1).$$

Proof. The third equation in (7.18) yields $u = c\dot{G}(s)$, which, in combination with the first two equations, gives

$$\ddot{u} = -c\dot{u} - c\dot{G}(s)[f(s) - D_1]$$
$$= c[D_1 \dot{G}(s) - \dot{s} - \dot{u}].$$
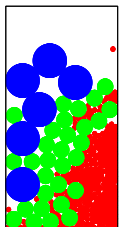
After integration,

$$\dot{u} = v_0 + c[D_1 G(s) - s - u] - c[D_1 G(s_0) - s_0 - u_0],$$

i.e. for $(s_0, u_0, v_0) = (1, 0, 0)$, system (7.18) is equivalent to

$$\begin{aligned} \dot{s} &= uf(s)/c, \\ \dot{u} &= c[D_1 G(s) - s - u + 1]. \end{aligned} \tag{7.19}$$

This proves proposition 7.5.1. □.

Due to proposition 7.5.1, the dynamics of the original system (7.18) is now completely described by

$$\begin{aligned} \dot{s} &= uf(s)/C, \\ \dot{u} &= c(D_1 G(s) - s - u) + \kappa. \end{aligned} \tag{7.20}$$

In particular, we can classify the stationary states as follows.

Proposition 7.5.2 (Classification of stationary states.) *The stationary states of system (7.20) are all the points on the s-axis, $(\bar{s}, \bar{u}) = \gamma(1, 0)$ for $\gamma \in \mathbb{R}$. The stability of these points depends on the constants c and D_1, as well as on the function f. We distinguish three cases.*
(a) If $f(\gamma) = c^2/4 + D_1$, then both $\lambda_{1,2}$ are negative reals. The stationary state is a stable node.
(b) If $f(\gamma) > c^2/4 + D_1$, then $\lambda_{1,2}$ are complex with negative real part. Hence, $(\bar{s}, \bar{u}, \bar{v})$ is a stable focus.
(c) If $f(\gamma) < c^2/4 + D_1$, there are three possibilities.
(c1) For $f(\gamma) = D_1$ we get $\lambda_1 = -c < 0$, $\lambda_2 = 0$, and we have a degenerate stable node.
(c2) For $f(\gamma) < D_1$, λ_1 is again negative, but λ_2 is positive, i.e. $(\bar{s}, \bar{u}, \bar{v})$ is a saddle.
(c3) Finally, if $D_1 < f(\gamma) < c^2/4 + D_1$, then both $\lambda_{1,2} < 0$, and the equilibrium is again a stable node.

Proof. At each point $\gamma(1, 0)$ on the axis of stationary points, the Jacobian takes the form

$$\begin{pmatrix} 0 & f(\gamma)/c \\ c(D_1/f(\gamma) - 1) & -c \end{pmatrix}, \tag{7.21}$$

and the eigenvalues are $\lambda_{1,2} = -c/2 \pm \sqrt{c^2/4 + D_1 - f(\gamma)}$. Hence, the proposition follows directly. □.

The preceding observations are schematically resumed in figure 7.7.

We have now all the tools in hand to completely describe traveling wave fronts in the epidemic case, i.e. solutions of the three-dimensional system (7.18) which stay
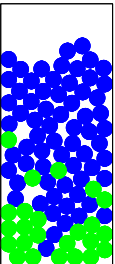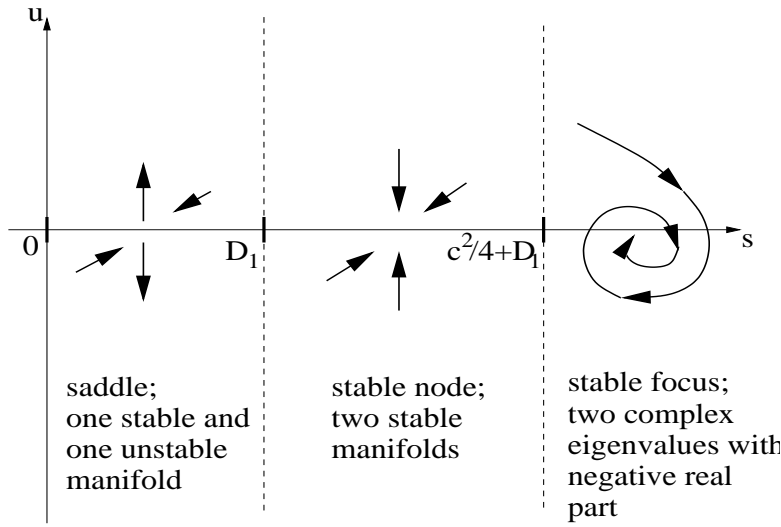
Figure 7.7: Stability and classification of the stationary points on the s-axis of system (7.18).

non-negative for all times. First of all, note that the initial condition (s_0, u_0, v_0) uniquely determines the parameter κ and thus the invariant manifold V_κ, in which the trajectory is embedded. Hence, for given (s_0, u_0, v_0), the feasible stationary states of (7.18) are given by the intersections of V_κ with the s-axis, i.e. by the solutions of

$$\kappa + c\,(D_1 G(s) - s) = 0. \tag{7.22}$$

Due to the monotonicity of f, the function G is concave. Hence, (7.22) can have at most two solutions. Clearly, if κ is small enough such that V_κ does not intersect the s-axis, then (7.20) has no stationary states and u becomes negative at some time for any initial value on the manifold. The stationary states of (7.18), which yield traveling wave fronts, are those solutions of (7.22), which are locally stable nodes, i.e. for which the parameters satisfy conditions (a) or (c3) in proposition 7.5.2. If $\kappa = \kappa^*$ is chosen in a way that (7.22) has a unique solution s^*, then the latter is given by $f(s^*) = D_1$ (differentiation of (7.22)). Finally, if (7.22) has two distinct solutions, the one with the smaller value of s is always the unstable equilibrium, while the other one is locally stable.

For $\kappa \geq \kappa^*$, we can give a lower bound for the wave speed c.

Proposition 7.5.3 (Wave speed estimate.) *The minimal feasible wave speed for system (7.17) is given by*

$$c^* = 2\sqrt{f(\gamma) - D_1}.$$
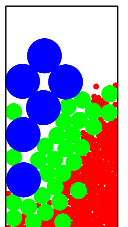
Proof. Consider case (a) in proposition 7.5.2. For given f and D_1 and for a given set of initial conditions (s_0, u_0, v_0), the point $(\gamma, 0, 0)$ is a stable node if and only if $f(\gamma) \geq D_1$ and $c^2/4 = f(\gamma) - D_1$. In case (c3), we need $f(\gamma) \geq D_1$ and $c^2/4 > f(\gamma) - D_1$. In any case, the minimal feasible wave speed is c^*. $\square$

The statement of proposition 7.5.3 is consistent with the linear conjecture:

Conjecture 7.5.4 (Linear conjecture.) *Consider a reaction-diffusion equation of the form*

$$u_t = Du_{xx} + g(u) \tag{7.23}$$

for a sufficiently smooth function g. If $g(u) \leq g'(0)u$, then the minimal speed of traveling wave fronts of (7.23) is given by

$$c_0 = 2\sqrt{Dg'(0)}.$$

In [Bosch90], [Lewis02.1], [Lewis02.2] or [Weinberger82], more general conditions are given for the minimal wave speeds to be attained. In the case of system (7.17), the reaction term is the linear function

$$g_s(u) = u(f(s) - D_1).$$

Hence, $c_0 = c^*$.

7.6   Two examples of the invariant manifold

In this section, we illustrate the reduction of system (7.18) to the invariant manifold V_κ by means of two examples. In the first system, the traveling waves discussed in section 7.5 do not occur naturally, i.e. the traveling wave approach yields wave fronts exhibiting negative concentrations of the species u. In a second example, we choose the set of parameters, and especially the wave speed c, appropriately in order to create such a steady wave.

Let $D_1 = 0.5$, and choose f to be the identity, $f(s) = s$. If we take the wave speed to be equal to one, and if the parameter κ is chosen appropriately, then the invariant manifold V_1 is given by

$$v = \frac{1}{2}\ln s + 1 - s - u. \tag{7.24}$$

The graph of (7.24) is represented in figure 7.8. Two of the stationary states lie on the manifold V_1, namely $S_1 = (1, 0, 0)$ and $S_2 = (\chi, 0, 0)$, where χ is approximately equal to 0.2. Consider the reduced system (7.19) and calculate the derivatives. The general Jacobian is

$$J_{epi} = \begin{pmatrix} u & s \\ \frac{1}{2s} - 1 & -1 \end{pmatrix}.$$
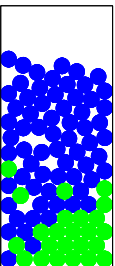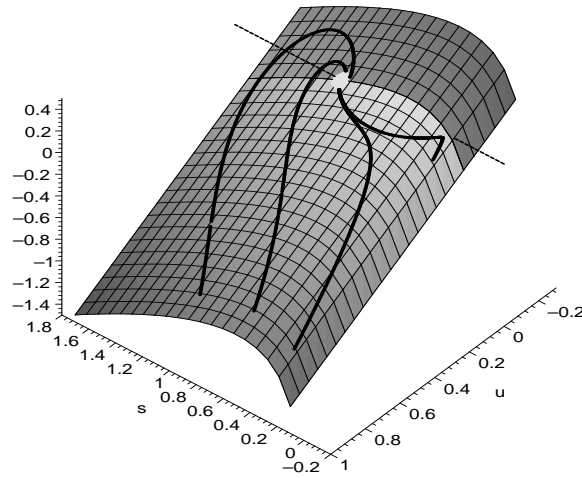
Figure 7.8: The invariant manifold V_c for $c = 1$. The trajectories starting in V_1 lie entirely in the manifold. The parameter D_1 is equal to 0.5, the function f is the identity, $f(s) = s$. The s-axis (dotted line) intersects V_1 twice, once in the stable focus $(s, u, v) = (1, 0, 0)$ (light grey patch) and a second time in an unstable equilibrium at $s \approx 0.2$. The dark shaded part of V_1 corresponds to negative concentrations of u.

Hence, the eigenvalues of the projected system are $\lambda^1_{1,2} = -1/2 \pm i/2$ at S_1 and $\lambda^\chi_{1,2} = -1/2 \pm \sqrt{1 + 4\chi(1/(2\chi) - 1)}$ at S_2. Consequently, S_1 is a stable focus (case (b) in proposition 7.5.2), while S_2 is a saddle (case (c2)). This example is not adequate to describe the propagation of traveling waves of our original system (7.17), since, due to the fact that the stable stationary state is a focus, all solutions become negative eventually.

In our second example, we choose the set of parameters in order to design a system exhibiting feasible traveling waves. Let $D_1 = 1/10$, $c = 1$ and $f(s) = s$. For $\kappa = 1/5 + \ln(5)/10$, the invariant manifold V_κ is given by

$$v = \left(\frac{1}{10}\ln s - s - u \right) + \frac{1}{5} - \frac{1}{10}\ln 5. \tag{7.25}$$

The graph of (7.25) intersects the s-axis of stationary states again in two points. One of them, at $s = 1/5$, is a stable node. As represented in figure 7.9, some trajectories approach this equilibrium coming from positive values of u. Hence, the corresponding traveling wave has positive concentrations everywhere.

7.7 Generalization to multi-consumer models

The discussion of traveling wave fronts appearing as solutions of chemostatic models with diffusion can be generalized to several consumers. For illustration, we
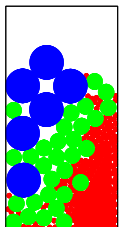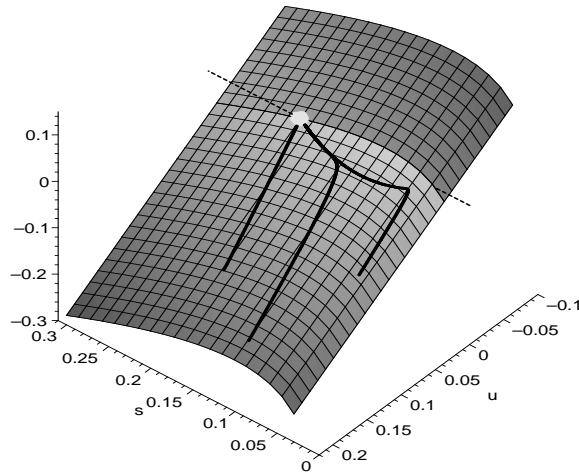
Figure 7.9: For $D_1 = 0.1$, $c = 1$ and $f(s) = s$, the invariant manifold V_κ with $\kappa = 0.2 + \ln(5)/10$ intersects the s-axis again twice. This time, one of these stationary states is a stable node (light grey patch), located at $s = 0.2$. The other one is unstable.

reconsider a system of two species u_1 and u_2, feeding on a single resource s, as the one analyzed in section 6.2 of chapter 6. For clarity reasons we restrict to constant washout rates $D_i(x_i) \equiv D_i = const$ for $i = 1, 2$. Thus, consider the model

$$\begin{aligned}
\dot{s} &= D_0(1 - s) - u_1 f_1(s) - u_2 f_2(s), \\
\dot{u}_1 &= u_1(f_1(s) - D_1), \\
\dot{u}_2 &= u_2(f_2(s) - D_2).
\end{aligned} \qquad (7.26)$$

As in chapter 6, we impose that the nutrient uptake rates f_i are strictly monotonously increasing with $f_i(0) = 0$. Under these assumptions, we saw that system (7.26) can have four different stationary states. The substrate-only equilibrium $S = (1, 0, 0)$ always exist, while the two one-consumer stationary points E_1 and E_2 appear only if $f_1(1) > D_1$ and $f_2(1) > D_2$ respectively. Necessary and sufficient conditions for the existence of a coexistence point are discussed in section 6.3 of chapter 6. Let us assume that the parameters in system (7.26) are chosen in a way that the coexistence state E exists. Since E is stable, we can distinguish two kinds of typical trajectories, the heteroclinic orbit connecting S to E as well as the two heteroclinic orbits going from the one-consumer states to the coexistence point (see figure 7.10). As in section 7.2, we consider a model incorporating diffusion of the species, i.e. we implicitly allow the concentrations to vary in space and time. Thus, consider

$$\begin{aligned}
s_t &= D_0(1 - s) - u_1 f_1(s) - u_2 f_2(s), \\
u_{1t} &= u_1(f_1(s) - D_1) + \delta_1 u_{1xx}, \\
u_{2t} &= u_2(f_2(s) - D_2) + \delta_2 u_{2xx}.
\end{aligned} \qquad (7.27)$$
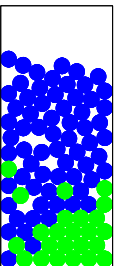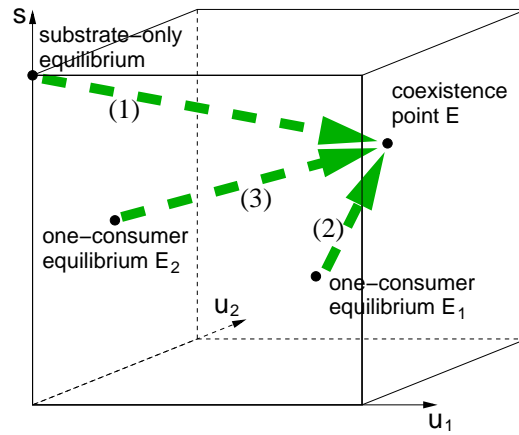
Figure 7.10: Simplified illustration of the heteroclinic orbits of system (7.26) connecting the substrate-only state S (arrow (1)) as well as the one-consumer equilibria E_1 and E_2 ((2) and (3)) to the coexistence point E.

For each one of the heteroclinic orbits described above, we expect to find a traveling wave solution of system (7.27). Figure 7.11 illustrates a wave front connecting S to E.
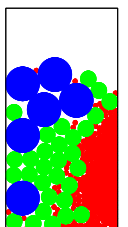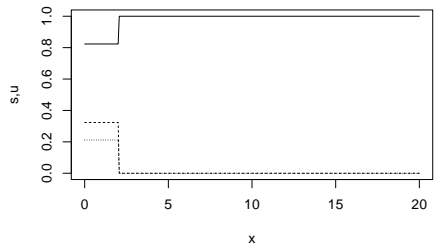
(a) The initial distribution is a step function.
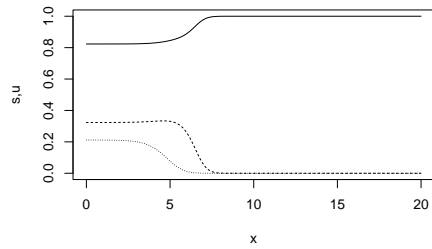
(b) The solution at $t = 28$.
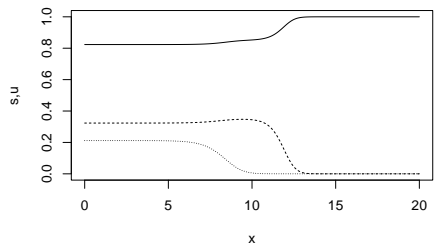
(c) $t = 56$.
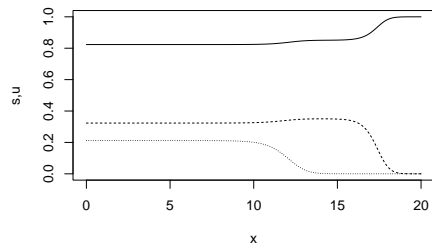
(d) $t = 84$.

Figure 7.11: Solution of the three-dimensional system (7.27) for $D_0 = 2$, $f_1(s) = s$, $f_2(s) = s/2$, $D_1(x_1) = x_1 + 0.5$, $D_2(x_2) = x_2 + 0.2$ and $\delta_1 = \delta_2 = 0.01$. The solid line represents the substrate concentration s, while the dashed and dotted lines are the consumer concentrations u_1 and u_2, respectively. The sequence of pictures illustrates a traveling wave moving to the right, connecting the trivial substrate-only equilibrium $S = (1, 0, 0)$ (values on the right boundary) to the coexistence point E (left boundary).
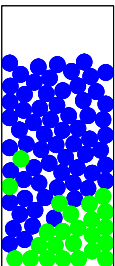
Chapter 8

Particle simulations

Summary. In this section, we develop a model to simulate the microscopic behavior of multi-particle systems. On the basis of partly elastic inter-particle collisions, repeatedly introduced kinetic energy and gravitation, the simulations show the frequently discussed phenomena of shaken or stirred granular material, such as sedimentation, compaction and particle segregation due to differences in size and specific weight. The present model does not account for rotation of the individual particles and deals with perfectly spherical grains only.

8.1 Introduction

The convection-diffusion models developed mainly in chapters 2 and 3 describe sedimentation and segregation effects of granular material under the influence of gravitation. The aim of the present chapter is to get a first verification of these theoretical results with the help of a model predicting the change of position of every individual particle. Even though there are still many restrictions and simplifications, imposed mainly by the limited computer resources, we tried to construct complex processes for the mixing of granular material as accurately as possible.

Numerous authors have devoted themselves to the study of shaken or vibrated granular mixtures. In [Luding01], an equation of state for two-dimensional hard sphere systems is set up in order to compare the theoretical results with computer simulations and to experiments conducted in [Clément91]. Computer simulations are used in [Jullien92] and [Rosato87] in order to study segregation in bi-disperse granular mixtures with particles differing in size, while [Duran93] presents results of segregation experiments in two- and three-dimensional vessels. Finally, [Pöschel95] investigates the development of convection cells within a vibrated granular mixture.

In section 8.2, we describe the mechanism used to model collisions between parti-

cles, the only means of interaction in our model (rolling and gliding effects are not accounted for). In section 8.3, we explain in short the way we process the data obtained in form of particle and density diagrams. We also track the evolution of the total potential energy during the segregation procedure, which gives us more insight into the microscopic process of particle interaction. Finally, the plots and diagrams are collected in section 8.4.
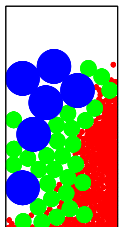
8.2   Modeling collisions of particles

The present simulation is based on the numerical solution of the Newtonian equations of motion of spherical particles in a container with impermeable walls and solid lid and bottom. A certain number N of such grains are introduced into the vessel at the same time. Instead of choosing their initial positions at random, we form layers in an order different from that of the anticipated outcome. For example, when shaking a mixture of small and large grains of the same specific weight, we start with a distribution in which the large particles are at the bottom, thus establishing the *worst possible* initial situation. That way, the effect of the segregation becomes more obvious. Due to the gravitational force acting on each one of the grains, they accelerate and start to fall down. In the process of falling, particles can collide with each other. In order to keep calculations simple, we restrict to two-particle collisions and neglect the effect of several grains touching at the same time. In an experiment, the actual collisions are of course partly inelastic. But instead of modeling the deformation of the two collision partners itself, we first calculate the new directions of the trajectories after the impact as if the collisions were fully elastic and then add a *friction parameter R*, which controls the loss of kinetic energy (see figure 8.1).

The major drawback of our model is the lack of rotational movement of the particles. As far as the particle collisions are concerned, this means that the grains are perfectly smooth. The exchange of energy due to an impact is performed only at the level of translational kinetic energy. Evidently, waiving the implications of particle rotation saves a lot of computing time and enables us to simulate systems of the order of $N = 10^4$ particles. The major disadvantage is the fact that two grains lying on top of each other cannot roll. They can only *glide*, a process which takes more time and hence slows down the sedimentation and compaction (see figure 8.2). In order to eliminate pattern formation resulting from a fixed order of handling the particles, we use a random sweep method to choose and move grains at each discrete time step. The various effects of different sweep methods have been studied intensively, among others in the context of cellular automata (see for example [Schönfisch99]).

While the N particles fall towards the bottom of the vessel and collide with each other, they gradually lose energy and settle to the ground. This sedimentation
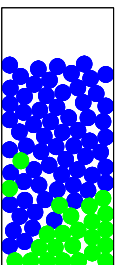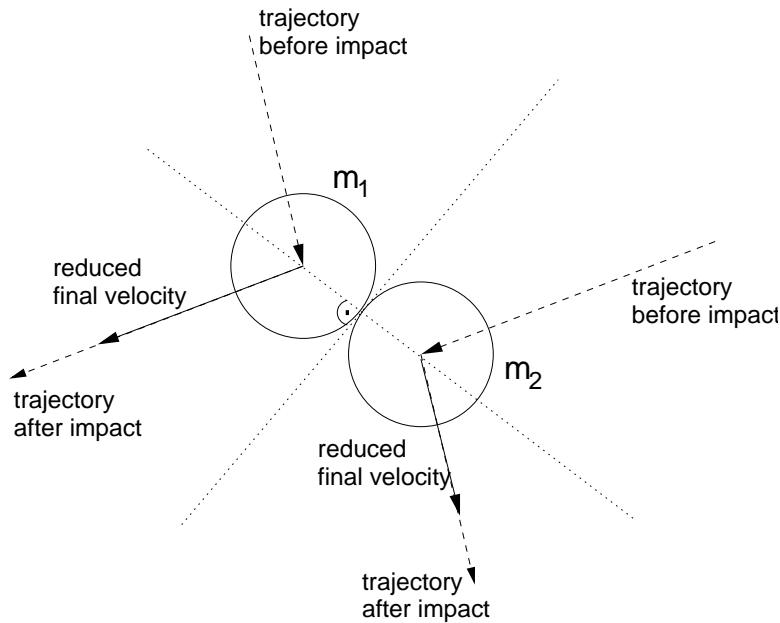
Figure 8.1: Schematic depiction of a collision between two spherical particles. Given the angles of incidence, the angles under which the balls leave the collision locus are calculated as if the collision were fully elastic. Afterwards, the final velocity is reduced according to the actual elasticity coefficient.

is accompanied by the compaction of the granular material. While the grains still have a certain velocity, gaps appear between them and smaller grains fall into these gaps. Once all particles have settled and their velocity has come down to a minimum, the whole container is shaken. In regular time intervals, we push each grain towards the top by adding a fixed velocity. Now, the process of sedimentation and compaction starts again.

Notice that, instead of pushing the grains upward at fixed time intervals, one could also constantly add kinetic energy to the system. Thus, the particles would never come to a complete rest and a certain minimal *temperature* of the *granular gas* would be maintained. This method, however, does not model the experiment we have in mind. Instead, it advances the compaction of the material and is less suitable for modeling segregation due to the Brazil nut effect.

8.3   Density diagrams and energy plots

In addition to studying the individual spherical grains and their positions in the vessel, we generate a *particle density plot* right before every shake, i.e. when the granular material has had enough time to settle completely to the ground. These

(a) If particles can only glide off of each other, the sedimentation process takes more time.

(b) Angular momentum and the possibility of the grains to roll off of each other would accelerate the sedimentation process.
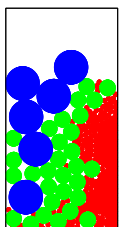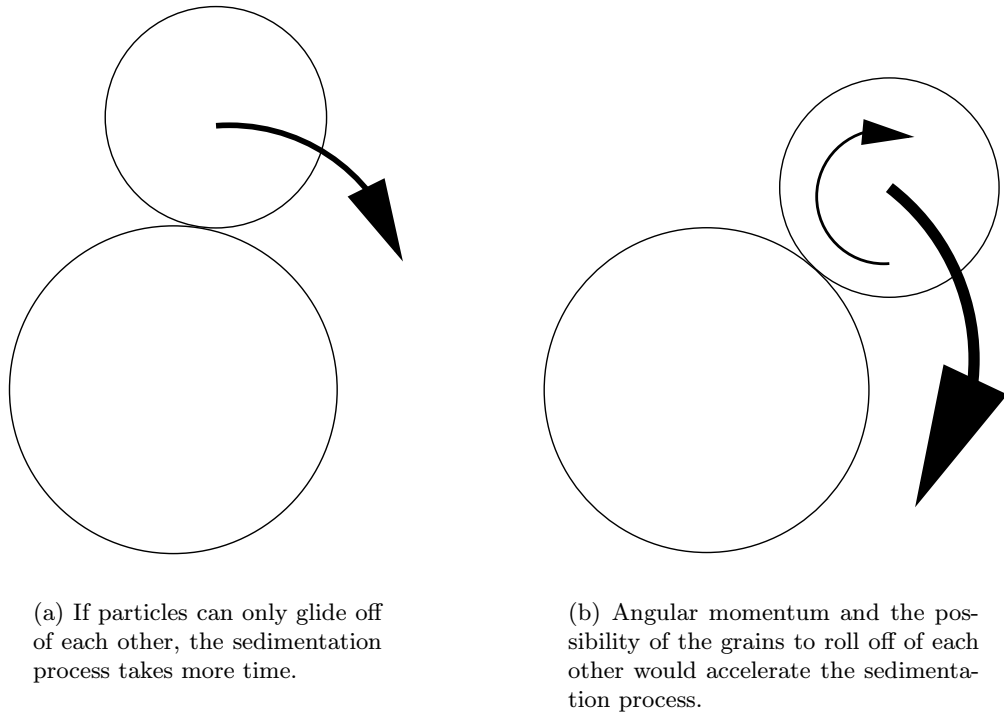
Figure 8.2: Particles gliding and rolling off of each other.

plots show the volume occupied by grains of the various types as a function of the height in the container, thereby giving information about the degree of segregation in the mixture. In order to achieve this task, we divide the vessel into 50 layers, each with a thickness equal to $l/50$, and count the number of grains in each such layer. The parameter l designates the container height.

Finally, an interesting issue in the context of segregation of granular material is the change in total potential energy E_{pot}. As we have already discussed in chapter 2, the shaking process, as it is modeled in the present simulations, does not necessarily reduce E_{pot}. In fact, the Brazil nut effect drives large particles to the top, even if their specific weight is slightly larger than the one of the smaller grains. Thereby, the system reaches locally stable (due to the friction of the grains) but globally unstable energy states (in the sense that the heavy large grains would move back down if only enough space were provided between the small particles). The driving force is the shaking, which repeatedly introduces energy. In the absence of the shaking, the only observable effects are the sedimentation and the compaction of the material, both of which tend to reduce potential energy.
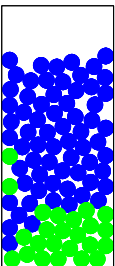
8.4 Simulations

Aside from the sedimentation of a single grain species, which does not as much depend on the interaction of the individual grains, the simplest scenario is the segregation of a granular material composed of two grain types. Figure 8.3 depicts the subsequent stages in the segregation process. In order to demonstrate the effect in the most obvious way, we chose an initial grain distribution, in which the small grains form the top layer. As the last image of the sequence indicates, the final state exhibits again two distinct layers. Only this time, the large grains are on top. Obviously, this is what we expected. Nevertheless, it is very surprising to observe the way this final situation attunes. Instead of seeping through the layer of large balls, the small particles move down as a block on one side of the vessel. It is not completely understood, why the segregation takes place in such an unsymmetric manner, but the effect resembles the circular convective flow which we observed in our experiments (see chapter 9) and which also occurs in the *Rayleigh-Bénard* effect in fluid dynamics. Besides the fitfulness of the shaking movement, which seems to influence to a large extent the sedimentation procedure in the experiments, there seem to be other factors causing horizontal inhomogeneity. The boundary of the container, of course, could be one reason.

The energy paradox described in section 8.3 is shown in figure 8.4. Here, we added two large grains to a large number of relatively small particles. While the specific density of the small grains is still equal to one, that of the big ones has been increased by 20 percent. The corresponding evolution of the total potential energy of the system is shown in figure 8.5. As we can see in figure 8.4, the large balls move to the top one after the other in small steps. The corresponding energy jumps are clearly visible.
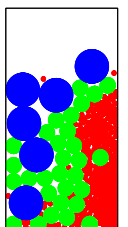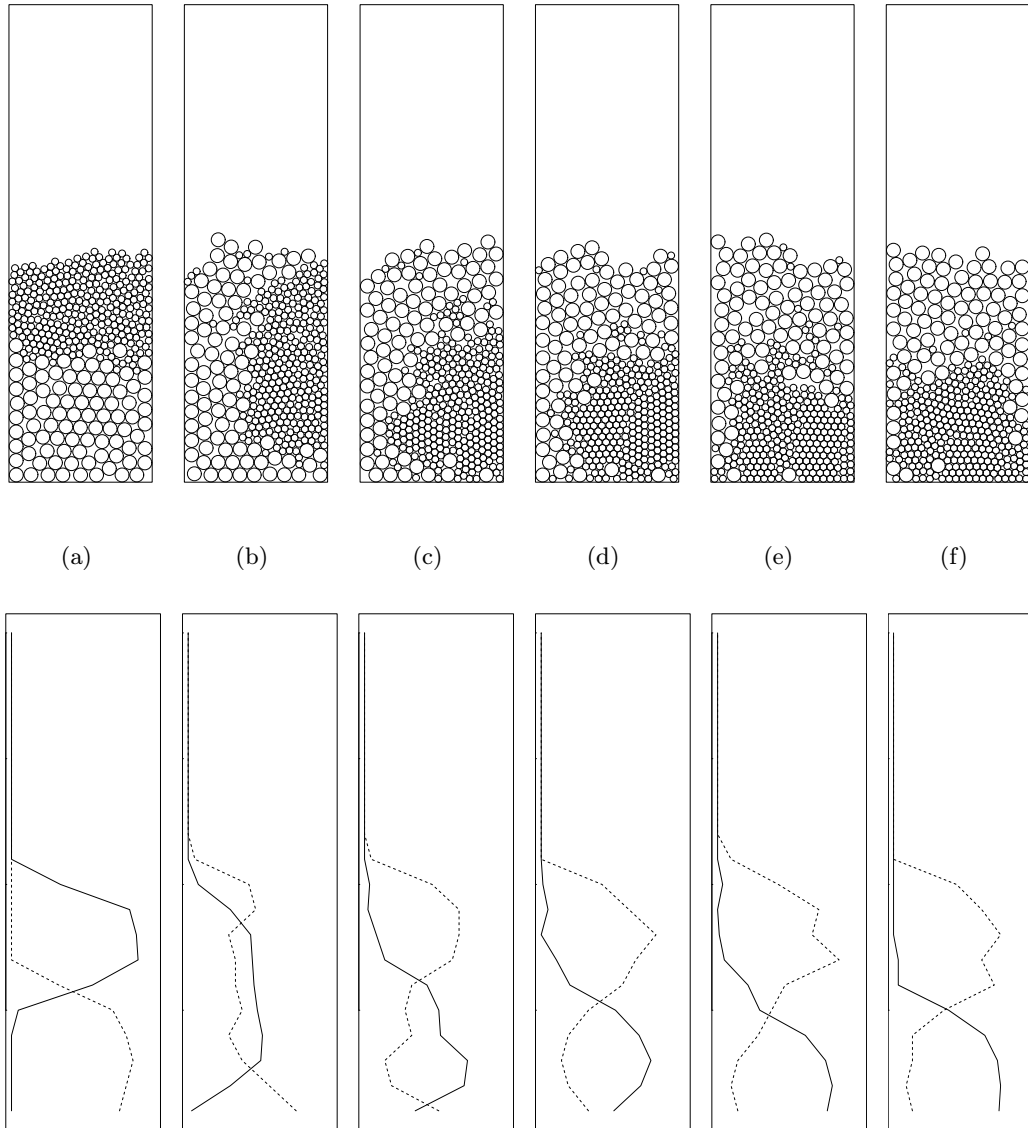
Figure 8.3: Representation of the particle density distribution in the vessel. The top row shows the individual particles in the vessel. The figures in the bottom row give relative particle densities between zero and one (horizontal axis) as a function of the height in the vessel (vertical axis). We observe segregation. The larger particles tend to move up. Particle numbers are $N_1 = 300$, $N_2 = 90$. Both have the same specific weight, $\rho = 1$. We used a friction parameter of $R = 0.01$. (a) Initial distribution. (b) After 2 shakes. (c) After 4 shakes. (d) After 6 shakes. (e) After 8 shakes. (f) After 39 shakes.
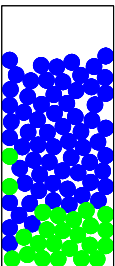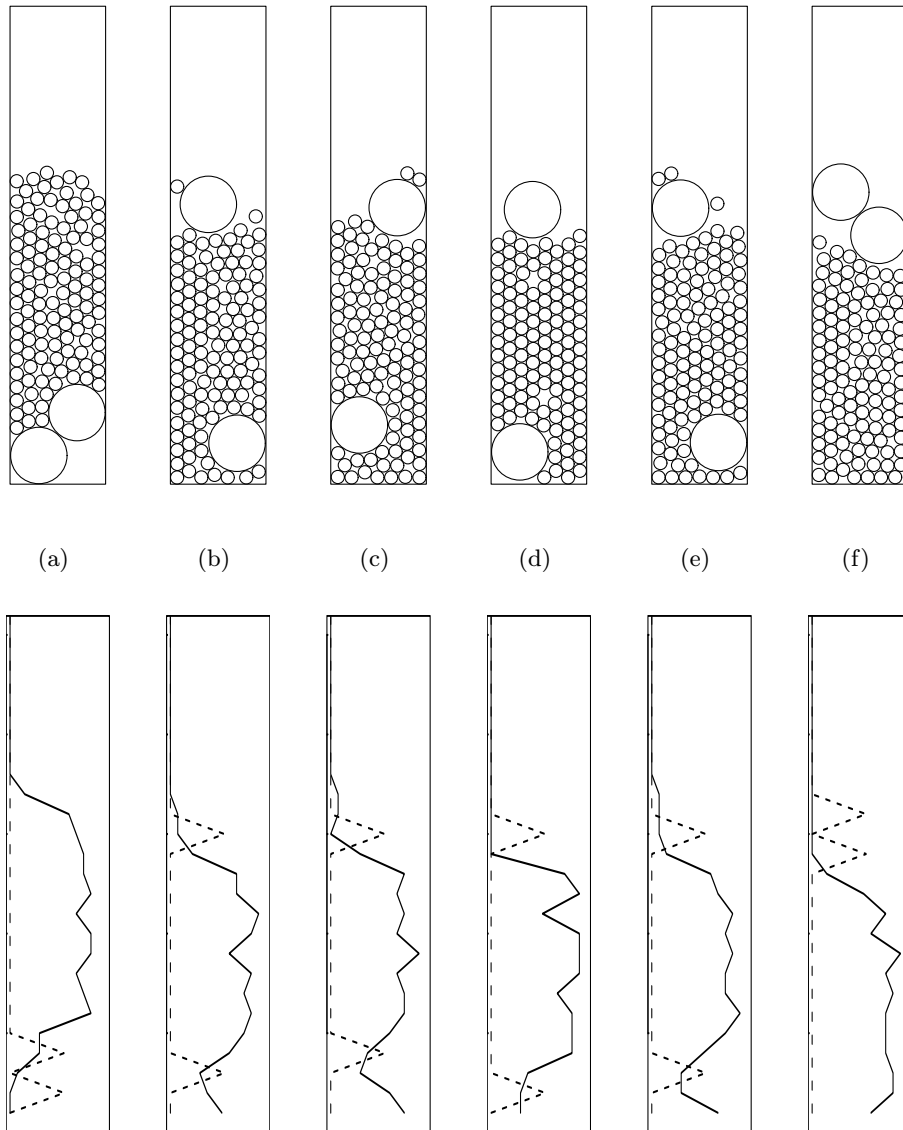
Figure 8.4: Representation of the particle density at each height in the vessel. The top row shows the individual particles in the vessel, the figures in the bottom row give relative particle densities (horizontal axis) as a function of the height (vertical axis). We observe segregation of the granular material. The larger grains tend to move up, the smaller ones move down. Particle numbers are $N_1 = 0$, $N_2 = 120$, $N_3 = 2$. The small grains have specific weight $\rho = 1$, the bigger ones $\rho = 1.2$. Finally, we used a friction parameter of $R = 0.007$. (a) Initial distribution. (b) After 50 shakes. (c) After 100 shakes. (d) After 150 shakes. (e) After 200 shakes. (f) After 386 shakes.
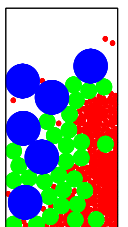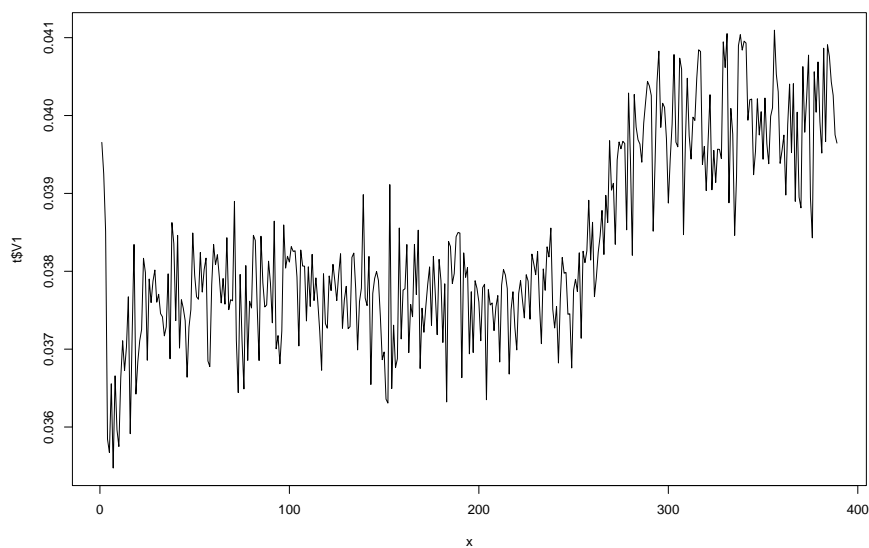
Figure 8.5: The energy plot corresponding to the simulation illustrated in figure 8.4. While the first large ball is driven to the top already after a few shakes, the second one starts to move up only after about 250 joggles. Each time, the total potential energy increases by approximately the same amount.
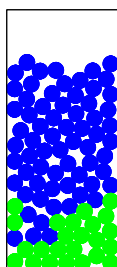
Chapter 9

Segregation experiments

Summary. In chapters 2, 3 and 4, we used different theoretical approaches to modeling segregation effects in shaken or vibrated granular mixtures. While the aim of chapter 8 was to verify the above models via computer simulations, we also conducted simple shaking experiments in order to confirm the theoretical results. The fruit of these runnings are analyzed in the present chapter.

9.1   Introduction

Several authors have studied of shaken or vibrated granular mixtures, and some of the effects giving rise to segregation or mixing of particles have been analyzed. While [Gallas96], [Luding96.2] and [McNamara99] discuss different segregation mechanisms in both two- and three-dimensional systems in general and compare computer simulations to experimental data, [Farkas02] and [Wambaugh02] attach particular importance to the so-called *ratchet-induced* segregation. [Duran93] treats the simple but very instructive case of one large spherical particle surrounded by material composed of very small grains and discusses the segregation procedure on a microscopic level. So-called *arching* and *vault* effects are made responsible for particle fluctuations due to this difference in size. The issue of convection cells appearing in vibrated granular mixtures is treated in [Pöschel95]. Finally, [Barker93] gives a brief overview on segregation approaches and mentions in particular the influence of vibration frequency and amplitude on experimental results. Despite the lively interest, which research in this field has experienced over the past years, some questions remain to date unexplained. Complex phenomena, as for example the appearance of convection cells in vibrated material, the equivalent of the so-called *Rayleigh-Bénard* experiment in fluid dynamics (see [Getling98], [Tritton77]), confront the scientists with unresolved problems. But also the well-known *Brazil nut* effect, which favors segregation due to differences in grain size, has as yet only been explained heuristically.

In the present chapter, we support our segregation theory developed mainly in
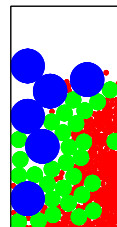
chapter 2 and formalized in chapter 3 by experiments, thus complementing the results obtained by our computer simulations in chapter 8. In section 9.2, we briefly describe the experimental setup. While section 9.3 contains the results concerning bi-disperse granular mixtures, section 9.4 deals with three kinds of species. Finally, the appearance of convection rolls, an effect similar so the Rayleigh-Bénard effect in fluid dynamics, is discussed in section 9.5.

9.2   The experimental setup

As we have mentioned in previous chapters, segregation in mixtures of granular material mainly depends on two properties of the individual particles, namely their size and their specific weight. While a higher material density privileges the downward movement in the container, an increase in size favors the so-called *Brazil nut* effect, driving grains to the top. In order to eliminate denticulation and friction effects, which might favor the one or the other particle species in their tendency to ascend, we attached importance to using grains with nearly spherical shape and smooth surfaces. Thereby, the results can be directly compared to our computer simulations in chapter 8, which are designed for perfect spheres.

We chose seeds of amaranth (*Amaranthus caudatus*), green gram (*Vigna radiata*), small lead balls and balls made of cotton batting with a larger diameter. The physical properties of these four particle types are collected in table 9.1.   At

	Amaranth	Green gram	Lead	Cotton batting
shape	lentil	ellipsoid	spherical	spherical
diameter	1-1.5mm	4mm	4mm	13mm
thickness	0.7-1mm	5-6mm	4mm	13mm
density	$1215\text{kg}/\text{m}^3$	$1310\text{kg}/\text{m}^3$	$10725\text{kg}/\text{m}^3$	$270\text{kg}/\text{m}^3$

Table 9.1: Shapes, sizes and specific densities of the particles used in the shaking experiments.

each case, two or three of these four particle types were filled into a transparent tube with closed bottom. For some experiments, we used a glass container with circular cross section, measuring 35mm in diameter, for others, an acrylic glass cylinder with a diameter of 46mm was used. In order to guarantee the accuracy and reproducibility of the runnings, the shaking movement was induced by a membrane vibrating with a constant frequency.   The vibration amplitude was
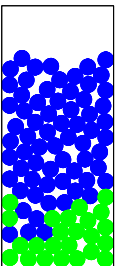
always between 2mm and 3mm, the frequency was adjusted to values between 10Hz and 14Hz, depending on the properties of the mixture and the fill level. We thereby made allowance for the following circumstances: When pushed upwards from an oscillating table, a single bouncing ball needs a certain well-defined time to move up to the peak and back down to the ground. Obviously, this period of time depends on the momentum the ball inherits from the table at each contact (i.e. after all on the oscillating amplitude and frequency of the table) as well as on the air friction and the energy loss of the partly inelastic collision (see [Tufillaro92] for an overview on the subject of the bouncing ball). Granular matter essentially obeys the same rules. Only in this case, the energy loss is much more important due to the large number of collisions during each shaking cycle. When pushed upwards with a certain force, the material has an intrinsic settling time. In our experiments, we adapted the frequency of the oscillating membrane in order to match this settling time. Thereby, we obtained a maximal oscillating amplitude of the grains in the container. During the segregation process, the vibration was stopped at regular intervals in order to record its effect. Photographs show the grain distribution after each shaking period.

9.3 Two interacting particle species

In a first run, we filled lead and cotton batting balls into the acrylic glass cylinder in a way, that the resulting mixture was more or less homogeneous. The vibration was conducted at about 10Hz with an amplitude of 2mm. The resulting sequence of pictures is shown in figure 9.1. Due to the relatively large differences in particle size and specific weight, we clearly expect that the cotton balls move up during the shaking process. This is verified in the experiment.

In a second run, amaranth seeds and green gram were shaken in the glass container at 13Hz with an amplitude of 2.5mm (see figure 9.2). Here, the difference in size is less important than in the previous case, and the specific weight, which is slightly higher for green gram, favors the small particles to move up. Nevertheless, the Brazil nut effect dominates, and we end up with a segregated material with the large grains on top.

The Brazil nut effect became even more obvious, when we studied the segregation properties of a mixture of amaranth with lead balls. Even though the specific weight of lead is about nine times higher than that of amaranth, the latter moved down, while the lead balls rose to the top (see figure 9.3). This illustrates, how important the size difference is in comparison to other particle properties, such as weight, shape or surface quality.
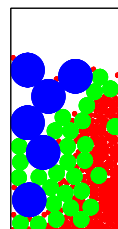
9.4   Three particle species

In the case of three interacting species, our predictions also match with the experimental results. We used a mixture of green gram, amaranth seeds and lead balls. The segregation process is illustrated in the sequence of photographs in figure 9.4. Here, both the Brazil nut effect on the one hand and the simple downward movement of heavy grains on the other hand, are nicely visible. While the small amaranth seeds, initially forming the top layer in the vessel, seep through the second layer of lead balls and gather at the bottom, green gram moves up. Due to its specific density, which is much lower than that of lead, the grains go all the way to the top. In the end, we distinguish again three layers, with the lead balls forming the middle one. In contrast to the situation in the initial distribution in figure 9.4(a), the roles of the small amaranth particles and the green gram seeds are now interchanged.

9.5   Convection rolls

It was interesting to yet another effect observe during the shaking experiments. In one case, a mixture of green gram and small lead balls was vibrated. Both particle types have about the same diameter, and the ellipsoid shape of the green gram seeds is not very pronounced. Thus, also the latter ones can be considered as nearly spherical, and the driving force in the segregation process was merely the difference in specific weight, which is by far higher for the lead balls. Even though we expected a distinct segregation of the material, driving green gram to the top, the result was a different one. Instead of a continuous separation of the two grain types in the vessel, we observed a convectional movement generating periodic fluctuation of the particle concentrations. The result was very similar to that of the classical Rayleigh-Bénard experiment (see [Getling98] or the chapter on convection in horizontal layers in [Tritton77]), in which a fluid heated from below moves up through the center of the so-called *Rayleigh-Bénard cell* and sinks again at its edges. The granular material rose on one side, while it descended on the other (simplified illustration see figure 9.5(a)). Due to the difference in the specific material density, the fluctuations were faster for one grain type than for the other, resulting at the same time in a horizontal segregation of the particle species (see photograph, figure 9.6(a)). It is not clear, what the trigger for this phenomenon is and how the direction of the horizontal segregation is determined. Nevertheless, it seems that the system is very sensitive to the nature of the shaking process itself. Not only the vibration frequency, but to a large extent also the shaking amplitude and direction have proven to influence the final result. Against this background, it seems to be manifest, that the appearance of convection rolls in shaken granular mixtures is due for the most part to a tilt of the container. If the shaking movement is performed at an angle deviating only slightly from the vertical, the rotational convection comes into effect and quickly
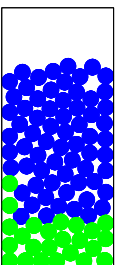
dominates other segregation activity. Moreover, the effect seems to become stronger with diminishing diameter of the container.

In another run, we observed a similar effect. Only this time, the mixture was composed of green gram and amaranth. While the pure Brazil nut effect would have driven the smaller amaranth particles to the bottom of the container, they again performed a circular movement resembling that of the fluid in the Rayleigh-Bénard cell. What was rather surprising was the fact, that only the amaranth particles seem to perform this kind of fluctuation, while the green gram grains only slightly changed the state of their distribution (see figure 9.6(b)). Hence, the mixture formed an amaranth source in its center. The grains ascending to the surface at this point were driven towards the edges of the vessel, where they descended again (illustration see figure 9.5(b)). The elementary nature of this phenomenon is very complicated and has not yet been fully understood. At this point, we will content ourselves with a heuristic interpretation helping understand the observations. One of the driving forces in the formation of sources in granular mixtures seems to be the so-called *ratchet effect* (see figure 9.7 for illustration). On the microscopic level, the surfaces of the individual grains in the mixture show a more or less pronounced throatiness. In some cases, especially if this microscopic shape is asymmetric and distinguishes one direction (as it is the case for the saw-tooth shaped surface of the grains in figure 9.7), this leads to an obstruction of the particle movement. The resulting motion becomes biased, driving different grain types in opposite directions. This ratchet effect seems to be at least one determining factor in the formation of particle sources. While a certain species is driven up through the center of the column (the amaranth seeds in the above example of a mixture with green gram), the material seeks regions where it can redescend, preferentially close to the boundary, where the gaps between the particles are usually larger. Here, in addition, the ratchet effect is usually less pronounced, since the surface of the container (glass or acrylic glass) is very smooth. This also explains the fact that particle sources are observed more frequently in narrow cylinders than in large vessels.
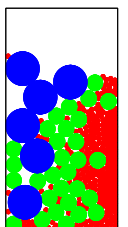
(a) Initial distribution.   (b) 100 cycles.   (c) 300 cycles.

(d) 1800 cycles.   (e) 3000 cycles.   (f) 5100 cycles.

Figure 9.1: A mixture of lead and cotton batting balls is shaken with an amplitude of approximately 2mm. As we expect, the cotton balls move to the top one by one, until the material is almost completely segregated.

(a) Initial distribution.   (b) 130 cycles.   (c) 260 cycles.

(d) 390 cycles.   (e) 520 cycles.   (f) 650 cycles.
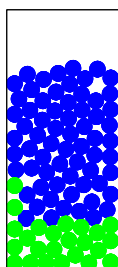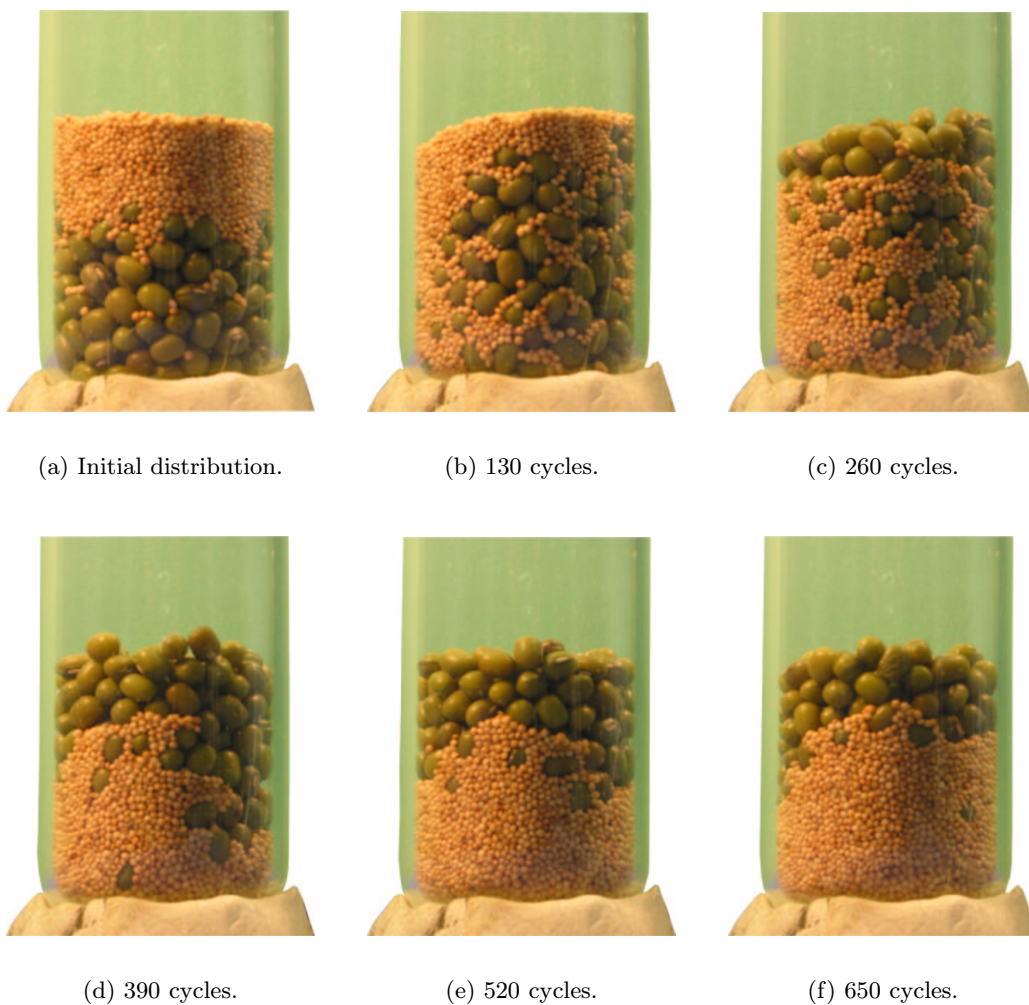
Figure 9.2: Vibration of a mixture of amaranth and green gram. Again, the large grains *win* and the Brazil nut effect drives green gram to the top.

(a) Initial distri-   (b) 500 cycles.   (c) 1500 cycles.   (d) 3000 cycles.
bution.

(e) 4500 cycles.   (f) 6000 cycles.   (g) 7500 cycles.   (h) 9000 cycles.
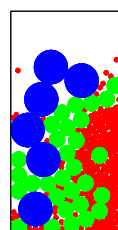
Figure 9.3: Vibration of a mixture of amaranth and lead balls. The Brazil nut effect
dominates and drives the lead balls to the top in spite of their high specific weight.

(a) Initial distri-
bution.
(b) 500 cycles.
(c) 1000 cycles.
(d) 1500 cycles.

(e) 2250 cycles.
(f) 3000 cycles.
(g) 4500 cycles.
(h) 6000 cycles.
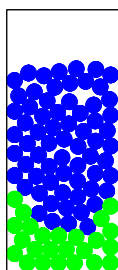
Figure 9.4: Vibration of a mixture of green gram, amaranth and lead balls. Again, the large seeds of green gram come to rest on top, while amaranth forms the bottom layer. In spite of their high specific weight, the lead balls of intermediate size form the middle layer.
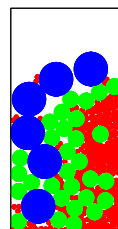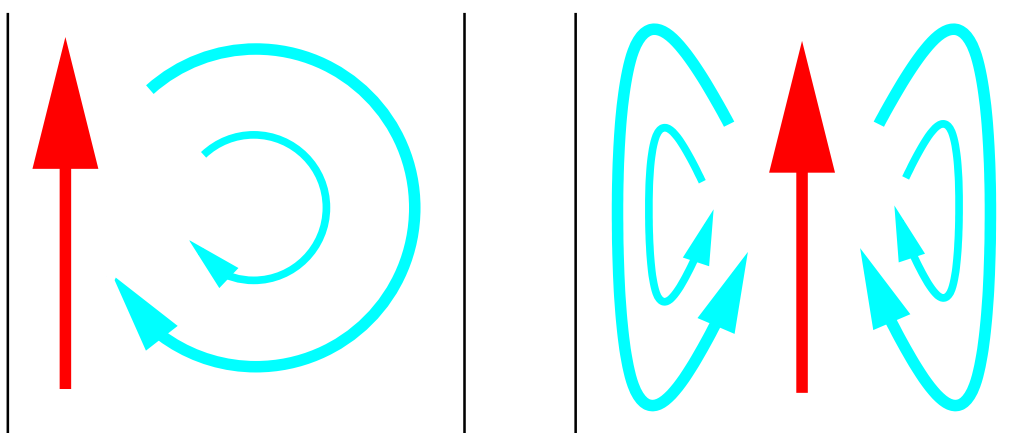
(a) The asymmetric convection roll, observed in a shaken mixture of green gram and lead balls of about equal size.

(b) The symmetric source of amaranth seeds in a mixture with green gram.

Figure 9.5: Schematic illustration of the convection rolls observed in vibrated granular mixtures. On the one hand, due to slight discrepancy between the shaking direction and the orientation of the gravitational force, a rotational convection drives particles up on one side of the vessel, while they sink back down on the opposite side (a). On the other hand, the ratchet effect can counteract the Brazil nut effect and form particle sources in the mixture (b).
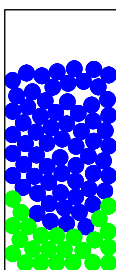
(a) Convection roll in a shaken mixture of green gram seeds and lead balls. The snapshot shows horizontal segregation with green gram on the left and lead balls on the right.

(b) Convection roll in green gram with amaranth. Again, horizontal segregation due to the periodic movement is visible.

Figure 9.6: Convection rolls. Some mixtures of granular material exhibit horizontal segregation and produce periodic fluctuations similar to the ones in the classical Rayleigh-Bénard cell.
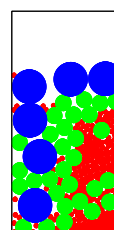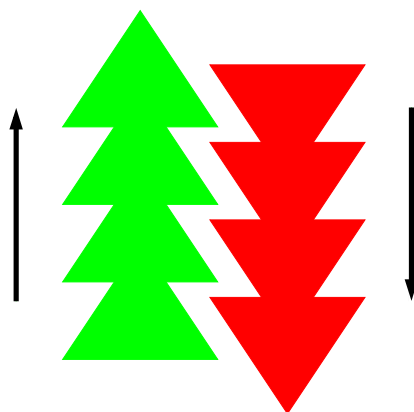
Figure 9.7: Due to surface structure or microscopic throatiness, particles can lose their ability to pass each other and jam. As a consequence, the introduced shaking energy is transformed into unidirectional particle motion. This so-called *ratchet effect* can antagonize the Brazil nut effect, which is dominating under normal conditions.
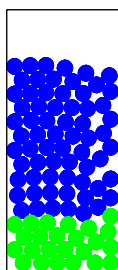
Bibliography

[Amann83] H. Amann, *Gewöhnliche Differentialgleichungen*, de Gruyter, 1983

[Amann89] H. Amann, *Dynamic theory of quasilinear parabolic systems. Part III. Global existence*, Math. Z. **202**, pp. 219-250, 1989

[Anderson93] R. S. Anderson, K. L. Bunas, *Grain size segregation and stratigraphy in aeolian ripples modelled with a cellular automaton*, Nature **365**, pp. 740-743, 1993

[Aste00] T. Aste, D. Weaire, *The Pursuit of Perfect Packing*, Institute of Physics Publishing, 2000

[Bantang02] J. Bantang, M. Lim, C. Monterola, C. Saloma, *Gravity-assisted segregation of granular materials of equal mass and size*, Phys. Rev. E **66**, pp. 041306 ff., 2002

[Barker90] G. Barker, M. Grimson, *Physics of Muesli*, New Scientist, May 26, 1990

[Barker93] G. C. Barker, A. Mehta, *Size segregation mechanisms*, Nature **364** (5), pp. 486-487, August 1993

[Batchelor82.1] G. K. Batchelor, *Sedimentation in a dilute polydisperse system of interacting spheres. Part 1. General theory*, J. Fluid Mech. **119**, pp. 379-408, 1982

[Batchelor82.2] G. K. Batchelor, C. S. Wen, *Sedimentation in a dilute polydisperse system of interacting spheres. Part 2. Numerical settling of polydisperse suspensions and three-dimensional particle-scale simulations*, J. of Engineering Mathematics **0**, pp. 1-21, 2000

[Bosch90] F. van den Bosch, J. A. J. Metz, O. Diekmann, *The velocity of spatial population expansion*, J. Math. Biol. **28**, pp. 529-565, 1990

[Boutreux99] T. Boutreux, H. A. Makse, P. G. Gennes, *Surface flows of granular mixtures III, Canonical model*, Eur. Phys. J. B **9**, pp. 105-115, 1999

[Braun01] J. Braun, *Segregation and sedimentation of granular media by diffusion and convection*, Phys. Rev. E **64**, pp. 011307 ff., 2001

[Brunovsky92] P. Brunovsky, P. Polacik, B. Sandstede, *Convergence in general periodic parabolic equations in one space dimension*, Nonlinear Analysis TMA **18** (3), pp. 209-215, 1992

[Britton] N. F. Britton, *Reaction-Diffusion Equations and Their Applications to Biology*, Academic Press, 1986

[Bürger00.1] R. Bürger, F. Concha, K.-K. Fjelde, K. Hvistendahl Karlsen, *Numerical simulation of the settling of polydisperse suspensions of spheres*, Powder Technology **113**, pp. 30-54, 2000

[Bürger00.2] R. Bürger, K.-K. Fjelde, K. Höfler, K. Hvistendahl Karlsen, *Central difference solutions of the kinematic model of settling of polydisperse suspensions and three-dimensional particle-scale simulations*, J. of Engineering Math. **0**, pp. 1-21, 2000

[Bustos99] M. C. Bustos, F. Concha, R. Bürger, E. M. Tory, *Sedimentation and Thickening*, Kluwer Academic Publishers, 1999

[Butler83] G. J. Butler, S. B. Hsu, P. Waltman, *Coexistence of competing predators in a chemostat*, J. Math. Biol. **17**, pp. 133-151, 1983

[Butler85.1] G. J. Butler, G. S. K. Wolkowicz, *A mathematical model of the chemostat with a general class of functions describing nutrient uptake*, SIAM J. Appl. Math. **45**, pp. 138-151, 1985

[Butler85.2] G. J. Butler, S. B. Hsu, P. Waltman, *A mathematical model of the chemostat with periodic washout rate*, SIAM J. Appl. Math. **45**, pp. 435-449, 1985

[Butler86] G. J. Butler, G. S. K. Wolkowicz, *Predator-mediated competition in a chemostat*, J. Math. Biol. **24**, pp. 167-191, 1986

[Butler87] G. J. Butler, G. S. K. Wolkowicz, *Predator-mediated coexistence in a chemostat: Coexistence and competition reversal*, Math. Modelling **8**, pp. 781-785, 1987

[Cizeau99] P. Cizeau, H. A. Makse, H. E. Stanley, *Mechanism for spontaneous granular stratification and segregation in two-dimensional silos*, Phys. Rev. E **59**, pp. 4408-4421, 1999

[Clément91] E. Clément, J. Rajchenbach, *Fluidization of a bidimensional powder*, Europhys. Lett. **16** (2), pp. 133-138, 1991

[Cubiotti01] P. Cubiotti, B. DiBella, *Two-point problem for higher-order systems*, J. Math. Anal. Appl. **253**, pp. 243-249, 2001

[Deimling74] K. Deimling, *Nichtlineare Gleichungen und Abbildungsgrade*, Springer, 1974

[deLarrard99] F. de Larrard, *Concrete Mixture Proportioning, A Scientific Approach*, E&FN Spon, 1999

[DiBella02] B. Di Bella, *A two-point problem for first-order systems*, Arch. Math. **78**, pp. 475-480, 2002

[Dippel95] S. Dippel, S. Luding, *Simulations on size segregation: Geometrical effects in the absence of convection*, J. Phys. I (France) **5**, pp. 1527 ff., 1995

[Dunbar83] S. R. Dunbar, *Travelling wave solutions of diffusive Lotka-Volterra equations*, J. Math. Biology **17**, pp. 11-32, 1983

[Dunbar84] S. R. Dunbar, *Travelling wave solutions of diffusive Lotka-Volterra equations: A heteroclinic connection in $I\!R^4$*, Trans. Amer. Math. Soc. **283** (2), pp. 557-594, 1984

[Dunbar86] S. R. Dunbar, *Travelling waves in diffusive predator-prey equations: Periodic orbits and point-to-periodic heteroclinic orbits*, SIAM J. Appl. Math. **46**, pp. 1057-1079, 1986

[Dung99] L. Dung, H. L. Smith, P. Waltman, *Growth in the unstirred chemostat with different diffusion rates*, Fields Institute Communications **21**, pp. 131-142, 1999

[Duran93] J. Duran, J. Rajchenbach, E. Clément, *Arching effect model for particle size segregation*, Phys. Rev. Lett. **70** (16), pp. 2431-2434, 1993

[Eigen79] M. Eigen, P. Schuster, *The Hypercycle: A Principle of Natural Self-Organization*, Springer 1979

[Epheser55] H. Epheser, *Über die Existenz der Lösungen von Randwertaufgaben mit gewöhnlichen, nichtlinearen Differentialgleichungen zweiter Ordnung*, Math. Zeitschr. **61**, pp. 435-454, 1955

[Farkas02] Z. Farkas, F. Szalai, D. E. Wolf, T. Vicsek, *Segregation of granular binary mixtures by a ratchet mechanism*, Phys. Rev. E **65**, pp. 022301 ff., 2002

[Feroe86] J. A. Feroe, *Existence of travelling wave trains in nerve axon equations*, SIAM J. Appl. Math. **46** (6), pp. 1079-1097, 1986

[Feroe83] J. A. Feroe, *Traveling waves with finitely many pulses in a nerve equation. Oscillations in mathematical biology* (Garden City, N.Y., 1982), Lecture Notes in Biomath. **51**, pp. 61-101, Springer, 1983.

[Fife79] P. C. Fife, *Mathematical Aspects of Reacting and Diffusing Systems*, in: *Lecture Notes in Biomathematics* **28**, Springer, 1979

[Friedman64] A. Friedman, *Partial Differential Equations of Parabolic Type*, Prentice-Hall, 1964

[Gale65] D. Gale, H. Nikaidô, *The Jacobian matrix and global univalence of mappings*, Math. Ann. **159**, pp. 81-93, 1965

[Gallas96] J. A. C. Gallas, H. J. Herrmann, T. Pöschel, S. Sokolowski, *Molecular dynamics simulation of size segregation in three dimensions*, J. Stat. Phys. **82**, pp. 443-450, 1996

[Gantmacher59] F. R. Gantmacher, *Applications of the Theory of Matrices*, Interscience Publishers, New York, 1959

[Gantmacher90] F. R. Gantmacher, *The Theory of Matrices*, Chelsea Publishers, 1990

[Gause34] G. F. Gause, *The Struggle for Existence*, Williams and Wilkins, 1934

[Gerhardt95] M. Gerhardt, H. Schuster, *Das Digitale Universum*, Vieweg, 1995

[Getling98] A. V. Getling, *Rayleigh-Bénard Convection: Structures and Dynamics*, World Scientific, 1998

[Gray97] J. M. N. T. Gray, K. Hutter, *Pattern formation in granular avalanches*, Continuum Mech. Thermodyn. **9**, pp. 341-345, 1997

[Gray98] J. M. N. T. Gray, Y. C. Tai, *Particle size segregation, granular shocks and stratification patterns*, H. J. Herrmann et al., eds., Physics of Dry Granular Media, Kluwer Academic Publishers, pp. 697-702, 1998

[Haken96] H. Haken, H. C. Wolf, *The Physics of Atoms and Quanta*, 5th edition, Springer, 1996

[Hansmann57] A. Hansmann, *Die Sylvien der Insel Sardinien*, Naumannia **7**, pp. 404-429, 1857

[Hardin60] G. Hardin, *The competitive exclusion principle*, Science **131**, 1960

[Hethcote94] H. W. Hethcote, *A thousand and one epidemic models*, Lecture Notes in Biomath. **100**, pp. 504-515, Springer, 1994

[Hofbauer98] J. Hofbauer, K. Sigmund, *Evolutionary Games and Population Dynamics*, Cambridge University Press, 1998

[Hong01] D. C. Hong, P. V. Quinn, S. Luding, *The reverse Brazil nut problem: competition between percolation and condensation*, Phys. Rev. Lett. **86**, pp. 3423-3426, 2001

[Horn91] R. A. Horn, C. R. Johnson, *Topics in Matrix Analysis*, Cambridge Univ. Press, 1991

[Hsu93] S. B. Hsu, P. Waltman, *On a system of reaction-diffusion equations arising from competition in an unstirred chemostat*, SIAM J. Appl. Math. **53** (4), pp. 1026-1044, 1993

[Hsu94.1] S. B. Hsu, H. L. Smith, P. Waltman, *Dynamics of competition in the unstirred chemostat*, Can. Appl. Math. Q. **2** (4), pp. 461-483, 1994

[Hsu94.2] S. B. Hsu, P. Waltman, G. S. K. Wolkowicz, *Global analysis of a model of plasmid-bearing, plasmid-free competition in a chemostat*, J. Math. Biol. **32** (7), pp. 731-742, 1994

[Hsu95] S. B. Hsu, T.-K. Luo, P. Waltman, *Competition between plasmid-bearing and plasmid-free organisms in a chemostat with an inhibitor*, J. Math. Biol. **34** (2), pp. 225-238, 1995

[Hutchinson78] G. E. Hutchinson, *An Introduction to Population Ecology*, Yale University Press, 1978

[Johnson10] R. H. Johnson, *Determinate evolution in the color-pattern of the lady-beetles*, Carnegie Institution of Washington **122**, pp. 104 ff., 1910

[Jullien92] R. Jullien, P. Meakin, A. Pavlovitch, *Three-dimensional model for particle-size segregation by shaking*, Phys. Rev. Lett. **69** (4), pp. 640-643, 1992

[Karolyi98] A. Karolyi, J. Kertesz, S. Havlin, H. A. Makse, H. E. Stanley, *Filling a silo with a mixture of grains: Friction-induced segregation*, Europhys. Lett. **44**, pp. 388-393, 1998

[Kermack27] W. O. Kermack, A. G. McKendrick, *Contributions to the mathematical theory of epidemics (I)*, Proceedings of the Royal Society **115A**, pp. 700-721, 1927

[Krapivsky93] P. L. Kapivsky, E. Ben-Naim, *Collective properties of adsorption-desorption processes*, J. Chem. Phys. **100** (9), pp. 6778-6782, 1993

[Krasnosel'skii64] M. A. Krasnosel'skii, *Topological Methods in the Theory of Nonlinear Integral Equations*, in *International Series of Monographs on Pure and Applied Mathematics*, Vol. **45**, Pergamon Press, 1964

[Kynch52] G. J. Kynch, *A theory of sedimentation*, Trans. Faraday Soc. **48**, pp. 166-176, 1952

[Lätzel00] M. Lätzel, S. Luding, J. Herrmann, *Macroscopic material properties from quasi-static, microscopic simulations of a two-dimensional shear-cell*, Granular Matter 2(3), pp. 113-121, 2000

[Lewis02.1] M. A. Lewis, B. Li, H. F. Weinberger, *Analysis of linear determinacy for spread in cooperative models*, J. Math. Biol. **45**, pp. 183-218, 2002

[Lewis02.2] M. A. Lewis, B. Li, H. F. Weinberger, *Spreading speed and linear determinacy for two-species competition models*, J. Math. Biol. **45**, pp. 219-233, 2002

[Lotka32] A. J. Lotka, *The growth of mixed populations: two species competing for a common food supply*, J. Wash. Acad. Sci. **22**, pp. 461-469, 1932

[Luding96.1] S. Luding, E. Clément, J. Rajchenbach, J. Duran, *Simulations of pattern formation in vibrated granular media*, Europhys. Lett. **36** (4), pp. 247-252, 1996

[Luding96.2] S. Luding, J. Duran, E. Clément, J. Rajchenbach, *Segregation of particle solids: Segregation via convection*, Pharmaceutical Technology, pp. 42-44, August 1996

[Luding97] S. Luding, *Stress distribution in static two dimensional granular model media in the absence of friction*, Phys. Rev. E **55** (4), pp. 4720-4729, 1997

[Luding98] S. Luding, M. Huthmann, S. McNamara, A. Zippelius, *Homogeneous cooling of rough, dissipative particles: Theory and simulations*, Phys. Rev. E **58**, pp. 3416-3425, 1998

[Luding99] S. Luding, O. Strauss, S. McNamara, *Segregation of polydisperse granular media in the presence of a temperature gradient* in: *Segregation in Granular Flows*, IUTAM symposium, A. D. Rosato, D. L. Blackmore, eds., Kluwer Academic Publishers, pp. 297-303, 1999

[Luding01] S. Luding, *A global equation of state of two-dimensional hard sphere systems*, Phys. Rev. E **63**, pp. 042201 ff., 2001

[Luo95] T.-K. Luo, S. B. Hsu, *Global analysis of a model of plasmid-bearing, plasmid-free competition in a chemostat with inhibitions*, J. Math. Biol. **34** (1), pp. 41-76, 1995

[Makse97.1] H. A. Makse, *Stratification instability in granular flows*, Phys. Rev. E **56**, pp. 7008-7016, 1997

[Makse97.2] H. A. Makse, S. Havlin, P. R. King, H. E. Stanley, *Spontaneous stratification in granular mixtures*, Nature **386**, pp. 379-381, 1997

[Makse97.3] H. A. Makse, P. Cizeau, H. E. Stanley, *Possible stratification mechanism in granular mixtures*, Phys. Rev. Lett. **78**, pp. 3298-3301, 1997

[Makse98.1] H. A. Makse, H. J. Herrmann, *Microscopic model for granular stratification and segregation*, Europhys. Lett. **43**, pp. 1-6, 1998

[Makse98.2] H. A. Makse, R. C. Ball, H. E. Stanley, S. Warr, *Dynamics of granular stratification*, Phys. Rev. E **58**, pp. 3357-3367, 1998

[Makse99.1] H. A. Makse, *Kinematic segregation of flowing grains in sandpiles*, Eur. Phys. J. B **7**, pp. 271-276, 1999

[Makse99.2] H. A. Makse, *Continuous avalanche segregation of granular mixtures in thin rotating drums*, Phys. Rev. Lett. **83** (16), pp. 3186-3189, 1999

[Masliyah79] J. H. Masliyah, *Hindered settling in a multiple-species particle system*, Chem. Eng. Sci. **34**, pp. 1166-1168, 1979

[Matano78] H. Matano, *Convergence of solutions of one-dimensional semilinear parabolic equations*, J. Math. Kyoto Univ. **18**, pp. 221-227, 1978

[Matano88] H. Matano, *Asymptotic behavior of solutions of semilinear heat equations on S^1*, in *Nonlinear Diffusion Equations and their Equilibrium States*, B. Peletier, J. Serrin, eds., pp. 139-162, Springer, 1988

[McGehee77] R. McGehee, R. A. Armstrong, *Some mathematical problems concerning the ecological principle of competitive exclusion*, Journal of Differential Equations **23**, pp. 30-52, 1977

[McNamara99] S. McNamara, S. Luding, *A simple method to mix granular materials*, in IUTAM Symposium on Segregation in Granular Flows, A. D. Rosato, ed., Kluwer Academic Publishers, 1999

[Merriam-Webster93] Merriam-Webster's *Third New International Dictionary*, 1993

[Michaelis13] L. Michaelis, M. I. Menten, *Die Kinetik der Invertinwirkung*, Biochem. Z. **49**, pp. 333-369, 1913

[Murray93] J. D. Murray, *Mathematical Biology*, second edition, Springer, 1993

[Okubo80] A. Okubo, *Diffusion and Ecological Problems: Mathematical Models*, Springer, 1980

[Ortega70] J. M. Ortega, W. C. Rheinboldt, *Iterative solution of nonlinear equations in several variables*, Academic Press, 1970

[Othmer97] H. J. Othmer, A. Stevens, *Aggregation, blowup, and collapse: The ABC of taxis in reinforced random walks*, SIAM J. APPL. MATH. **57** (4), pp. 1044-1081, 1997

[Perko96] L. Perko, *Differential Equations and Dynamical Systems*, second edition, Springer, 1996

[Picard08] M. E. Picard, *Traité d'Analyse, Tome III*, Gauthier-Villars, Paris, 1908

[Picard30] M. E. Picard, *Equations Différentielles*, Gauthier-Villars, Paris, 1930

[Pöschel95] T. Pöschel, H. J. Herrmann, *Size segregation and convection*, Europhys. Lett. **29** (2), pp. 123-128, 1995

[Poundstone87] W. Poundstone, *The Recursive Universe*, Oxford Univ. Press, 1987

[Prottere84] M. H. Protter, H. F. Weinberger, *Maximum Principles in Differential Equations*, Springer, 1984

[Radach74] G. Radach, E. Maier-Reimer, *The vertical structure of phytoplankton growth dynamics, a mathematical model*, Proc. of the Sixth Colloquium on Ocean Hydrodynamics, Liège, 1974

[Rapaport01] D. C. Rapaport, *Mechanism for granular segregation*, Phys. Rev. E **64**, pp. 061304 ff., 2001

[Raudkivi76] A. J. Raudkivi, *Loose Boundary Hydraulics*, Pergamon Press, 1976

[Renardy93] M. Renardy, R. C. Rogers, *An Introduction to Partial Differential Equations*, Springer, 1993

[Richardson54] J. F. Richardson, W. N. Zaki, *Sedimentation and fluidization I*, Trans. Inst. Chem. Engrs. (London) **32**, pp. 35-53, 1954

[Ristow99] G. H. Ristow, *Mixing and segregation in rotating drums*, IUTAM Symposium on Segregation, Cape May, USA, June 5th-10th, 1999

[Rosato87] A. Rosato, K. J. Strandburg, F. Prinz, R. H. Swedsen, *Why the Brazil nuts are on top: size segregation of particle matter by shaking*, Phys. Rev. Lett. **58**, pp. 1038-1040, 1987

[Schönfisch99] B. Schönfisch, A. de Roos, *Synchronous and asynchronous updating callular automata*, Biosystems **51**, pp. 123-143, 1999

[Smith95] H. L. Smith, *Monotone Dynamical Systems - An Introduction to the Theory of Competitive and Cooperative Systems*, in *Mathematical Surveys and Monographs*, Vol. 41, American Mathematical Society, 1995

[Smoller83] J. Smoller, *Shock Waves and Reaction-Diffusion Equations*, Springer, 1983

[So91] J. W. H. So, *Inertial manifold for a reaction diffusion equation model of competition in a chemostat*, J. Austral. Math. Soc. B **33**, pp. 9-15, 1991

[Stemmons00] E. D. Stemmons, H. L. Smith, *Competition in a chemostat with wall attachment*, SIAM J. Appl. Math. **61** (2), pp. 567-595, 2000

[Stokes51] G. G. Stokes, *On the effect of the internal friction on the motion of pendulums*, Trans. Cambridge Phil. Soc. **9** (2), pp. 8-106, 1851

[Tarjus92] G. Tarjus, P. Viot, *Generalized car parking problem as a model for particle deposition with entropy activated rate process*, Phys. Rev. Lett. **68** (15), pp. 2354-2357, 1992

[Tritton77] D. J. Tritton, *Physical Fluid Dynamics*, Van Nostrand Reinhold, 1977

[Tufillaro92] N. B. Tufillaro, J. Reilly, T. Abbott, *An Experimental Approach to Nonlinear Dynamics and Chaos*, Addison-Wesley, 1992

[Vladimirova99] N. Vladimirova, A. Malagoli, R. Mauri, *Two-dimensional model of phase segregation in liquid binary mixtures*, Phys. Rev. E **60** (6), pp. 6968-6977, 1999

[Volterra26] V. Volterra, *Variationi e fluttuazioni del numero d'individui in specie animali conviventi*, Mem. R. Acad. Naz. dei Lincei **2**, pp. 31-113, 1926

[Volterra28] V. Volterra, *Variations and fluctuations of the number of individuals in animal species living together*, J. Conseil Permanent Internat. pour l'Exploitation der la Mer. **3**, pp. 3-51, 1928

[Wackenhut02] M. Wackenhut, *Modeling compaction of polydisperse particles*, master thesis, October 2002

[Walter70] W. Walter, *Differential and Integral Inequalities*, Springer, 1970

[Wambaugh02] J. F. Wambaugh, C. Reichhardt, C. J. Olson, *Ratchet-induced segregation and transport of nonspherical grains*, Phys. Rev. E **65**, pp. 031308 ff., 2002

[Weinberger82] H. F. Weinberger, *Long-time behavior of a class of biological models*, SIAM J. Math. Anal. **13**, pp. 353-396, 1982

[Wörz-Busekros76] A. Wörz-Busekros, *Solutions to a degenerate system of parabolic equations from marine biology*, J. Math. Biol. **3**, pp. 393-406, 1976

[Wolkowicz92] G. S. K. Wolkowicz, Z. Lu, *Global dynamics of a mathematical model of competition in the chemostat: General response functions and differential death rates*, SIAM J. Appl. Math. **52** (1), pp. 222-233, 1992

[Wolkowicz95] G. S. K. Wolkowicz, M. M. Ballyk, S. P. Daoussis, *Interaction in a chemostat: Introduction of a competitor can promote greater diversity*, Rocky Mt. J. Math. **25** (1), pp. 515-543, 1995

[Wolkowicz96] G. S. K. Wolkowicz, M. M. Ballyk, Z. Lu, *Microbiological dynamics in a chemostat: Competition, growth, implications of enrichment*, Z. Deng et

al., ed., Differential equations and control theory. Proceedings of the international conference, Wuhan, People's Republic of China, 1994. New York: M. Dekker. Lect. Notes Pure Appl. Math. **176**, pp. 389-406, 1996

[Wolkowicz97] G. S. K. Wolkowicz, H. Xia, *Global asymptotic behavior of a chemostat model with discrete delays*, SIAM J. Appl. Math. **57** (4), pp. 1019-1043, 1997

[Wolkowicz98.1] G. S. K. Wolkowicz, X. Q. Zhao, *N-species competition in a periodic chemostat*, Differ. Integral Equ. **11** (3), pp. 465-491, 1998

[Wolkowicz98.2] G. S. K. Wolkowicz, Z. Lu, *Direct interference on competition in a chemostat*, J. Biomath. **13** (3), pp. 282-291, 1998

Curriculum Vitae

November 1, 1971	born in Göttingen
1977-1981	attendance at the elementary school in Rösrath-Hoffnungsthal
1981-1983	attendance at the Freiherr-von-Stein high school in Rösrath
1983	move of the family to Markdorf at the Lake of Constance
1983-1991	attendance at the high school in Markdorf
June 13, 1991	graduation from high school (*Abitur*)
1991-1992	civil service at the *Beratungsstelle für Landespflege, Obst- und Gartenbau* in Stockach
1992-1994	college (*Diplom Grundstudium*) in mathematics and physics at the Ruprecht-Karls University of Heidelberg
August 10, 1994	graduation from college, majors in mathematics and physics
1994-1995	attendance at the master program in mathematics at the State University of New York at Stony Brook, USA, with a scholarship of the Fulbright Commission
December 19, 1995	master of arts degree in mathematics
1996-1997	*maîtrise* program in mathematics at the Denis Diderot University in Paris, France, with an Erasmus/Sokrates scholarship
February 1997	*maîtrise* graduation
1997-1998	*DEA* program at the Pierre et Marie Curie University in Paris, France
September 18, 1998	*DEA* graduation with major in dynamical systems and population dynamics; thesis (*rapport de stage*) entitled *Modèles Écologiques de Dynamique Simple: Des Individus aux Populations*
1998-2003	PhD program at the Eberhard-Karls University of Tübingen with major in dynamical systems and partial differential equations
2000-2003	position as a scientific assistant at the University of Tübingen
May 2003	completion of the doctoral thesis entitled *Convection-Diffusion Models for Competition and Segregation in Granular Material*
July-September 2003	practical course in the laboratory of the Physiological Institute of the University of Tübingen

Academic teachers

Ruprecht-Karls University of Heidelberg

Mathematics: A. Brandis, H. G. Bock, S. Böge
Physics: K. Tittel, K. D. Rothe
Chemistry: P. Comba

State University of New York at Stony Brook, USA

Mathematics: L. Jones, B. Maskit, L. Takhtajan
Physics: C. N. Yang

Denis Diderot University, Paris 7, France

Mathematics: J. Le Potier, C.-M. Marle

Pierre et Marie Curie University, Paris 6, France

Mathematics: I. Kupka, J.-P. Françoise

Eberhard-Karls University Tübingen

Mathematics: K. P. Hadeler, F. Loose, B. Leeb
Human Physiology: F. Lang, J. P. Ruppersberg
Botany and Plant Physiology: W. Frommer, R. Haupp